Synthesis and Characterization of some Selenazone Complexes and Nanoadsorbent Surfaces from Industrial Waste for Removing some Carcinogenic Dyes and Heavy Metals from Water

A Dissertation Submitted To

The College of Science, University of Basrah In Partial Fulfillment of

the Requirements for

Degree of Doctor of Philosophy of Science In Chemistry

By:

Zuhair Ali Abdulnabi

B.Sc. in Chemistry, 2000, University of Basrah

M.Sc. in Chemistry, 2013, University of Basrah

Supervised By :

Prof. Dr. Hassan T Abdulsahib   Prof. Dr. Faris A J Al-doghachi

2021 A.D   1442A.H

جمهورية العراق

وزارة التعليم العالي والبحث العلمي

جامعة البصرة ـ كلية العلوم

قسم الكيمياء

تحضير وتشخيص بعض معقدات السلينازون والسطوح الممتزة النانوية من المخلفات الصناعية لأزالة بعض الأصباغ المسرطنة والعناصر الثقيلة من المياه

أطروحة مقدمة الى

كلية العلوم/ جامعة البصرة

وهي جزء من متطلبات نيل درجة الدكتوراه

في فلسفة علوم الكيمياء

من قبل الطالب

زهير علي عبدالنبي

بكلوريوس في علوم الكيمياء   ٢٠٠٠

ماجستير في علوم الكيمياء   ٢٠١٣

<table>
<tr><td>أ.د فارس عبدالرضا جاسم الدوغجي</td><td>أ.د حسن ثامر عبدالصاحب</td></tr>
<tr><td>٢٠٢١ م</td><td>١٤٤٢ هـ</td></tr>
</table>

بسم الله الرحمن الرحيم

(قَالُوا سُبْحَانَكَ لَا عِلْمَ لَنَا إِلَّا مَا عَلَّمْتَنَا إِنَّكَ أَنْتَ الْعَلِيمُ الْحَكِيمُ)

صدق الله العلي العظيم

-الاية (   )

Dedication

To

The candle which lit my life and awarded me everytning………………

My parents

The supporters that helped me throughout the study period…

My brother, My sister

The hand that helped me and the patience she kept with me……………

My wife

The flowers that awarded me love………………………………………

My Sons

Zuhair

Acknowledgments

Firstly , praise to Almighty Allah who awarded me force , health and patience in order to achieve this project. My thanks and gratitude also go to the first teacher in our life who lit the torch for knowing and teaching , the prophet Muhammad (may Allah's peace be upon him and his household) .

I would like to express my deep appreciation to my supervisors, Prof. Dr. Hassan T Abdulsahib and Prof. Dr. Faris A J Al-doghachi for all their guidance and support during my study period. My sincere thanks and gratitude extend to the deanship of the College of Science, the presidency of the department of chemistry and all their staff members. In more love, I would like to express my appreciation and thanks to all staff members of the Marine Sciences Center for supporting me to achieve this work.

Finally, I am pleased to express my thanks , appreciation and gratitude to my family , my friends and everyone who supported me in order to achieve success.

Zuhair

Recommendation of Supervisors

We certify that this dissertation was carried out under our supervision at the Chemistry Department in the College of science at the University of Basrah, Iraq, as a partial fulfillment of the requirements for the degree of doctor of philosophy in the science of Chemistry.

Signature

Prof. Dr. Hassan T Abdulsahib

Date: /   /2021

Signature

Prof. Dr. Faris A J Al-doghachi

Date: /   /2021

Recommendation of the Head of the Department

In view of available recommendation, I forward this dissertation for debate by the examining committee.

Signature

Prof. Dr. Zaki Nassir Kadhim

Head of the Department of Chemistry

College of Science

University of Basrah, Iraq

Date: 23/ 11 /2021

Committee Certification

We the examining committee, certify that we have read this thesis entitled " **Synthesis and Characterization of Some Selenazone Complexes and Nanoadsorbent Surfaces From Industrial Waste For Removing Some Carcinogenic Dyes and Heavy Metals From Water**" and we have examine the student Zuhair Ali Abdulnabi, in its contents, and that, in our opinion it is accepted as a thesis for the degree of Doctor of philosophy of scince in chemistry Appreciated Excellence.

Signature

Chairman: Prof. Dr.Nadhum Abdulnabi Awad
Address: University of Basrah
Date   /   2021

Signature
Member: Prof. Dr. Adnan Sultan Abdulnabi
Address: University of Basrah
Date   /   /2021

Signature
Member: Prof. Dr. Alaa Kadhim Jasim
Address: University of Southern technical
Date   /   /2021

Signature
Member: Assist.Prof. Dr.Ala Ismael Ayoob
Address: University of Mosoul
Date   /   /2021

Signature
Member: Assist.Prof. Dr.Laila Saleh Zaalan
Address: University of Basrah
Date   /   /2021

Signature:
Supervisor and Member:
Prof. Dr. Hassan T Abdulsahib
Address: University of Basrah
Date: /   /2021

Signature
Supervisor and Member:
Prof. Dr. Faris A J Al-doghachi
Address: University of Basrah
Date: /   /2021

Approval of the committee on postgraduate studies

Signature
Assist.Prof. Dr. Muwafaq F. Al-Shahwan
Dean college of science
University of Basrah
Date: /   /2021

Abstract

The current work comprises two basic parts of inorganic and analytical study. The first part adopts a new method for preparing of 1,5-diphenylselenocarbazone (Selenazone) nanoparticle and their complexes with Pb^{+2}, Cd^{+2}, Co^{+2} and Ni^{+2} ions. The ligand and its complexes were characterized by using FT-IR,Uv-Vis, ^{1}H-NMR, ^{13}C-NMR, XRD, EI-mass spectrometry, SEM, hydride generation (HG), flame-atomic absorption spectrophotometer, thermal analysis (TG/DTA) and molar conductance measurements. The result of ligand mass spectrum was shown the structure of ligand is dimer. The measurements of molar conductance in all complexes recorded low values, (3.3-7.27 ohm^{-1} cm^2 mol^{-1}) in hot DMSO indicating that all the metal complexes were non-electrolytes excepted for the nickel complex which recorded a higher molar conductance at 80.71 ohm^{-1} cm^2 mol^{-1} and possessed an electrolytic nature. Kinetic and thermodynamic parameters of complexes (A ,E ,ΔH ,ΔS and ΔG) have been computed using three kinetic models such as Coast-Redfern , Broido and Horowitz-Metzger, that illustrated the decomposition reactions in all steps which were nonspontaneous, endothermic and negative values of entropy. Thermogravimetric analyses (TG/DTA) were consistent with the atomic spectroscopy data, proving that the geometry shape of all the complexes was octahedral by molar ratio 1:2 (M:L).

The second part included six adsorbent surfaces were used to water treatment from some carcinogenic dyes and heavy metals, Four adsorbent surfaces were prepared by adopting different methods such as graphene oxide from graphite powder (GO), modification of graphene oxide(GOZ) , activated carbon (ACZ) and silica gel (SGZ) with selenazone ligand. Two adsorbents surface nanoparticles such as graphitic oxide (sGO) and Iron oxide (sFe) were separated from soot waste by using various solvents. The prepared adsorbents were characterized by using FT-IR, UV-Vis, EDX, XRD, FESEM, Thermal analysis (TG,DTG and DSC), the surface area , pore size and specific pore volume (BET&BJH analysis). The

Abstract

crystals size were calculated by Debye Scherrer's equation from XRD data which were 23.9, 4.5, 27.1, 32.5, 54.1 and 42.2 nm for adsorbents ACZ, SGZ, GO, GOZ, sGO and sFe respectively.

The optimum conditions included contact time , temperature , pH level , concentration and agitation speed were investigated for increasing the removal efficiency of Mordant Red 3, Congo Red, Basic Brown and Rhodamine dyes, as well as, mercury and lead ions from their aqueous solutions by using the prepared adsorbents. The removal percentage of dyes from their aqueous was recorded a highest percentage for Basic Brown dye onto all adsorbent surfaces while the lowest removal percentage recorded for Mordant Red 3 dye onto all adsorbent surfaces excepted onto ACZ adsorbent. Mercury and lead ions were recorded highest the removal percentage onto ACZ and GOZ respectively.

Adsorption equilibrium isotherms were determined by utilizing four models as Langmuir , Freundlich , Temkin and Dubinin-Radushkevich. The adsorption process of Mordant Red 3 dye onto ACZ, GO and GOZ adsorbents was found to be more appropriate with Langmuir model whilst , Freundlich model was more consistent than othr isotherms for SGZ and sGO adsorbents. The model of Langmuir was more fitted to describe the adsorption process of Congo Red dye onto ACZ, GO, GOZ and sGO adsorbents while, Temkin model was more suitable for SGZ and sFe adsorbents than other isotherm models.

The adsorption mechanism of Basic Brown dye is more corresponding with Freundlich model which refers to multilayer adsorption , Langmuir model which was more suitable to adsorb Basic Brown dye onto GO adsorbent while the adsorption process of Basic Brown dye onto sFe adsorbent was found to be more appropriate with D-R isotherm. The isotherms of Langmuir, Temkin and Freundlich were found to be more consistent to describe the adsorption process of rhodamine B dye onto ACZ, GO and GOZ adsorbents respectively .

Abstract

The Freundlich model was more suitable than other isotherm models to describe the adsorption process of Mercury ions onto all adsorbents surface except for their adsorption onto ACZ material that is corresponding with D-R models. While lead ions was more fitted with Langmuir isotherm onto ACZ, GO and GOZ adsorbents, Freundlich model was more suitable than other adsorption isotherms to adsorb lead ions onto SGZ, sGO and sFe adsorbents.

Thermodynamic parameters of the adsorption process were computed included $\Delta G°$, $\Delta S°$ and $\Delta H°$. The results of free energy of all adsorption process revealed the spontaneous reaction of adsorption and showed the physisorption process that agreed with results of adsorption energy (E KJ/mol). The data of enthalpy $\Delta H°$ recorded positive and negative values that refered to the endo-exothermic adsorption while , the positive and negative values of the entropy $\Delta S°$, pointing to increase or decrease the affinity towards the interaction between the adsorbate molecules with adsorbent surface.

The desorption process was studied by utilizing three solvents that were different in polarity which were distilled water , methanol and ethanol for recovering the dyes molecules while , heavy metals were recovered from the adsorbent surface after their adsorbed by using different concentrations of HCl (0.5 , 1 and 2N) . The data showed good solvent recoveries for dyes molecules which were methanol while, the best concentration of HCl was approximately 0.5 N.

The adsorption-desorption system was applied by using three different types of water included distilled , river and sea water, using four dyes (Mordant red 3, Congo red, Basic brown and Rhodamine B). The ionic strength for solutions was impacted positively or negatively on the adsorption efficiency. The percent of desorption efficiency recorded high values by utilizing methanol as solvent.

المستخلص

تتضمن الدراسة الحالية على محورين أساسيين:

المحور الأول يتضمن تحضير جسيمات نانوية للمركب المناظر للدايثيزون (Selenazone) ‎1,5-diphenylselenocarbazone وبعض معقداتها مع Ni^{+2} , Co^{+2}, Cd^{+2}, Pb^{+2} بأستخدام الميثانول الساخن كمذيب، شخصت المركبات المحضرة بأستخدام التقنيات التالية : مطيافية الأشعة تحت الحمراء FT-IR، مطيافية الأشعة المرئية- فوق البنفسجية UV-Vis، مطيافية الرنين النووي المغناطيسي للبروتون HNMR[1] ، مطيافية الرنين النووي المغناطيسي لنظير الكاربون CNMR[13]، حيود الأشعة السينية XRD، مطيافية الكتلة ، المجهر الألكتروني الماسح(SEM)، مطياف الأمتصاص الذري اللهبي وتقنية توليد الهيدريد HG، التحليلا الحرارية (TG/DTA)، وقياس التوصيل المولاري لمحاليل المعقدات بأستخدام مذيب DMSO الساخن ، أظهرت نتائج طيف الكتلة التركيب الثنائي لليكاند المحضر ، سجلت قياسات التوصيلية المولارية قيم منخفضة بحدود (٣,٣ – ٧,٢٧ أوم$^{-1}$ سم^2 مول$^{-1}$) والتي تشير نتائجها الى الطبيعة غير الألكتروليتية لمحاليل المعقدات بأستثناء محلول معقد النيكل الذي يكون ذو طبيعة الكتروليتية (٨٠ أوم$^{-1}$ سم^2 مول$^{-1}$) ، تم حساب بعض الدوال الثرموديناميكية والحركية مثل (A، E،ΔH، ΔS و ΔG) بأستخدام ثلاث موديلات حركية مثل Coast-Redfern ، Broido و Horowitz-Metzger، تشير النتائج الى تلقائية جميع تفاعلات التحلل الحراري للمعقدات ، تفاعلات ماصة للحرارية وكذلك تظهر قيم سالبة للتغير بالأنتروبي. تتفق نتائج التحليل الحراري الوزني (TG/DTA) للمعقدات مع نتائج المطيافية الذرية والتي تشير الى الشكل الهندسي لجميع المعقدات المحضرة هو شكل ثماني السطوح وبنسبة مولية ١: ٢.

يتضمن المحور الثاني من الدراسة هو التطبيقات التحليلية لأزالة بعض الأصباغ المسرطنة والعناصر الثقيلة من محاليلها المائية من خلال أستخدام ستة أسطح ممتزة محضرة ضمن الحدود النانوية. حضرت أربع أسطح ممتزة بطرق مختلفة مثل أوكسيد الكرافين وتم تحميل مركب السلينازون المحضر على سطح أوكسيد الكرافين GOZ و الكاربون المنشط ACZ والسليكا جل SGZ. أستخلص سطحين من المواد المازة من النفايات السخام مثل اوكسيد الكرافيت sGO وأوكسيد الحديد sFe بأستخدام مذيبات مختلفة للأستخلاص.

شخصت السطوح المازة بأستخدام تقنيات مختلفة مثل مطيافية الأشعة تحت الحمراء FT-IR، مطيافية الأشعة المرئية- فوق البنفسجية UV-Vis، حيود الأشعة السينية XRD، المجهر الألكتروني الماسح(FeSEM)، تحليل EDX، التحليل الحراري TG وDTG و DSC وكذلك تم قياس المساحة السطحية وقطر المسامات وحجومها بأستخدام تحليل BET و BJH. حددت حجوم البلورات لجميع السطوح المازة من بيانات تحليل حيود الأشعة السينية بواسطة أستخدام معادلة ديباي شرر، أضهرت النتائج لحجوم

المستخلص

البلورات على النحو التالي : ٢٣,٩ ، ٤,٥ ، ٢٧,١ ، ٣٢,٥ ، ٥٤,١ و ٤٢,٢ نانومتر والتي تعود الى الأسطح المحضرة ACZ، SGZ، GO، GOZ، sGO وsFe على التوالي .

درست الظروف المثالية مثل زمن التوازن ، درجة الحرارة، سرعة المزج و الدالة الحامضية لزيادة كفاءة أزالة الأصباغ المدروسة بالأضافة الى ايونات الزئبق والرصاص من محاليلها المائية بواسطة الأسطح الممتزة المحضرة، أظهرت النتائج أزالة عالية لصبغة Basic Brown من محاليلها المائية بينما سجلت قيم منخفضة لأزالة صبغة Mordant Red 3 على سطوح جميع الممتزات بأستثناء سطح ACZ . سجل أزالة عالية لأيونات الزئبق والرصاص من محاليلها المائية على سطح ACZ و GOZ على التوالي .

درست أربع موديلات من الأيزوثرم مثل Langmuir ، Freundlich، Temkin و -Dubinin Radushkevich لأمتزاز الصبغات المدروسة و أيونات الزئبق والرصاص، حيث تشير النتائج لأزالة صبغة Mordant Red 3 بواسطة الأسطح ACZ، GO و GOZ والتي تتفق مع نموذج Langmuir ، بينما أزالة الصبغة بواسطة SGZ و sGO تتفق مع نموذج Freundlich .

تتفق عملية أمتزاز صبغة Congo Red على أسطح المواد الممتزة التالية ACZ، GO ، GOZ و sGO مع نموذج Langmuir ، بينما يمكن وصف عملية الأمتزاز الصبغة على سطح SGZ و sFe بواسطة موديل Temkin أكثر من السطوح المتبقية .

يمكن وصف ودراسة ميكانيكية الأمتزاز صبغة Basic Brown من محلولها المائي بواسطة نموذج Freundlich أكثر من الأيزوثرمات الأخرى والتي تشير الى أمتزاز متعدد الطبقات ، بينما تتفق النماذج Langmuir و D-R على دراسة ووصف ميكانيكية امتزاز الصبغة على سطح GO و sFe على التوالي .

تعتبر نماذج الأيزوثرمات التالية Langmuir ، Temkin و Freundlich أكثر دقة لوصف ميكانيكية الأمتزاز لصبغةّ Rhodamine B من محلولها المائي على سطح ACZ، GO و GOZ على التوالي .

تتفق جميع عمليات ألأمتزاز لأيونات الزئبق بواسطة جميع الأسطح المازة مع نموذج Freundlich أكثر بالمقارنة مع الأيزوثرمات الأخرى المدروسة والذي يشير الى أمتزاز متعدد الطبقات بأستثناء سطح ACZ الذي يتفق مع D-R أيزوثيرم لأمتزاز أيونات الزئبق من محاليل المائية.

المستخلص

عملية امتزاز أيونات الرصاص من محاليلها المائية بواسطة بعض الأسطح الممتزة مثل ACZ، GO و GOZ يمكن وصفها بدقة عالية بأستخدام نموذج Langmuir ، بينما الأسطح الممتزة الأخرى تتطابق بشكل أكبر مع أيزوثيرم Freundlich لأزالة أيونات الرصاص من محاليلها المائية.

حددت الدوال الثرموديناميكية لعمليات أمتزاز للأصباغ وأيونات الرصاص والزئبق من محاليلها المائية مثل التغير بالطاقة الحرة ΔG° و التغير بالمحتوى الحراري ΔH° والتغير بالعشوائية ΔS°، حيث تشير النتائج التغيير بالطاقة الحرة على ان جميع عمليات الأمتزاز تحدث بشكل تلقائي والتي تتفق نتائجها مع نتائج طاقة الأمتزاز المحسوبة من أيزوثيرم D-R والتي تحدد نوعية الأمتزاز كأمتزاز فيزيائي. تشير نتائج التغير بالمحتوى الحراري على حدوث أمتزاز ماص وباعث للحرارة، بينما القيم الموجبة والسالبة للتغير بالعشوائية تشير الى زيادة او نقصان الألفة نحو أمتزاز المادة المراد أمتزازها على السطح الماز .

درست عمليات الأسترجاع للصبغات وأيونات الزئبق والرصاص بعد أمتزازها على الأسطح المازه بأستخدام ثلاث مذيبات مختلفة القطبية مثل الماء المقطر، الميثانول و الأيثانول المطلق لأسترجاع الصبغات الممتزة، بينما درست تأثير ثلاث تراكيز من حامض الهيدروليك (٠,٥ ، ١ و ٢ نورمالي) لأسترجاع أيونات الزئبق والرصاص الممتزة على جميع السطح المازة . تظهر النتائج الى ان مذيب الميثانول أفضل من المذيبات المدروسة لأسترجاع الصبغات بعد أمتزازها من على جميع الأسطح الممتزة المدروسة ، بينما كان التركيز المثالي لحامض الهيدروليك هو ٠,٥ نورمالي لأسترجاع أيونات الزئبق والرصاص من على جميع الأسطح الممتزة.

طبقت عملية الأمتزاز والأسترجاع للصبغات المدروسة من خلال تحضير نماذح حقيقية تحاكي عملية التلوث بالأصباغ في النظام المائي حيث أستخدمت ثلاث أنواع من المياه مختلفة القوة الأيونية لتحضير محاليل الصبغات مثل ماء مقطر ، مياه نهرية ومياه بحرية ، تشير البيانات على تأثير القوة الأيونية للمياه المستخدمة على عملية أمتزاز الصبغات المدروسة نحو زيادة او نقصان بكفاءة عملية الأمتزاز. درست عملية الأسترجاع الصبغات المدروسة بكفاءة أسترجاع عالية من على جميع الأسطح الممتزة بواسطة أستخدام مذيب الميثانول كمحلول أسترجاع .

Table of Contents

Table of Contents

Table of Contents

Table of Contents

Table of Contents

Table of Contents

List of Tables

List of Tables

List of Tables

List of Schemes

List of Figures

List of Figures

List of Figures

List of Figures

List of Figures

List of Figures

List of Symbols and Abbreviations

Nomenclature	Symbols
Gawlamd Chemical Company	G.C.C
British Drug House	B.D.H
Riedel − De Haen AG Seelze − Hannover	R.D.H
John Townsend Baker	J.T. Baker
Melting Point	M.P.
Fourier transform infrared spectroscopy	FT-IR
Proton Nuclear Magnetic Resonance	^{1}H-NMR
Carbon-13 Nuclear Magnetic Resonance	^{13}C-NMR
Mass Spectra	MS
Electron Impact Ionization	EI
Flame-Atomic Absorption Spectroscopy	F.A.A.S
Hydride Generation	HG
Electron Volte	eV
Hertz	Hz
Chemical Shift	δ
Part Per Million	ppm
Dimethylformamide	DMF
Dimethylsulphoxide	DMSO
Tetra methyl Silane	TMS
Degree Celsius	
Molar Conductance	Λ_m

List of Symbols and Abbreviations

Molar Concentration	C
Specific Conductance	K
Conductance	G
Cell Constant	A(Λ)
Thermo gravimetric Analysis	TGA
Drevitives Thermal gravimetric	DTG
Differential Thermo Analysis	DTA
Differential Scanning Calorimetry	DSC
Arrhenius factor	A(TGA)
Gas constant	R
Activation energy	E
Heating rate	θ
Barrett Joyner Halenda	BJH
Tetramethylethylenediamine	TMEDA
N,N'-dicyclohexylcarbodiimide	DCC
Field Emission scanning electron microscopy	**FeSEM**
X-Ray Diffraction	**XRD**
Brunauer Emmett Teller	**BET**
Energy Dispersive X-ray	**EDX**
The extracted graphite oxide	**sGO**
The extracted iron oxide	**sFe**
Graphene oxide	**GO**

List of Symbols and Abbreviations

Graphene oxide-Selenazone	**GOZ**
Activated carbon-Selenazone	**ACZ**
Silica gel-Selenazone	**SGZ**
The maximum wavelength	$\boldsymbol{\lambda_{max}}$
Mass to charge ratio	**m/z**
2Theta	$\boldsymbol{2\Theta}$
Angstrom	$\mathbf{A^o}$
Initail temperature	$\mathbf{T_i}$
The max temperature	$\mathbf{T_m}$
The final temperature	$\mathbf{T_f}$
The standard enthalpy change	ΔH°
The standard entropy change	ΔS°
The standard free energy change	ΔG°
Activation energy	**E**
The correlation coefficient	$\mathbf{R^2}$
Carbon/Oxygen ratio	**C/O**
The Adsorption percentage	**%Ad**
The Desorption percentage	**%De**
Initial concentration	$\mathbf{C_o}$
The residual concentration	$\mathbf{C_e}$
Adsorption capacity	$\mathbf{Q_e}$
The maximum of adsorption capacity	$\mathbf{Q_{max}}$

List of Symbols and Abbreviations

Weight	**W**
Volume	**V**
Langmuir constant	$\mathbf{K_L}$
Separation factor	$\mathbf{R_L}$
Heterogeneity factor	**1/n**
Freundlich constant	$\mathbf{K_f}$
Temkin constant	$\mathbf{b_T}$
Temkin constant	$\mathbf{A_T}$
Dubinin-Radushkevich	**D-R**
D-R isotherm constant	**β**
Polanyi potential	ε
Total Desolve Solid	TDS
Electrical Conductivity	EC
Selenazone or (E)-1,5-diphenylselenocarbazone	Z

Chapter One

Introduction

1. Introduction

1.1. Organoselenium compounds

Selenium was separated for the first time in 1817 by the Swedish Chemist Jons Jacob Berzelius [1] . Selenium has a symbol Se, it belongs to chalcogen group in the periodic table and has the four natural oxidation states that are set as follows: elemental selenium (0), selenide (II), selenite (IV) and selenate (VI). The selenium compounds are classified into two groups organic and inorganic compounds such as: selenocysteine and selenomethionine, they are considered the main species that exist in vegetables and grains while the inorganic selenite and selenate represent the dominant class in waters, additionally both selenite and selenate are highly available forms of selenium for living organisms[1,2]. Selenium is a complex class owing to its important properties of being both essential and toxic, the levels of selenium in many organisms, especially human and animal are important whereas,both the excesses and deficiencies in the selenium concentration are known to cause endemic disease[2-4]. Organoselenium compounds are chemical compounds containing carbon -to- selenium chemical bonds [4], they are shown as follows :
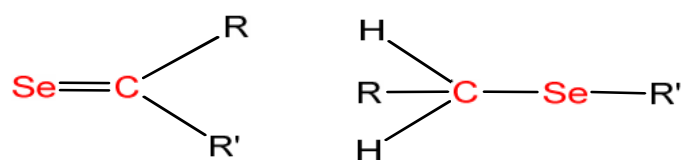
Where R , R' is H atom , alkyl , Aryl , heterocyclic

Organoselenium compounds were known for the first time in 1847 by Wöhler and Siemens when the first synthesis of ethyl selenol ,the novel functional groups in some organic compounds are synthesized by using organoselenium compounds as useful intermediates under mild conditions such as: alkyl selenoxide which was synthesized from alkyl selenides by using oxidant agents [5]. There are many

compounds of organoselenium that were synthesized and took various forms [4,5], as shown in Figure 1.1.
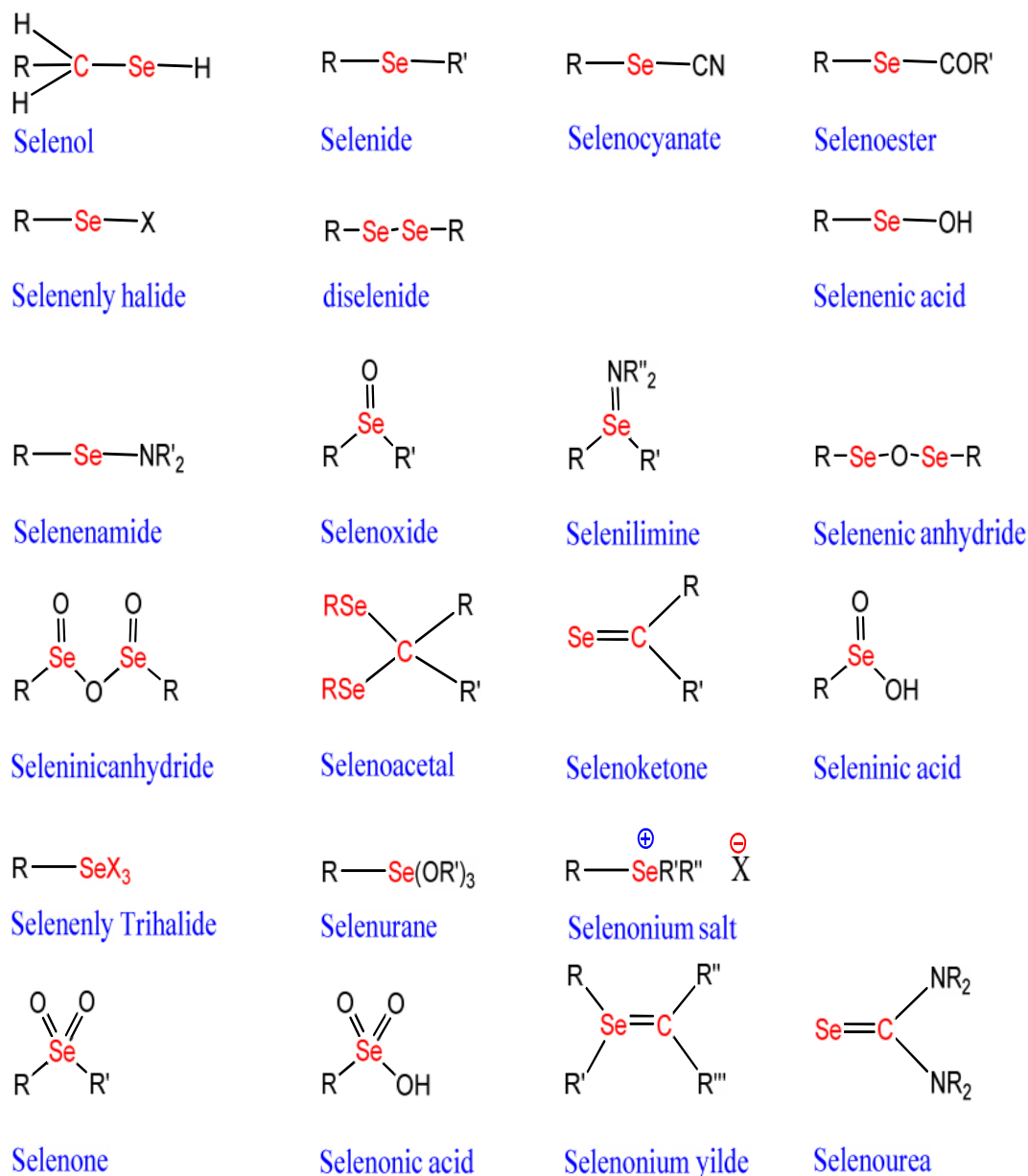
Figure 1.1 : Organoselenium compounds[5]

1.1.1. Reactions of organoselenium compounds

Organoselenium compounds appeared high activity as useful intermediates in synthesizing several of the organic compounds during the last few decades , moreover , the acivity of these compouns due to the existence of selenium and its

ability to be inserted in different organic reactions by employing three ways can be intrduced as an electrophile, nucleophile and as a radical form. Generally it combines chemo - , regio - , and stereoselectivity with mild experimental conditions [6] . The electrophilic properties of organoselenium compounds are important in the reaction of organic chemistry, where, it can provide useful and powerful reagents in the synthetic chemistry, especially the selenofunctionalization of olefins that represent an important method for the rapid introduction of vicinal functional groups, often found with the associated formation of rings and stereocenters as shown in scheme 1.1 . Furthermore , the electrophilic of selenium reagents were used the α - selenenylation for carbonyl compounds that are available for the important intermediates in the synthesis of α , β – unsaturated compounds and thier derivatives [7] and also the preparation of 1,2 - diketones through a seleno - Pummerer reaction [6,8] .
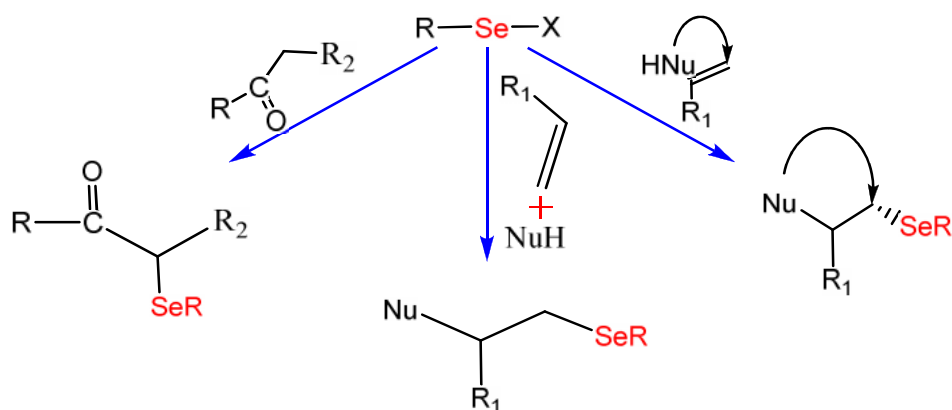
Scheme 1.1 : The reactivity of selenium reagents as an electrophile[6]

The synthesis of selenium electrophile compound is regarded the main reagents, derived from some phenylselenenyl derivatives like chloride, bromide, and N – phenylseleno phthalimide. Recently, the selenium electrophile reagents are commercially obtainable and are considered the most common electrophilic reagents, used to introduce selenium into organic molecules [6].

The behavior of selenium as nucleophilic reagents began in 1973 when the scientific team for Sharpless offered a simple method to prepare a benzene selenolate[[PhSeB(OEt)3]- Na+], its utility in the nucleophilic ring opened various epoxides as it is explained in scheme 1.2 [5] .

PhSeSePh $\xrightarrow[\text{Ehanol}]{\text{NaBH}_4}$ [PhSeB(OEt)$_3$]$^\ominus$ Na$^\oplus$
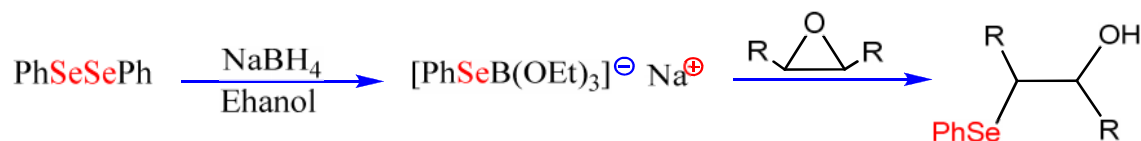
Scheme 1.2 : The reactivity of selenium reagent as nucleophilic[5]

Ever after Sharpless' discovery, several of nucleophilic reactions by using sodium phenylseleno(triethoxy)borate complex were developed, including substitution reactions with halides , addition reactions to cyclic ethers, nucleophilic reductions of α,β-epoxy carbonyl compounds . On other hand , these reactions are important and useful in the organic synthesis. Additionally, it is used in the preparation of biologically active organoselenium compounds and other diverse materials that contain selenium. There are many methods that have been developed to synthesis different nucleophilic reagents for selenium. The other method than Sharpless method, included the insertion of selenium into lithium and Grignard reagents , reduction of diselenides, selenocyanates, and elemental selenium by using many reducing reagents, like alkali metals, alkali hydrides, hydrazine and samarium reagents [5] . The reactivity of synthetic selenium as nucleophile depends on the preparation route, employed additionally, it depends on the additives that exist in the solution.Generally, these species of selenium nucleophilic are highly reactive and usually cannot be separated. Nowadays, new species of nucleophilic selenium reagents have high stability because they have formation bond between selenium and the main group elements, on other hand these reagents have contributed to the wide spread of nucleophilic selenium species and their various application in the all branches of chemistry [9] .

The radical reactions are important reactions in widely ranges of chemistry and several of the compounds have played an important role in the sophistication of radical reactions, especially the Organoselenium compounds. Selenium compounds are utilized in a wide range of synthetic radical reactions as radical precursors are used (scheme 1.3) , for inclusion of selenium into target products and several of other important applications like radical trapping. A number of precursors are adequate for useing in common radical chemistry such as the reactions that are facilitated by the use of tributyltin hydride (Bu3SnH) [5] or triphenyltin hydride (Ph$_3$SnH) [6] . The radical applications for selenium compounds are various and furthermore they are more facilitated in form because the selenium atom has the polarizability. Also, these compounds have the weak bonds for C – Se and Se – H in their structures . Generally , the Selenium compounds are available, easy to prepare and not overly costly [5,6].
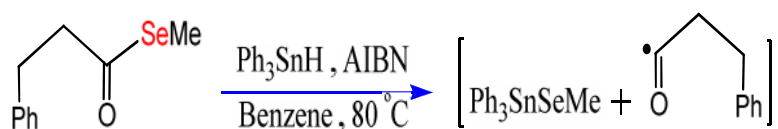
Scheme 1.3 : The reactivity of selenium reagent as radical[5]

1.1.2. Preparation methods of organoselenium compounds

There are many routes used for the insertion of the selenium atom in the organic compounds, these new compounds formation that different properties and a variety of chemical and biological activities. The insertion of selenium atom in the organic compounds are utilized by adopting three forms such as an electrophile, nucleophile and as a radical form. This insertion depends on various conditions such as pH , temperature of reaction , type of solvent and nature of catalysts agent . Several of the synthetic compounds of selenium are explained in Figure 1.1. Selenoketon compounds are one species that belongs to organoselenium compounds and thus can be defined as the chemical compounds that have double

bond between carbon and selenium atoms. In general, these species of organoselenium compounds are relatively more stable than the other species of selenium compounds. Through it has stability, but still it keeps a high reactivity which leads to show unique reactions [5,6]. In order to synthesize the selenoketon compounds, it used three methods based on the patterns of reaction instead of the types of compounds , these methods are known as follows the insertion of selenium atom as an electrophile or nucleophile into the structure of organic molecules. Additionally, the other methods are the heterocumulenes that contain selenium atoms as a starting material [5].

Selenocarbonyl compounds have been prepared by using elemental selenium through the smooth reaction and their behavior as electrophile with carbanion ions , Nakayama et al. carried out the preparation of selenocarbonyl compounds as intermediate compound by using elemental selenium and heat [10], as is shown in equation 1.1 .

$R_1, R_2 = CN , CO_2ET , H$ X= S or Se
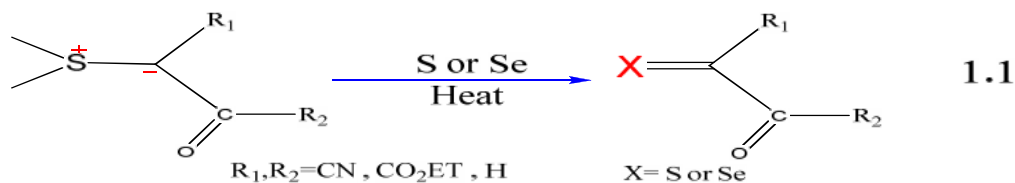
Selenium is used as nucleophile reagent which belongs to selenide species (Se^{2-}) through the reduction process of elemental selenium and by using the reduced agents, for example the reduction process of selenium element (Se^0) with $NaBH_4$ as reduced agent in ethanol alcohol at 0°C for 30 min or used the water as solvent rather than ethanol to produce the selenide species as NaHSe. These species are utilized to construct double bonds between carbon and selenium atoms which lead to form the selenocarbonyl compounds [6] . The study for Raghavendra et al.[11] has explained to prepare 2-Seleno-3-formylquinoline from the reaction between 2-chloro-3-formylquinoline with sodium hydroselenide in ethanol as solvent for 1h under refluxed that are shown in equation 1.2.

1.2
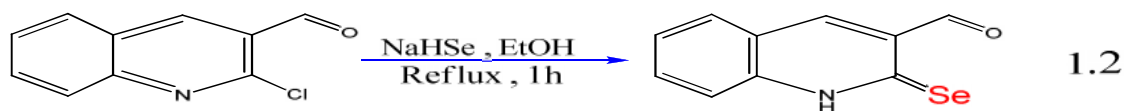
Carbon diselenide (CSe_2) was utilized as an initialed material for a long time like the reduction process for carbon diselenide with sodium and followed by benzoylation for gaving 1,3-diselena-2-selone [5] , these process are explained in equation 1.3 .

1.3
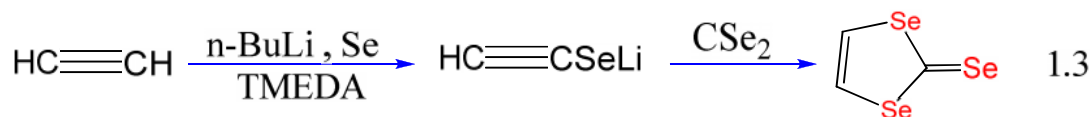
1.1.3. Biological importance of Organoselenium compounds

The intramolecular interaction between selenium and nitrogen or oxygen atoms in structure of organoselenium compounds is particularly interesting because these interactions are employed to improve the biological activity of the selenium compounds [6]. Furthermore , Selenium has promoted redox reactivity when it is compared with sulfur, and on other hand , selenium forms become weaker σ-bonds when they are compared with the analoge element such as sulfur and thus , selenium bonds are have undergone the faster cleavege than the sulfur bonds, so the selenium compounds usually appear higher chemical and biological activities than sulfur compounds [5,6]. Many organoselenium compounds are usually used in biological system such as the selenocyanates compounds that are used as intermediates in the synthesis of diorganoselenates and are investigated as antitumor drugs [8]. Generally , the organoselenium compounds have basically greater bioavailability when compared with inorganic selenium compounds where the organoselenium compounds reflected more importance because these compounds usually exist in less toxic forms than the inorganic ones [1] . The organic compounds of selenium have been used as antioxidant activity where , in

1973 were known by the selenium as an essential component for the enzyme glutathione peroxidase (GPx) . This enzyme is present in most of the body tissues and is responsible for catalyzing the breakdown of hydrogen peroxide and convert into water. There are five forms from enzyme glutathione peroxidase, all these types are done to reduce hydrogen peroxide and lipid hydroperoxides [12,13]. The activity of organoselenium compound as an antitumor started with dietary P-methoxy benzeneselenol , moreover, the study carried out by Rao et al. exhibited some compounds of organoselenium such as P-Phenylen bis(methylene) Selenocyanate that was utilized as a superior cancer chemopreventive agents [14].

There are many of synthesized organoselenium compounds that have shown activity as antiviral like selena zofran which was used against Type 1 herpes simplex virus . On other hand several properties of organoselenium compounds have been studied as antimicrobial for example ,ebselen(2-phenyl-1,2-benziso selenazol-3-(2H)-one) which were studied as anti-inflammatory,anti atherosclerotic ,cytoprotective and antimicrobial against Staphylococcus aureus where, it indicated high activity [12].

1.1.4. Complexes of organoselenium compounds

Organoselenium compounds played an important role in development of coordination chemistry through the complexes formation with several transition metals. Organoselenium compounds are considered good chelating agents for many elements, that due to their capability on donate electrons and bonds formation such as covalent or coordination covalent linkages because they contained empty orbitals in their external levels . In contrast , hetero atoms in the structure of organoselenium compounds contributed to the active forms for complexes formation with the transition metals such as sulfur , nitrogen , oxygen and selenium [15]. The organic compounds of selenium and their complexes are acquired for

more interest in various important applications such as analytical chemistry , medical field and industrial field [16] .

Ramakrishna and Irving (1969) study referred to extraction of some different ions from their aqueous solutions in various pH values such as (Ag^+,Mn^{2+}, Fe^{2+}, Co^{2+}, Ni^{2+}, Cu^{2+}, Zn^{2+}, Cd^{2+}, Hg^{2+}, Pb^{2+}, Tl^+ and Bi^{3+}) by using selenazone compound. Additionally , this study identified a high selectivity towards some extraction ions as Ag^+, Hg^{2+} , Ni^{2+} and Pd^{2+} by using diselenide compound more than used of selenazone or dithizone [17].

Some organoselenium compounds identified a high activity in the medical field, especially in chemotherapy , where , the scientific team by Zec et.al. have recorded the first evidence by using complexes formation from Zn^{2+} , Cd^{2+} and Ni^{2+} with 2,6-diacetyl pyridine bis(selenosemicarbazone) as anti-proliferative [18]. The prepared organoselenium compound and their complexes are shown in Figure 1.2 below .
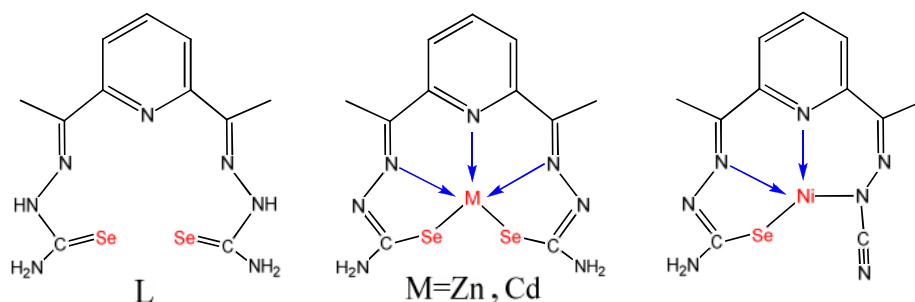
Figure 1.2 : Ligand and their complexes with
Zinc , Cadmium and Nickel[18]

Todorovic et.al. Prepared some new complexes for Zn^{2+} , Cd^{2+} and Ni^{2+} with 2-quinolinecarboxaldehyde selenosmicarbazone. The prepared compound and their complexes are given in Figure1.3 . The synthesized complexes are characterized by various techniques as NMR , IR and X-ray moreover, these complexes have been existed in their aqueous solutions by two forms like the major as tetrahedral while the octahedral is the minor form [19] .
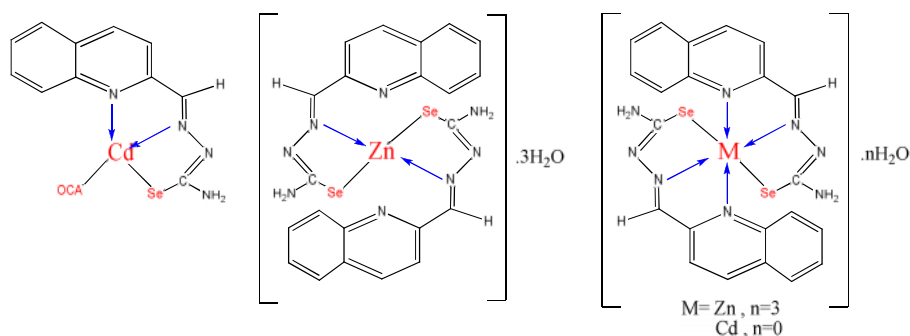
Figure 1.3 : The complexes for Zinc and Cadmium [19]

A new selenosemicarbazone and their complex with copper was synthesized by Shen et.al., the complex has worked the efficient generates oxidative stress and down-regulates the 90-kDa heat shock protein (HSP90AA1) and its client proteins (PIM1, AKT1) in U2os and HeLa cells. These results explain the possible application of this complex in cancer therapy [20]. The prepared compound are shown in Figure 1.4 .
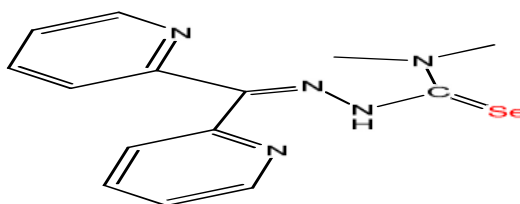
Figure1.4 :The selenosemicarbazone [20]

1.2. Environmental Pollution

The environmental pollution is one the complex problems facing humanity as it results from the increasing of many activities such as a variety industrial development , urban growth , agriculture activities , combustion of coal and oil , movement of wind and rain water, all these reasons lead to increasing the pollution of ecosystem as soil , water and air , affect negatively on biodiversity and human health [21] . There are many sources of pollution that are involved into ecosystem.

In general, the pollution sources are divided into two categories according to origin of pollutants such as natural or anthropogenic sources.

The natural sources are often related with natural phenomena which occur without human activities like earthquakes, floods, drought, cyclones , movement of wind , erosion of rock and rain water[2]. All these phenomena lead to increasing of several contamination in ecosystem . In addition , the anthropogenic sources are ones in which the insertion of pollutants into ecosystem is done by human activities such as refining oil , effluent urban , agricultural activities , effluent industrial , waste incineration and mining operations[21] . All these pollution sources have worked to raise the levels of pollutant concentrations in ecosystem that resulted from the increasing of pollutants released by variety industrial activities [22,23]. Additionally the pollution has distributed according to their nature and classified into physical , chemical and biological pollutants .

Physical pollutants are one species of environmental pollution that are associated with physical phenomena such as heat change , electromagnetic radiation , noise, earthquakes , volcanic eruptions and cyclones[24] . All physical properties in the ecosystem are affected by these pollutants , while the chemical contaminants are represented the other challenge that faced the ecosystem, they are divided into two groups given as follows :

The contaminants of the organic origin included a large number of natural materials such as dyes ,domestic waste , industrial waste , pesticides , fertilizes , oil, oil derivatives, in contrast to the other type in which the inorganic origin such as inorganic acids , heavy metals , emitted gases from volcanoes and the gases emission from combustion of coal and oil. The chemical contaminants are introduced into environment by several industrial activities , thus they are transferred into air , water , soil and sediment and lead to increasing of the concentration pollutants in ecosystem that affects negatively on human health [23].

The biological contaminants contained many types of microorganism like bacteria, viruses, fungi and algae. All these types have harmful effect which causes several human diseases [24,25]. Generally , the pollution can be defined as any substance as solid , liquid and gases that exist in such concentration as may be or tend to be harmful to the environment. Therefore, any change of concentration in environmental limits leads to imbalance in ecosystem [26]. The various pollutants are transferred by different routes that were inserted into environment via air , water , soil and sediment, in accordance with type of pollutants released as gases , liquid or solid materials. In addition, all these pollutants are collected through different mechanisms that lead to be transferred into aquatic system as is shown in Figure 1.5 [26].
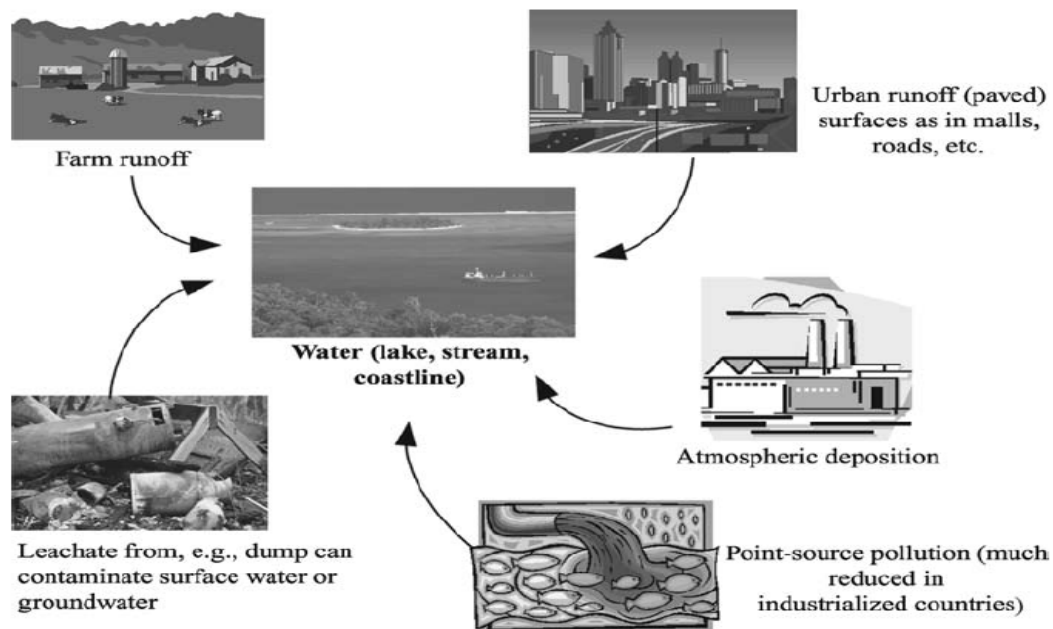
Figure 1.5 : Pollution sources for aquatic system [26]

The pollution in aquatic system resulted from releasing the several pollutant materials like the increasing of the development of industry and urban growth, many chemical substances have been introduced in most of the material industries that need many human activities such as pharmaceutical industry, cosmetics,

electrical industries, pesticide, dyes, mining, and leather industries [24,27]. All these industries are necessary for human life but, it produces chemical compounds that can be harmful and toxic to human health when it reaches to the aquatic system, for example the heavy metals and dyes that are released by many industries like oil extraction , leather and foods , these materials are known by their toxicity and ability on accumulation in most tissues in organisms of water as fish causes many diseases for human like cancer disease when it is transferred to human via foods chain [21 ,23] .

1.2.1. Dyes

Many natural and industrial materials have appeared different forms and colors, these colors depend on their contents varying from organic or inorganic materials and their capability to absorb visible radition. Additionally, it is known the visible light is divided into several colors starting in blue color at 350 nm and ending in red color at 800 nm. Dyes can be defined as chemical substances organic or inorganic which are used to impart colors to textiles, paper, leather,foods , buldings and other materials where the colouring is not readily changed by washing, heat, light or any other factors [28]. Dyes differ from pigments where most dyes belong to organic compounds which they contain carbon atoms in their structure , while the pigments may consist of inorganic or organic compounds and keep on their constant when it is related with target material by coloring operation. Here the dyes are of lower constancy than pigments, furthermore, pigments give brighter colours than dyes [25] . Mauveine was considered the first synthetic dye when it was discovered by Perkin in 1856. The reactive dye has been known for the first time in 1954 and their commercial launch in 1956 where it was used in different industries like the ink-jet printing of textiles, especially cotton [29].

1.2.1.1. Classification methods of dyes

There are several routes for the classification of dyes that depend on chemical structure , uses and application methods, they are given as follows :

The dyes can be classified according to their chemical structures and divided into many species such as azo , xanthene ,anthraquinone , thiazine and triaryl methan dyes. They are shown as follows[29]:
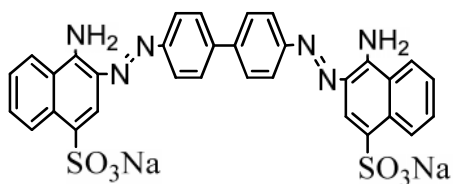
Congo red as azo dyes   Xanthene dyes   Triaryl methan dyes
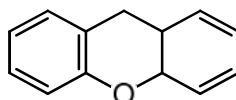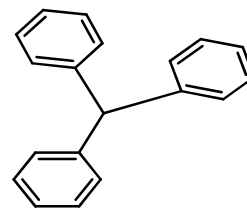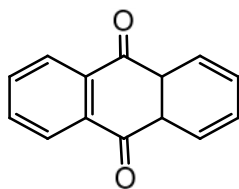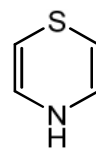
Anthraquinone dyes   Thiazine dyes

This classification is mostly used and regarded as a suitable system which has many benefits where it easily identifies dyes when it belong to group that has diagnosed properties such as azo dyes that belong to a group which has some useful properties such as strong, easily prepared, good all-round properties and cost-effective, while the other type is anthraquinone dyes that has some unuseful properties as weak and expensive, moreover , dyes can be characterized by a change of colors, for example the easily known of azo yellow, anthraquinone red and a phthalocyanine blue by observing the change of colors [29]. Additionally , the other classification of dyes depending on their uses in the principal system adopted by the color index indicated by relationship between the dyes and textile fibers from type cotton and polyester [30,31]. The last classification of dyes is based on their uses and application methods where , dyes have been also utilized in various technological applications, like in the medical sciences, electronics and especially the nonimpact printing industries. They have also been used in electrophotography whether in photocopying or laser printing . This classification

consists of several classes that depend on their uses and application[29,30], they are explained as follows:

Reactive dyes are important dyes that were discovered in 1954. They depend on the covalent bond formation between dyes and fibers. In general, the cotton is used in the coloring operation although it is utilized also, to a certain extent in wool and nylon.

Disperse dyes belong to nonionic class of dyes that are insoluble in water, therefore, it is used in coloring operation for hydrophobic fiber such as polyester and to a certain in nylon, cellulose, cellulose acetate, and acrylic fibers, this class is used in different applications, especially in electronic photography through using thermal transfer printing and dye diffusion thermal transfer .

Direct Dyes , are considered from ionic dyes as a class that have the ability in water solubility so, this class has high affinity towards cellulosic fibers, therefore, it is used in the dyeing of cotton and regenerated cellulose, paper, leather and to a lower extent for nylon. All the dyes in this class are polyazo compounds, along with some stilbenes, phthalocyanines and oxazines.

Vat dyes belong to water insoluble dyes that have been applied principally to cellulosic fibers as soluble leuco salts after their reduction in an alkaline solution, many of the chemical species belong to this class but the main types of these chemical species are anthraquinone and indigoid.

Sulfur dyes , have been applied to cotton by using sodium sulfide to reduce agent in their alkaline solution .

Basic dyes belong to a class that have water solubility and release cation ions in their aqueous solution. So, this class is also called the cationic dyes . Basic dyes were carried out on paper, polyacrylonitrile , modified nylons and modified polyesters , some of the chemical classes belong to the basic dyes such as

diazahemicyanine, triarylmethane, cyanine, hemicyanine, thiazine, oxazine, and acridine. Furthermore , some of the basic dyes show biological activity , therefore , it is used in medical field as antiseptics.

Acid dyes , are within water soluble class that released anions in their aqueous solutions therefore are also called as anionic dyes and are utilized to some extent for paper, leather, ink-jet printing, food, and cosmetics.

Solvent dyes, are insoluble in water, but they have their solubility in non-polar solvents that are used for dyeing different materials such as plastic, gasoline, oil, and wax. The principal group of chemical classes belong to solvent dyes such as azo dyes , anthraquinone while the phthalocyanine and triarylmethane dyes to a lower extent are used .

1.2.2. Heavy metals

Heavy metals can be defined as metals and metalloids that have their densities greater than 5 gm/cm^3 . The term "heavy metals" are known as the metals that exist between group II and VI in periodic table according to their definition given the by United States environmental protection agency [32]. Moreover , heavy metals exist naturally in the earth's crust by less concentration than 0.1%, therefore, they are also known by another term as trace elements [33]. In general, trace elements are divided into two principal groups as essential and unessential elements . The essential elements are important nutrients that are needed for human ,animals and plants such as zinc , iron , copper , manganese , molybdenum and cobalt. Additionally , these elements participate in several activities of the biological systems, like the involvement in the formation of proteins structure and pigment , redox operations, keeping on ionic balance , the osmotic pressure regulation and having the activity as an enzyme component of the cells [32,34] . In contrast, the excess of the concentration for these elements about allowable limit is considered harmful and may have toxic properties for human , animals and plants while the

deficiency of concentration to a lesser than the allowable limit also leads to cause many diseases for human , animals and plants . On other hand, the unessential elements are useless for the biological system and also cause several problems for human. Some of the heavy metals have toxic properties in their lower concentration like cadmium , lead , mercury …..etc., all these elements have the capability to be transferred by different mechanisms from the surround environment to the tissues of human ,animals and plant. These elements start to increase their levels in tissues by the accumulation processes ,that cause many risks for human health [32,33]. The pollution of heavy metals resulted from many activities such as natural and anthropogenic , usually from the different industries that have released a large amount from the untreated waste which is included in heavy metals, especially the oil industries towards the environment whether to air , water and soil . The riskiness of heavy metals are shown by its unable on the environmental degradation in different physico-chemical conditions it only appeard their ability in converting from one form to another through the change in its oxidation states. So , they can be considered as the constant and stable contaminants in ecosystem that causes the increase of their concentration in environment through the accumulation processes which affect on human health and animals [34,35] .

Generally ,the gas pollutants which contain heavy metals are transfered from the source pollution of gas to atmosphere, especialy from the industries of oil extraction. A larg amount of heavy metals pollutants as the oxides form, affects on the life for various birds. This leads to many risks on human health. Likewise, all these pollutants can be transfered into aquatic system from several activities via different routes for example the stations of the generator of electrical power which use some heavy metals in painting of the cooling pipes of water that causes pollution in cooling water which leads to the environmental pollution when it is released without treatment [36, 37] .

1.3. Treatment methods of waters

There are many methods for the treatment of water have been used in order to obtain a good quality of water which can convert polluted water into clean water by using many processes. The clean water has been used in several activities such as drinking water , irrigation water and different industries that are based on water purity, like soft drink . The methods are explained as follows :

1.3.1. Precipitation method

Chemical precipitation methods are important methods for the removal of pollutants from water in which the change occurs in the form of materials, dissolved in water into solid particles. These particles are formed by adding some chemical compounds to polluted water in order to occur deposited of some pollutants by increasing of conglomeration for their molecules through the reduction of negative charges for colloids which easily for their conglomerations formation of pollutant molecules , for example in order to remove of clays from water through adding some chemical compounds that contain hydroxyl and sulfate groups or via their relation with some chemical compounds that work as precipitating agent [38] .

1.3.2. Membrane Osmosis method

In general , the membranes are divided into two types as isotropic and anisotropic in which , the isotropic type is uniform in their composition and physical nature while , the anisotropic type is non-uniform in its composition and physical nature. They consist of many layers which vary in their chemical structures . The water purification methods employ many types of the membranes such as microfiltration (MF) , ultrafiltration (UF) , nanofiltration (NF) and reverse osmosis (RO), these membarnes have been graded in their poros sizes. So, the RO and NF membranes are considered the best methods that have been used to remove

many contaminants from waters like dissolved organic materials and inorganic materials [39,40].

1.3.3. Ion –exchange method

Ion exchange resins can be described as one of polymer types which are capable of exchanging particular ions in the structure of polymer with other ions that are found in solution which has passed through them . This operation is also carried out in natural systems such as soil and living cells, furthermore, these systems are alowed for removing the pollution in order to obtain clean water [24,41] .

1.3.4. Adsorption method

In order to remove several pollutants from water such as toxic compounds , heavy metals , dyes , hydrocarbons and other organic compounds that do not have the ability to be destroyed by biodegradation , and can not be removed by using the traditional methods, the adsorption method was used for water treatment. The adsorption method is used in various industrial application, it is also important for environmental treatment. So, it gains more interest when it is compared with another methods because it is commercial availables , low-cost , easily prepared , high efficiency and variety sources of adsorbent materials [25] .

Adsorption operation can be defined as the tendency of materials molecules for liquids or gases to collect on the outer surface for solid materials. This tendecy may be as resulted from the mutual attraction between the molecules of solid materials with materials molecules of gases or liquids. This attraction due to exist for weak force that occurs between molecules because of the different charges between them, this force is called Van der Waals force , which occurs in decrease condition of temperature and energy .

The outer surface of solid materials that occurs above the adsorption process is know as adsorbent , while the liquid or gas molecules which are adsorbed on the

solid surface are know as adsorbate [42,43] .The associated terms for adsorption process are explained in Figure 1.6 .

The adsorption process can be classified into two types as the positive and negative adsorption , according to the attraction forces or the ejection for adsorbate molecules through the outer surface of solid materials .
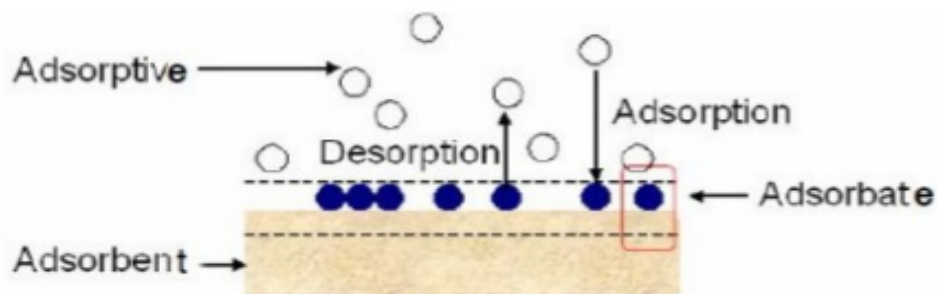
Figure 1.6 : The description for adsorption process

The concentration of adsorbate molecules are increased on the outer surface of solid materials when it occures. It can be attracted between adsorbate molecules with adsorbent, this type of adsorption is calld as positive adsorption , while the other type of adsorption that occures when the concentration of adsorbate molecules was decreased as gradualy on the outer surface of solid materials which leads to increase the concentration of adsorbate molecules in bulk solution when it is compared with outer surface for adsorbent. So, this type is known as a negative adsorption [25] . Moreover , there is another classification for adsorption that depends on nature of bond which occures between adsorbate molecules with outer surface for adsorbent and it is also divided into two types as follows :

1.3.4.1. Physical adsorption

The adsorption process, basically occures by the intraction between adsorbate molecules with outer surface for adsorbent material , this mutual intraction between them may occur through an electron transfer between adsorbate molecules and

adsorbent material , moreover , if no electrons transfer between the outer surface for adsorbent and adsorbate molecules ,in this case the adsorption process also occurs but this requires for low energies level that rang from 5-40 KJ/mol. So, the desorption operation more probably occurs and this process can be described as reversible one. This type of adsorption is known as the phyical adsorption or physisorption. In addition, multilayer adsorption may occur due to the mutual attraction between the outer surface of solid materials and the adsorbate molecules such as electrostatic forces, hydrogen bonds, van der Waals forces and dipole-dipole attraction[44- 46] .

1.3.4.2. Chemical adsorption

The chemical adsorption or chemisorption occurs as a resultant from the mutual interaction between adsorbate molecules and outer surface for solid materials that leads to transfer of electrons and strong bonds formation between them like ionic or covalent bonds . The chemisorption process requires for high energies level when it is compared with physisorption ,which ranges from 40-800 KJ/mol and, consequently, the desorption process hardly occurs, therefore, this operation is irreversible, furthermore, this type is occurred as monolayer adsorption and of highly specific properties [44, 45].

The probability to change the adsorption type from physical adsorption into chemical adsorption can be increased as function to temperature , when the temperature starts to raise which leads to the change of type adsorption which happens due to the increase of desorption process. In contrast, the contribution of electrons between adsorbent surface and adsorbate molecules will be increased and new bonds are formed as ionic or covalent bonds , which refers to a change from the adsorption type into chemisorption [24] .

1.4. The factors affecting adsorption operation

There are many factors that have some effects on the efficiency of adsorption process through the increasing or decreasing of their efficiency, the factors are shown as follows :

1.4.1. Effect of pH

pH is an important parameter that directly affects on the efficiency of adsorption operation in which any change in pH values for solutions will affect on the nature of functional groups for adsorbent surface , adsorbate molecules and solvents . In this case, the adsorbent materials which contain the polarized groups or charged on its outer surface will be affected when any change occurs in pH value of their solution, for example the adsorbent that includes the hydroxyl group in their outer surface will be affected in the basic medium and thus it undergoes for deprotonation process which is converted into phenoxide ions , that leads to increase complex with adsorbate molecules when it has positive charge . In general , the change of pH value in solution leads to an increase of competition on uptake H^+ and OH^- ions among active sites on adsorbent surface , adsorbate molecules and solvent molecules , that directly reflected on adsorption efficiency as positive or negative [47].

1.4.2. Effect of temperature

The temperature of solution plays an important role through its effect on the adsorption efficiency , where their effect depend on many factors like adsorption type , nature of both adsorbate materials and adsorbent surface . The adsorption operation is increasing with the decrease of temperature level that occurs especially in exothermic process , while the endothermic process leads to an increase of adsorption efficiency with increasing of temperatures level. This may occur in limited temperatures, furthermore, the thermodynamic parameters have been determined by using the temperature[25,47].

1.4.3. Effect of adsorbent and adsorbate nature

In general, the efficiency of adsorption process is affected by the nature of adsorbent surface , active sites (functional groups) on the outer surface of adsorbent materials and surface area of adsorbent , where the adsorption capacity is increased by the increase of surface area for adsorbent materials. Moreover, the surface area depends on several parameters such as particles size of adsorbent materials, nature and type of active sites and adsorbent dose. In addition, the adsorption process is also affected by the physical and chemical properties for adsorbate materials , where the adsorption capacity increases with the raise of molecular weight for adsorbate material and it is also impacted by the functional groups in adsorbate materials in case of it is found [24,25].

1.4.4. Effect of contact time

The contact time is an important parameter, it can be defined as the time that needs for outer surface of solid materials in order to reach a maximum limit for adsorption process , that depends on the surface area for adsorbent and their chemical structure. So, it significantly impacts on the adsorption operation and the determination of its adsorption kinetics [48].

1.4.5. Effect of initial concentration of adsorbate material

In order to Know the best concentration of adsorbate materials the fixed amount of adsorbent materials is used. So, the adsorption capacity increases with the increase of adsorbate concentration but in some times the adsorption process may be limited by monolayer from adsorbate dissolved in solution. Therefore, the increasing for concentration of adsorbate in solution may not increase adsorption process ,which is attributed to saturation of the outer surface of solid materials by the crystalline lattice for adsorbate materials [33].

1.4.6. Effect of ionic strength and solvents

Generally , the ionic strength generated by electrolytic salts in solution impacts on the adsorption efficiency which happens due to the competition among adsorbate materials with electrolytic salts ions in order to relate with the active sites on adsorbent surface. In this case the increase of salts ions affinity to linkage with active sites on adsorbent surface leads to decrease of adsorption efficiency for adsorbate materials.

In contrast, the solvent has the same effect of ionic strength on the adsorption efficiency through the competition relation to relate with the active sites on adsorbent surface that occurs between adsorbate materials and solvent molecules which also leads to decrease adsorption percent for adsorbate materials [24] .

1.5. Adsorption Isotherms

The equilibrium isotherms can be described as the linkage relationship between the amount of adsorbate materials which is adsorbed on the outer surface of adsorbent with the equilibrium concentration of adsorbate materials in aqueous phase . The curve of equilibrium isotherms helps to elucidate and understand some the associated phenomena in adsorption process, so, the isotherm shape does not only supply information on the affinity between the molecules but it also gives the probable mechanism , which may occur by the interaction between adsorbate and adsorbent materials . The isotherm curves have been classified for liquid - solid adsorption system given by Giles at el. In 1960 in which they provide some suggestions about using the shape of isotherm curve in order to characterize the adsorption mechanism. Consequently, the information regarding of the adsorption process was obtained as the physical nature of adsorbate and adsorbent materials and the specific surface area measurements for adsorbent surface were obtained too. This classification are explained in Figure 1.7 .
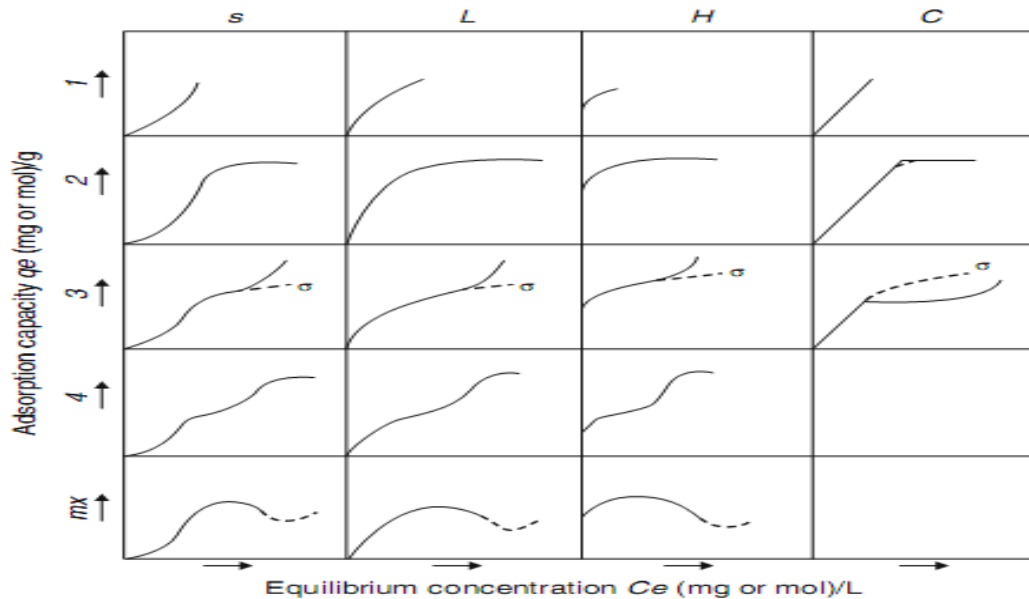
Figure 1.7: The shape of adsorption isotherm [44]

Where the S class represent the orientation of adsorbate molecules that are vertical or tilted on the adsorbent surface and also refers to high attraction for adsorbate molecules towards the adsorption layer , while the L class refers to the orientation of adsorbate molecules that are horizontal with adsorbent surface. This type refers the adsorption that ocuurs relatively by weak forces, like van der Waals forces.

The H class tends to high affinity adsorption towards the adsorbate molecules where , this type can occur in diluted solution of adsorbate molecules it also refers to chemical adsorption type which occurs by electrostatic forces.

The last type of isotherms is C class that refers to constant partition between adsorbate molecules and solvent on one hand and with the adsorbent surface on the other hand, this type suggests the adsorbate concentration which is proportional with the adsorption capacity up the maximum probable adsorption and then a sudden change to a horizontal front occurs [33] .

Several of hypotheses have been suggested to describe the adsorption mechanism and the shape of isotherm via various studies were carried out by scientists like Langmuir , Freundlich , Temkin , Dubinin–Radushkevich (D-R) , Fowler , Sips and BET [44] .

1.5.1. Adsorption isotherme models

1.5.1.1. Langmuir Isotherm

In 1916, Langmuir model was applied to describe the gas adsorption of the surface of solid materials and then was used in liquid-solid system, Langmuir isotherm depended on computing the surface coverage in the dynamic equilibrium state between the adsorbate molecules with the homogenous of adsorbent surface where , the surface coverage of adsorbent depended on the adsorbate concentration by occupying the active sites in the adsorbent surface, so, the balance between the adsorption and the desorption for the adsorbate molecules onto adsorbent surface leads to describe the adsorption nature therefore Langmuir isotherm tends towards monolayer adsorption [44,45, 49] . The relation of Langmuir model is given as follows :

$$\frac{C_e}{Q_e} = \frac{1}{Q_{max}\ K_L} + \frac{C_e}{Q_{max}}$$

Where : C_e is the concentration of adsorbate in fluid at the equilibrium state (mg/l) , Q_e is represent the adsorption capacity at the equilibrium state (mg/g) , Q_{max} is considered as the maximum of adsorption capacity that occurs when all active sites onto adsorbent surface are occupied by the adsorbate molecules that formed monolayer adsorption and K_L (L/mg) is Langmuir constant which is related with the adsorption energy [49,50]. The fundamental characteristics of Langmuir isotherm can be summarized by a constant value that was defined as the separation factor R_L which can be explained as follows :

$$R_L = \frac{1}{1+K_L \, C_o}$$

Where : C_o represents the initial concentration of adsorbate solution (mg/l) . The adsorption process can be characterized by the separation factor value where , the adsorption is unfavorable when the separation factor is more than $1(R_L>1)$, adsorption is linear when $R_L=1$, the adsorption process is favorable when $0< R_L<1$ while , if the separation factor is equal to zero this shows that the adsorption process is irreversible [49-52].

1.5.1.2. Freundlich Isotherm

Freundlich model was used in 1906 in order to describe the relation between the adsorbate molecules and the adsorbent surface heterogeneous in which, this isotherm assumed an increase of adsorption capacity with the increases of the adsorbate concentration that tend to give a multilayer adsorption , the Freundlich relation is given by [49,52, 53,54]:

$$Log\,Q_e = Log\,K_f + \frac{1}{n}\,Log\,C_e$$

Where : K_f is Freundlich constant that is releated with the adsorption capacity (L/g) while the term $1/n$ is called the heterogeneity factor and refers to the adsorption intensity , n value points to the adsorption nature where the adsorption process is unfavorable when the n value is located between 0 and 1 ($0 <n <1$) , the isotherm is irreversible when n value is equal to zero (n=0) whilst ,if the n value is more than 1 (n>1) that refers to the isotherm is favorable [44, 53,55] .

1.5.1.3. Temkin Isotherm

Temkin isotherm is utilized to calculate the indirect effect of the interaction happens between the adsorbate and the adsorbent in the adsorption operation. This

isotherm assumed the adsorption heat of all molecules in a layer decline linearly with the coverage that was attributed to the interaction made between adsorbate and adsorbent, the adsorption is identified by organizing distribution of the binding energies . The relation of Temkin isotherm model is shown as follows [44,49 ,52,53] :

$$Q_e = \frac{RT}{b_T} \ln A_T + \frac{RT}{b_T} \ln C_e$$

Where : R is the gas constant (8.314 J/ mol.K) , T is the absolute temperature , A_T is the Temkin isotherm constant that denotes to the equilibrium binding (L/g) and b_T is Temkin constant that is related with the adsorption heat (J/mol) .

1.5.1.4. Dubinin-Radushkevich Isotherm

Dubinin-Radushkevich (D-R) isotherm is an experimental adsorption model that was carried out to express the adsorption mechanism with Gaussian energy distribution onto heterogeneous adsorbent surface. The D-R isotherm is more interesting to describe the adsorption nature as a chemical or a physical property of a single solute system , the D-R relation can be given as follows [44, 49, 56, 57]:

$$\ln Q_e = \ln Q_{max} - \beta \varepsilon^2$$

Where : β is D-R constant that is related to the mean free energy of adsorption per mol of adsorbate (mol^2/J^2) , ε is Polanyi potential which can be computed by relation as it is given in the following [44 , 53,56]:

$$\varepsilon = RT \ln(1+(1/C_e))$$

The β value is related to the adsorption energy E (KJ/mol) which can be calculated by the relationship as follows :

$$E = 1/(2\beta)^{1/2}$$

Where the E value used in order to suggest the adsorption nature such as the physical adsorption when the E value is located between the range 1 to 8 KJ/mol , if E value is located between 8 to 16 KJ/mol in this case the process related to the ion-exchange while , the chemisorption occurs when the E value is between 20 to 40 KJ/mol [53,57,58].

1.6. The adsorbent surfaces

Adsorbent materials have been used in the treatment operations for the polluted water because it is available , low-cost and of high efficiency to remove the pollutants, moreover, the adsorbent materials are utilized for the remediation of water such as active carbon , metals oxides particularly the magnetic oxides for mineral , red mud , green sand and nano particles[24,59].

1.6.1. Carbon-based materials as adsorbent

In general , the materials based on carbon have been used for the removal of several pollutants from water, which result from the important properties like high capacity of adsorption , the large of surface area , extensive porosity and also, they have high affinity to linkage towards many pollutants[46]. The well-known classes of carbon-based materials as adsorbent surfaces are activated carbon , graphite , graphite oxide , carbon nanotubes , fullerene , grapheme and grapheme oxide [60-66] .

1.6.1.1. Activated carbon

Basically active carbon are carbonaceous materials that were efficiently utilized in many pollution control systems due to its high adsorption capacity that consist of two types as granular activated carbon and powdered activated carbon .The particles shape of granular activated carbon are irregular shape and have size ranging from 0.5 to 2.5 mm , while the size of particles for powdered activated carbon predominantly is less than 0.15 mm. Additionally, the activated carbons in

both types are prepared from heterogeneous materials that contain a high carbon content in their structure and also ,low inorganic components such as bituminous coal, charcoal, lignite, coconut shells, palm and wood. The activated carbon consist of multilayer's of graphite and have extensive porosity and very large obtainable surface areas ranging from $300 – 2500 \ m^2/g$.

Moreover , the surface of activated carbon also contains a variety of heteroatom's like oxygen, hydroxyl group, carboxyl group, nitrogen, phosphorus and sulfur, that are inserted to carbon surface by using different chemicals processes. The oxidation process leads to increase the content of hydroxyl and carbonyl groups on outer surface of activated carbon while, the oxidation which execute in liquid phase leads to increase, especially the content of carboxyl groups. Furthermore, these groups are responsbile for increasing the affinity between the surface of the activated carbons for the pollutants and the chemical bonding formation between them. This leads to increase the efficiency of adsorption process [46,60] . The cross-section of activated carbon surface is shown in Figure 1.8 .
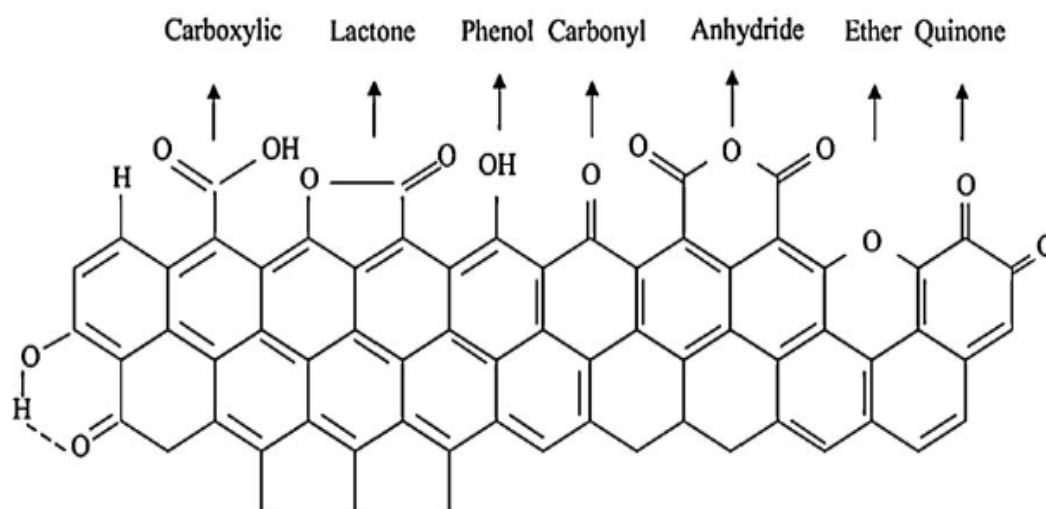
Figure 1.8 : Functional groups for activated carbon surface [60]

1.6.1.2. Graphite

Graphite is one carbon-based material in their structure (Figure 1.9) which consists of only fused hexagons of sp2 carbons, that form basically a planar layer and have homogeneous structure that can be obtained by using a high heat for carbon black materials in the range of 2700-3000°C and in an inert atmosphere . Moreover it is considered non-specific material and have the small surface area in the range of 100-210 m^2/g. So, it is used as anion-exchanger that it is attributed to the existence of positively charged groups on their surface therefore , it is widely utilized as adsorbent surface to the removal of polar organic pollutants from water but their use to remove a heavy metals is still very rare [61] .
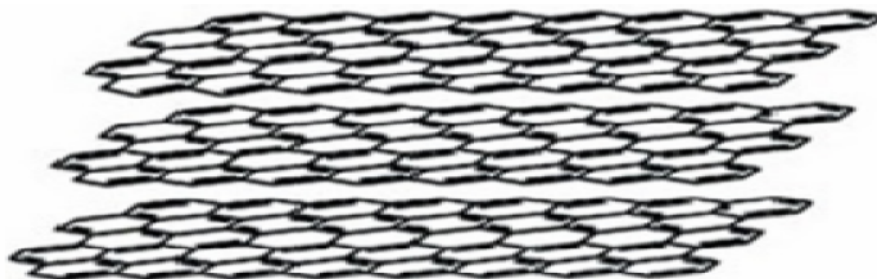
Figure 1.9 : Graphite Structure[61]

1.6.1.3. Graphene and graphene oxide

Graphene and graphene oxide are important compounds that derivatives from graphite where, the graphene is considered as a single layer of graphite which consists of two-dimensional carbon allotrope. Furthermore, it has important properties such as physical and chemical properties that due to unique their structure . Graphene oxide comprises of many important functional groups that are introduced by the oxidation operation for graphite. So, graphene oxide is considered as an important adsorbent surface and thus, it has attracted by many researchers to use as an adsorbent to remove pollutants from their solutions . This is it posseses more attractive properties such as, a low-cost when compared with graphene , decreased particles size in the range nanoscale , large surface area and

high adsorption efficiency [65,66] .The graphene oxide structure is depicted in Figure 1.10.
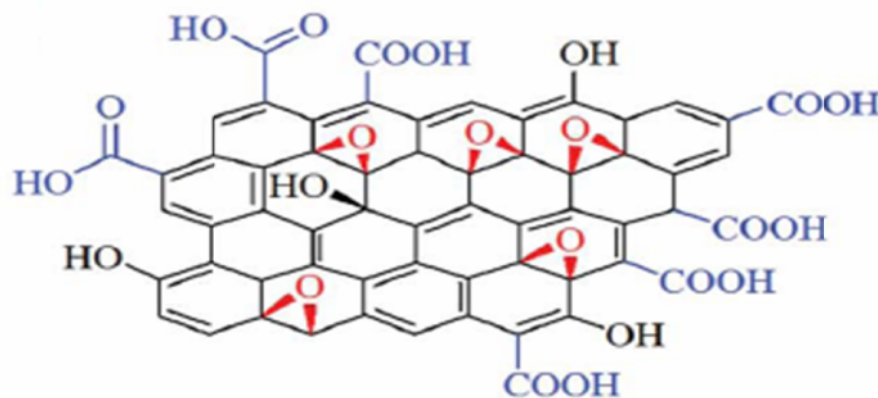
Figure 1.10 : Graphene oxide structure [65]

1.6.2. Metal oxides nanoparticles as adsorbent

The metal oxides are particularly regarded as the magnetic oxides that are used as adsorbent surface in order to remove different pollutants, especially the heavy metals that are attributed to exist in empty orbital's on adsorbent surface which was prepared to accept electrons and, thus the chemical bond is formed between them. Metal oxides nanoparticles are prepared from various metals such as Iron , titanium ,copper , manganese, magnesium , silica , zinc and aluminum that possess a variety of characteristic properties such as electronic, physical and chemical properties which are different in their bulk particles. Characteristic properties of metal oxides are found due to the band gap which decreases with the decrease in average size of oxides particles and consequently, the electrons that exist in oxides surface will have more freedom of movement and are transferred in order to form LSPR spectrum (the Localized Surface Plasma Resonance). Moreover , these properties for metal oxides of nanoparticles will gain new and unique properties whenever there are decreases of their particles size like conductivity, chemical reactivity, optical and electronic properties, the large surface area and high adsorption

capacity. The elemental oxides nanoparticles were used in adsorption processes to give high efficiency for removing some pollutants from their solution as excellent adsorbent surface [62,65] .

1.7. Desorption method

Both of the adsorption and the desorption processes are associated together with the removal of pollutants from their aqueous solution and then, its recover once again for each of the adsorbent and the adsorbate. So, the desorption process is an important for the recovery of the adsorbent surface that can be reused several times to remove the adsorbate molecules from their aqueous solution [56,67, 68] . The desorption process can help to understand the adsorption mechanism of adsorbate molecules after its adsorbed onto the adsorbent surface . The primary process occurs by removing the reversible molecules of adsorbate onto the adsorbent solid materials [56]. The efficiency of desorption process was computed by the following relation [69] :

$$\% \text{ De} = [(A_o - A_r) / A_o] \times 100$$

Where A_o is total of the adsorbed amount to the adsorbate molecules and A_r is represented the residual of adsorbed amount onto adsorbent surface after carried out the desorption process .

1.8. Literature survey

New adsorbent surface of magnetic nanocomposite γ Fe_2O_3 with activated carbon was prepared by Fayaz et.al. [70], that was utilized to remove the dye of alizarin S red from their aqueous solution. The high adsorption capacity was obtianed in about 108.69 mg/g. Moreover, the equilibrium isotherm like Langmuir and Freundlich also has been studied and the data appeared their consistent with the Langmuir model more than Freundlich model. The other study has been carried out in order to remove alizarin S red from its aqueous phase by using three adsorbent surfaces as an activated carbon powder , treated activated carbon and

activated carbon powder / γ Fe$_2$O$_3$ by Kamarehie et.al.[71]. The results of adsorption capacity for the adsorbent surfaces showed various values when compared with treated activated carbon and activated carbon powder / γ Fe$_2$O$_3$ as 24.5 , 57.8 and 112.56 mg/g respectively. Furthermore, the adsorption isotherms and kinetic were evaluated and the data obtained shows that Langmuir model is more fit than Freundlich model. Also, the kinetic study exhibited the pseudo first-order as a fit model.

The pea peels modified with citric acid as adsorbent were utilized in order to remove the basic brown and crystal violet dyes from the aqueous phase by Khan et.al. [72]. The optimum conditions of adsorption process have been studied and the adsorption capacity was calculated through Langmuir model and showed 5.37 and 17.61 mg/g from basic brown and crystal violet, respectively. The sips isotherm model is fit to describe adsorption process for removal the basic brown dye when it is compared with other isotherm models that were studied such as Freundlich , Langmuir , Redlich-Peterson and Radke-Prausnitz. The study of Maderova and others [73] used magnetically the modified activated sludge as adsorbent surface to remove four types of organic dyes like basic brown Y , aniline blue , nile blue and safranin O. The adsorption capacity was calculated and showed 246.9 ,768.2 , 515.1 and 326.8 mg/g, respectively.

The biowaste was also used as low-cost adsorbent surfaces in order to remove congo red dye from their aqueous solutions by Kaur et al. [54], using ground nut shells charcoal and eichhornia charcoal under different opimum conditions such as the effect of contact time , pH , ionic strength , tempareture changed , dye concentration and adsorbent dose . Several isotherm models have been studied such as Freundlich , Langmuir , Dubinin-Radushkevih , Temkin and Generalized, The results of the adsorption process appeared a high adsorption capacity to remove congo red when it used ground nut shells charcoal as adsorbent than using

eichhornia charcoal   about 117.6 and 56.8 mg/g respectively. The congo red dye was removed from it's aqueous solutions under certain opimum conditions by using the activated carbon which is prepared from coffee waste. This study was carried out by Lafi et.al.[74], in which the equilibrium results show Langmuir model more proper than when it is compared with Freundlich, Dubinin-Radushkevih and Temkin models, in order to remove the dye of congo red through the adsorption capacity that reaches 90.90 mg/g.

Abdolrahimi and Tadjarodi [75] study was carried out to remove rhodamine B dye from their aqueous phase by using activated carbon which was prepared from almond shell after applying the chemical treatment by H_2SO_4. The study referred to an increase in the removal ratio of rhodamine dye with an increase in pH value where the removal ratio reaches 70 % in pH 11 , furthermore , the Langmuir isotherm is best model to describe the adsorption operation as it indicated that the adsorption capacity was 255.39 mg/g. The low-cost adsorbent has been used to remove the rhodamine and methylene blue from their aqueous phases by using waste of seeds of aleurites moluccana that were prepared by Postai et.al.[76]. The removal ratio also depended on changing of pH values which noted increases of pH value in range, 3-9 that was associated with the increase of removal ratio by three fold . The adsorption isotherm was analyzed by using Sips , Langmuir , Freundlich and Redlich-Peterson isotherms and also, the results indicated that the best isotherm is Sips as it was more consistent with the removal rhodamine dye and methylene blue by adsorption capacity 117 and 178 mg/g, respectively.

The activated carbon has been prepared from fertilizer waste as adsorbent surface by Mohan et.al. [77], in order to remove mercury (II) from the polluted water under the optimal condition of adsorption process. Moreover, the adsorption efficiency increases with the decrease of pH level in solution and also , the thermodynamic parameters and isotherms have been studied under pH 2. The data

obtained showed that the adsorption process was spontaneous and exothermic, while the study of isotherms revealed that the Langmuir isotherm was more suitable to describe the adsorption operation than Freundlich isotherm. The study of Silva et.al. [78] marks removal of mercury (II) from liquid solutions onto the modified activated carbon surface in order to improve the specific properties of surface and their pore volume using H_2SO_4 and CS_2. The activated carbon exhibited high efficiency to uptake mercury (II) from it's solutions after their treatment by H_2SO_4 when it was compared with the activated carbon and activated carbon- CS_2 that due to increase of sulfonates groups onto surface, additionally, the Freundlich isotherm is fitted to describe the adsorption process.
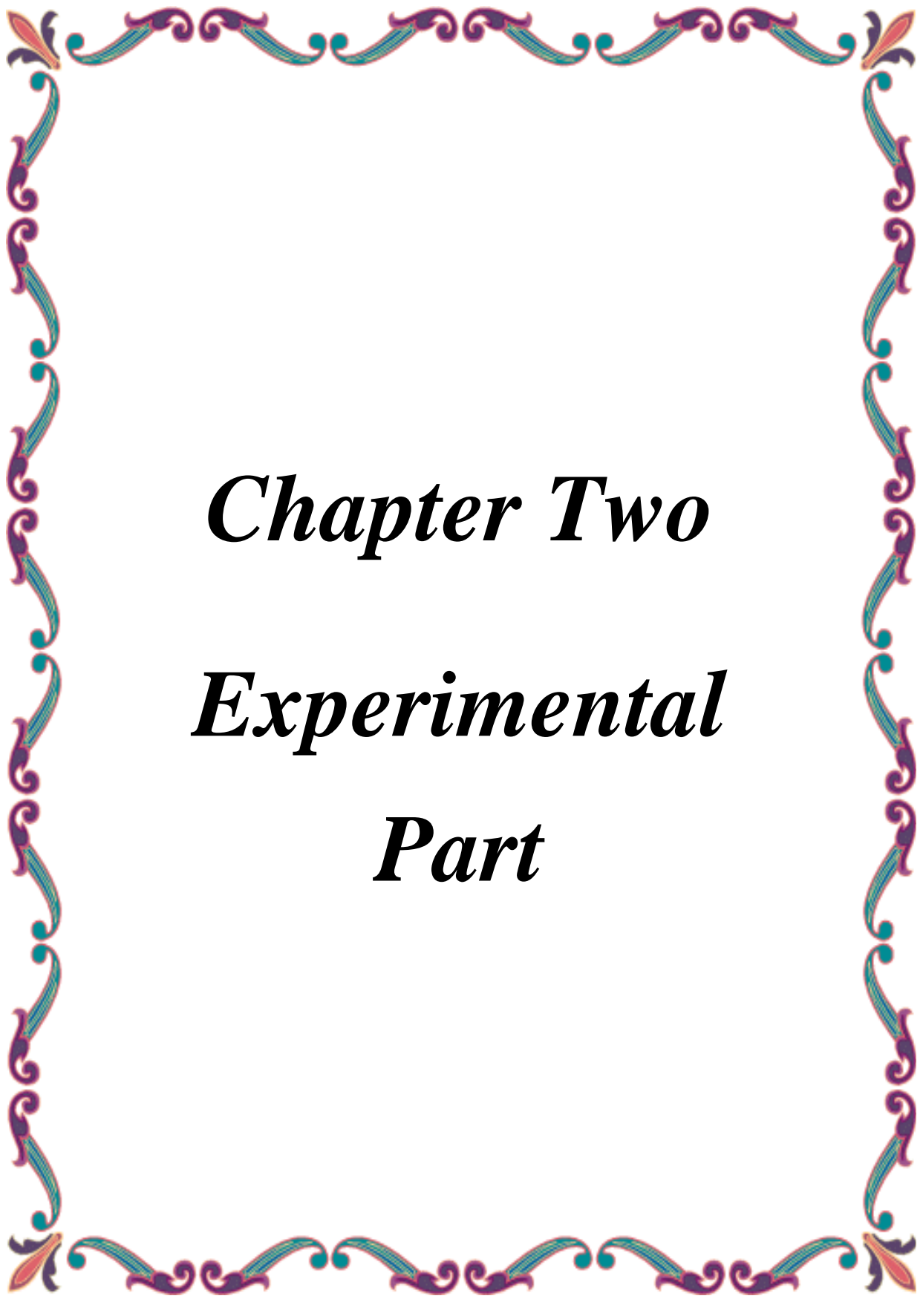
Lead has high toxic properties that introduce to the environment by using natural and anthropogenic sources, particularly the oil extraction industries. So, the study of Ketsela et.al. [79] focused on removing lead (II) from their aqueous solution by using an activated carbon derived from white lupine under different conditions included contact time , pH , lead concentration ,tempareture and adsorbent amount. In order to obtain the best condition and high efficiency adsorption, the results appeared the adsorption capacity to reach 5.7 mg/g at 328K. The Freundlich models is more proper to describe the adsorption process than Langmuir models. To enhance of efficiency of adsorption process to remove lead (II) from their aqueous phase , Salihi et.al.[80] prepared the activated carbon from sugarcane bagasse. The results obtained exhibted the maximum of removal lead (II) percent was found at pH 5, adsorbent amount 10g/l and adsorption capacity 23.4mg/g. Langmuir isother is considered as the best isotherm to describe the adsorption process when it is compared with Freundlich isotherm.

1.9. Aims of study

Nowadays , there are many challenges that face humanity which happened as a consequence for increasing development promoted of many industrial activities.

The current study focuses on the treatment operation of the polluted water using the prepared nanoparticles compounds that are used as adsorbent surface. The objectives of this study can be summarized as follows :

1- Synthesis and spectroscopic characterization of selenazone ligand (z) derived from dithizone and some complexes .

2- Identification the structures formula of the prepared complexes by using their thermal study and calculate the kinetic and thermodynamic parameters using Coats-Redfern , Broido and Horowitz and Metzger equations.

3- Separated of nanoparticles as new and low cost of adsorbent surfaces derived from waste soot .

4- Preparation of new adsorbents surfaces derived activated carbon , Silica gel and graphene oxide .

5- Investigating the adsorption efficiency of the adsorbent surfaces to remove some dyes (Mordant Red 3, Congo Red , Basic Brown and Rhodamine B) and some toxic elements (Hg and Pb) found onto prepared adsorbent surfaces and assessment of the factors affecting adsorption efficiency .

6- Investigating the adsorption isotherms of Langmuir , Freundlich , Temkin and Dubinin-Radushkevih isotherms models, and calculated of the thermodynamic parameters as ΔG , ΔH , ΔS and E .

7- Study the desorption process from the prepared adsorbent after completion of the adsorption.

8- Studing the applications of the above surfaces on real water samples .

Chapter Two

Experimental Part

2. Experimental Part

2.1. Chemicals

2.1.1.Chemical Materials

Many chemical compounds in different phases as solid and liquid were utilized in order to achieve this work, all information about these compounds like molecular formula and the companies supplies it, are explained in Table 2.1.

Table 2.1 : The chemical materials

Chemical Materials	Molecular formula	%Purity	Company producing
Absolute ethanol	CH_3CH_2OH	99.9	J.T. Baker
Activated carbon	-	-	Carlo-Erba
Cadmium nitrate tetrahydrate	$Cd(NO_3)_2 .4H_2O$	98	B.D.H
Carbon tetrachloride	CCl_4	99	Alpha Chemika-India
Cobalt nitrate hexahydrate	$Co(NO_3)_2 . 6H_2O$	98	B.D.H
Diethyl ether	$CH_3CH_2OCH_2CH_3$	99.5	Scharlau
Dimethylformamide	C_3H_7NO	99.8	GCC
Dimethylsulfoxide	C_2H_6SO	99.9	Himedia
Dithizone	$C_{13}H_{12}N_4S$	98	Analar
Graphite powder	-	-	Hopkin&Williams
Hydrochloric acid	HCl	37	GCC
Hydrogen Peroxide	H_2O_2	50	Scharlau
Lead nitrate	$Pb(NO_3)_2$	99	B.D.H
Lead standard solution (1000 mg/l)	Pb	-	Thomas Baker India
Mercury standard solution (1000 mg/l)	Hg	-	Merck
Methanol	CH_3OH	99.9	Himedia
Methyl iodide	CH_3I	99	Merck
N,N'-Dicyclohexylcarbodiimide	$C_{13}H_{22}N_2$	99	Aldrich
n-Hexane	C_6H_{14}	95	J.T. Baker

Nickel chloride hexahydrate	$NiCl_2 . 6H_2O$	98	B.D.H
Nitric acid	HNO_3	70	GCC
Potassium Permanganate	$KMnO_4$	99.7	GCC
Selenium powder	Se	99.95	Merck
Sodium borohydride	$NaBH_4$	97	Riedel-de haen ag seelze-hannover
Sodium Carbonate	Na_2CO_3	99.9	Analar
Sodium hydroxide	NaOH	99	Merck
Sodium Nitrate	$NaNO_3$	99	Sigma Aldrich
Sulfuric Acid	H_2SO_4	95	J.T. Baker
Toluene	$C_6H_5CH_3$	99.8	Scharlau

2.1.2. Dyes

Four different type of dyes were used as adsorbate. In order to remove these dyes from their aqueous solutions by using batch adsorption experiments. Nowadays , many dyes are used more by human and are introduced through a variety of industries such as pharmaceutical , foods , biological dying , cosmetics and textile [81]. The physico-chemical properties of the used dyes are explained in Table 2.2.

Table 2.2 : The physico-chemical properties of dyes used as adsorbate

Characteristic	Mordant Red 3	Congo Red	Basic Brown	Rhodamine B
Chemical formula	$C_{14}H_7NaO_7S$	$C_{32}H_{22}N_6Na_2O_6S_2$	$C_{18}H_{18}N_8 .2HCl$	$C_{28}H_{31}ClN_2O_3$
Company producing	Himedia	Riedel-de haen ag seelze-hannover	Chroma-Gesellsch schmid&Co.	B.D.H
Molecular weight g/mol	342.253	696.665	419.31	479.02
Type	anionic	anionic	cationic	cationic
$\lambda_{max (nm)}$	260 ,441.5	495	455.5 , 210	553.5
Solubility in	Soluble	Soluble at pH 4-9	Soluble at pH 3-8	Soluble

water		Partial soluble at pH 3	Partial soluble at pH 9	
Color change at pH	3-4 pall yellow 6.5 Dark yellow 7-9 reddish pink	3-5 Dark violet 6-9 Orange	3-4 Redish orange 5-9 Redish yellow	Pink

2.2. Instrumentions

Several instruments were utilized in order to achievement this work , the instruments used are shown as follows :

1- The balance-instrument was used , type : Citizen Cy 204 , department of chemistry , college of science , University of Basrah .

2- Hot plate magnetic stirrer , type : Velp , Italy , department of marine chemistry , Marine science center , University of Basrah .

3- Melting point instrument , type : Thermo Fisher electrically heated , department of chemistry , college of science , University of Basrah .,

4- Oven , type : Baird&Tatiock ,England ,department of chemistry , college of science , University of Basrah .

5- Uv-vis measurments have been carried out at range 200-800 nm by using Uv-vis spectrophotometer , doubal beam , Shimadzu 1800 , department of marine chemistry , Marine science center , University of Basrah .

6- FT-IR spectra was measured by FT-IR 8400S , Shimadzu , Japan , department of chemistry , education college of pure science , University of Basrah .

7- The instrument of X-ray diffraction (XRD) was used , type : Philips, PW1730 , Beamgostar laboratory , Iran .

8- The scanning electron microscopy images (SEM) and Energy-dispersive X-ray (EDX) using Zeiss microscopy at 10.00 Kv, Beamgostar laboratory , Iran .

9- Mass spectrum was measured by EI technique , Agilent technology (HP) , model :5973 Network mass selective detector , Iran .

10- ^{1}H-NMR and ^{13}C-NMR spectra were preformed on a Bruker DRX (500 MH$_z$ and 100 MH$_z$ respectively) , Beamgostar laboratory , Iran .

11- Incubator shaker was used by LH Fermentation model MK 10 Refridse , United Kingdom and Sartorius , Certomat IS , Germany, Marine science center , University of Basrah .

12- Atomic absorption spectrophotometer , type : AA7000 Shimadzu , Japan , department of marine chemistry , Marine science center, University of Basrah.

13- Centerifuge , type: Baird&Tatlock ,Mark IV , Germany ,department of marine chemistry , Marine science center , University of Basrah .

14- pH meter ,Crison-Basic 20, department of chemistry , college of science , University of Basrah.

15- Conductivity meter , Cond 3110 set1, WTW , Germany, department of marine chemistry , Marine science center , University of Basrah .

16- TGA/DSC ,SDT Q600 v20.9 build20 , Beamgostar laboratory , Iran .

17- Blender grinder was utilized on FriTsch , Germany , department of marine chemistry , Marine science center , University of Basrah .

18- Surface area was measured at 450ºC under N_2 gas as an adsorptive analysis on BEL , model BEL SORP MINI II , Japan . Beamgostar laboratory , Iran .

2.3. Synthesis of Selenazone ligand and their complexes

2.3.1. Synthesis of selenazone ligand (Z)

1,5-diphenylthiocarbazone (4.10g , 16mmol) has been dissolved in 50 ml absolute ethanol followed by adding (2.84 g, 20 mmol) of methyl iodide. The reaction mixture was stirred for 15 min at room temperature and was left under reflux for 1h (Solution A) [20].

For preparing solution B, sodium carbonate (1.06g , 10 mmole) was dissolved in 20ml of warm deionized water and then transferred to a round bottom flask of three necks (100 ml) containing (1.97 g, 25 mmol) of selenium powder and (1.13g, 30 mmol) of sodium borohydride, the mixture was then stirred at 100 ℃ for a short time under inert atmosphere of argon gas, in which the colour of the solution was changed from black to colorless. Consequently, the ethanolic solution (solution A) was added to the solution B. The mixture was then left at a room temperature with a continuous stirrer under the inert gas as argon for 3hours. The resulting blackish brown precipitated solid was filtered and washed for several times by using absolute ethanol and deionized water , then it was recrystallized by utilizing methanol:water (1:5). The precipitate was dried and showed some physical properties such as blackish brown color, m.p :119-120 ℃ and a yield 65%. These results obtained are consistent approximately with the previous study [17]. The synthesis of selenazone (Z) was carried out in accordance with the reaction in the scheme2.1.
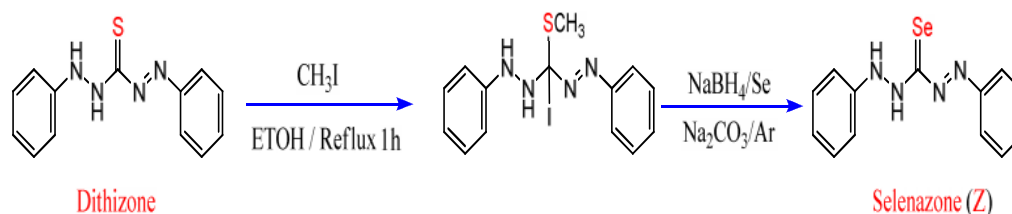
Scheme 2.1 : Preparation of selenazone ligand (Z)

2.3.2. Synthesis of Pb(Z)₄ complex

Selenazone ligand (0.606g, 2 mmol) was dissolved in 50 ml of warm methanol and then (0.311g, 1mmol) of lead nitrate that dissolved in 50ml of methanol was added to it. The mixture was stirred and left under reflux for 3hours. Upon the forming of the blackish gray precipitate, the precipitate was filtered and washed with warm methanol several times. The obtained precipitate was then dried in oven at 70ºC. It displayed some physical properties : blackish gray color, m.p : >300 and a yield 35%.

2.3.3. Synthesis of Cd(Z)₄ complex

(0.606g, 2 mmol) of selenazone ligand (Z) was dissolved in 50 ml of warm methanol and then added to (0.308g,1mmol) of Cd(NO₃)₂. 4H₂O in 50ml of methanol.The solution was mixed with continuous stirring and left under reflux for 6 hours. A dark brown precipitate was formed. The formed precipitate was filtered and washed with warm methanol several times and was dried at 70ºC in oven. The precipitate showed dark brown color, m.p : >300 and a yield 30%.

2.3.4. Synthesis of Ni(Z)₄ complex

The nickel complex was prepared in a similar procedure of the lead complex by mixing 50 ml methanolic warm solution (0.237g,1mmol) of NiCl₂.6H₂O with 50ml methanolic solution of the prepared ligand (Z) (0.606g,2mmol).The mixture was left under the reflux for 3 hours with continuous stirring and was left over night at room temperature. The mixture solution was filtered, dried and washed by diethyl ether several times. The precipitate has brown color, m.p : >300 and a yield 75%.

2.3.5. Synthesis of Co(Z)₄ complex

50 ml of methanolic solution of ligand (Z) containing (0.606g,2mmol) has been mixed with 30 ml of methanolic solution of Co(NO₃)₂.6H₂O (0.291g,1mmol). The

resulted mixture was changed its color immediately to reddish black under the refluxing for 4hours with continuous stirring. The mixture was filtered and washed by hot methanol several times. The precipitate was collected and revealed some physical properties like brown color, m.p : >300 and a yield 30%.

2.4. Metals determination

The metals content have been determined by using the instrument of flame atomic absorption spectrophotometer (FAAS). 0.01 g of prepared complexes were taken and dissolved in 5 ml concentrated nitric acid , then the solution put was on hot plate at 80 ºC with a continuous stirrer , until the solution became clear and thus the solution diluted to a volume 25 ml . Then ,1ml from the diluted solution was taken and diluted to a volume 50 ml by deionized water [82]. The same procedure was performed to estimate the selenium content in selenazone ligand (Z) by using hydride generation system . All physico-chemical properties of selenazone ligand (Z) and their complexes are shown in Table 2.3 .

Table 2.3 : The physico-chemical properties of prepared compounds

Symbol Comp.	Molecular formula & molecular weight	Physical state	Color	Melting point ºC	Reaction time (h)	Yield %	Λ Ohm^{-1} cm^{2}mol^{-1}
Z	$C_{13}H_{12}N_4Se$ 303.22	powder	Blackish brown	119-120	3	65	-
ZPb	$C_{52}H_{52}N_{16}O_3PbSe_4$ 1472.11	powder	blackish gray	>300	3	35	7.27
ZCd	$C_{52}H_{52}CdN_{16}O_3Se_4$ 1377.33	powder	Dark brown	>300	6	30	3.3
ZCo	$C_{52}H_{53}CoN_{16}O_{3.5}Se_4$ 1332.86	powder	Brown	>300	4	30	4.48
ZNi	$C_{52}H_{61}Cl_2N_{16}NiO_{6.5}Se_4$ 1459.58	powder	Brown	>300	3	75	80.71

2.5. Graphite oxide (sGO) separation

The graphite oxide nanoparticle was separated from soot waste in chimney after their collection from Alnajebia electric generation station that uses crude oil as fuel , where , graphite and graphite oxide produced from incomplete combustion for fuel in which due to the amount of oxygen is inadequate for the combustion operation. The combustion process that leads to increase of the temperature may be upto 1500 ℃ , where part of the hydrocarbon compounds including graphite is converted into carbon vapor under high temperatures and it returns to condensation and carbon compounds are formed , when the decreased temperature is under 250 ℃. The scheme 2.2 appeared the combustion steps and gases of the generated movement in boilers in Alnajebia electric generation station .
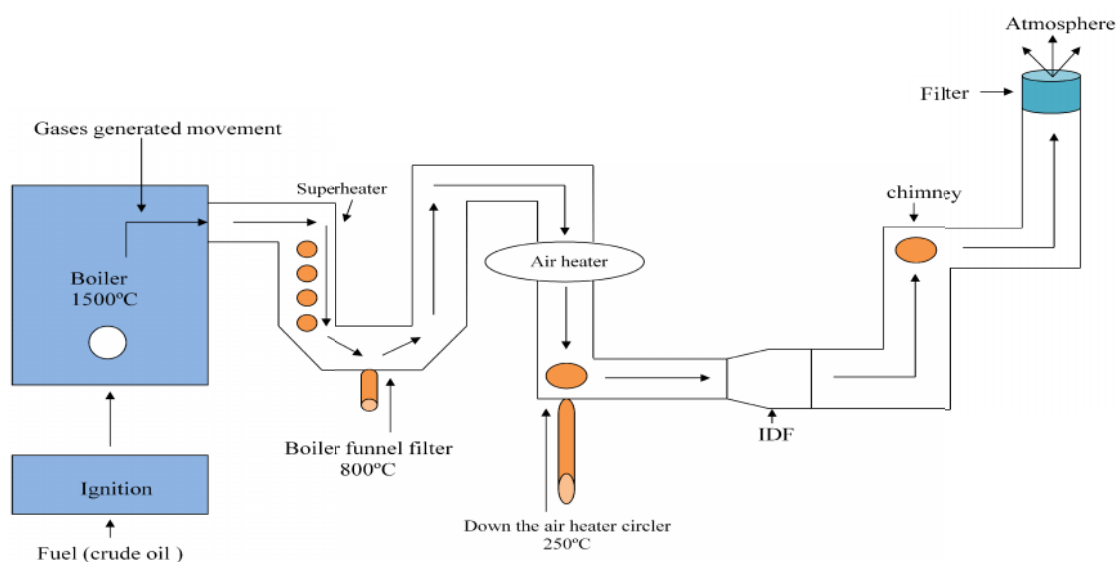
Scheme 2.2 : The combustion steps and gases generated movement

Soot waste sample was collected from Alnajebia electric generation station in Basra governorate, Iraq, then it was kept in polyethylene containers and transferred to the laboratory in order to execute the extraction operation of graphite oxide nanoparticles . 100 g of soot waste was take from funnel filter site and then it was put in round flask (1L) , then 500 ml of toluene was added over it and left at a

temperature ranging from 50-70ºC with stirring for 10h. The mixture was filtered and the precipitate was washed with methanol, n-hexane and diethylether several times. The resulting was also washed in deionzed water several times and then, it was dried at 80ºC for 10h [83]. 19.85 g of the dark blackish brown (Figure 2.1) precipitate was obtained .

2.6. Separation of Iron oxide (sFe) nanoparticles

Soot waste has been collected from the boiler site according to scheme 2.2. Iron oxide nanoparticles was separated by applying the same procedure of graphite oxide nanoparticles separation. The precipitate remained insoluble in toluene solvent that was taken and washed by deionized water several times , 61g of brown color solid (Figure 2.1) was obtained after their drying at 80ºC for 10 h [83].
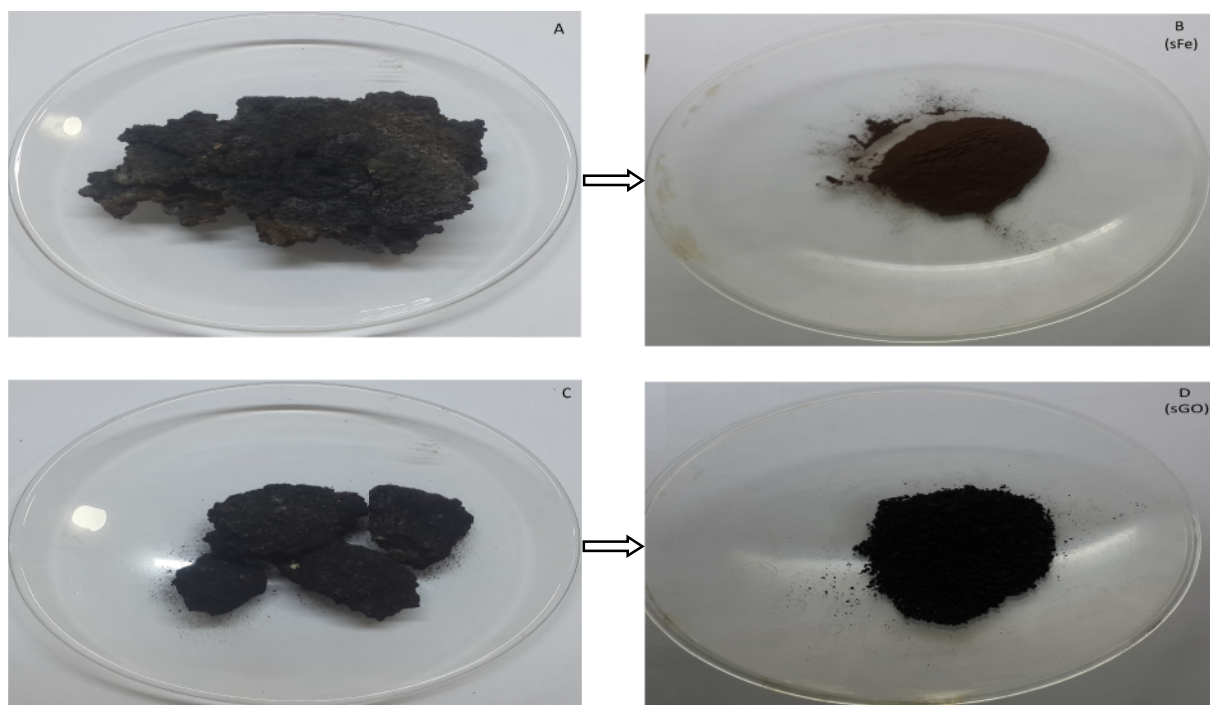
Figure 2.1 : Separation of Iron oxide (B) and graphite oxide (D)
nanoparticles from soot waste (A ,C)

2.7. Preparation of graphene oxide nanoparticles from graphite

The well-known graphene oxide nanoparticles can be prepared by various methods like Brodie, Staudenmaier and Hummers , in this work the modified Hummers method was utilized, it can be simply and briefly described : 1g of graphite powder was weighted and transferred into a beaker (600 ml) , 0.5 g of sodium nitrate was added with 23 ml of concentrated sulfuric acid into graphite powder under a continuous stirrer at room temperature for one hour . Then , 3g of potassium permanganate has been added into the mixture after their put in an ice bath to avoid overheating under the stirring continuously with the maintenance of temperature level, less than 20ºC for 20 hours. The mixture is diluted to 200 ml by deionized water with a keeping stirrer for 30 min where, the change of color solution is observed from black to reddish brown, 300 ml of deionized water was added once again with 10 ml 50% H_2O_2 under stirring , where it was clearly observed that the color of solution was changing from reddish brown to yellowish brown (Figure 2.2) . The precipitate was separated and collected by using centrifuge at 2500 rpm for 10 min and then rinsed with 5% HCl by following deionized water several times , in order to obtain graphene oxide , the product needs to be dried at 70ºC for 24h [84-86] .
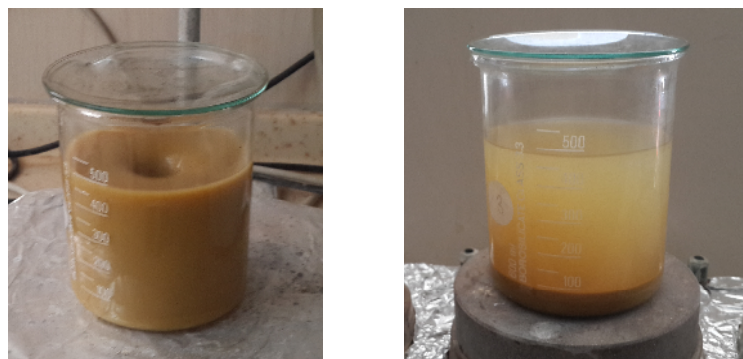
Figure 2.2 : The preperation of graphene oxide

2.8. Preparation of adsorbent surfaces

In order to increase the adsorption efficiency with increases of surface area the modification process was used via new functional groups which have been inserted

into adsorbent surfaces . The current study focuses on the modified version of some materials as nanoparticles and microparticles with selenazone ligand (Z) for using them as adsorbent surfaces such as graphene oxide , silica gel and activated carbon as well as. Separated nanoparticles from the soot waste as graphite oxide and iron oxide were used as good adsorbent surfaces.

2.8.1. Modification of graphene oxide with selenazone ligand (Z)

Graphene oxide nanoparticles were used as a good adsorbent surface to remove many pollutants from their aqueous phase. Therefore, to increase the surface area of graphene oxide by adding new functional groups [87] to their structur such as the reaction that occurs between carboxly groups which was found in structure of graphene oxide with amine group to produce a new group as amide group. So, 1g of graphene oxide was taken and transferred into beaker (250 ml) **,** 1g of DCC was added above it after their dissolved in 20 ml DMF solvent and left with constant stirrer at room temperature for 30min thereafter , 60 ml of methanolic solution has been added to the mixture which contain 0.1 g of selenazone ligand (Z) . Then, the solution is left at 60ºC for 24 hours under a constant stirring. The resulting mixture was separated at 2500 rpm using centrifuge subsequently and was washed by DMF-Methanol solution and then by deionized water several times [88] , the gray precipitate was obtained after their drying at 70ºC for 10 hours . The scheme 2.3 shows the preparation method of GOZ adsorbent.
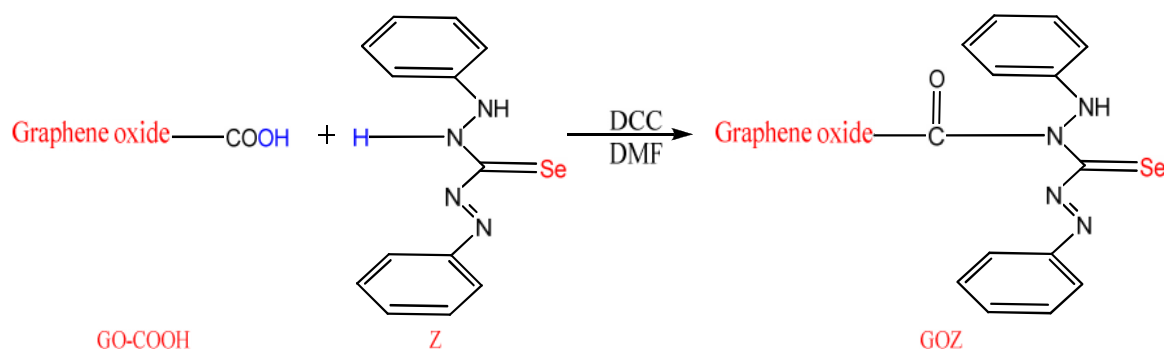
Scheme 2.3 : Preparation of GOZ adsorbent

2.8.2. Modification of silica gel with selenazone ligand (Z)

A new adsorbent surface was prepared from silica gel (scheme 2.4) after its activating with hydrochloric acid and its chlorination with thionyl chloride. The procedure can be summarized as follows: 10 g of silica-gel (100-200 µm) was treated with 150 ml HCl (1:1) and left at a room temperature for 20 hours under a continuous stirrer , then silica gel was filtered and washed by deionized water several time in order to remove the excess amount of acid until it reaches the neutral state of pH . The product needs to be dried at 120ºC for 2 hours . The chlorination process is applied on silica gel after its activation, 5g of activated silica gel was mixed with 30 ml $SOCl_2$ under a refluxing process at 77ºC for 48h , the mixture was dried at 60ºC for 15h .

After the completion of the chlorination process, 0.5g of selenazone ligand (z) was taken and dissolved in 30ml of carbon tetrachloride solvent ,this solution was added into chlorinated silica gel, then it is left under a continuous stirrer at a room temperature for 48hours . The mixture was filtered and rinsed by CCl_4 , ethanol and deionized water several times to confirm a complete removal of the unreacted selenazone ligand (Z) , the obtained product(SGZ) has a pale pink color after their drying at 60ºC for 4h [89] .
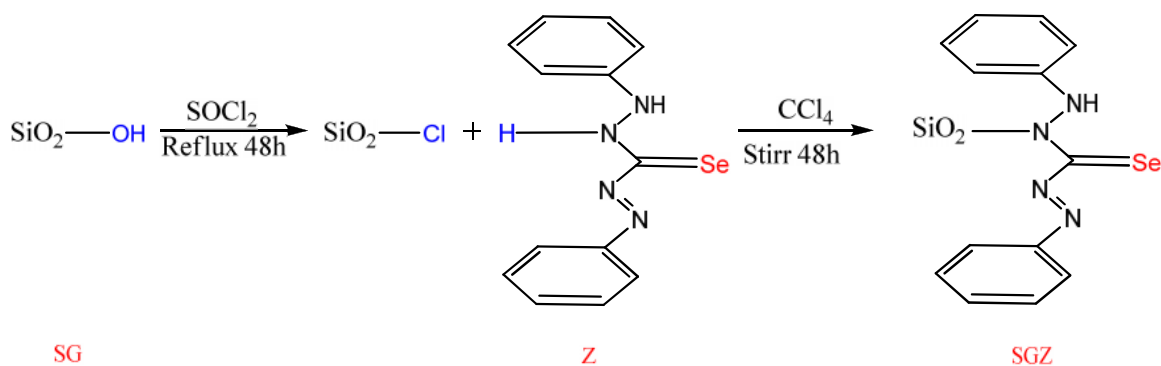
Scheme 2.4 : Preparation of SGZ adsorbent

2.8.3. Modification of Activated carbons with selenazone ligand (Z)

The activated carbon is considered as microparticles that contains many functional groups and also has a large surface area ranging from 300- 2500 m^2/g. The modification operation of the activated carbon was aimed for increasing a new functional groups that lead to raise the adsorption afficiency , this operation can be completed through many steps which can be explained as follows: in order to purify the activated carbon from the impurities by taking 20 g of the activated carbon and putting them into a beaker (600 ml) which mixed with 300 ml of HCl(10%) by using a constant stirrer at room temperature for 24 hours. The mixture was filtered and washed several times by deionized water and dried at 80ºC for six hours. The oxidation process is performed to activate carbon at a later step after their purification by adding 300 ml of nitric acid (32.5%) to 10 g of the activated carbon pure into a beaker (600ml) which covers it by a watch glass, then it is left with stirring at 60ºC for 5 hours . Black precipitate is obtained after their filteration and rinsing by the deionized water until it reaches neutral state, and consequently dried at 80ºC for 10 hours . The activated carbon became containing the carboxyl groups more than the other groups after the completion of the oxidation operation .

Generally , the modification process was applied to activate carbon (scheme 2.5) after oxidizing by taking 5g of activated carbon and mixing with 5g of N,N'-Dicyclohexylcarbodiimide (DCC) after dissolved in 100ml DMF solvent. The mixture was stirred at a room temperature for 15mins and then 100ml of selenazone ligand (Z) solution (that was prepared by dissolving 2g of ligand(Z) in 100ml methanolic solution) were added. The mixture is left at 60ºC for 24 hours under constant stirring . The resulting (ACZ) is filtered and washed by DMF-Methanol solution and then with deionized water for several times. Finally, the black product was dried at 70ºC for 10 hours [88 ,90] .
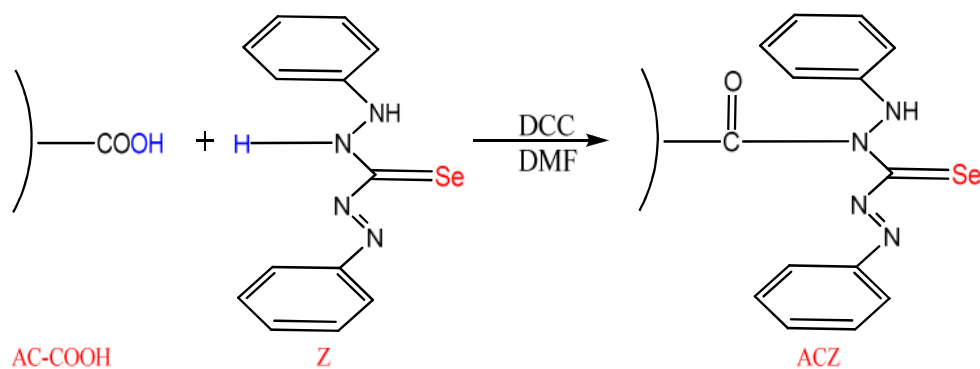
Scheme 2.5 : Preparation of ACZ adsorbent

2.8.4. Separated nanoparticles from soot waste as adsorbent

After the executing of the extraction operation for iron oxide and graphite oxide nanoparticles from soot waste as previously described , 28 ,19.85 g of brown and blackish brown solid substances respectively were obtained after their crushed and sieved by using the sieve 75 µm. The brown precipitate has some physical properties such as its attraction towards magnet , brown color. Also, both of the extracted oxides are insoluble in water therefore it is utilized as adsorbent surface in order to remove pollutants from its aqueous solutions .

2.9. Preparation of adsorbate materials

The adsorbate materials have been prepared as aqueous solutions from their pure primary substances . In this work it was focused onto remove some toxic materials such as some dyes (Mordant Red 3 , Congo Red , Basic Brown and Rhodamine B) and some toxic element (lead and mercury) from their aqueous phase . The method for preparing the adsorbate solution are explained as follows :

2.9.1. Preparation of dyes solutions as adsorbate

There are many dyes inserted into a variety of industries that are more consumed from human activities furthermore , dyes are classified as toxic materials, so, it causes to the increase toxic pollutants concentration in

environment. The current study is concerned with the selection four different types of dyes that possess a variety of applications as dyeing textile , dyeing of biological cells and cosmetics[81,91] . The dyes solutions were prepared and used as adsorbate material, they should be known by the wavelength that occurs at a maximum absorbance for dyes solutions and by the limitation of linearity relationship between absorbance and concentrations that it belong for aqueous solutions for dyes according to the Beer- Lambert law .

2.9.1.1. Selection of the maximum wavelength (λ_{max}) of dyes

To select the extremity wavelength of each dye by preparing 1×10^{-4} M of dyes solutions after their dissolved in deionized water , the dyes solutions are diagnosed by using UV-Vis spectrophotometer instrument that scans ranging between 200-800 nm . The results of maximum wavelength of dyes are shown in Table 2.2 and Figures (2.3 -2.6) .
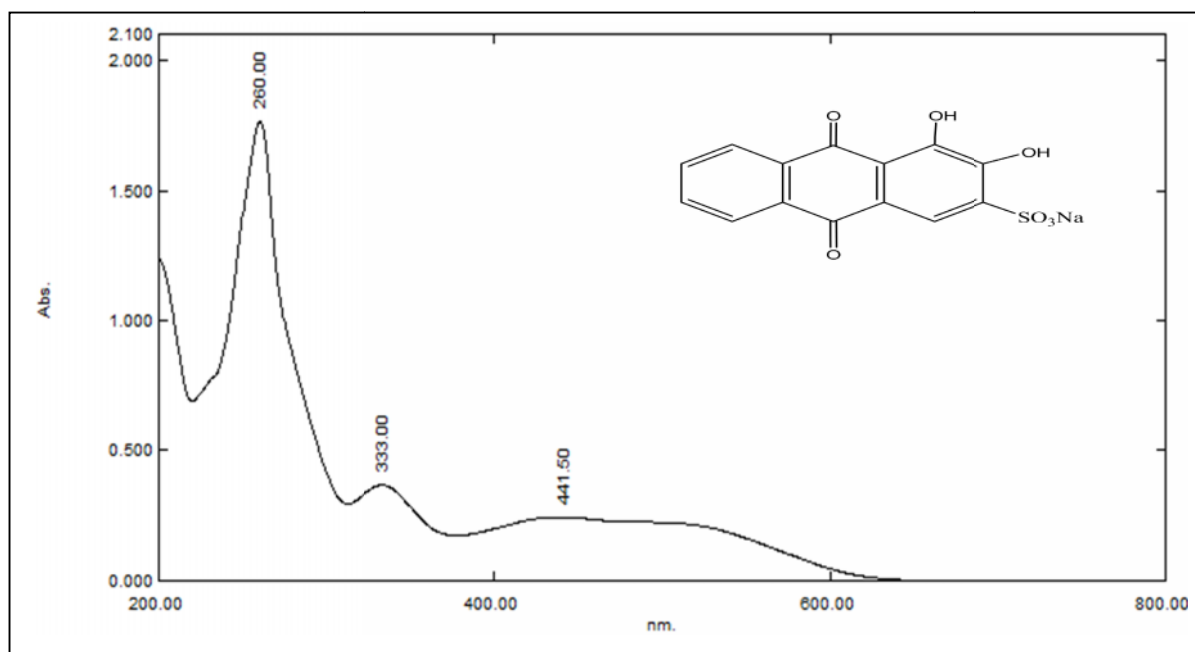
Figure 2.3 : The UV-Vis spectrum of Mordant Red 3 dye
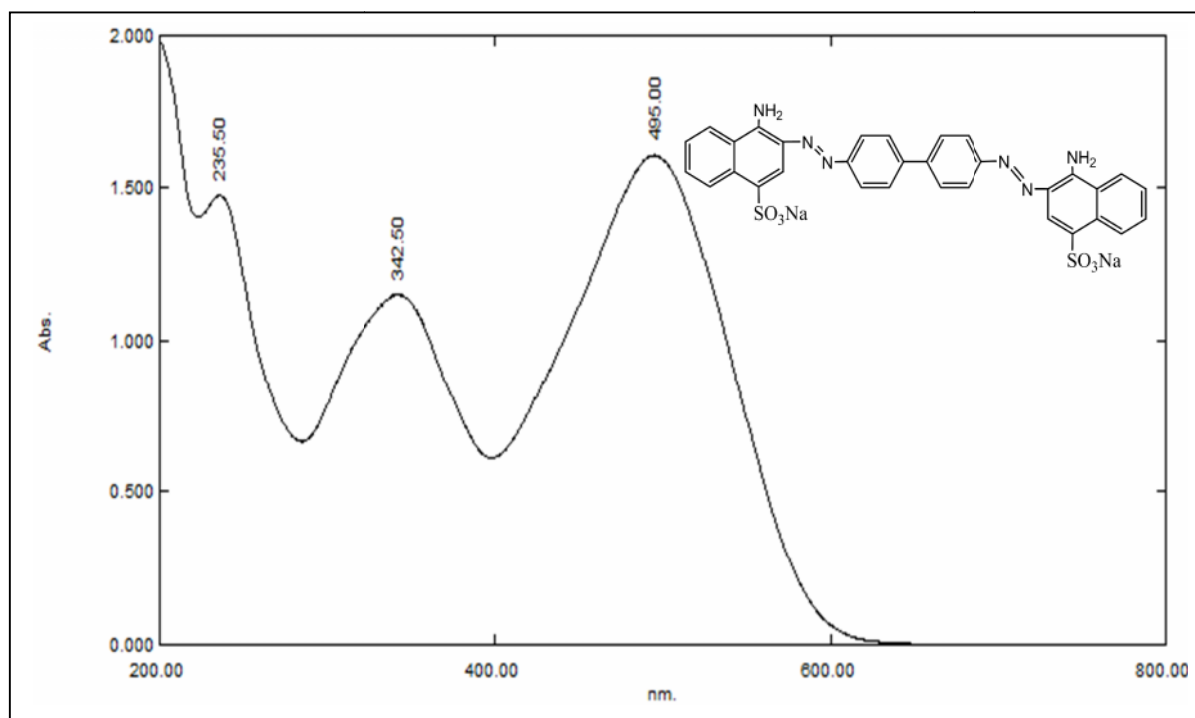
Figure 2.4 : The UV-Vis spectrum of Congo Red dye
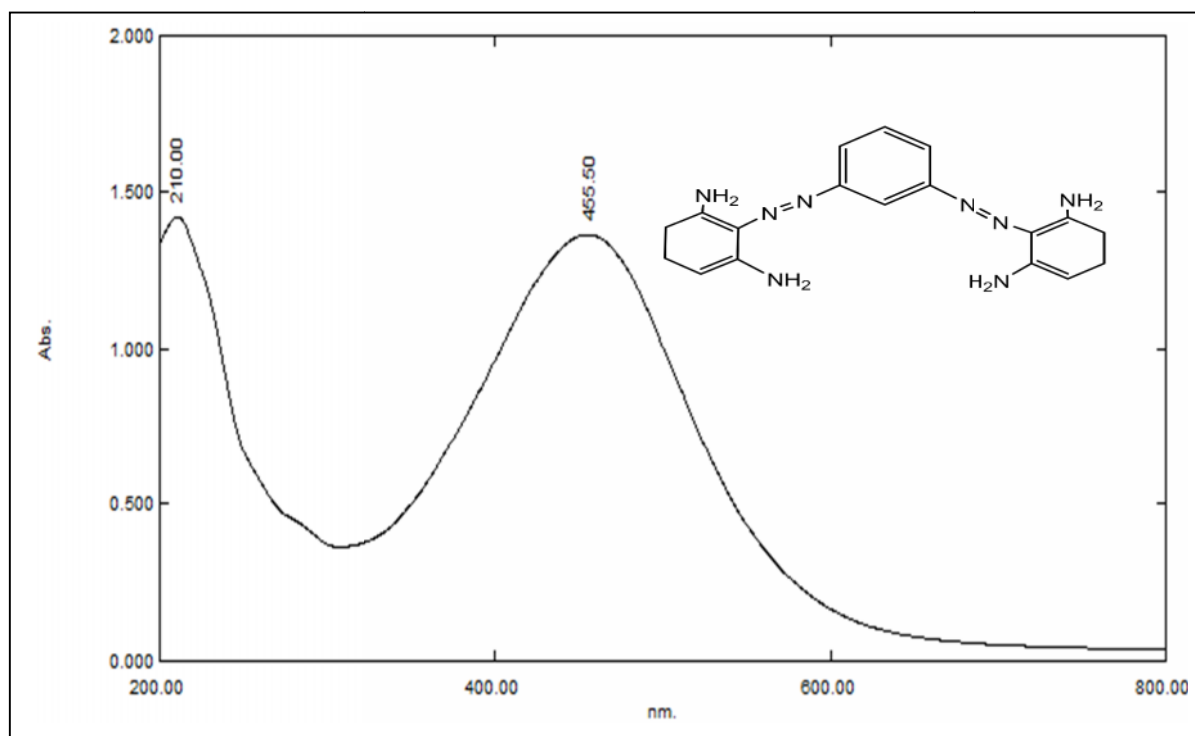
Figure 2.5 : The UV-Vis spectrum of Basic Brown dye
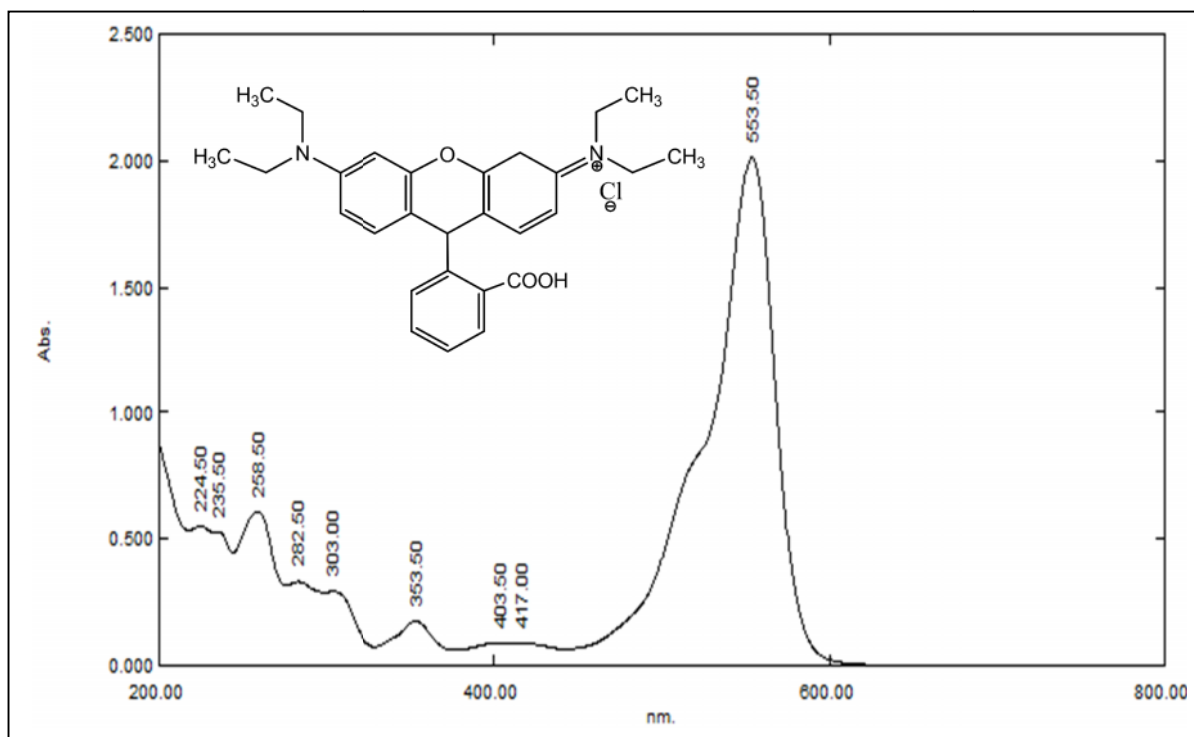
Figure 2.6 : The UV-Vis spectrum of Rhodamine B dye

2.9.1.2. limitation of Linearity relationship for standard curve of dyes

In order to determine the linearity relationship between the concentrations with absorbance at a maximum wavelength for each dye, the concentration series for dyes are prepared that contain (0.1 , 0.5 , 1 , 3 , 5 , 10 , 20 , 30 , 40 , 50 , 100 , 150 , 200 , 250 mg/l) in a 25ml volumetric flask . The results obtained from the plot between the series concentration versus the maximum of wavelength for each dye exhibit, according to Beer's law ranging from (0.1-40 mg/l) , (0.1 - 150 mg/l) , (0.1-50 mg/l) and (0.1-10 mg/l) that belong for dyes Mordant Red 3 , Basic Brown , Congo Red and Rhodamine B respectively as shown in Figures (2.7 - 2.10) .
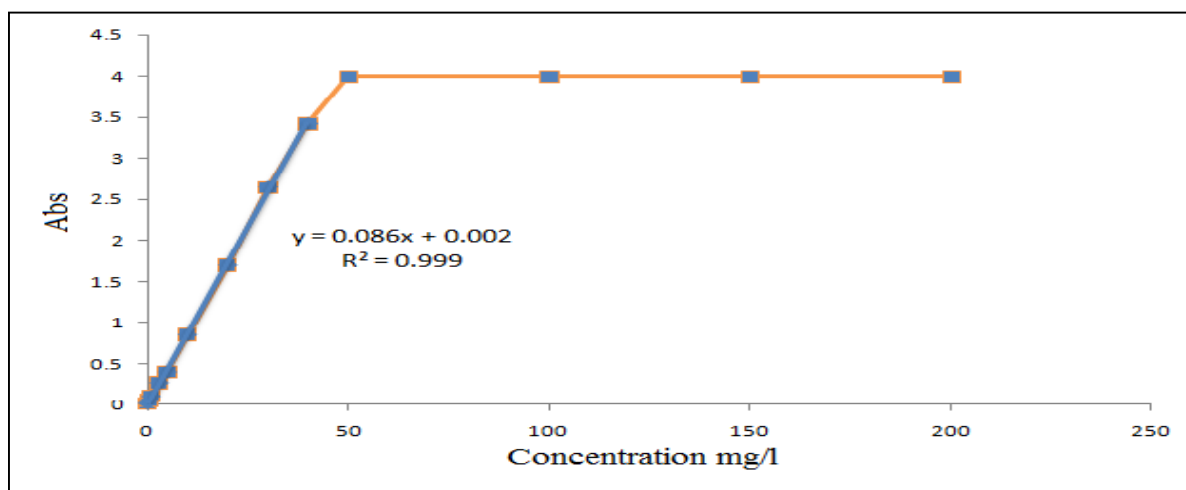
Figure 2.7 : Standard curve of Mordant Red 3 dye
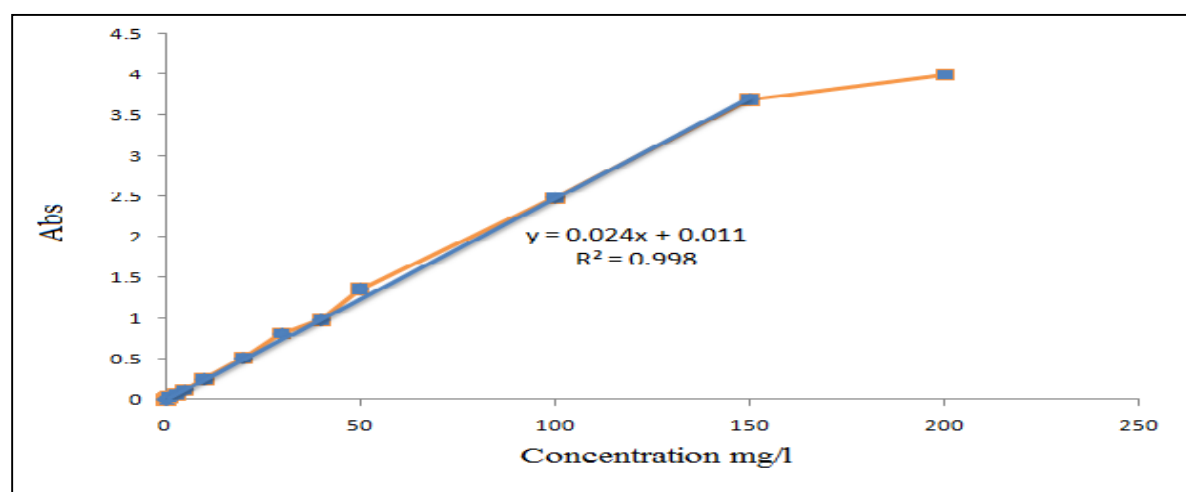
Figure 2.8 : Standard curve of Basic Brown dye
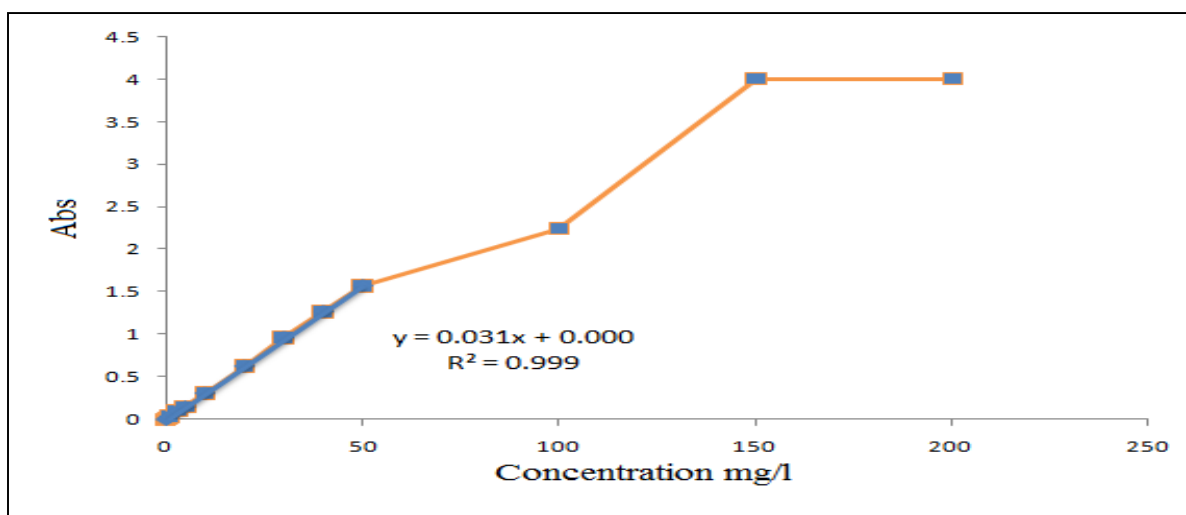
Figure 2.9 : Standard curve of Congo Red dye
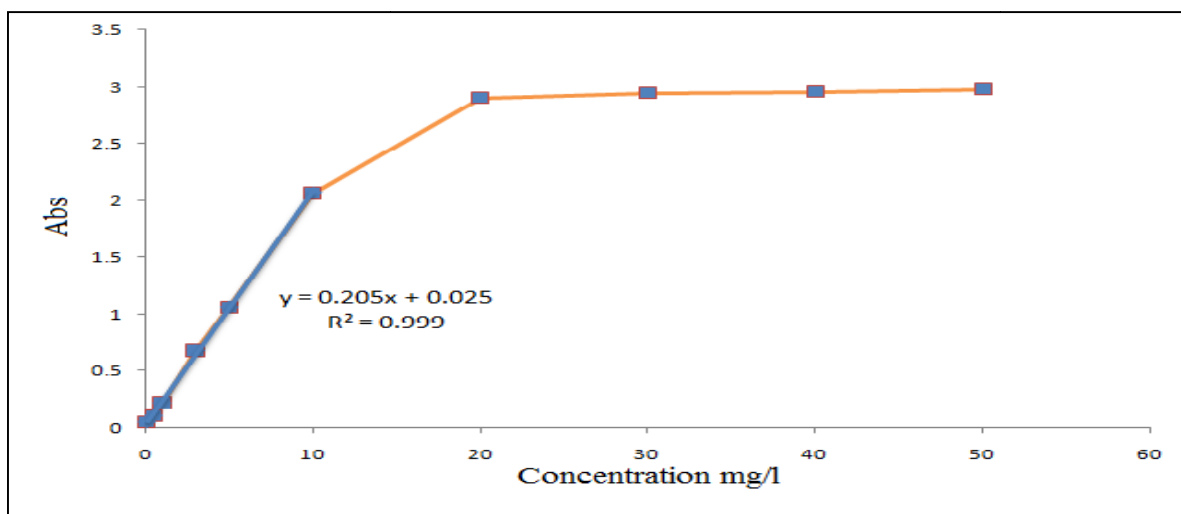
Figure 2.10 : Standard curve of Rhodamine B dye

2.9.2. Preparation of Mercury and Lead stock solutions

The stock solutions (1000 mg/l) of mercury and lead are available commercially and were used for preparing the sequence concentration that obeyed to Beer-Lambert law in the range of 1-20 µg/l for mercury and measured by the cold vapor atomization method , while the lead ion in the range of 1-25 mg/l was measured by FAAS method. The results can be explained in Figure 2.11.
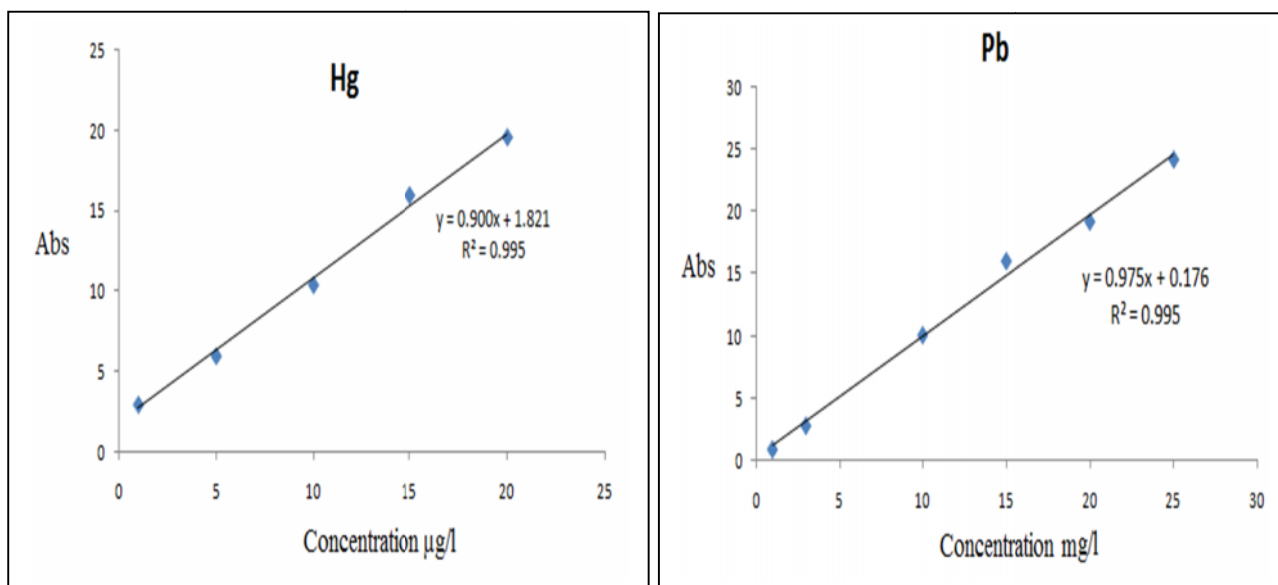
Figure 2.11 : Standard curve of mercury and lead ions

2.10. Selection of optimum conditions for adsorption process

There are many parameters affecting negatively on the adsorption efficiency. So, the current work focuses on the optimum conditions and the highest removable ratio for pollutants as it is demonstrated follow.

2.10.1. Initial concentration

The initial concentration of adsorbate solutions was selected by using different concentration of each dye ,mercury and lead solutions which were (10 , 20 , 30 , 40 , 50 ,100 , 150 , 200 mg/l) , (500 , 1000 , 1500 , 2000 , 5000µg/l) and (4 ,8 , 14 , 28 mg/l), respectively. Also , the constant conditions were utilized as 10 ml of volume solution , fixing temperature at (20ºC) , 0.01g of adsorbent surface , 130 rpm as mixing speed and 4h as contact time . The analysis are executed in natural pH of each solution .

2.10.2. Effect of contact time

In order to select the contact time between the adsorbent surface with the adsorbate solution by using constant weight of adsorbent surface (0.01g) and 10 ml of adsorbate solution and then , different times that are chosen for shaking solution (0 , 5,10 ,20 ,30 , 40, 50, 60, 90,120,180, 240 min) at 20ºC , fixing of shaking speed at 130 rpm and concentration of adsorbate solution at 50 mg/l for dyes , 1000 µg/l for mercury and (4 and 14 mg/l) for lead ions . Furthermore, the analysis is applied to natural pH of each solution .

2.10.3. Effect of temperature

To determine the best temperature which is given the highest value of the removal ratio, therefore, six degrees (25 , 35 , 45 ,55 ,65 ,75) are selected with the remain of the other conditions constant such as 0.01 g of adsorbent surfaces ,10 ml of each adsorbate solution , 50 mg/l , 1000 µg/l and (4 and 14 mg/l) for dyes , mercury and lead solutions respectively , mixing speed at 130 rpm by using the

contact time selected previously of each adsorbent surface . Additionly , the study of temperature affects on the adsorption efficiency which was carried out in natural pH level of each solution .

2.10.4. Effect of pH levels

The pH value was adjusted of adsorbate solutions by utilizing 0.1M of NaOH and HCl solution. In order to achieve this examination , various levels of pH are chosen at ranging between 3-9 with the remain of the other conditions fixed as 50 mg/l , 1000 µg/l and (4 and 14 mg/l) for dyes , mercury and lead solutions respectively, 10 ml of each adsorbate solution , 0.01 g of adsorbent surface ,mixing speed at 130 rpm. Also, the contact time is used as it was selected previously at 20ºC.

2.10.5. Effect of mixing speed

The effect of shaking speed was studied for the adsorption efficiency utilizing 0.01 g of adsorbent surface and four different shaking speeds (50 , 100 , 150 and 200 rpm) by using shaker incubator at 20ºC and limited pH value of solution according to the natural value of each solution, the volume and the concentration constant were used as follow: 10ml of each adsorbate solution , 50 mg/l , 1000 µg/l and (4 and 14 mg/l) for dyes , mercury and lead solutions respectively . While , the contact time is constant as it was selected previously for each adsorbent surface with the adsorbate solutions .

2.11. Adsorption isotherms

The adsorption isotherms and thermodynamic study were applied on the solutions of dyes , mercury and lead by taking different concentration in the range (10 ,20 , 30 , 40 and 50 mg/l) , (500 , 1000 , 1500 , 2000 µg/l) and (4 and 14 mg/l) of dyes , mercury and lead solutions, respectively. They were studied with the change of temperatures at (25 , 35 , 45 and 55 ºC) of each concentration by using

10 ml of adsorbate solution , 130 rpm as mixing speed. The contact time was used as it was selected previously at natural pH of each solution. Then, the solutions were centrifuged and separated . The equilibrium concentration were estimated by using UV-Vis spectroscopy and atomic spectroscopy .

2.12. Desorption experiment

The desorption process was studied by using three solvents that have different polarity such as distilled water , methanol and ethanol for 24h under the continuous shaking in order to recover the dyes from the adsorbents surface while, the heavy metals were recovered from adsorbent surface after their adsorption by using different concentrations of HCl at (0.5 , 1 and 2N) .

2.13. Environmental experiment

The sample of river water was collected from al-Najebia station that is located on Shatt Al-arab River , while the sea water sample was collected from the zone, which is nearby khor Alamaya port in Basrah governorate by utilizing water collector instrument at depth, 15 cm from the surface water in summer season. Also, the double distillation water was used. The mixture of dyes solutions containing 50 mg/l of each dye, were prepared by utilizing three different types of waters.

Chapter Three

Results and Discussion

Synthesis ,spectroscopic characterization and thermal study of some complexes derived from selenazone ligand derived from dithizone
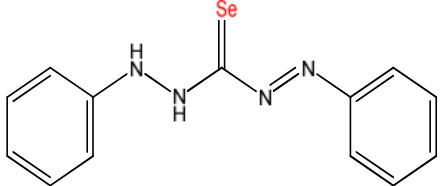
3. Characterization of selenazone ligand and their complexes

The current work includes the prepared selenazone ligand (Z) and it's complexes , new prepared compounds are characterized by using various techniques that are explained as follows :

3.1. Characterization of ligand (Z)

The ligand (Z) was prepared from dithizone after the replacement of the sulfur atom by the selenium atom, using the reduction process in the basic medium under an inert atmosphere of argon. The blackish brown color compound was obtained and also it was observed that the product compound has a good solubility in some common solvents as methanol, toluene, diethyl ether, dichloromethane and xylene. On the other hand, it is insoluble in ethanol, water and hexane. Furthermore, the structure of selenazone ligand was named according to IUPAC system which is shown in Table 3.1.

Table 3.1 : Structure of selenazone ligand (Z)

Symbol of ligand	IUPAC system	Structure formula
Z	(E)-1,5-diphenylselenocarbazone	

3.1.1. FT-IR Spectroscopy

The IR spectrum of selenazone ligand (Z) was measured by using KBr disk in the region 4000- 400 cm^{-1}. The IR spectrum demonstrated a new peak at 979.84 cm^{-1} that attributed to the group of C=Se in the ligand structure [92]. Some peaks disappered in the spectrum of selenazone ligand when compared with the dithizone spectrum such as C=S, C-S,C=N and S-H groups. The data obtained from the FT-IR spectrum confirmed the formation of selenazone ligand via the replacement of

the selenium atom rather than the sulfur atom. Moreover, the tautomeric forms disappeared in the selenazone ligand when they were compared to the dithizone spectrum through the absence of the imine group. All the information obtained from the infrared spectra for selenazone and dithizone are shown in Table 3.2 and Figures 3.1 and 3.2 .

Table 3.2 : The results of FT-IR for selenazone

ligand and its complexes

Functional group	Wavenumber(cm^{-1})					
	Dithizone	Z	ZPb	ZCd	ZCo	ZNi
N-H	3435,3400	3278	3266	3267	3280	-
O-H	-	-	3421	3450	3433	3404
C-H Arom.	3003,3091	3026 3047	3154 3131	3010	3159 3053	3062
N=N	1490	1494	1469	1490	1477	1485
C=C	1597-1444	1597- 1408	1597- 1405	1558- 1427	1600- 1400	1600- 1400
S-H	2530	-	-	-	-	-
C=S	894,860, 1062	-	-	-	-	-
C-S	501	-	-	-	-	-
Se-H	-	-	2207	2260	2177	2308
C=Se	-	979	-	-	-	-
C-Se	-	-	573	574	578	580
C=N	1627	-	1635	1645	1622	1633
C-N	1219	1226	1257	1222	1247	1263
M-N	-	-	455	626	648	501
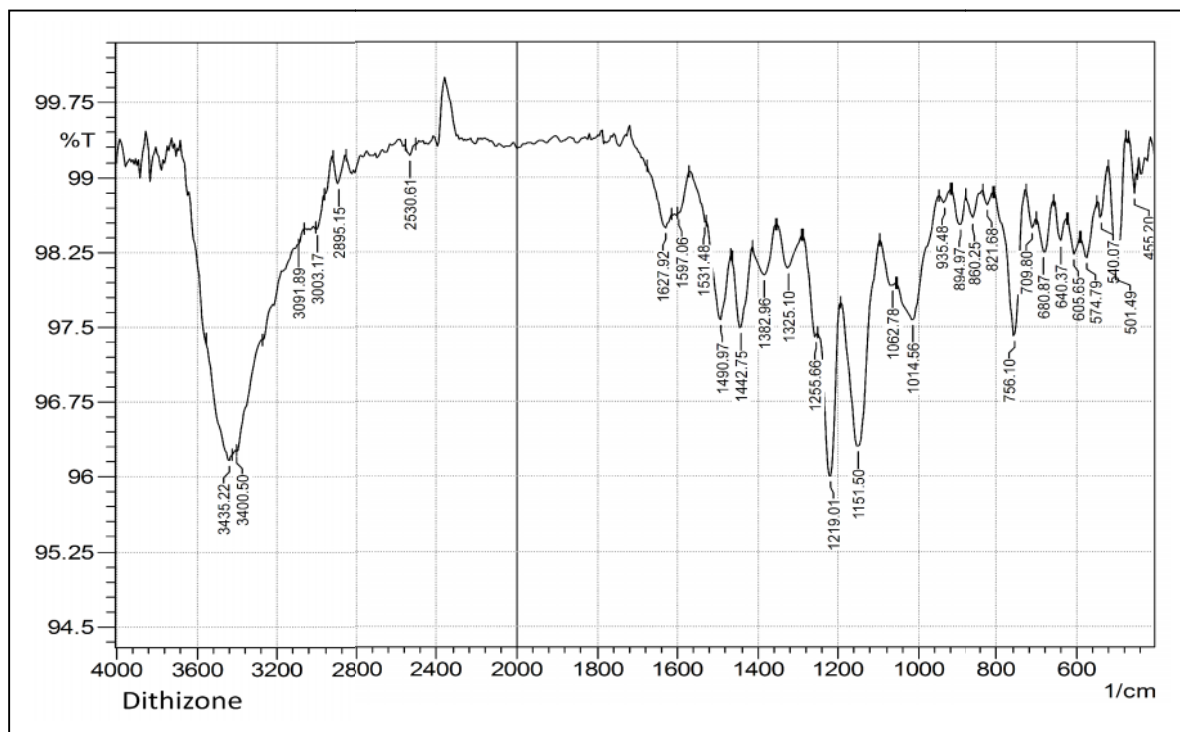
Figure 3.1 : FT-IR Spectrum of Dithizone
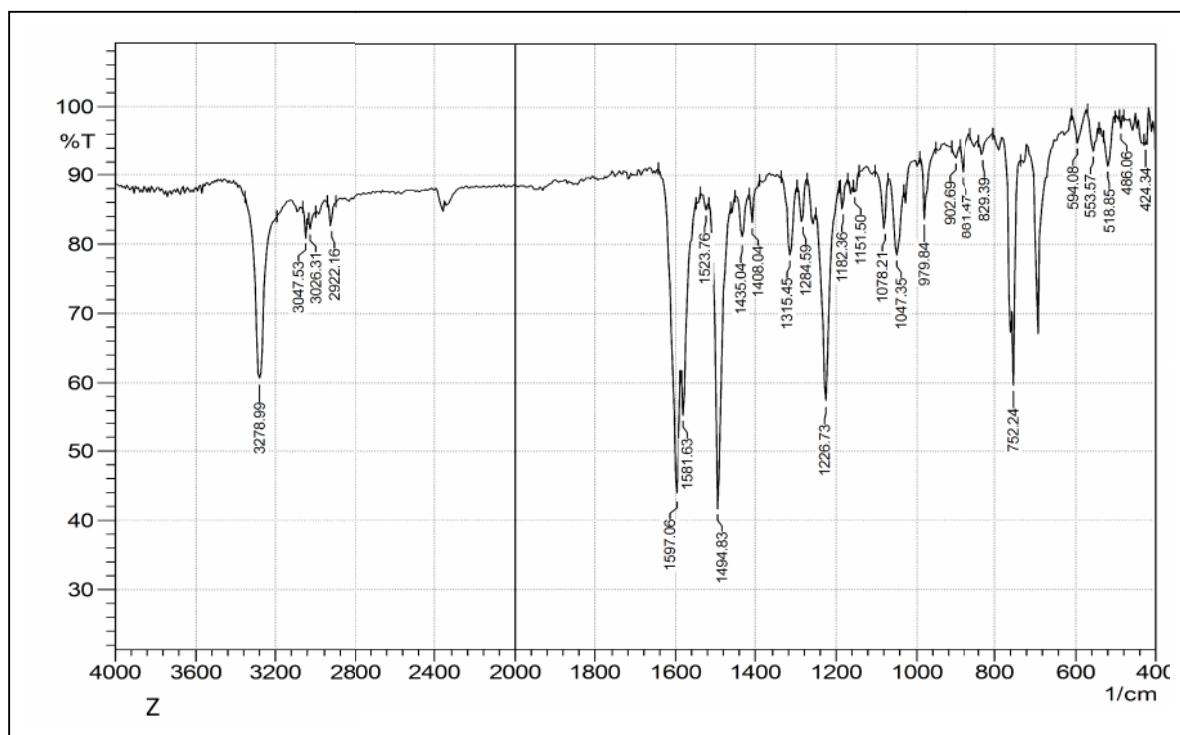
Figure 3.2: FT-IR Spectrum of Selenazone ligand (Z)

3.1.2. UV-Vis Spectroscopy

Ultraviolet-Visible spectroscopy is an important technique to characterize many functional groups in organic molecules and inorganic compounds by using the absorption radiation of electromagnetic in UV-Vis region through the scanning of the wavelengths in extent 200 -800 nm. The UV-Vis spectrum of dithizone in ethanol solvent (Figure 3.3) which appeared by many bands at 226, 266, 277, 295, 444 and 593 nm due to π-π^* and n-π^* transitions for carbon –carbon double bond in benzen rings , azo group , azomethine group , carbon-sulfur double bond and thiol - thione forms. The bands at 444 and 593 nm were attributed to thiol-thione formation these bands refer to the presence of tautomerism in dithiozone structure [17,93]. UV-Vis spectrum of selenazone ligand (Figure 3.4) which was measured in methanol solvent displayed four bands at 267,296,413 and 535 nm that attributed to π-π^* and n-π^* transitions with molar extinction coefficients at 8620, 5810, 10750, 3350 L mol^{-1} cm^{-1} respectively . These bands also confirm the formation of selenazone ligand and the disappearance of the tautomeric forms from the selenazone ligand structure [17].
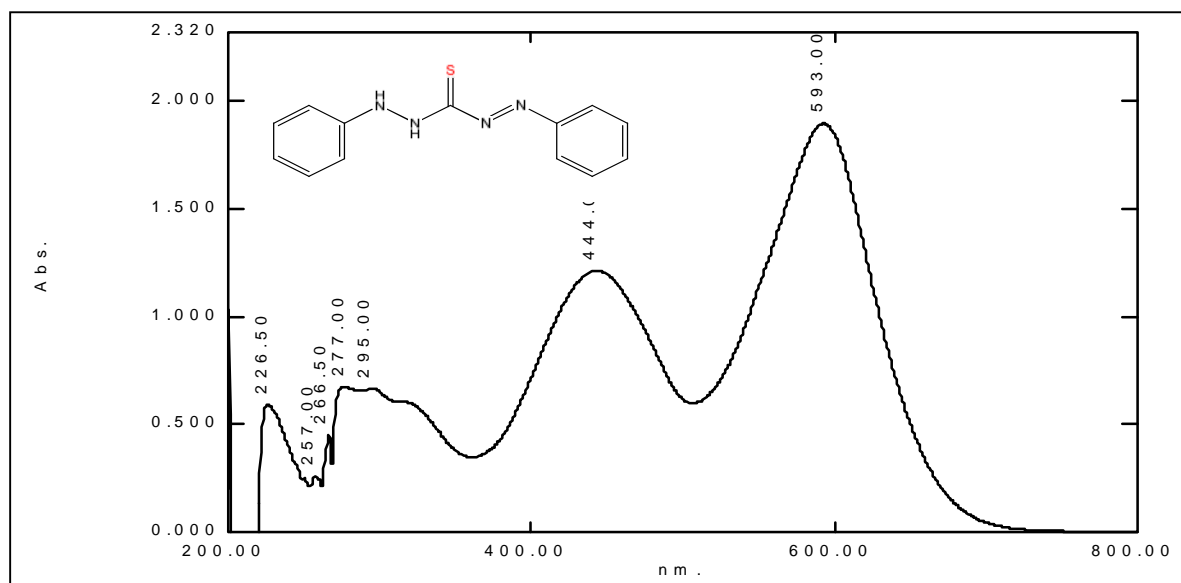
Figure 3.3: UV-Vis Spectrum of Dithizone
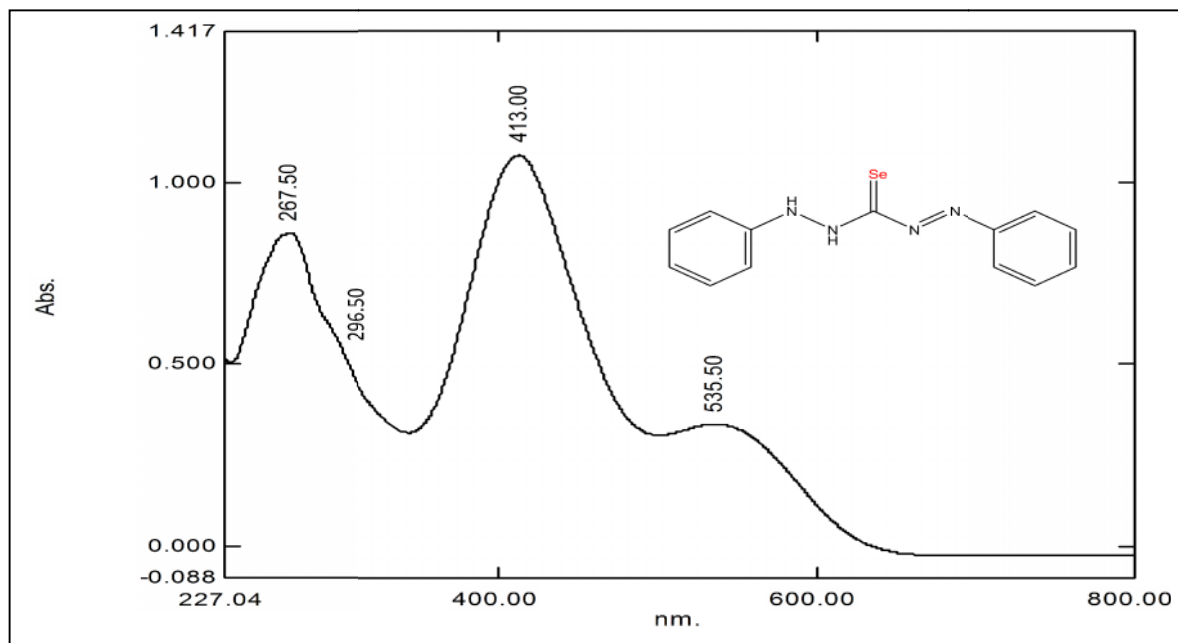
Figure 3.4: UV-Vis Spectrum of Selenazone ligand

3.1.3. Mass Spectrometry

The technique of mass spectrometry gives useful information about the synthetic compound by selecting the molecular ion to characterize the organic compounds in coordination chemistry. Also, it can be known as the fragment pattern of compounds that gives a good idea about the stability of fragments particularly with the base peak ion [94]. The Figure 3.5 shows the mass spectrum of selenazone ligand (Z) where the molecular ion was exhibited at m/z 303 with the relative abundance of (0.35%) and a base peak at m/z 77 (100%) . The molecular ion refers to the agreement with the molecular weight their suggestion structure for selenazone ligand (Z). On other hand, the fragment of molecular ion for selenium isotope (^{80}Se) was appeared at m/z 305 (0.01%). Furthermore, a new fragment has been revealed at m/z 606 (0.05%), this may indicate the formation of dimers structure of selenazone ligand (Z). The fragmentation of ions are shown in Figure 3.5 and scheme 3.1.
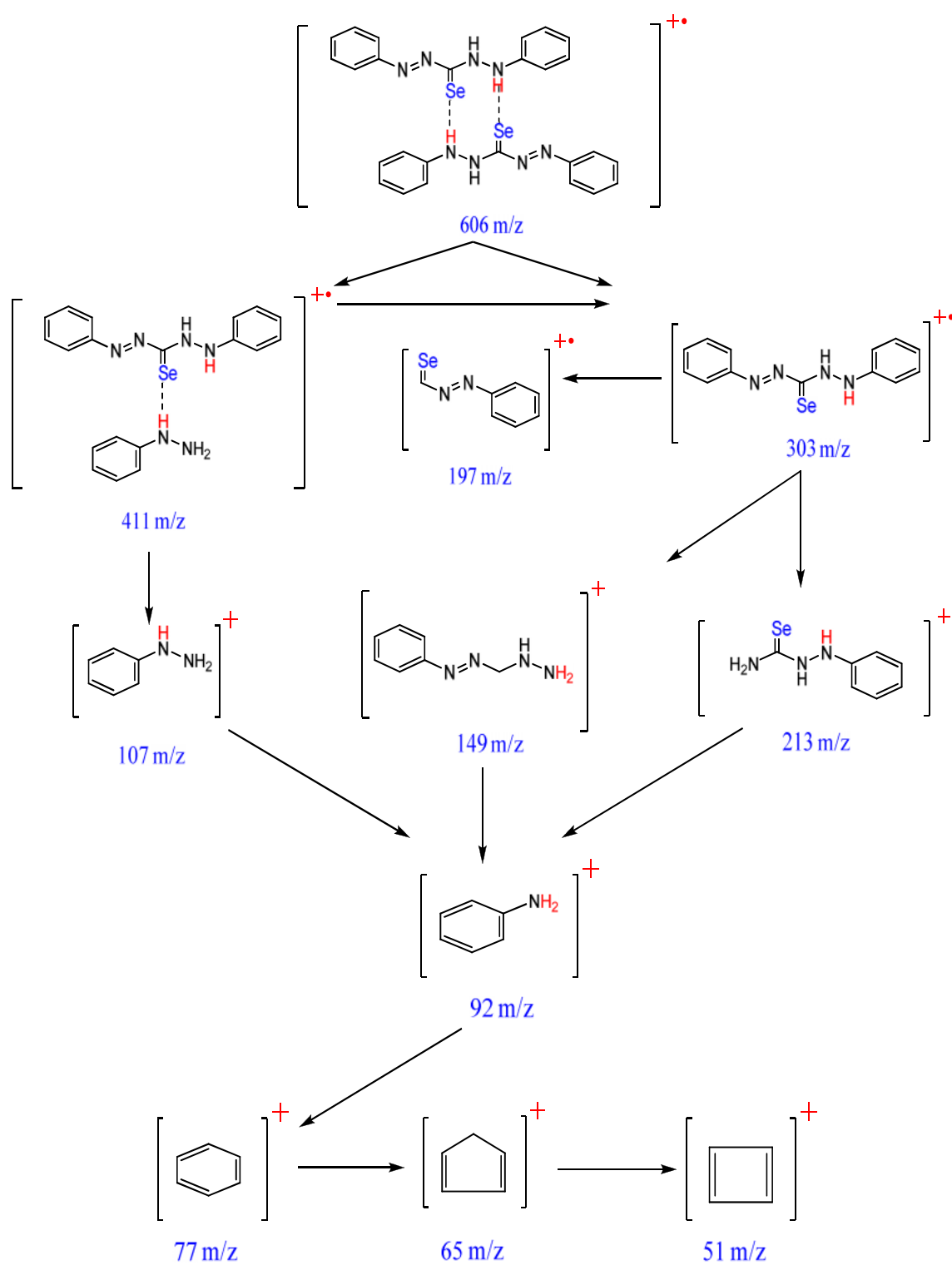
Scheme 3.1: Fragmentation of Selenazon ligand (Z)
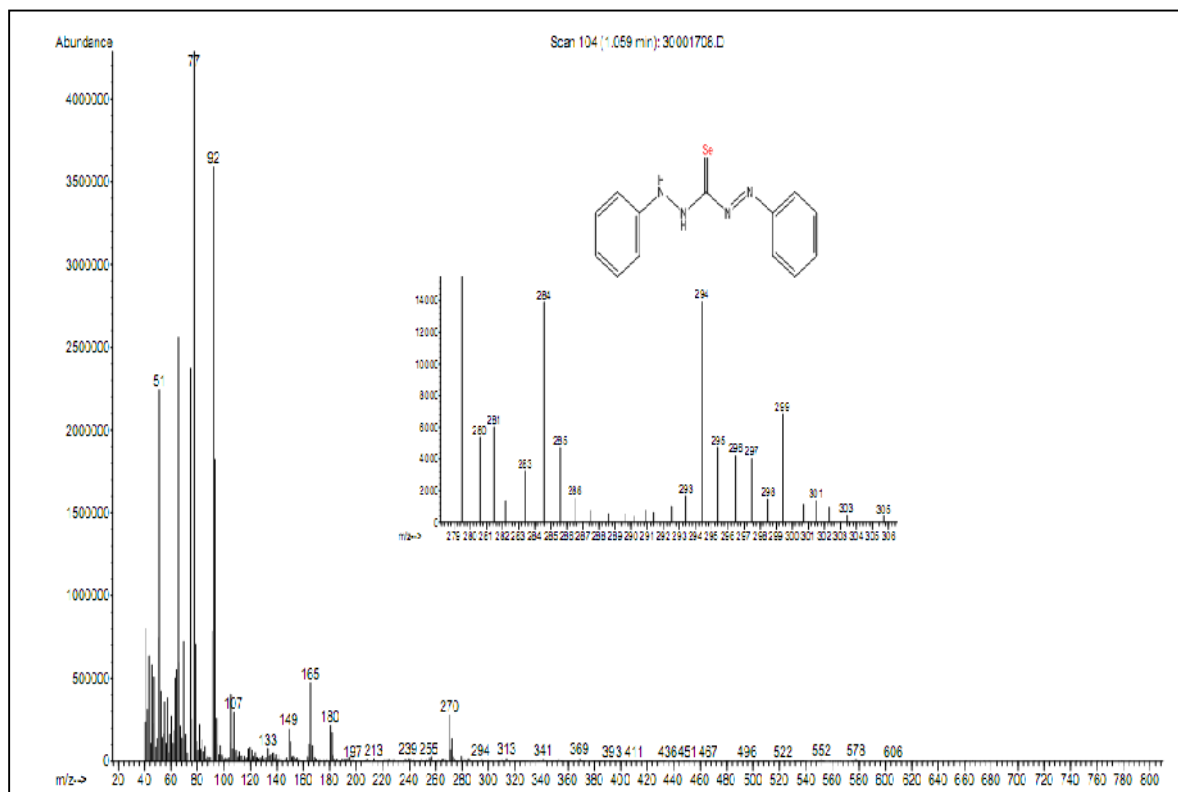
Figure 3.5: Mass Spectrum of Selenazone ligand (Z)

3.1.4. [1]H- Nuclear magnetic resonance spectroscopy

^{1}H-NMR spectrum of selenazone ligand has been recorded in methanol (CD$_3$OD) as a solvent by using the frequency at 500 MH$_z$, this technique is an important to select the magnetic nucleus in the solution it provided helpful information about the distribution of protons in the compound that was used to characterize several compounds in the organic and coordination chemistry [95]. The Figure 3.6 showed two signals by employing a chemical shift at δ=2.33 , 2.48 ppm that due to amine group (N-H)[96] which is consistent with two protons, while multi signals were appeared in the range of a chemical shift from 6.70 to 7.68 ppm where they are appropriate with ten protons which were attributed to protons of benzene rings[94]. The ^{1}HNMR spectrum result confirms the proposed structural elucidation of the selenazone ligand (Z) .
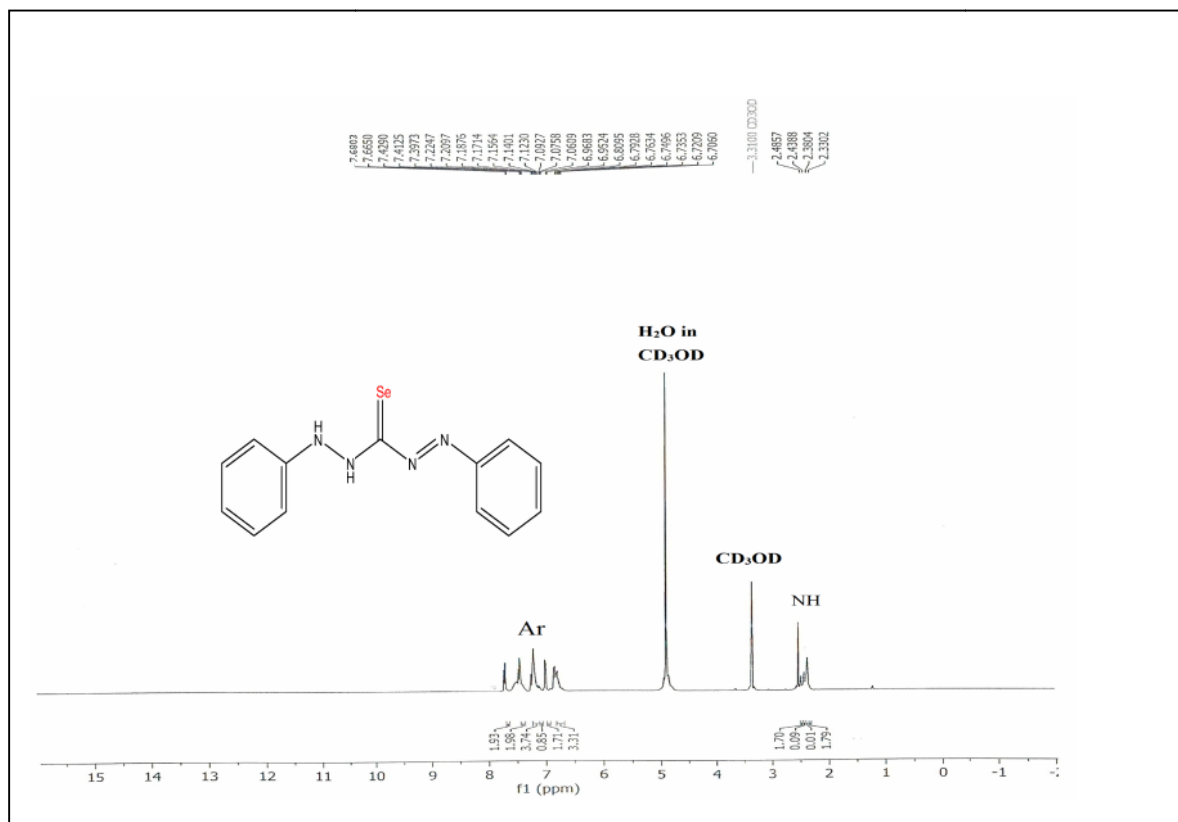
Figure 3.6: ^{1}H-NMR of Selenazone ligand (Z)

3.1.5. ^{13}C- Nuclear magnetic resonance spectroscopy

The chemical shifts of all carbon atoms in the selenazone ligand (z) were measured by using ^{13}C-NMR spectroscopy in frequency at 125 MH$_z$ in methanol (CD$_3$OD) as a solvent . The carbon atoms have been numbered in selenazone ligand (z) as is shown in Figure 3.7. Moreover, the magnetic equivalent carbon atoms have the same number.
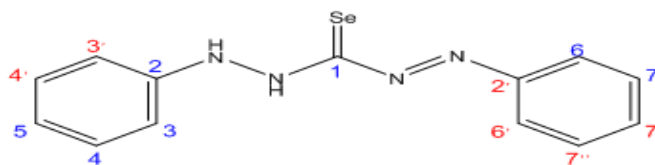
Figure 3.7: The numbering of carbon
atoms of selenazone ligand

The ^{13}C-NMR spectrum of selenazone ligand (z) was appeared multi signals in different chemical shifts where , the signal shows at δ=130.28 ppm   which is attributed to carbon atom which is connected directly with nitrogen atom ($C_{2,2'}$) in the ring system of benzeen furthermore , the ring system also, revealed several signals at δ=113 , 114, 119 ,129.72 and 129.86 [97] that due to carbon atoms for numbering $C_{3,3'}$, $C_{6,6'}$, C_5 , $C_{7,7',7''}$ and $C_{4,4'}$ respectively. On other hand, the signal of carbon atom that is connected with selenium atom has been disapeared in ^{13}C-NMR spectrum in this case may be attributed to the decrease of intensity of this signal because of the decrease of overhauser effect. Also, it can't be observed in spectrum with the existance of the noise signals [98]. The ^{13}C-NMR data are consistent with the number of carbon atoms of selenazone ligand as is elucidated in Figure 3.8 and Table 3.3 .

Table 3.3 : Chemical shifts of selenazone ligand and their complex in ^{13}C-NMR spectra

Carbon atoms	Chemical shift (ppm)	
	Z	ZNi
C_1	-	168.76
$C_{2,2'}$	130.28	130.77
$C_{3,3'}$	113	126.78
$C_{4,4'}$	129.86	134.56
C_5	119	126.78
$C_{6,6'}$	114	126.78
$C_{7,7',7''}$	129.72	133.27
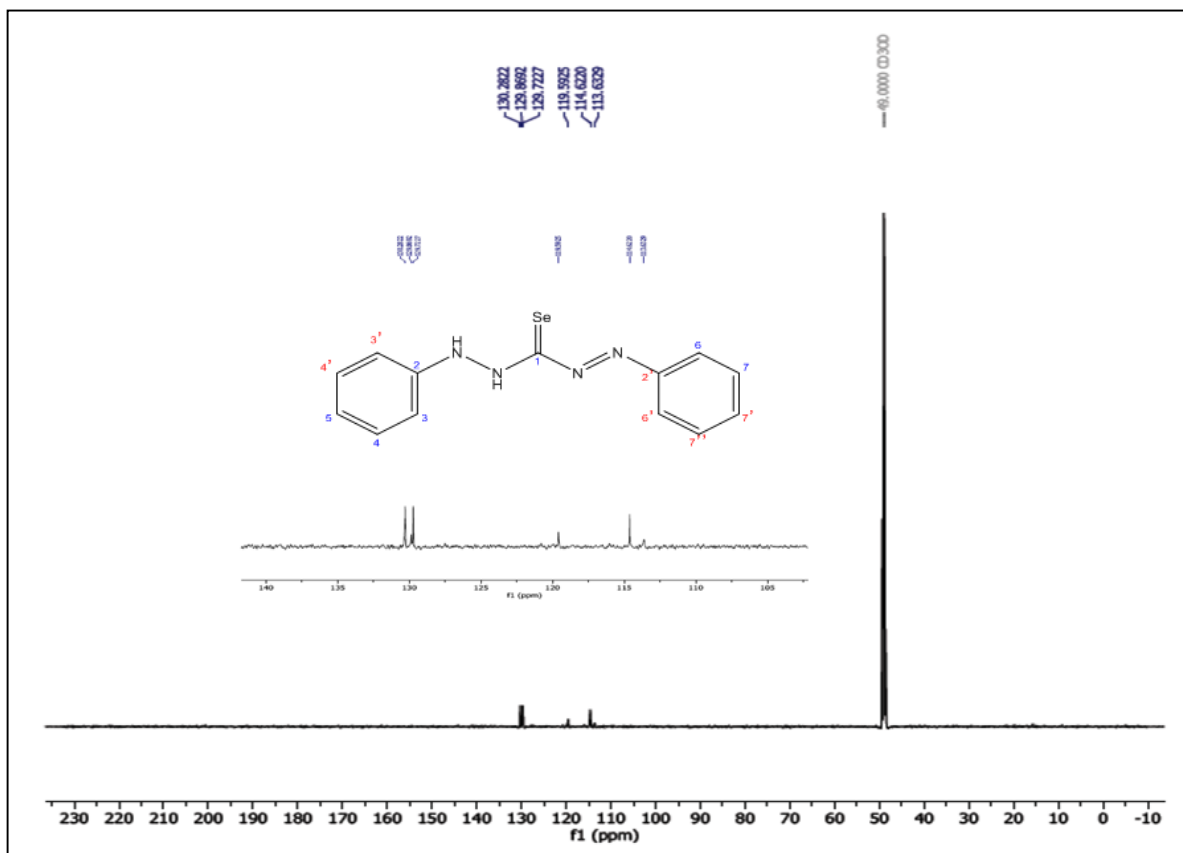
Figure 3.8: ^{13}C-NMR of Selenazone ligand (Z)

3.1.6. X-ray Diffraction Spectroscopy

X-ray spectroscopy is a useful technique that provides several information about the crystal size and crystalline phase which help for characterizing the compounds [99]. There are many techniques that utilized the principle of X-ray excitation in order to determine the electronic and geometric structures of the compounds like : X-ray absorption spectroscopy (XAS) , X-ray emission spectroscopy (XES) , X-ray photoelectron spectroscopy (XPS) and X-ray Auger spectroscopy [100] . Several important parameters were measured in XRD technique in which the diffractogram helps to diagnose many organic and organometallic compounds. Generally, the position of peak (2θ) and d-speacing (interplaner) the basic properties that are used for characterizing compounds because they have a special constant value to

each the metal or compound. The well-known crystallinity index (CI) can be calculated from XRD diffractogram by using equation as follows :

$$CI(\%) = [(I_m - I_{am})/ I_m] \times 100$$

Where : I_m and I_{am} (arbitrary units) represent the maximum intensity of the crystalline peak and the amorphous diffraction peak around 2θ respectively [67,100] . Interplaner speacing d has been calculated from Bragg's equation $(n\lambda = 2d \sin\theta)$ [67,99,100] .

The crystal size in compounds can be determined by knowing the full width of high maximum (FWHM) to each peak by using Debye sherrer's equation $(D=K\lambda/\beta \cos\theta)$, where K is constant whose value is about 0.9 , λ is the wavelength of the X-ray , β is the width of radians of the peak and θ is Bragg's diffraction angle [99] .

The X-ray diffraction pattern of the selenazone ligand (z) showed several bands that have positions at 2θ (18.9º, 23.5º, 26.6º, 29.6º, 41.4º , 43.6º , 45.4º , 51.74º , 56.2º , 61.7º , 65.4º and 71.7º) , the 2θ values corresponding to the crystal planes (Miller indices) (- ,100 , - , 101 ,110 , 102 , 111 , 201 , 112 , 202 , 210 and 113) respectively . The amorphous diffraction peak was revealed at 2θ (77.06º). Besides, the crystal size of selenazone (Z) was computed by using Debye Sherrer's equation, proving that the average crystals size (19.78 nm) of selenazone ligand was within the nanoparticles class. These bands in diffrectogram of selenazone ligand (z), due to the existence of selenium atom in the structural formula of selenazone ligand that is appropriate with the results that were obtained in the previous studies [99, 101, 102]. On the other hand, the bands of sulfur atom disappeard in the pattern of selenazone ligand that enhanced the formation of the suggested structure formula of selenazone ligand [103]. All the results of X-ray analysis are explained in Table 3.4 and Figure 3.9.

Table 3.4 : The results of X-ray analysis for selenazone ligand (z)

Pos. [°2Th.]	Height [cts]	FWHM Left [°2Th.]	d-spacing [Å]	Rel. Int. [%]	Miller indices (HKL)	Crystal size (D nm)	crystallinity index (CI)
18.9624	558.64	0.2952	4.68017	20.83	-	27.28	86.93255
23.5491	1027.11	0.4428	3.77798	38.29	100	18.32	92.89268
26.6454	448.61	0.2952	3.34557	16.72	-	27.65	83.72751
29.6836	2682.40	0.3936	3.00970	**100.00**	101	**20.88**	**97.27856**
41.4472	356.82	0.5904	2.17865	13.30	110	14.38	79.54151
43.6544	932.45	0.2460	2.07348	34.76	102	34.78	92.17116
45.4515	476.39	0.5904	1.99559	17.76	111	14.58	84.67642
51.7456	375.11	0.5904	1.76669	13.98	201	14.95	80.53904
56.2229	283.18	0.8856	1.63616	10.56	112	10.17	74.22134
61.7438	263.21	0.8856	1.50245	9.81	202	10.45	72.26549
65.4836	181.85	0.3936	1.42541	6.78	210	23.99	59.85703
71.7806	102.39	0.4920	1.31506	3.82	113	19.92	28.70397
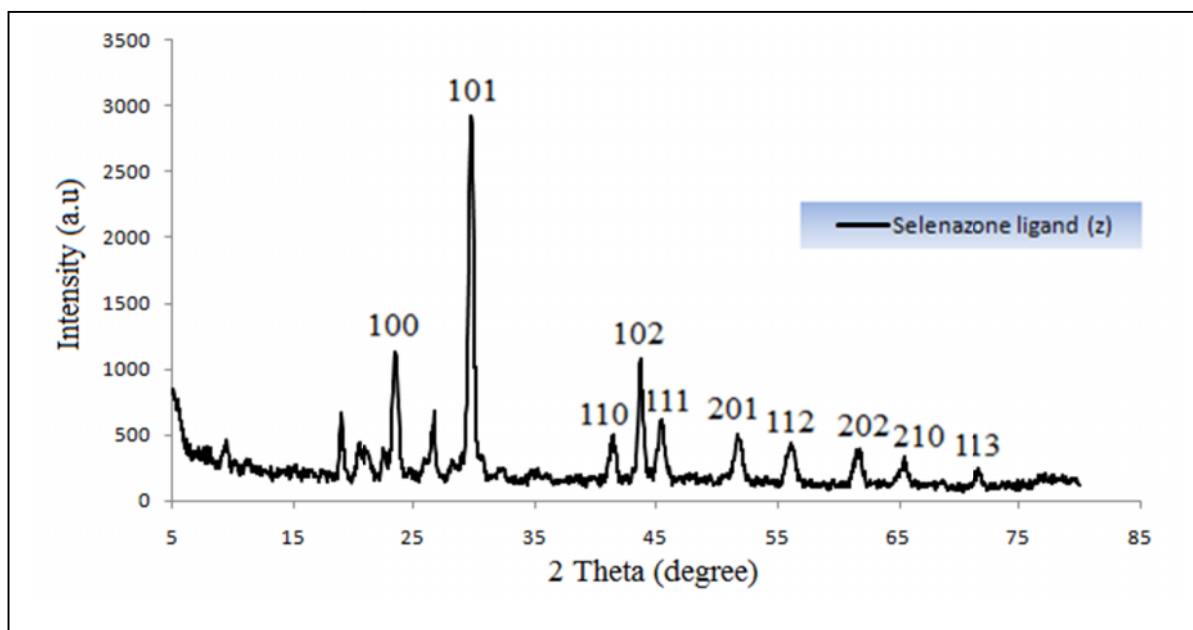
Figure 3.9: XRD spectrum of Selenazone ligand (Z)

3.1.7. Scanning Electron Microscopy (SEM)

The scanning electron microscope is one of the technique which provide images through the scanning of outer surface of sample after dyeing it by gold with a concentrated beam of accelerated electrons which are attractive with the atoms in the sample that leads to produce several signals which includ useful information about the overall shape and structure of the outer surface of sample [67,104]. The SEM image (Figure 3.10) was utilized in this work to prove the existence of a selenium atom in the structutre of selenazone ligand. The results revealed that the shape of nanorods were attributed to selenium atom. The SEM result was consistent with the previous study that was carried out by Fresneda et.al. [99] and proved the existence of selenium nanoparticles . The XRD analysis is consistent with SEM image which confirms the nanostructure of selenazone ligand (z) .
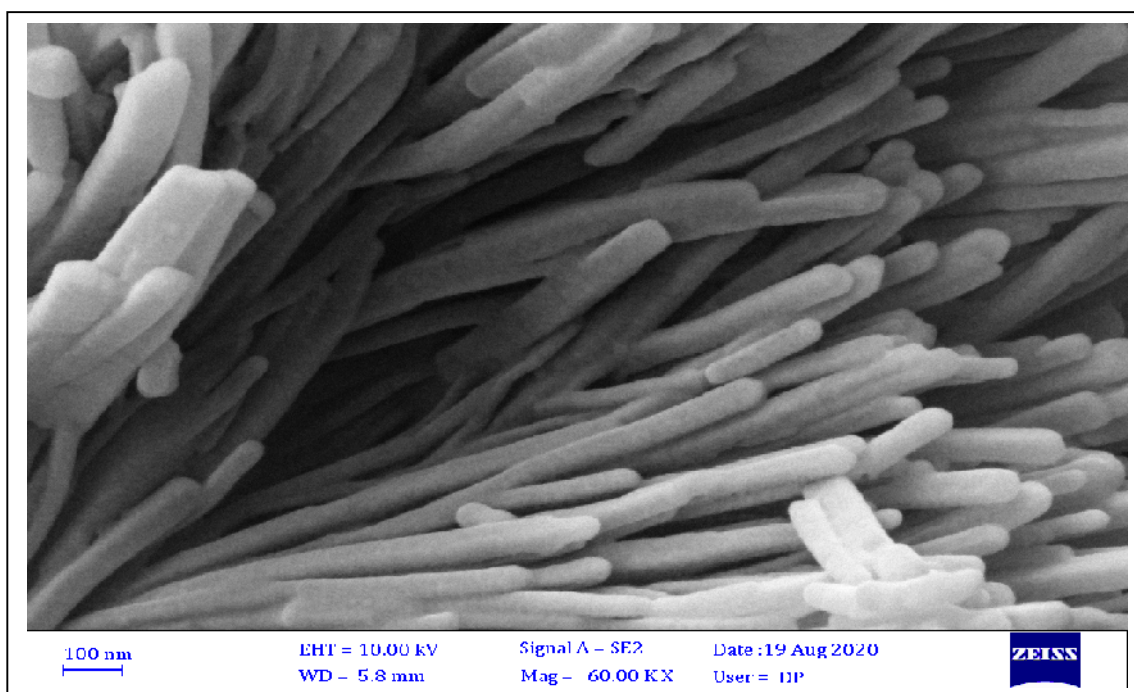
Figure 3.10: SEM of graph for Selenazone ligand (Z)

3.1.8. Determination of Selenium content in ligand (Z)

In order to investigate the selenazone ligand (z) structure, the selenium content in ligand (z) was measured by using atomic absorption spectrophotometer via hydride generation method that was carried out after the digestion operation for the sample in acidic medium [105]. The result indicates the agreement between the theoretical content value of selenium with the measured value of selenium in the sample. This agreement between the values refers to the correction for the suggested structural formula to selenazone ligand (z) as is exehibted in Table 3.1. The result of selenium content is shown in Table 3.5 .

Table 3.5 : The selenium content in Z ligand

Compound	M.Wt	Concentration from AAS (ppb)	Selenium content %	
			found	calculated
Z	303.2	18.911	26.86	25.72

3.2. Characterization of Complexes for ligand (Z)

The synthetic complexes have many physical properties such as the stability at room temperature , non hygroscopic and they are insoluble in most of the common organic solvents that were examined except for the nickel complex which is soluble in DMSO at a room temperature. Some physical properties of the prepared complexes appeared in Table 2.3. The complexes were characterized by using several techniques such as FT-IR spectroscopy, UV-Vis analysis, Nuclear magnetic resonance spectroscopy for hydrogen and isotopic of carbon, molar conductance measurements, Thermal analysis (TG/DTG) and the metals content of complexes have been measured by using atomic absorption spectroscopy.

3.2.1. FT-IR Spectroscopy

FT-IR spectrum gives a good proof about the sites of binding when it compared the ligand spectrum with IR spectra of their complexes . The IR spectra of complexes have revealed new bands when compared with IR spectrum of ligand at 573 , 574 , 578 and 580 cm^{-1} that due to stretching vibration of C-Se group in lead , cadmium , cobalt and nickel complexes respectively. On the other hand , the band of C=Se group that was shown in ligand spectrum at 979 cm^{-1} disappeared when compared with the complexes spectra, indicating the change in configuration formula of ligand structure after the complexation process through the convertion of carbon selenium double bond to a single bond . this leads to have new bands at 2207 , 2260 ,2177 and 2308 cm^{-1} in IR spectra of complexes , which were attributed to Se-H group [106,107]. This change that occurs in configuration formula of ligand during the complexes process leads to form imine group via proton transition from amine group into selenium atom that is connected with carbon neighbor atom. New bands in spectra complexes have appeared for lead , cadmium , cobalt and nickel complexes at 1635 , 1645 , 1622 and 1633 cm^{-1} respectively due to imine group formation . The stretching vibration of amine group shown in IR spectrum of ligand and their complexes at 3278 , 3266 ,3267 and 3280 cm^{-1} respectively occurs for changing in a wave number (Δv = 2-12 cm^{-1}) in complexes spectra due to the participation by the lone pair of electrons on the nitrogen atom to form the complexes. On the other hand, the band at 1226 cm^{-1} which results from C-N group in free ligand (z) is shifted to a higher wave number about (Δv = 21-37 cm^{-1}) in all complexes except for the cadmium complex which recorded the shift to a lower wave number at (Δv = 4 cm^{-1}). These results confirm the participation of amine group in complexes formation [94 ,108]. The azo group N=N was recorded in IR spectrum of free ligand at 1494 cm^{-1} that was shifted to a lower wave number about (Δv =4-25 cm^{-1}) in all complexes spectra which indicate

the participation of the azo group in coordination to the metal ions [109]. Furthermore , new bands in complexes spectrum were shown at (3404-3450) and (455-648) cm^{-1} which was attributed to hydroxyl and M-N groups respectively . All the results of IR spectra are shown in Table 3.2 and Figures 3.11 -3.14 .
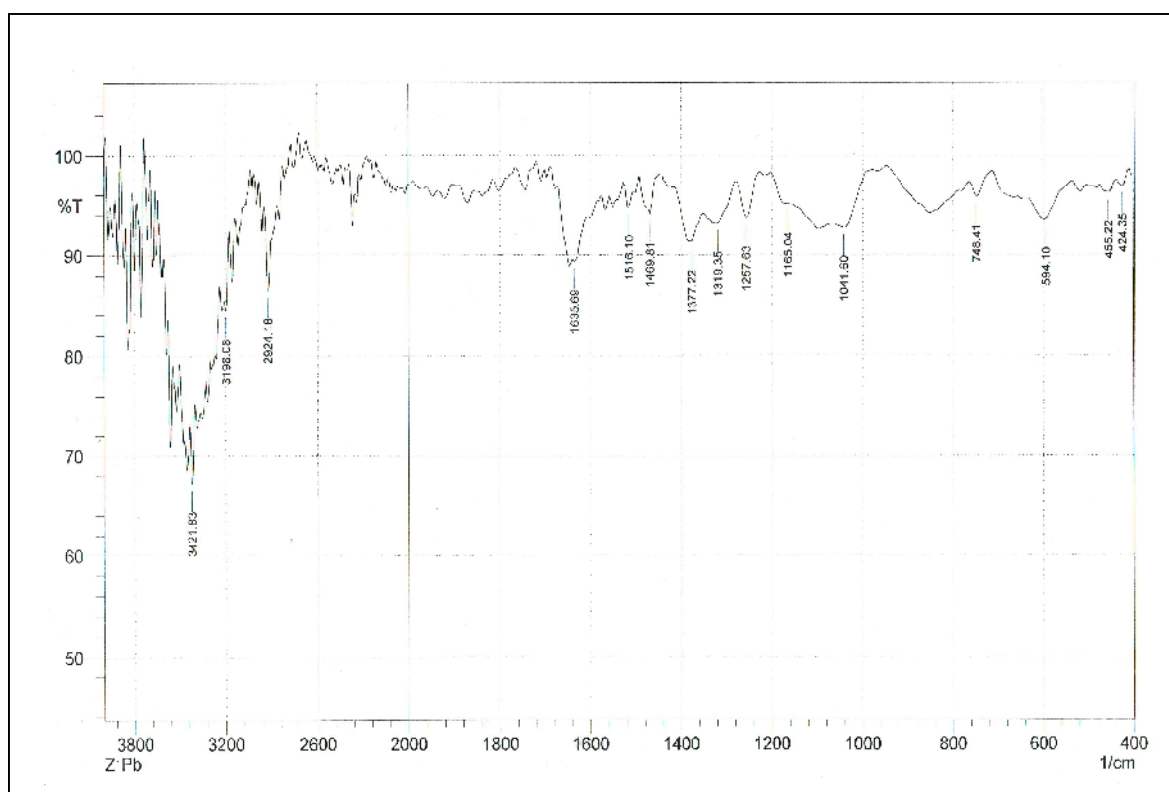
Figure 3.11: IR spectrum of Lead complex
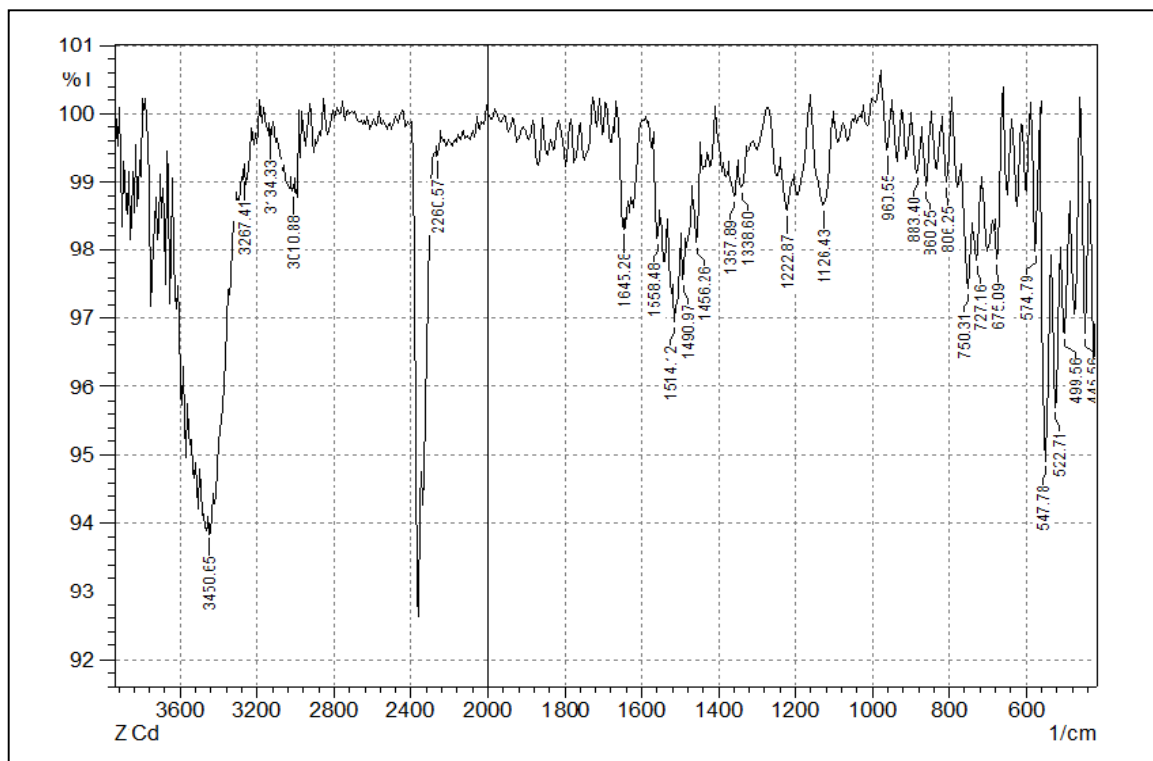
Figure 3.12: IR spectrum of Cadmium complex
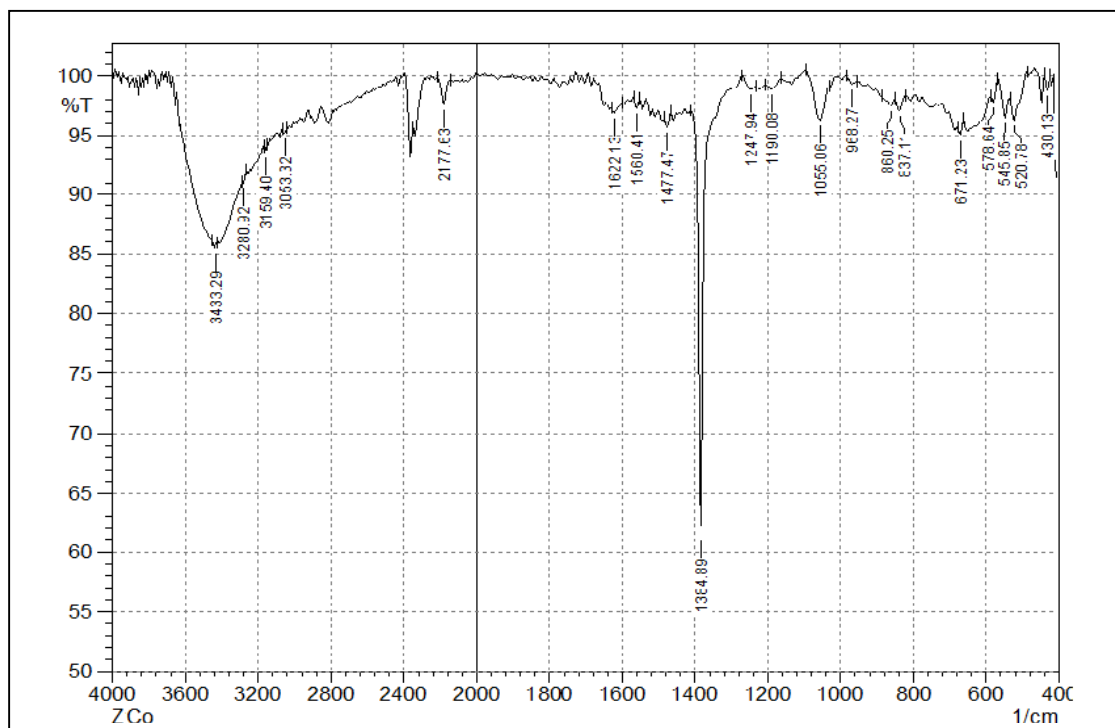
Figure 3.13: IR spectrum of Cobalt complex
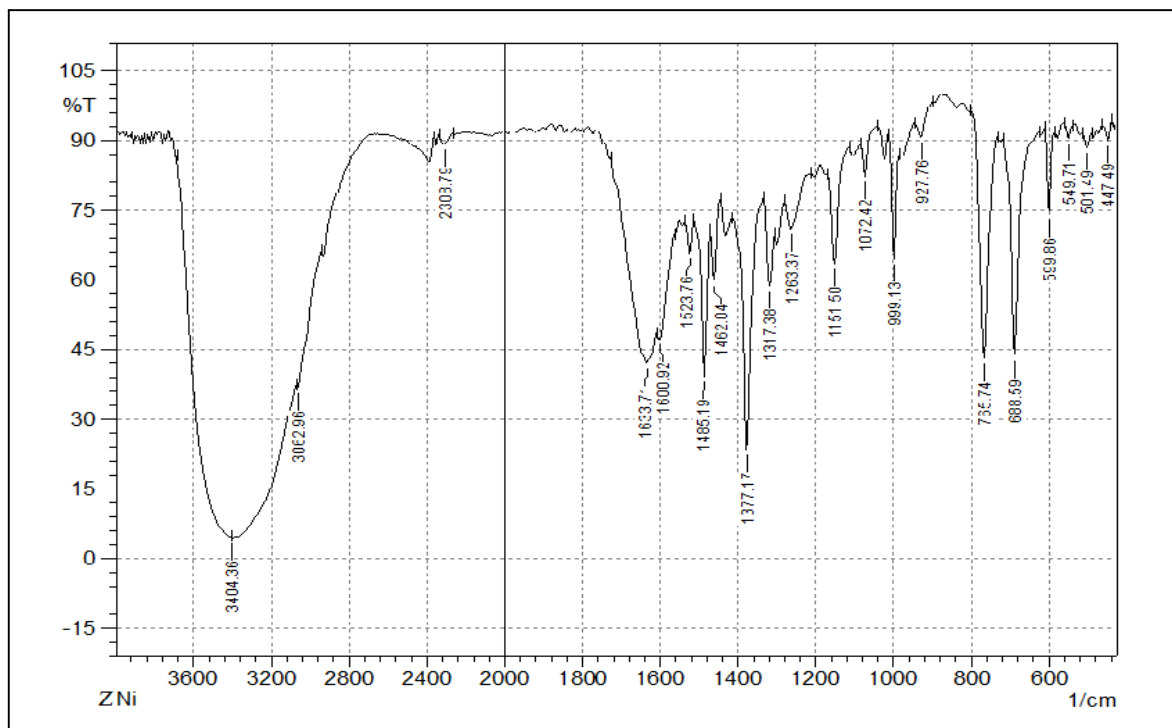
Figure 3.14: IR spectrum of Nickel complex

3.2.2. UV-Vis Spectroscopy

The ultraviolet-visible spectra have been utilized in order to characterize the ability for complexes formation by the participation of functional group (chromophore) that it is responsible for absorbing the light of ultraviolet-visible radiation in ligand structure towards the involvement with the metal ions [94 ,110]. The electronic absorption spectra of complexes have not been recorded because of their insoluble in several common organic solvents except for the nickel complex which is soluble in DMSO solvent at a room temperature. The electronic spectrum of nickel complex was recorded within the range 250-800 nm that exhibited the strong band at 261nm which is attributed to the transition motions of phenyl rings. Moreover, the wavelength of this peak is unchanged   when compared with selenazone ligand (z) spectrum where , the result refers relatively to the unshared phenyl rings in complexation formation. The transition bands that appeared in

ligand spectrum at 296 , 413 and 535 nm are shifted in nickel complex spectrum towards a red shift and hypochromic effect at 328 ,420 and 549 nm , indicating that the nitrogen atom in azo and amine groups were involved for coordinating the complexation with nickel ions. In this case, a new band was shown at 666 nm in complex spectrum that occurred due to d-d transition [111] .
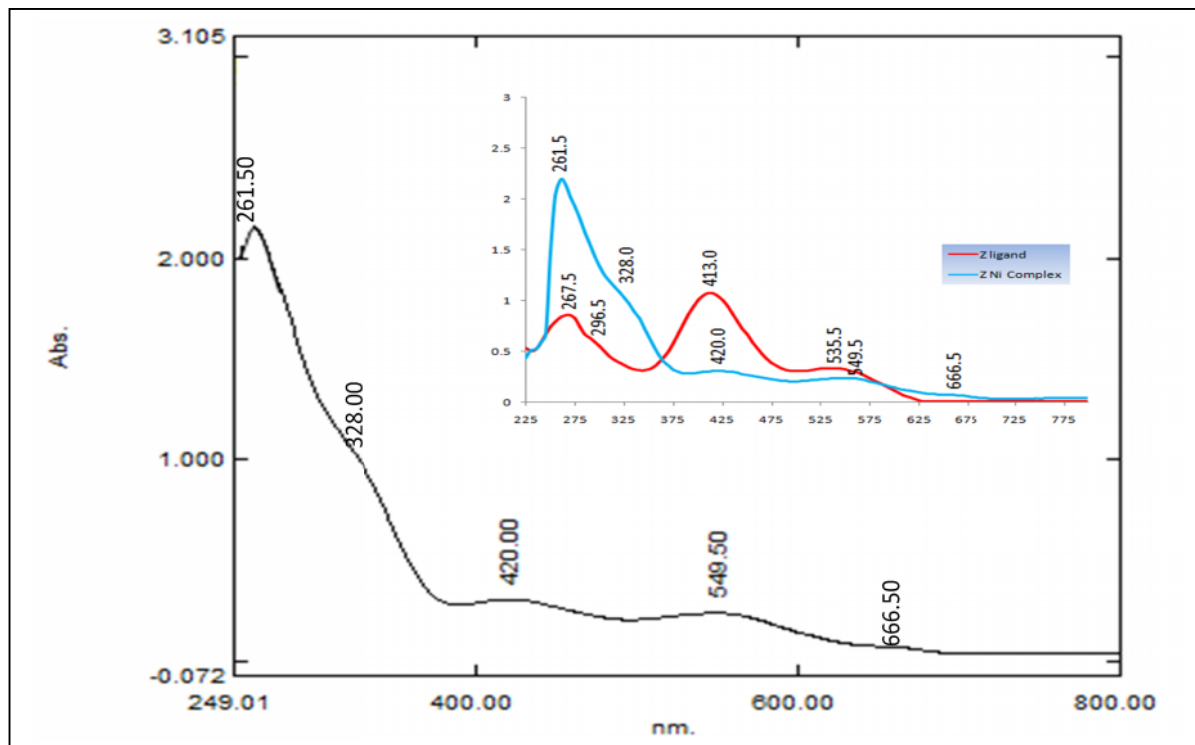
Figure 3.15The UV-Vis spectrum of Nickel complex

3.2.3. [1]H and [13]C- Nuclear magnetic resonance spectroscopy

In order to diagnose the complexes structure by knowing the functional group that have the ability to share for complexing process with metal ions. So, the ^{1}H-NMR and ^{13}C-NMR spectroscopy was utilized to characterize the organic and organometallic compounds, particularly in the coordination compounds when applied to the comparison spectral among the ligand with their complexes . Generally , the complexes that have paramagnetic properties can not be measured

in ^{1}H-NMR technique because the paramagnetic properties of materials affected on the relaxation time of proton. Thus the signals appeared as a broad [82,112]. The nuclear magnetic resonance of proton spectrum was measured for nickel complex by using the DMSO-d_6 as a solvent at ambient temperature using frequency at 400 MHz , the multi signals were exhibited in spectrum of nickel complex in the range δ= 7.63-7.79 ppm which was due to the aromatic protons. Furthermore, a singlet signal was recorded at δ= 2.89 ppm, while the same chemical shift was shown in ligand spectrum as singlet signal at δ=2.33 and 2.48 ppm, due to the two non-equivalent of NH protons. The results indicate that amine group has relatively affected on complex spectrum when compared with the ligand spectrum. Thus , this group was shared to formation of nickel complex. The result of ^{1}H-NMR data of nickel complex is shown in Figure 3.16 .

The ^{13}C-NMR spectrum of nickel complex was measured in DMSO-d_6 as a solvent by using frequency 100 MHz. The data of analog carbon spectrum refer to show a signal at δ=168.76 ppm that is attributed to carbon atom (C_1) which is contacted directly with selenium atom. The signal of carbon atom ($C_{2,2'}$) in phenyl ring that is connected directly with nitrogen atom which was revealed at δ= 130.77 ppm. This signal relatively affected on the complex spectrum of nickel that confirms the amine group which has been shared in coordination to metal ion. Moreover, several of the signals that appeared in chemical shift at δ= 126.78 , 133.27 and 134.56 ppm were attributed to carbon atoms for phenyl ring system . The data of ^{13}C-NMR of nickel complex are listed in Table 3.3 and Figure 3.17 .
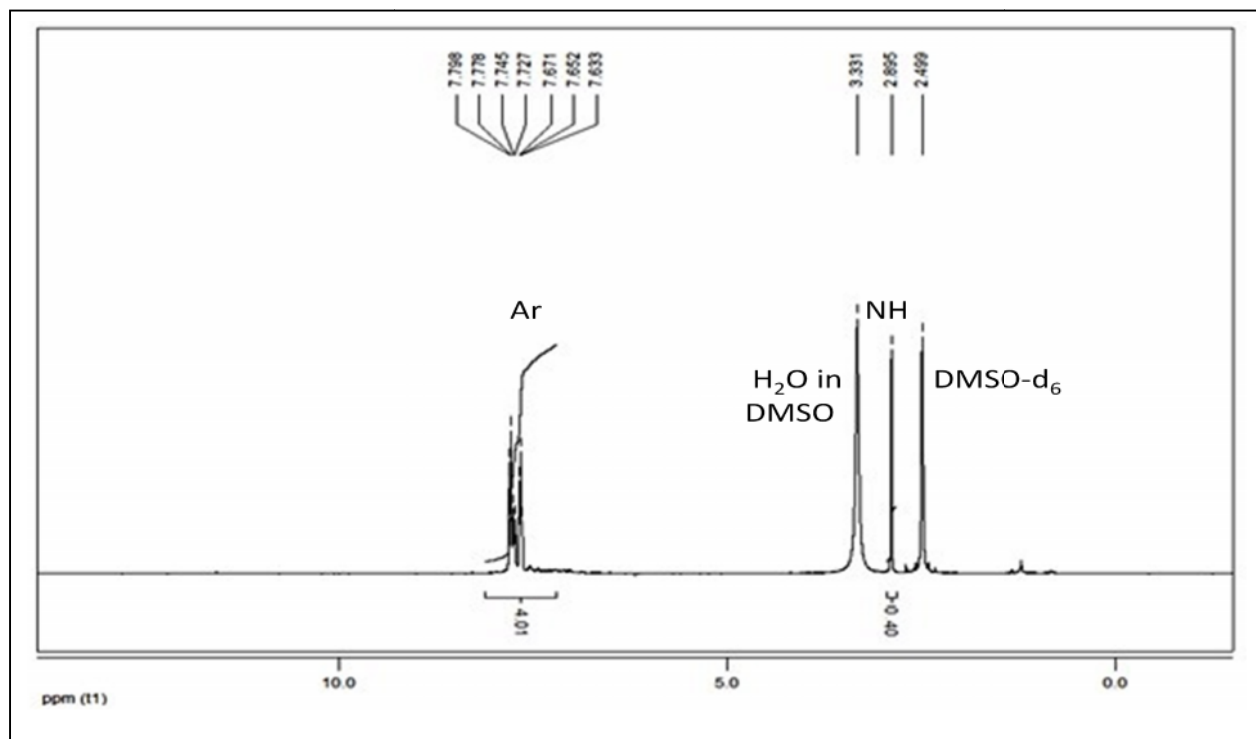
Figure 3.16: The ^{1}H-NMR spectrum of Nickel complex
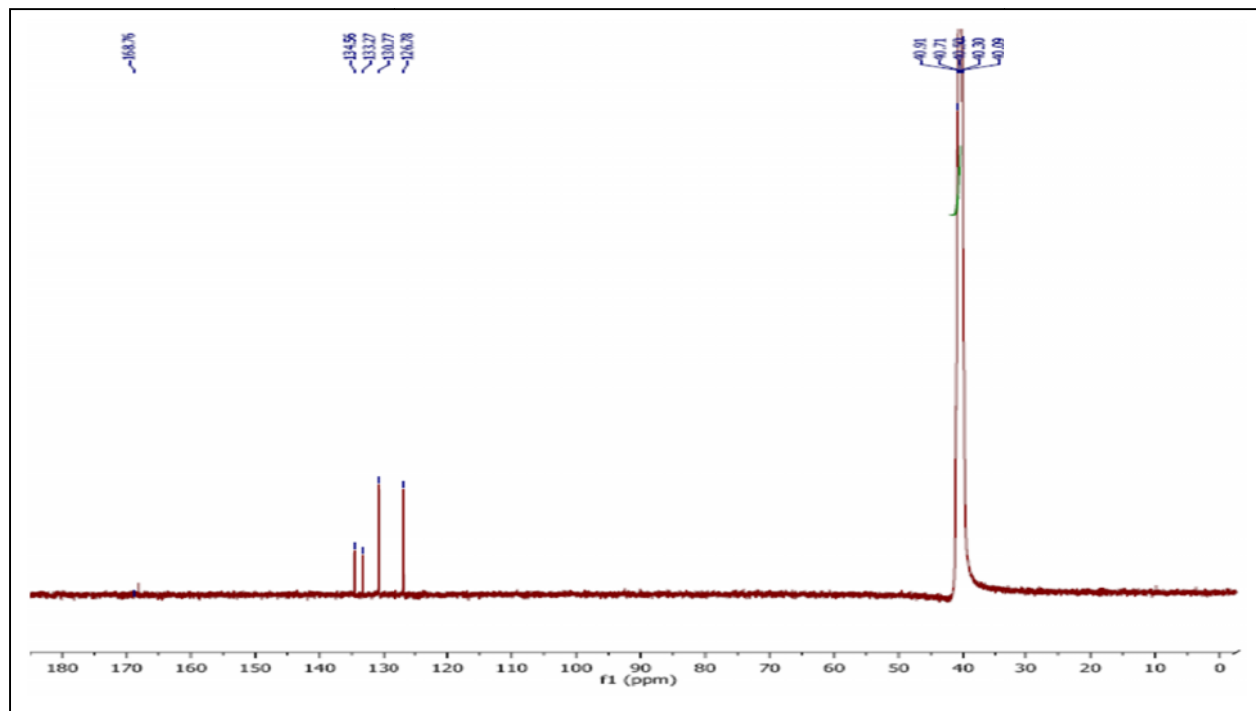
Figure 3.17: The ^{13}C-NMR spectrum of Nickel complex

3.2.4. Determination of metals content in complexes

The content ratio of complexes are measured through utilizing three methods are the continuous variation (Job method) , Mole-ratio and slope-ratio method. These methods are used for measuring the moles ratio between the ligand and the content of the metal in structure of complexes by using the UV-Vis spectrophotometer instrument [113,114]. There is another method for selecting the mole ratio of complexes by their destroyed in the acidic medium after its formation. Here, the solution of the complex is measured by using the atomic absorption spectroscopy moreover, this method is considered more accuracy , high resolution and fast when compared with other methods [94,115,116]. The current study employed the atomic absorption spectrophotometer as a method used to reveal the mole ratio for complexes after its synthesization. Generally, the results of the metals ratio measurements in synthetic complexes appeared consistent with the theoretical values which point out that the ligand associated with the metals in all complexes are 1:2 . The results of determination of metals in the configuration structure for complexes are listed in Table 3.6 .

Table 3.6 : Determination of metals content in synthetic complexes

Compound	M.Wt	Concentration from AAS (ppm)	Metal content %		Metal to ligand ratio
			found	calculated	
Pb(Z)₄	1472.1	1.262	14.21	14.07	1:2
Ni(Z)₄	1459.5	0.369	4.15	4.02	1:2
Co(Z)₄	1332.8	0.398	4.49	4.42	1:2
Cd(Z)₄	1377.3	0.732	8.25	8.18	1:2

3.2.5. The measurement of molar conductance

The measurement of molar conductance is carried out in order to determine the electrolytes nature of complexes in their solutions and identified the structural formula of these complexes. The high values of molar conductance refer to the electrolyte nature for complexes solution and also, confirm the existence of the anions, outside the coordination sphere, while the low values of molar conductance indicate the non-electrolyte nature for complexes solution which refer to absent the free anions in the outside of the coordination sphere [82,117, 118]. The molar conductance values have been calculated by using the equation is following :

$$\Lambda_m = \frac{K \times 1000}{C}$$

Where : Λ_m - Molar conductance (ohm^{-1} cm^2 mol^{-1})   , C- Concentration solution (mol L^{-1}) and K- Specific conductance (ohm^{-1} cm^{-1}) .

While the specific conductance can be calculated by using the equation,given below :

$$K = G \times A$$

Where **:** G - conductivity (ohm^{-1}) and A- Cell constant (cm^{-1}) .

The molar conductance data for complexes solution were measured in hot solvent of DMSO because the prepared complexes with lead, cadmium and cobalt are insoluble in most commonly solvents except for the hot DMSO, they suffered from the recrystallization process at less than 75 ℃ so, the measurements of molar conductance were carried out by utilizing hot DMSO at 75 ℃. The results have recorded low values of molar conductance for lead , cadmium and cobalt complexes that refer to the non-electrolyte nature [94,108,119], while the nickel

complex revealed a high value of molar conductance at $80.71[118](\text{ohm}^{-1}\text{cm}^2\text{mol}^{-1})$ which indicates the electrolyte nature. The data of molar conductance are shown in Table 2.3 .

3.2.6. Thermal analysis of complexes

Thermogravimetric analysis is a useful technique that provides more information about the configuration of the structure of organic and inorganic compounds, leading to the diagnosis of these compounds. The analysis can assist in studying the important parameters such as the thermal stability of the compound, water molecules (lattice or coordinated), compounds mechanism of decomposition and in determining the quality and quantity of the residual amount [120,121]. The thermal analyses such as thermogravimetric (TG) and differential thermo analyses (DTA) were recorded in the thermal range from a room temperature to 1200ºC under the nitrogen gas flow. Also, it used the heating rate at 10 ºC/min. The results of thermal analyses of all complexes are explained as follows :

- Thermal analysis of Lead complex $Pb(Z)_4$

   The thermal analysis curve (TG/DTA) of the lead complex(Figure 3.18) showed four decomposition steps. The first step is represented in two degradation steps, combined in the extent 20-255ºC (DTA_{max} 224ºC) with a weight loss ratio of 3.28 % (theoretical 3.66%). This is consistent with the loss of three molecules of water (one molecule of lattice water and two molecules of coordinated water) [94,119] as they are explained in the equation 1.

$$\text{Step 1}^{st}\, [Pb(Z_4)(H_2O)_2].H_2O \xrightarrow{\;20\text{-}255^0C\;} [Pb(Z_4)] \quad + 3H_2O \quad ....(1)$$
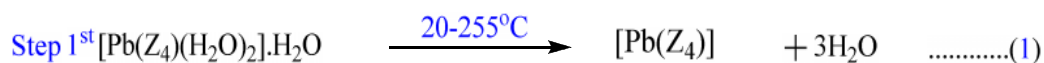
The second step start at 260ºC to 525ºC (DTA_{max}467ºC) with the mass loss of 72.22% (theoretical 72.51%) which indicates the loss of (two molecules of ligand (z) and two molecules of $C_8N_3H_6Se$) . The third and fourth steps started in the range

of 530-610ºC (DTA$_{max}$540) and 615-970ºC (DTA$_{max}$713ºC) with a mass loss of 7.16%(theoretical 7.18%) and 36.89%(theoretical 36.49%), respectively. This was attributed to the loss of one molecule of N$_2$and also, one molecule of C$_{10}$H$_{10}$. The residual amount ratio in the final of degradation steps is 15.02 % (theoretical 15.16%) which was attributed to lead oxide PbO. Generally, from these results the structural formula of lead complex can be suggested Pb(Z)$_4$ as follows :
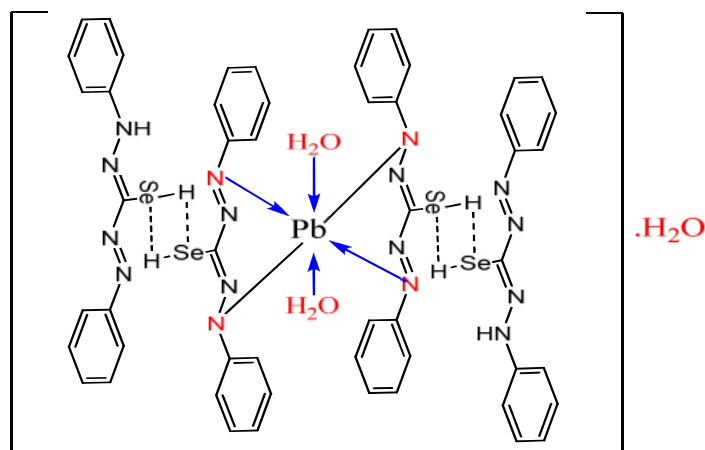
- Thermal analysis of Cadmium complex Cd(Z)$_4$

Three degradation steps were revealed in the thermal analysis curve of cadmium complex (Figure 3.19), showed the endo-exothermic peaks, indicating a change in the phases [120-122]. The first decomposition stage showed an endothermic peak at 102 ºC, refering to the loss of one molecule of lattice water in the range of 30-155ºC (DTA$_{max}$ 100ºC) with a weight loss ratio of 1.028 % (theoretical 1.3%). The second stage also exhibited an endothermic peak at 230ºC in the DTA curve by the decomposition range of 160-255ºC (DTA$_{max}$ 230ºC) with a weight loss ratio of 2.031 % (theoretical 2.64%). This was attributed to the loss of two molecules of coordinated water as is explained in equation 2 and 3.

Step 1st [Cd(Z$_4$)(H$_2$O)$_2$].H$_2$O $\xrightarrow{30\text{-}155ºC}$ [Cd(Z$_4$)(H$_2$O)$_2$] $+$H$_2$O ....(2)

Step 2nd [Cd(Z$_4$)(H$_2$O)$_2$] $\xrightarrow{160\text{-}255ºC}$ [Cd(Z$_4$)] $+$ 2H$_2$O ....(3)
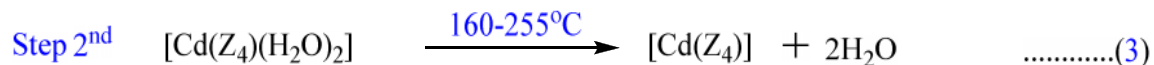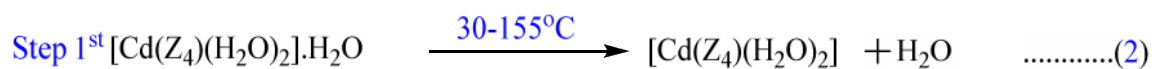
The third step appeared two exothermic peaks at 396.81 ºC and 508.11 ºC in the range 260-565ºC (DTA$_{max}$495ºC) with a mass loss 88.39% (theoretical 88.64%) that was appropriate with the loss $C_{49}H_{49}N_{16}Se_4$, while the residual amount ratio at 565 ºC is 11.61 % (theoretical 11.93%) was attributed to cadmium oxide CdO polluted with three carbon atoms [94,108]. Generally, from these results the structural formula of cadmium complex can be suggested $Cd(Z)_4$ it is corresponding with the form that is given below :
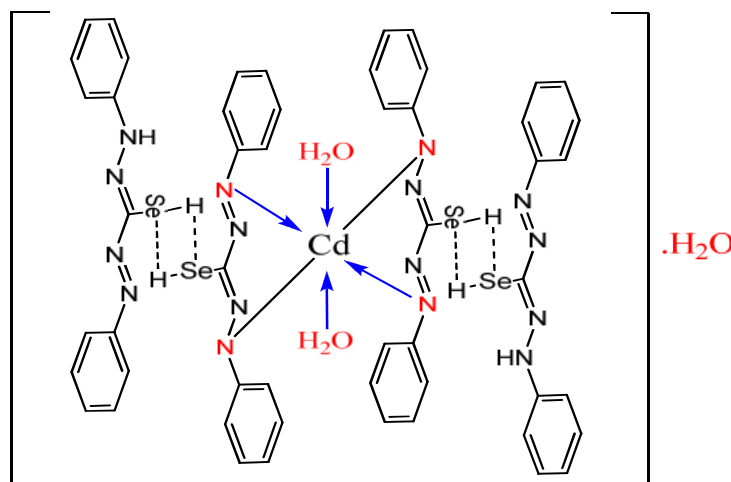
- Thermal analysis of Cobalt complex $Co(Z)_4$

The decomposition of the cobalt complex was revealed by employing five degradation steps (Figure 3.20). The first step was at the extent of 30-120ºC (DTA$_{max}$75ºC) with a weight loss ratio of 1.86% (theoretical 2.02%). That is appropriate with the loss of 1.5 molecules of lattice water. Additionally, two molecules of coordinated water with cobalt ion are lost in the range of 125-250ºC (DTA$_{max}$ 216ºC) that is corresponding with a ratio of 2.71% (theoretical 2.75%). the decomposition steps were explained clearly in the equation 4 and 5 .

Step 1st $[Co(Z_4)(H_2O)_2].1.5H_2O$ $\xrightarrow{30\text{-}120ºC}$ $[Co(Z_4)(H_2O)_2]$ $+ 1.5H_2O$ ....(4)

Step 2nd $[Co(Z_4)(H_2O)_2]$ $\xrightarrow{125\text{-}250ºC}$ $[Co(Z_4)]$ $+ 2H_2O$ ....(5)
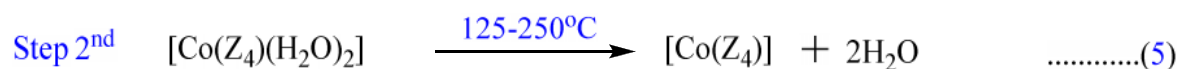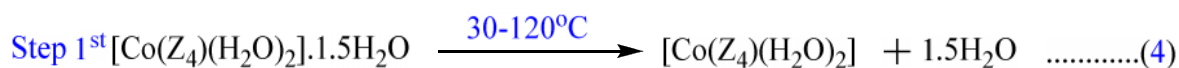
The third step start at 255ºC to 520ºC (DTA$_{max}$500ºC) with a mass loss 69.12% (theoretical 68.54%) which indicates the loss of two molecules of ligand (z) and two molecules of $C_7N_3H_5$, while the fourth and fifth steps started in the range 525-660ºC (DTA$_{max}$624) and 665-980ºC (DTA$_{max}$955ºC) with a mass loss 15.53 and 5.03 %, respectively. Hence, the remaining amount at 980ºC was identified as cobalt oxide with a constant weight ratio of 5.75 % (theoretical 5.62%). The results agree with the suggestion of the structural formula of cobalt complex Co(Z)$_4$ that shows the elucidation in the form, given as follows :
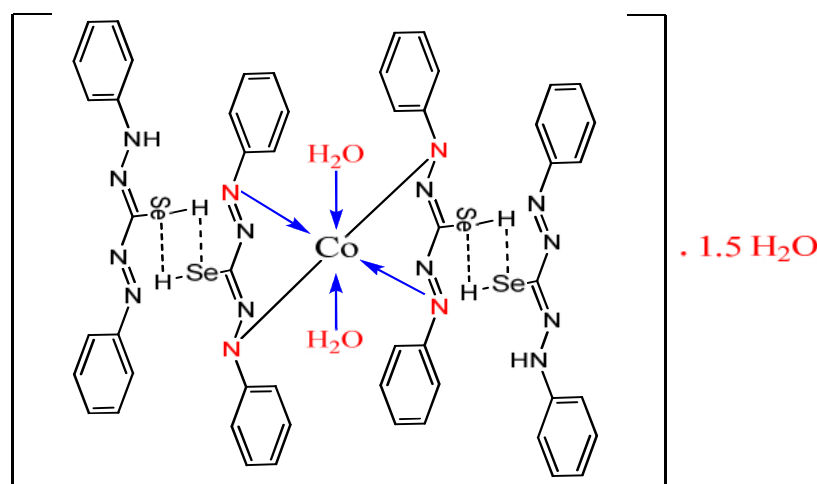
• Thermal analysis of Nickel complex Ni(Z)$_4$

Nickel complex has five degradation steps, appeared the endo-exothermic peaks at 90.86,259.40 , 427.13 and 565.96 ºC in the differential thermal analysis curve which was revealed in the Figure 3.21 . The first step starts in the range of 30-110ºC (DTA$_{max}$ 90ºC) with a weight loss ratio of 5.50% (theoretical 5.54%), that is consistent with the loss of 4.5 molecules of lattice water that is located out of the coordination sphere. On the other hand , the high value of molar conductance was measured for nickel complex solution in DMSO which confirms the existence of anions out of the coordination sphere. So, the second step was recorded in the range of 115-190ºC (DTA$_{max}$ 175 ºC) that attributed to the loss of two molecules of

coordinated water and one molecule of HCl. This is convenient with a lost weight of 5.49% (theoretical 5.25%) . The results are shown in the equation 6 and 7 .

Step 1st $[Ni(Z_4)(H_2O)_2].4.5H_2O.Cl_2 \xrightarrow{30-110^oC} [Ni(Z_4)(H_2O)_2].Cl_2 + 4.5H_2O$ ....(6)

Step 2nd $[Ni(Z_4)(H_2O)_2].Cl_2 \xrightarrow{115-190^oC} [Ni(Z_4)].Cl + 2H_2O + HCl$ ....(7)
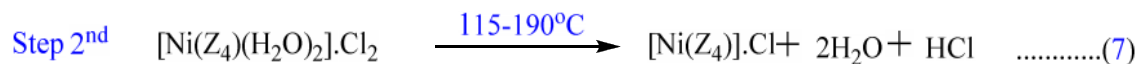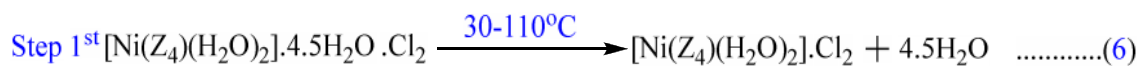
The strong peaks of exothermic appeared at 259.40 , 427.13 and 565.96 ℃ and reflected the change that occured in the phases during the thermal decomposition process . The residual amount after the last step at 690℃ was suitable with 4.99% (theoretical 5.12%) due to nickel oxide NiO. From these data, the structural formula of nickel complex $Ni(Z)_4$ can be suggested as follows :
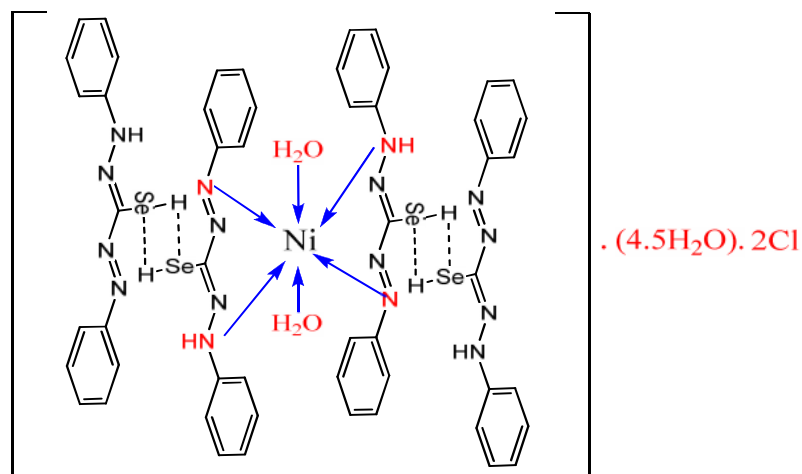
Accordingly, the spectroscopic and thermal results, the octahedral geometry structure was suggested in all the prepared complexes . The data of the thermal analysis for complexes are listed in Table 3.7 .

Table 3.7 : The degradation thermal steps for all complexes

derived from selenazone ligand (z)

Compound	TG / DTA				Mass loss %
	step	T_i °C	$T_m(DTA_{max})$ °C	T_f°C	
Pb(Z)₄	1st	20	224	255	3.28
	2nd	260	467	525	72.22
	3rd	530	540	610	7.16
	4th	615	713	970	36.89
Cd(Z)₄	1st	30	100	155	1.028
	2nd	160	230	255	2.031
	3rd	260	495	565	88.39
Cd(Z)₄	1st	30	75	120	1.86
	2nd	125	216	250	2.71
	3rd	255	500	520	69.12
	4th	525	624	660	15.53
	5th	665	955	980	5.03
Cd(Z)₄	1st	30	90	110	5.5
	2nd	115	175	190	5.49
	3rd	195	259	360	29.26
	4th	365	427	480	8.04
	5th	485	565	690	45.46
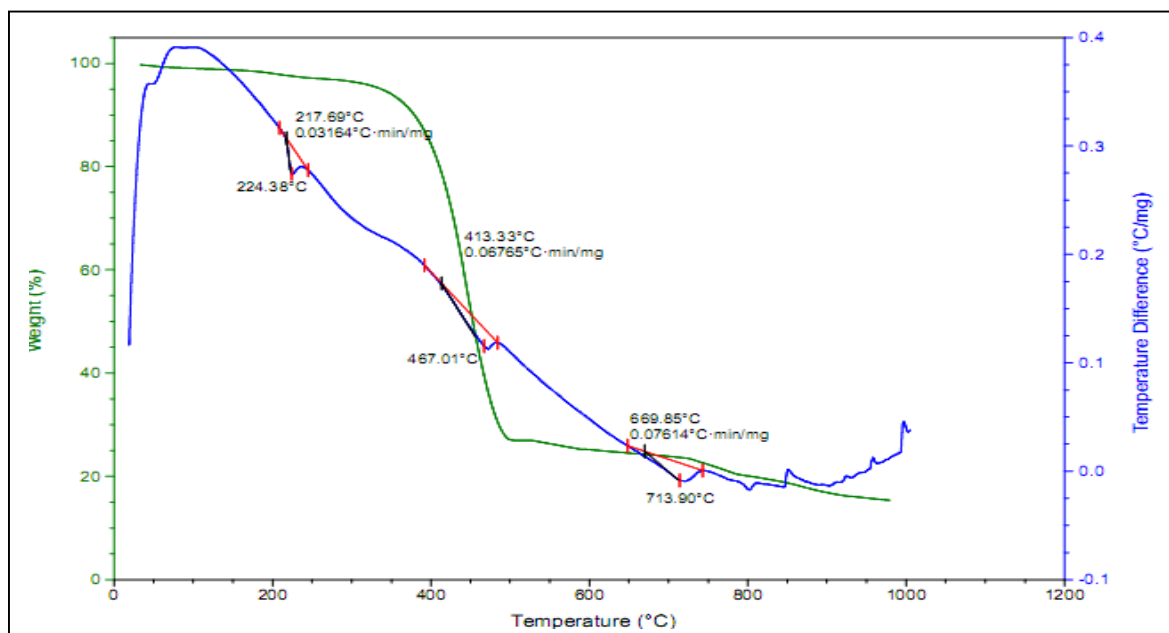
Figure 3.18: The TG/DTA curve of lead complex
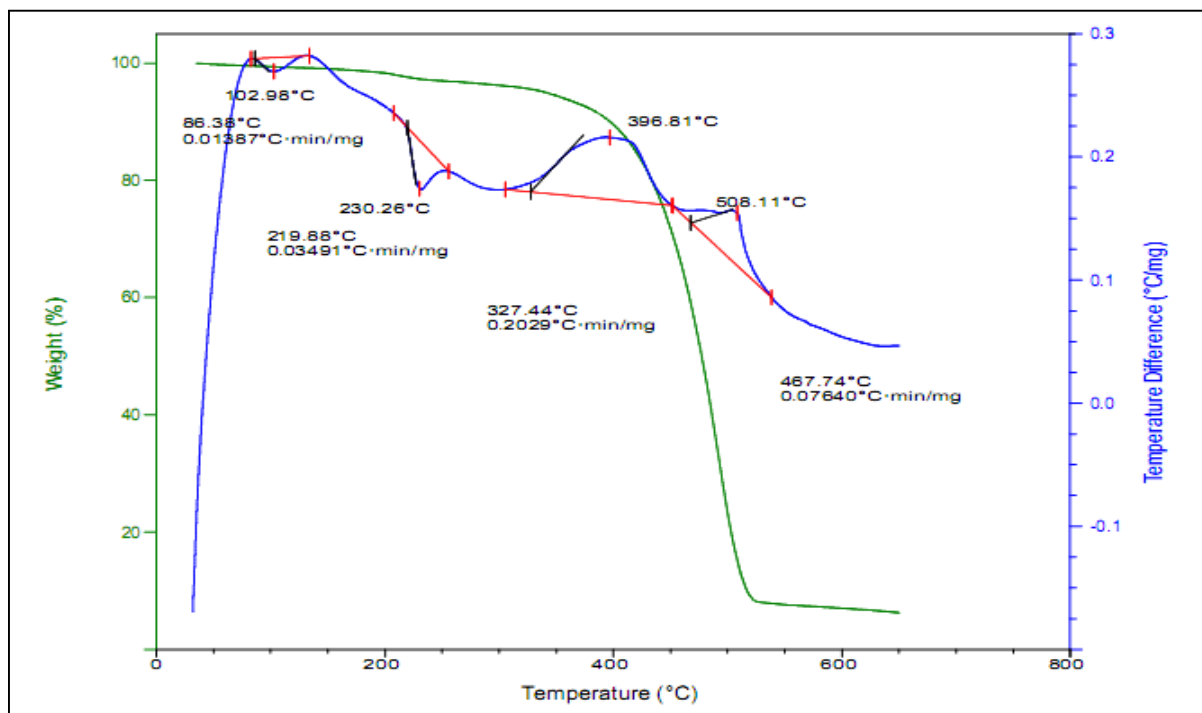
Figure 3.19: The TG/DTA curve of cadmium complex
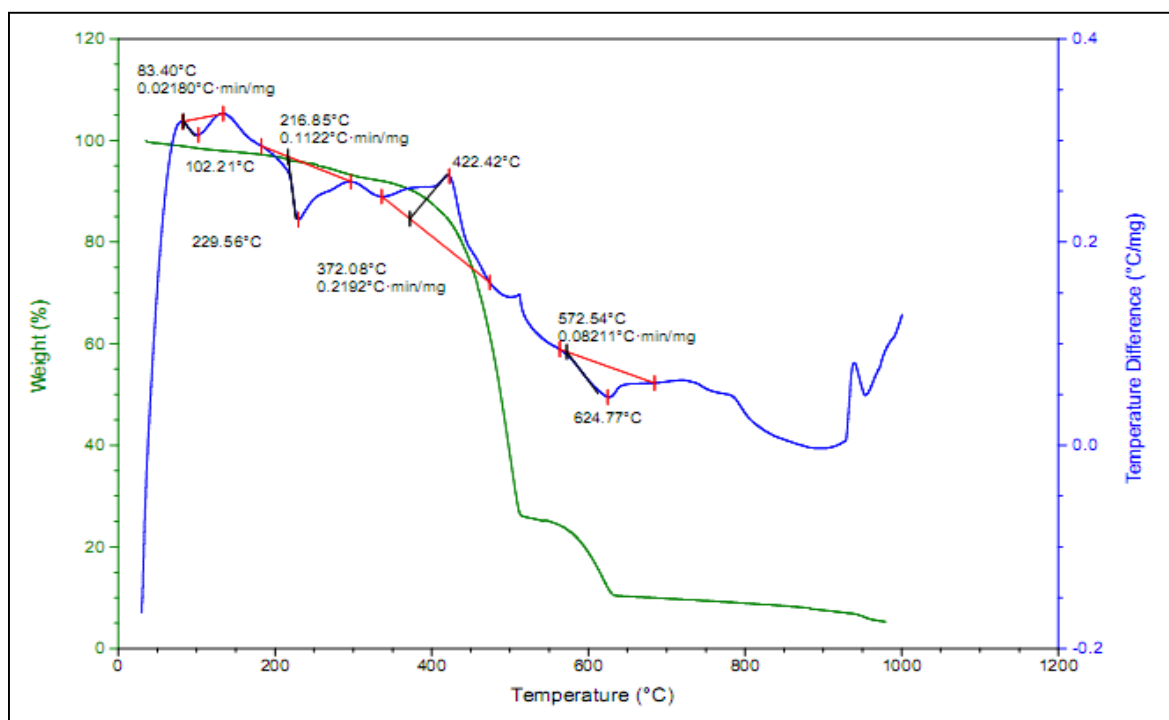
Figure 3.20: The TG/DTA curve of cobalt complex
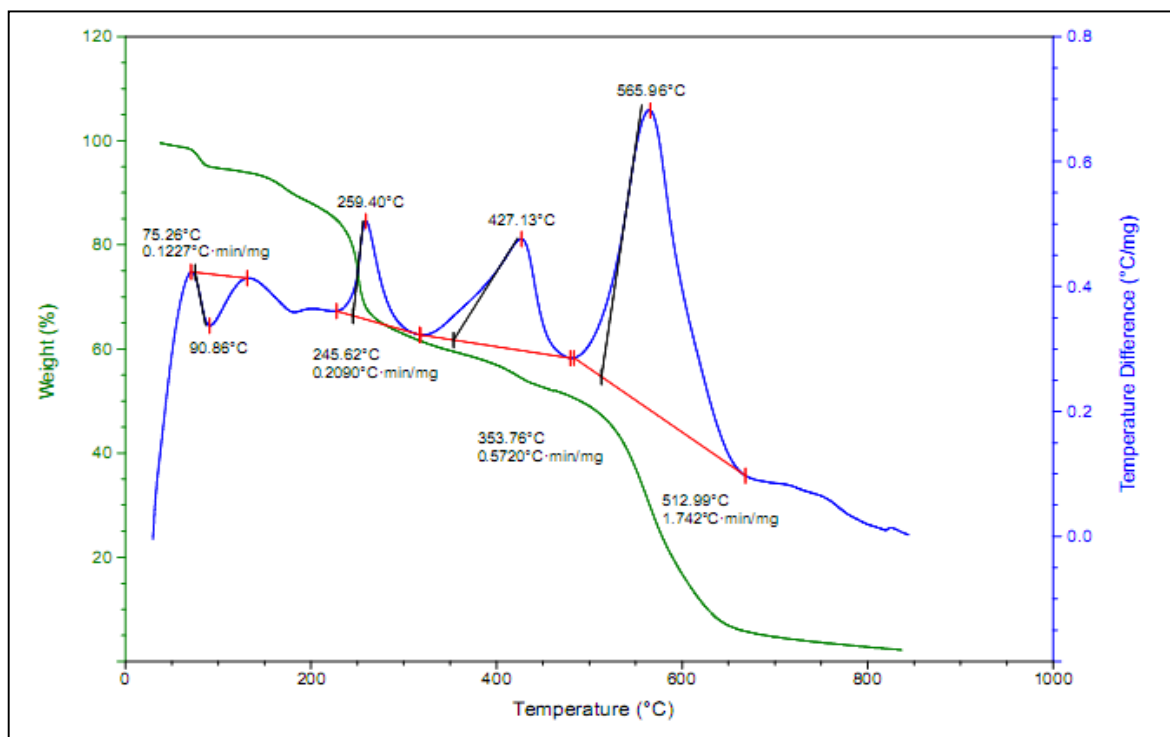
Figure 3.21: The TG/DTA curve of nickel complex

3.3. Calculation of kinetic parameters

The thermal dehydration and degradation of complexes have been studied kinetically by utilizing three types of kinetic models including Coast-Redfern , Broido and Horowitz-Metzger[123,124]. The thermogravimatric analysis TG provided more information about decomposition mechanism , thermal stability , endo-exothermic reactions and identified the spontaneous or the non-spontaneous decomposition reactions of complexes. Many of the thermodynamic activation parameters of degradation process and dehydration of complexes , reaction orders (n), activation energy (E), pre-exponential factors (A), enthalpy of activation (ΔH), entropy of activation (ΔS) and Gipps free energy change of the degradation (ΔG) are computed graphically from TG/DTA data by employing three kinetic models and carried out by making comparison among them. The values of activation energy (E), reaction order (n) and pre-exponential factors (A) are affected by several factors like flow rate and nature of gas used, heating rate and sample

weight. In addition, the mathematically methods that were used to evaluate the data [123]. The kinetic models that were utilized represent one of the integral methods for computing the thermodynamic parameters and they can be summarized as follows :

- **Coats-Redfern Method**

The integral methods represented more accurcy when compared with the others methods, Coast-Redfern method is considried a more accurate than the other methods that were used in the current study where ,the error ratio is approxmatly 1% in calculation of the activation energy and 2% for calculting Arrhenius factor (pre-exponential factor) , this values of error ratio are much less than the other kinetic models [124,125]. The relation of Coats-Redfern can be defined in the following form :

$$\log \left[\frac{\log \frac{Wf}{Wf\text{-}Wt}}{T^2} \right] = \log \left[\frac{AR}{\Theta E} \left(1\text{-} \frac{2RT}{E} \right) \right] \text{-} \frac{E}{2.303RT}$$

Where:

Wf : is equal of mass loss for during the thermal stage .

Wt   : is represent of mass loss at any temperature within the thermal stage .

T   : The absolute temperature .

R   : is the constant of gases (8.31 J mol^{-1} K^{-1})

A   : the Arrhenius factor (S^{-1}) .

Ɵ   : The heating rate 10 ℃/min .

E   : The activation energy (KJ mol^{-1}) .

The value of term 2RT is much less than activation energy so, the term(1-(2RT/E)) is neglected in all the previous studies [82,126,127]. The degradation steps in all complexes exhibit the consistent with the first order reaction in all steps. Moreover, the activation energy and Arrhenius factor are computed graphically

from slope and intercept respectively when plotting between the left-hand side in Coast-Redfern equation versus 1000/T , while the thermodynamic parameters have been computed by using the relations [128-130], that are explained as follows :

$$\Delta H^o = E - RT \quad , \quad \Delta G^o = \Delta H^o - T\Delta S^o \quad , \quad \Delta S^o = R \ln (A \, h/K_B T_S)$$

Where : h , is Plank's constant (6.6262×10^{-34} J S) . K_B , is Boltzmann constant (1.3806×10^{-23} J K^{-1}) . T_S , represents DTA$_{max}$.

- **Broido Method**

The activation energy for each step in the thermal analysis has been computed through developing kinetic model suggested by Broido where , Broido equation can be shown as follows[123] :

$$\ln \ln \left[\frac{1}{Y} \right] = \frac{-E}{RT} + \text{Constant}$$

Where :

$Y = (Wt - W\infty)/ (W_o - W\infty)$.

Wt , W_o and $W\infty$, are the weight loss at any temperature , initial weight and the weight at infinity time respectively . The activation energy is computed graphically from slope when plotting between the left-hand side in Broido equation versus 1000/T . The change of enthalpy for each pyrolysis step has been evaluated by using the equation described and shown above.

- **Horowitz -Metzger Method**

Horowitz and Metzger have conducted a new method for calculating the activation energy (E) to each thermal analysis step.The equation utilized for the calculation of activation energy is shown as follows :

$$\ln \ln \left[\frac{W_o}{Wt} \right] = \frac{\Theta E}{RT_s^2}$$

Where :

W_o , The initial weight .

Wt , The weight loss at any temperature .

Ꮎ   , is the difference between the peak temperature and the temperature at a particular weight loss ($Ꮎ = T - T_s$) .

   The activation energy can be obtained from slope when plotting between the left-hand side in Horowitz - Metzger equation against Ꮎ [123,124, 131] as well as , The pre-exponential factor (Arrhenius factor) was calculated by using the equation in the following form [131] :

$$\frac{E}{RT_s^2} = \frac{A}{Ꮎ \; EXP(-E/RT_s)}$$

    The thermodynamic parameters can be computed by using the same equations that have been mentioned earlier . The correlation coefficient (R^2) and the thermo-kinetic data that used three models of kinetic equations are summarized in Table 3.8 ,3.9 and 3.10 .

Table 3.8: Kinetic – Thermodynamic parameters using

Coats-Redfern equation

Complex	Step	A (S^{-1})	E $(KJmol^{-1})$	ΔH $(KJmol^{-1})$	ΔS $(KJmol^{-1}K^{-1})$	ΔG $(KJmol^{-1})$	R^2
$Pb(Z)_4$	1st	23.66×10^{-3}	13.567	9.634	-0.279	142.014	0.960
	2nd	1.47×10^5	108.724	102.755	-0.153	212.782	0.989
	3rd	1.04×10^{14}	267.774	261.015	0.015	248.726	0.957
	4th	1.22×10^2	110.611	101.815	-0.215	329.787	0.969
$Cd(Z)_4$	1st	2.8307	23.837	20.736	-0.238	109.555	0.926
	2nd	1.387×10^7	90.929	86.831	-0.112	142.227	0.985
	3rd	4.735×10^3	93.405	87.019	-0.182	227.115	0.976
$Co(Z)_4$	1st	20.2979	27.425	24.532	-0.221	101.497	0.987
	2nd	1.025×10^3	53.046	48.988	-0.191	142.376	0.987
	3rd	2.11×10^2	643.365	636.938	-0.208	797.975	0.905
	4th	1.67×10^{15}	299.292	291.868	0.0373	258.478	0.993

	5th	2.057×10^2	122.573	112.363	-0.212	373.182	0.894
Ni(Z)$_4$	1st	2.524×10^5	52.968	50.0338	-0.142	100.475	0.964
	2nd	1.21×10^8	89.112	85.388	-0.093	127.291	0.991
	3rd	95.21×10^{-2}	30.263	25.873	-0.250	157.910	0.895
	4th	7.989×10^7	142.96	137.156	-0.100	207.444	0.953
	5th	4.368×10^6	156.621	149.654	-0.126	255.562	0.941

Table 3.9: Kinetic – Thermodynamic parameters using

Broido equation

Complex	Step	E (KJmol^{-1})	ΔH (KJmol^{-1})	R^2
Pb(Z)$_4$	1st	14.815	10.882	0.995
	2nd	104.571	98.602	0.990
	3rd	185.99	179.230	0.866
	4th	111.248	102.451	0.929
Cd(Z)$_4$	1st	21.040	17.939	0.882
	2nd	72.597	68.498	0.935
	3rd	97.420	91.034	0.989
Co(Z)$_4$	1st	20.661	17.768	0.984
	2nd	46.216	42.159	0.973
	3rd	702.927	697.148	0.952
	4th	249.898	242.474	0.965
	5th	123.132	112.923	0.895
Ni(Z)$_4$	1st	40.710	37.776	0.972
	2nd	77.978	74.253	0.975
	3rd	15.175	10.785	0.756
	4th	116.619	110.816	0.891
	5th	151.873	144.906	0.908

Table 3.10: Kinetic – Thermodynamic parameters using

Horowitz -Metzger equation

Complex	Step	A (S^{-1})	E $(KJmol^{-1})$	ΔH $(KJmol^{-1})$	ΔS $(KJmol^{-1}K^{-1})$	ΔG $(KJmol^{-1})$	R^2
Pb(Z)$_4$	1st	0.108	20.278	16.346	-0.267	142.738	0.989
	2nd	0.282	123.820	117.850	-0.262	306.478	0.968
	3rd	0.304	171.744	164.985	-0.263	378.910	0.851
	4th	0.115	109.154	100.358	-0.273	389.574	0.884
Cd(Z)$_4$	1st	0.186	21.734	18.633	-0.260	115.885	0.833
	2nd	0.368	75.903	71.805	-0.257	198.696	0.911
	3rd	0.257	128.611	122.226	-0.264	325.033	0.987
Co(Z)$_4$	1st	0.264	26.905	24.012	-0.257	113.533	0.967
	2nd	0.258	51.933	47.876	-0.260	174.873	0.950
	3rd	0.197	99.724	93.298	-0.266	299.155	0.964
	4th	0.385	265.166	257.742	-0.261	491.660	0.951
	5th	0.121	154.310	144.100	-0.274	480.844	0.864
Ni(Z)$_4$	1st	0.411	43.273	40.338	-0.253	129.893	0.963
	2nd	0.505	86.286	82.561	-0.253	196.340	0.962
	3rd	0.054	12.592	8.202	-0.273	152.822	0.725
	4th	0.281	116.329	110.526	-0.262	293.766	0.866
	5th	0.239	142.522	135.555	-0.265	357.957	0.871

The positive values of Gibbs free energy change (ΔG) refer to nonspontaneous reaction in all decomposition steps of complexes while ,the change of enthalpy (ΔH) in all decomposition steps of complexes recorded positive values that refer to all decomposition steps that are endothermic . The results of ΔH differ when compared with DTA data that can be attributed to change in temperatures that are much less and have not affected on the total temperature of the system, so, the system temperature do not tend towards negative values , which indicated to prefer of products formation [132] .The increases of activation energy values refer to increase in the thermal stability while , the negative values of entropy indicate the decomposition reactions process that occurs at a very low rate [94,108]. The correlation coefficient (R^2) and activation energy demonstrated highest values in

Coast-Redfern method when compared with Broido and Horowitz-Metzger methods while the change of enthalpy recorded positive values in the kinetic models. The method of Coast-Redfern indicated high values than the other methods, the free energy change recorded lower values in Coast-Redfern model than of Horowitz-Metzger . The values of entropy appeared to be converging between Coast-Redfern method and Horowitz-Metzger method. The decomposition steps plot for all complexes in three kinetic models are shown in Figures from 3.22 to 3.30 .
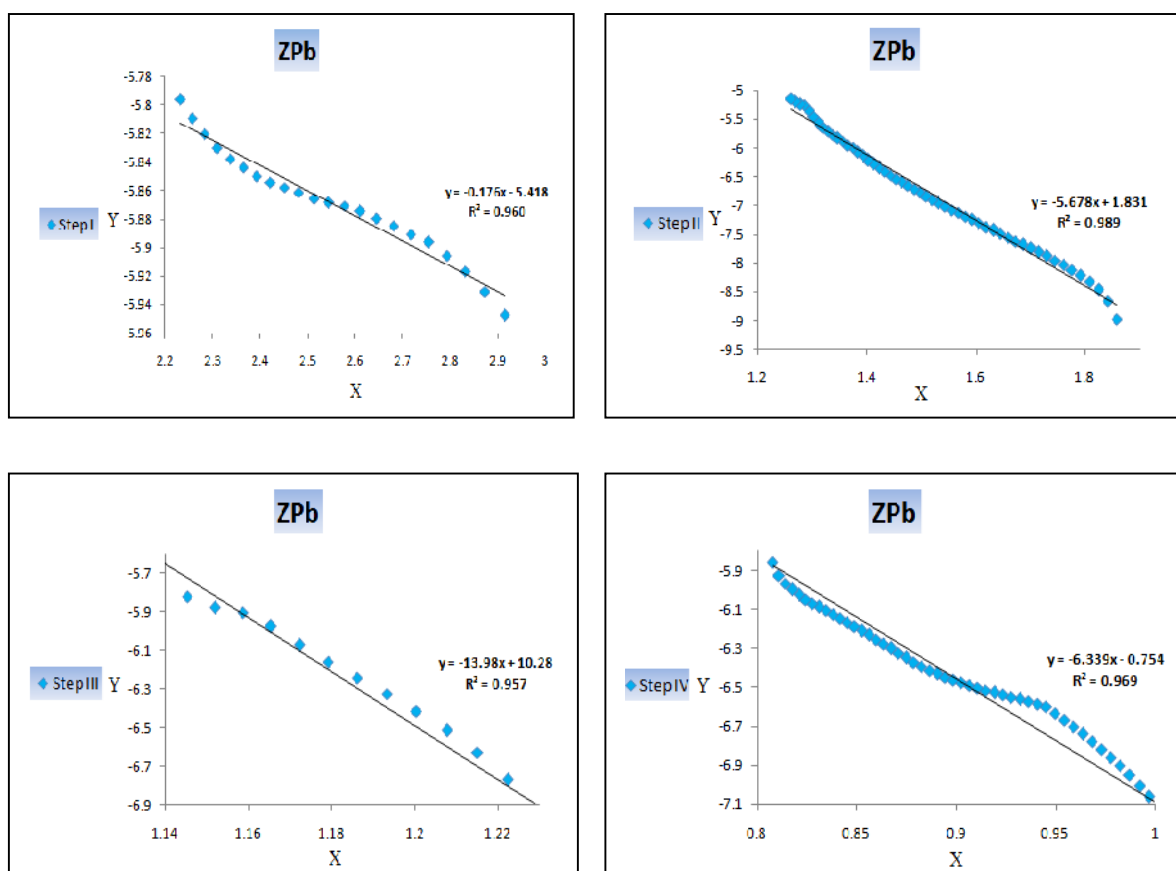
Figure 3.22 : Coast-Redfern plot of Pb complex
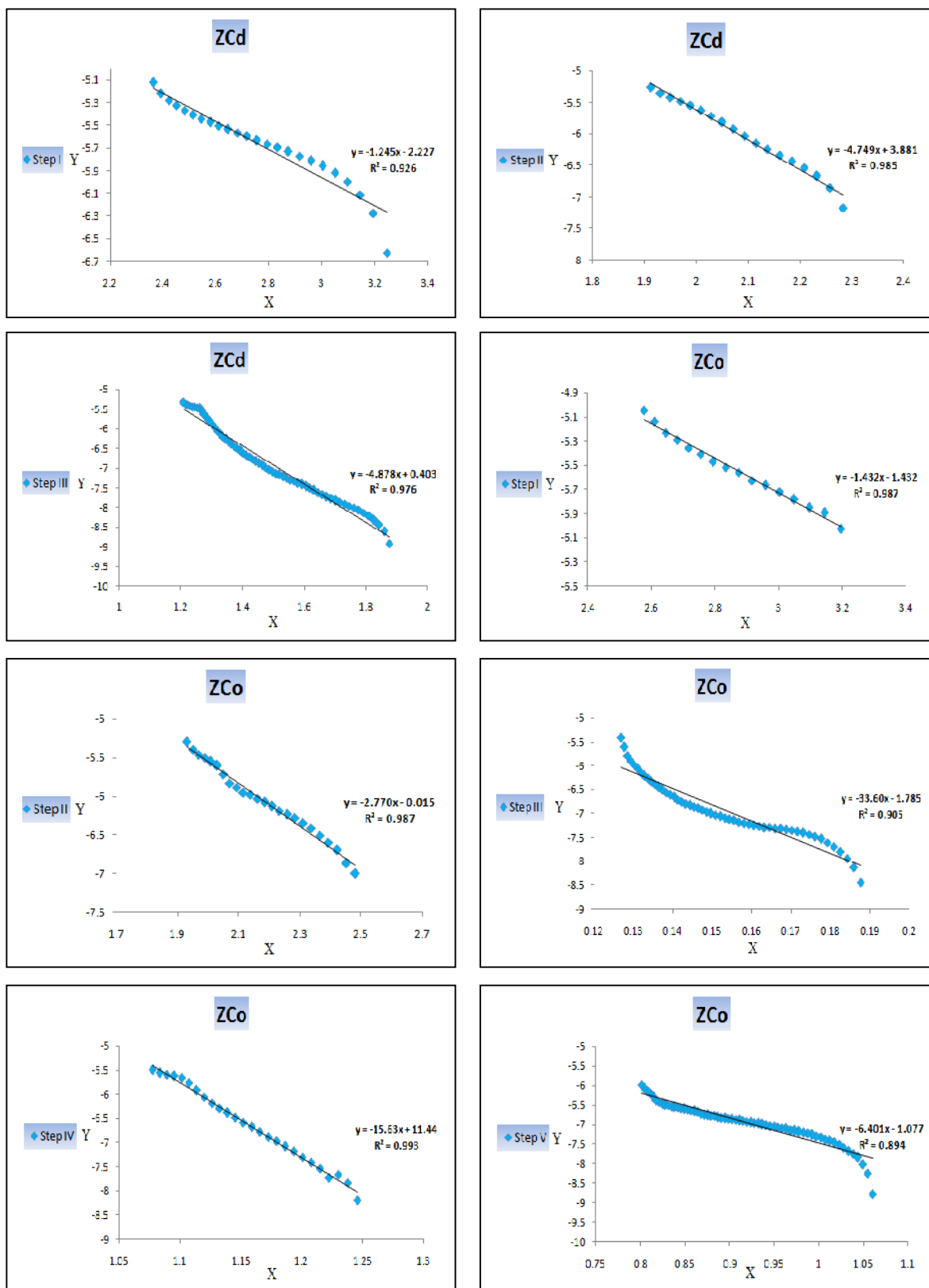
Figure 3.23 : Coast-Redfern plot of Cd and Co complexes
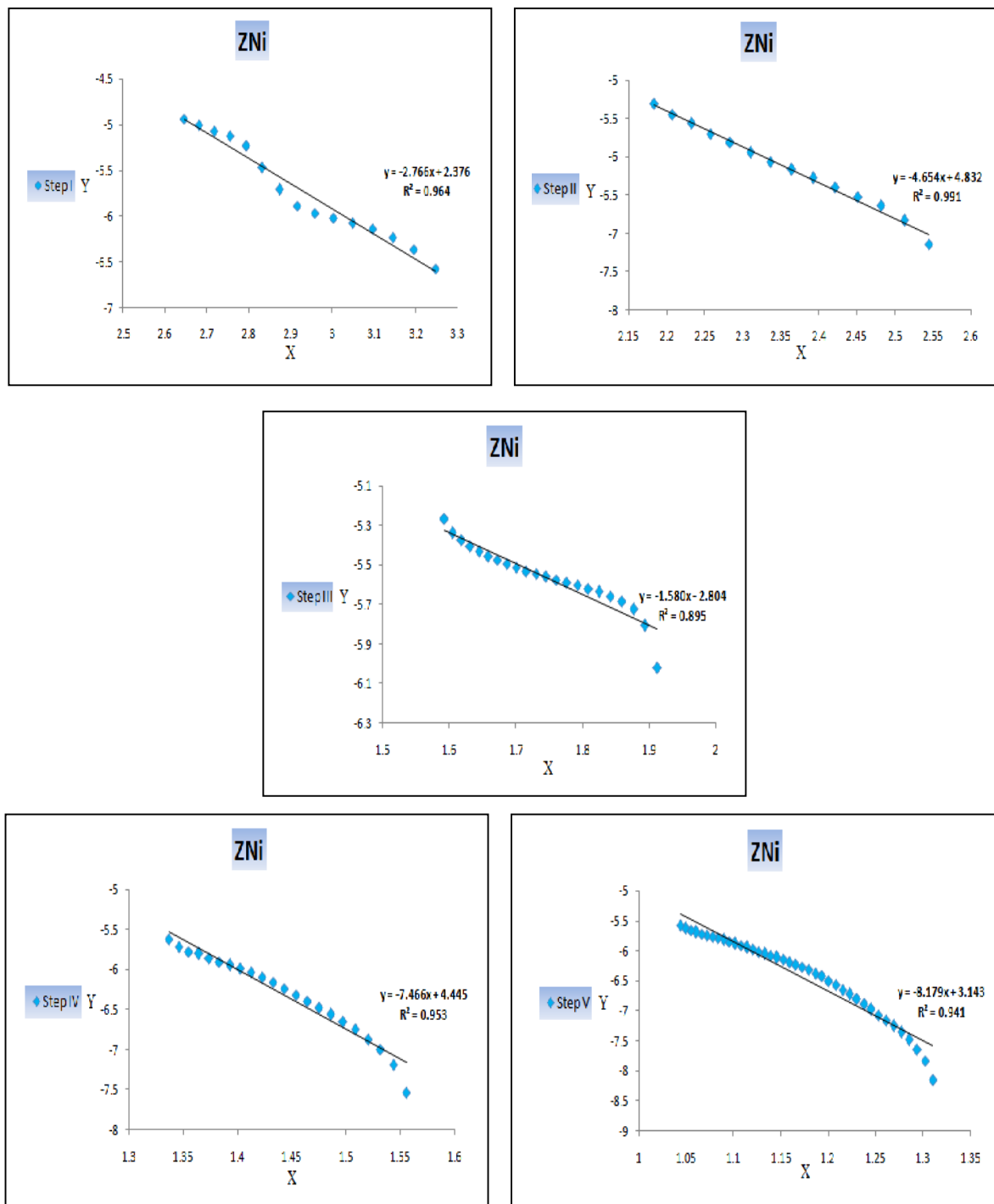
Figure 3.24 : Coast-Redfern plot of Ni complex
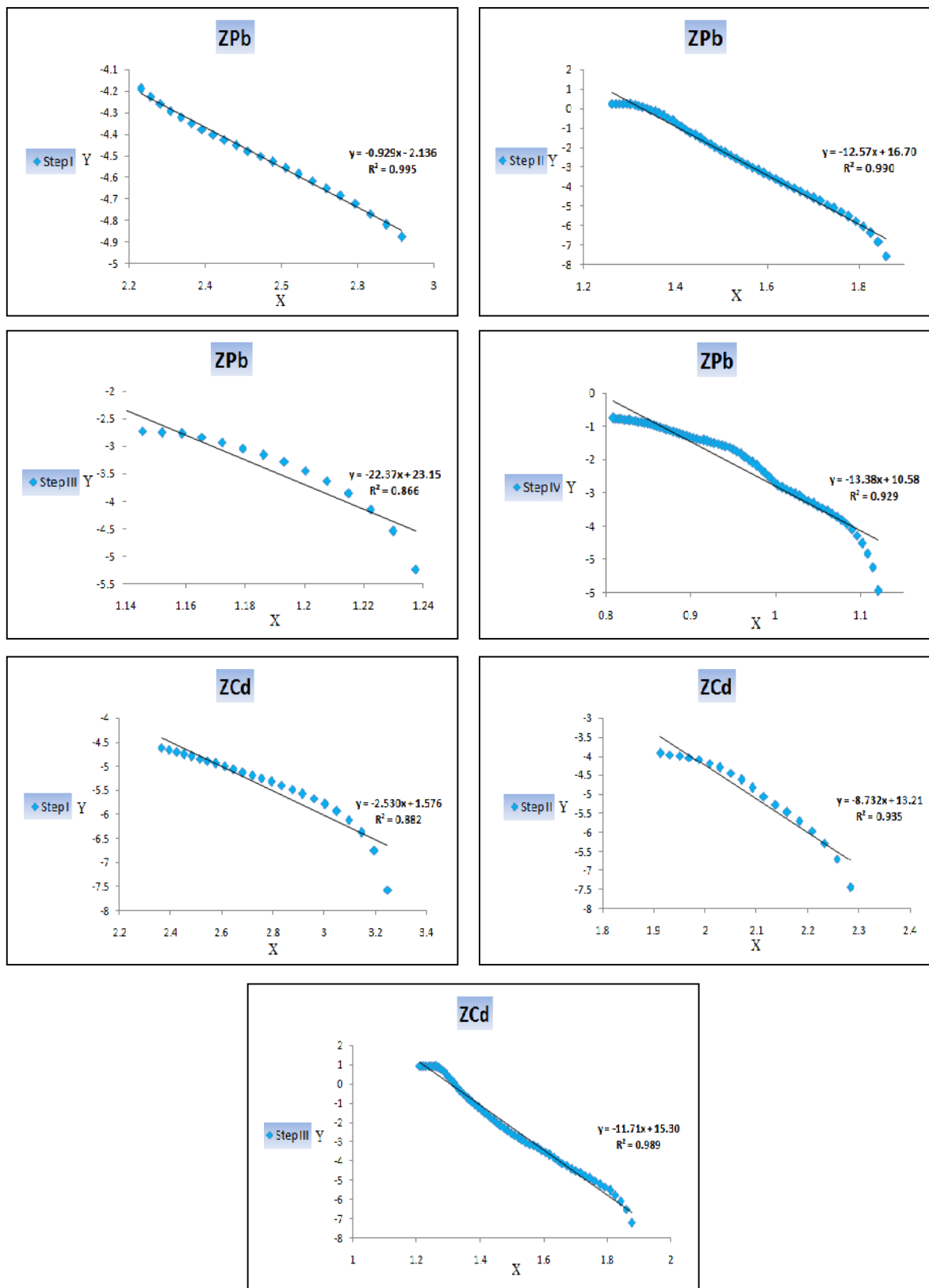
Figure 3.25 : Broido plot of Pb and Cd complexes
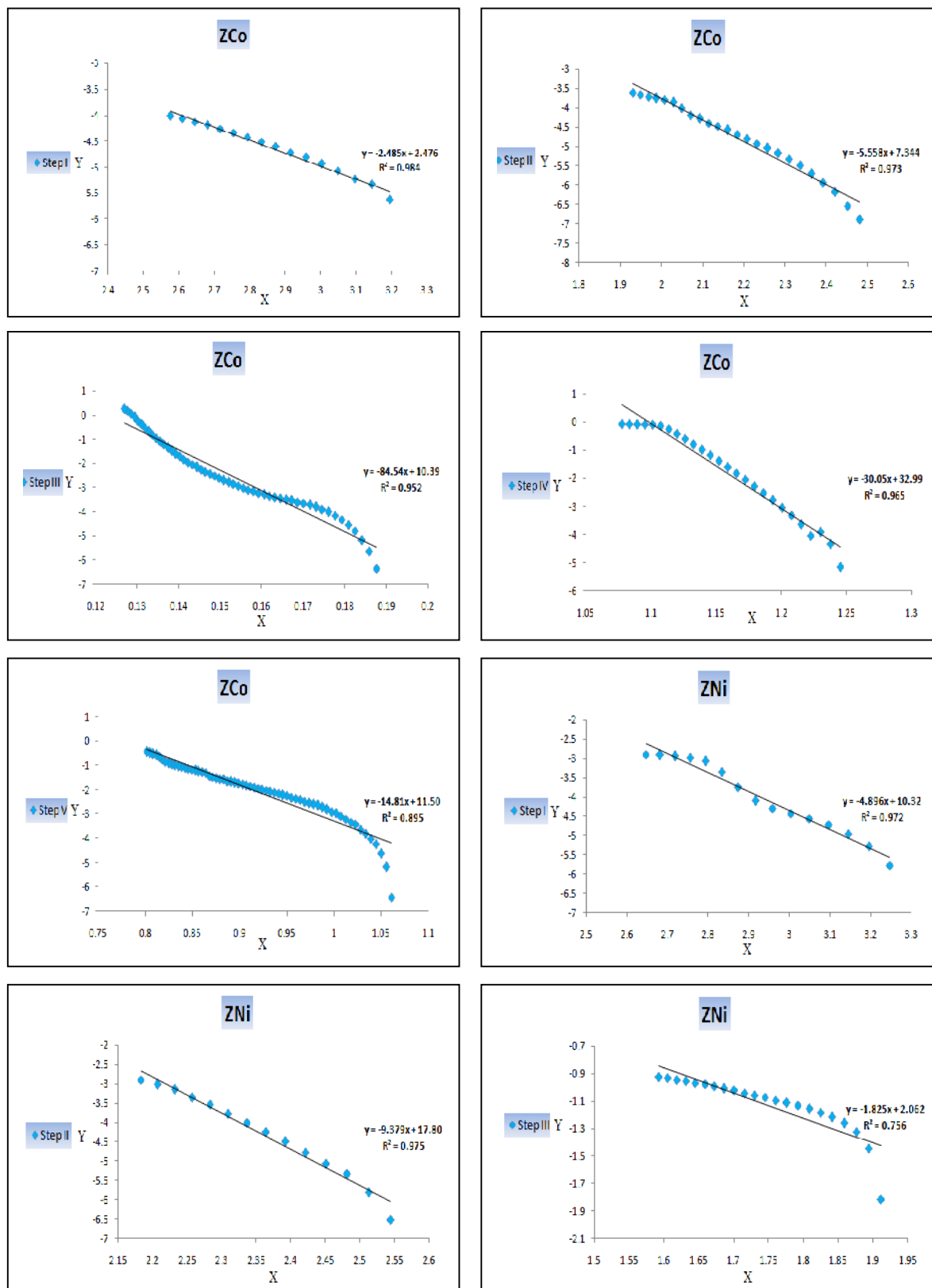
Figure 3.26 : Broido plot of Co and Ni complexes
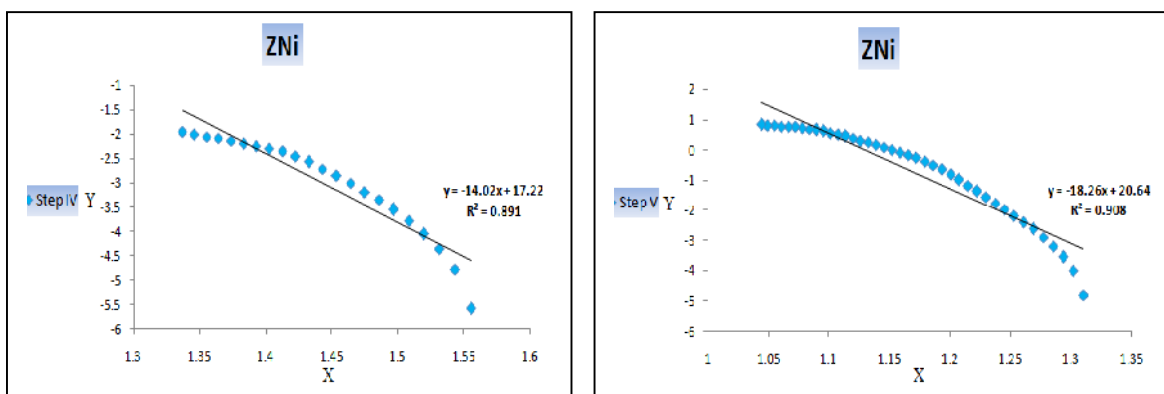
Figure 3.27 : Broido plot of Ni complex
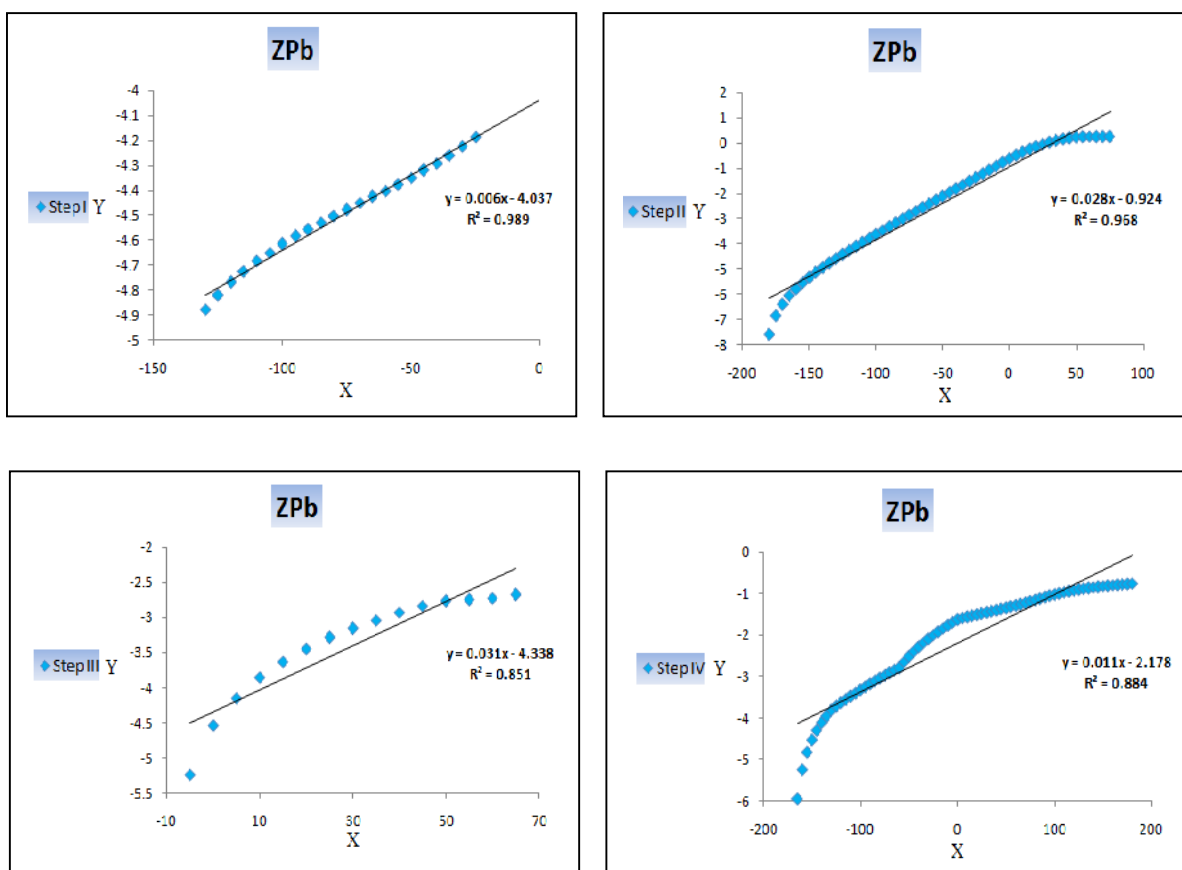
Figure 3.28 : Horowitz-Metzger plot of Pb
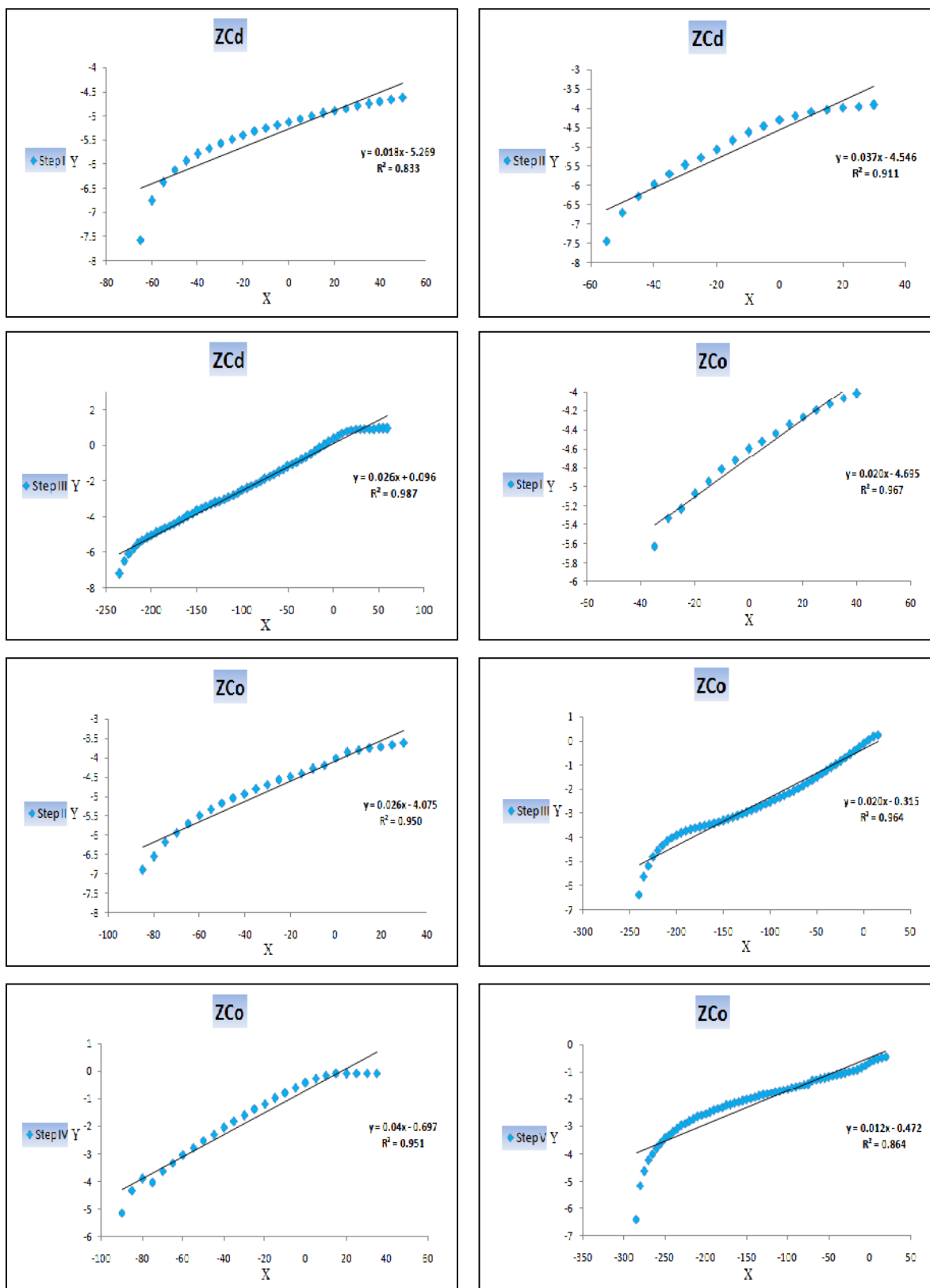
Figure 3.29 : Horowitz-Metzger plot of Cd and Co complexes
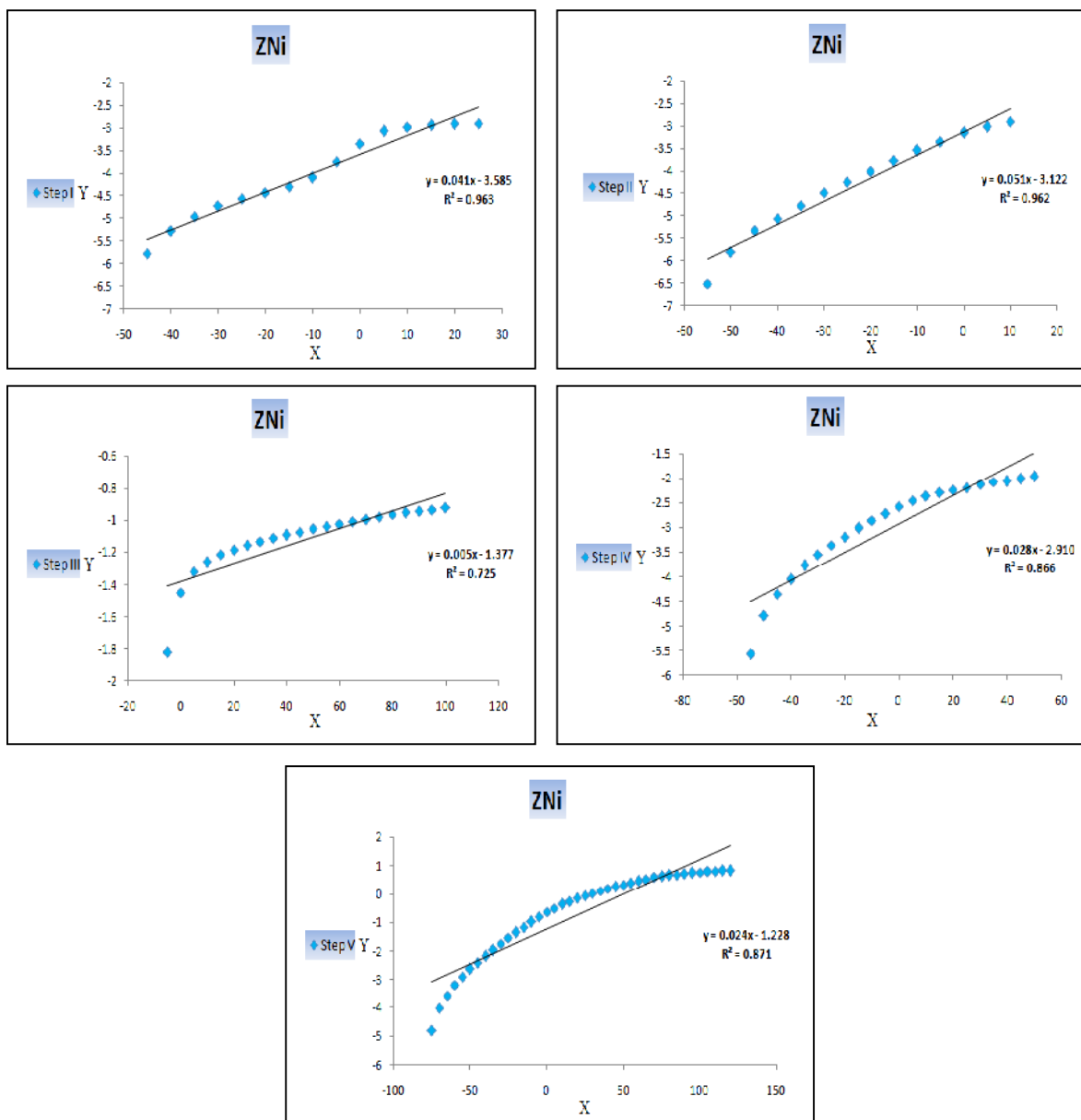
Figure 3.30 : Horowitz-Metzger plot of Ni complex

Chapter Four

Results and Discussion

Characterization of Adsorbent

4. Characterization of Adsorbent

This chapter focuses on the characterization of adsorbent surfaces by using several techniques that are explained as follows :

4.1. FT-IR Spectroscopy

The IR technique can supply useful information about the identification of the functional groups that exist in the structural formula of the adsorbent surfaces . The IR spectrum of the activated carbon (ACP) after it is purified (Figure 4.1) shows a special peak at 3435 cm^{-1} which is attributed to the stretching vibration of hydroxyl groups [89]. New prominent peaks are appeared in IR spectrum of the activated carbon after their oxidization (ACC) with nitric acid (Figure 4.2), particularly at 1747 and 1249 cm^{-1} due to the stretching vibration of carbonyl and C-O group respectively. These peaks indicates obviously the complement of oxidation process by adding carboxylic groups . The carboxylic activated carbon was modified with selenazone ligand(ACZ) which confirmed by decreasing the intensity of hydroxyl and carbonyl group peaks as well as, the peak of C-O group disappeared in IR spectrum of ACZ (Figure 4.3). In addition, the carbonyl peak is shifted towards a lower wave number at 1707 cm^{-1} ($\Delta\upsilon$=40 cm^{-1}) which confirms amide group[89] formation. Moreover , the clear peak appeared at 1543 cm^{-1} that was attributed to the vibration of N-H bending group .

The IR data analysis of silica gel spectrum after their purification with hydrochloric acid (Figure 4.4) revealed many peaks at 3421 , 1629 ,1180 , 1097, 802 and 470 cm^{-1} that pointing to hydroxyl stretching vibration , bending vibration of H-O-H , asymmeric stretching vibration of Si-O-Si , Si-O silicate , bending vibration of Si-O and bending vibration of O-Si-O groups respectively [35 ,133 , 134] . These peaks are unaffected in IR spectrum for silica gel modified with selenazone ligand (SGZ) excepted for the wave number at 1097 cm^{-1}, which is

shifted towards a lower value at 1087 cm^{-1} (Figure 4.5). This is because , some groups of hydroxyl that are connected directly with Si in structural formula of silica gel are replaced to selenazone molecules via nitrogen atom. In addition, a new peak appeared at 1537 cm^{-1} that assigned the vibration of N-H bending group [88] where , this result refers to the modification process with selenazone.

After the complement of oxidation process of graphite powder to graphene oxide. The IR spectrum of graphene oxide (GO) exhibited the several peaks as a broad peak at 3396 cm^{-1} that indicate the stretching vibration of hydroxyl groups while, the peak at 1722 cm^{-1} is pointed to the stretching vibration of C=O group. Also , the strong peak appeared at 1625 cm^{-1} which corresponded to the stretching vibration of C=C groups . Many peaks are observed at 1396 , 1076 and 1033 cm^{-1} that attributed to the deformation vibration of hydroxyl groups , asymmetrical and symmetrical stretching vibration of C-O-C groups.

These peaks in IR data of graphene oxide spectrum (Figure 4.6) are consistent with the results of the previous studies [135-137]. A new adsorbent (GOZ) was synthesized by modifying the graphene oxide with selenazone ligand (Figure 4.7) through the replacement of hydroxyl group within the carboxylic group to selenazone via amine group. Thus, the IR spectrum of GOZ was appeared decreases of intensity peaks in the stretching vibration of hydroxyl and carbonyl groups that was attributed to replace some hydroxyl groups in graphene oxide with selenazone ligand, on the other hand, peak at 1625cm^{-1} in graphene oxide spectrum was shifted to a longer wave number at 1647 cm^{-1} due to form carbonyl group of amide. A new peak has been revealed at 1244 cm^{-1}, that corresponds to the stretching vibration of C-N group , from this IR analysis data of GOZ adsorbent confirm the suggested modification method of graphene oxide with selenazone ligand .
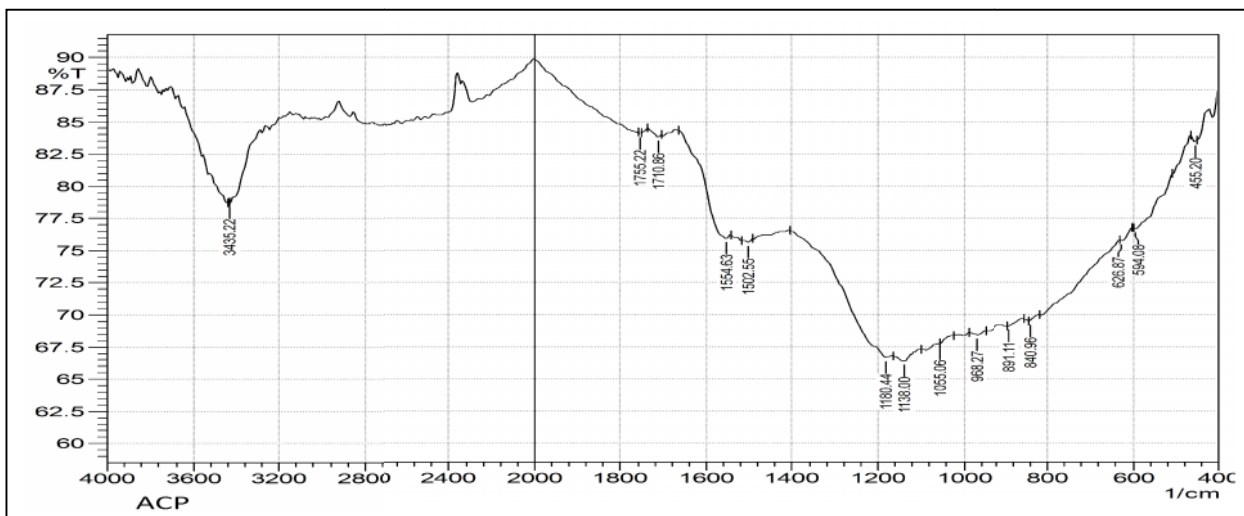
Figure 4.1 : IR spectrum of pure activated carbon
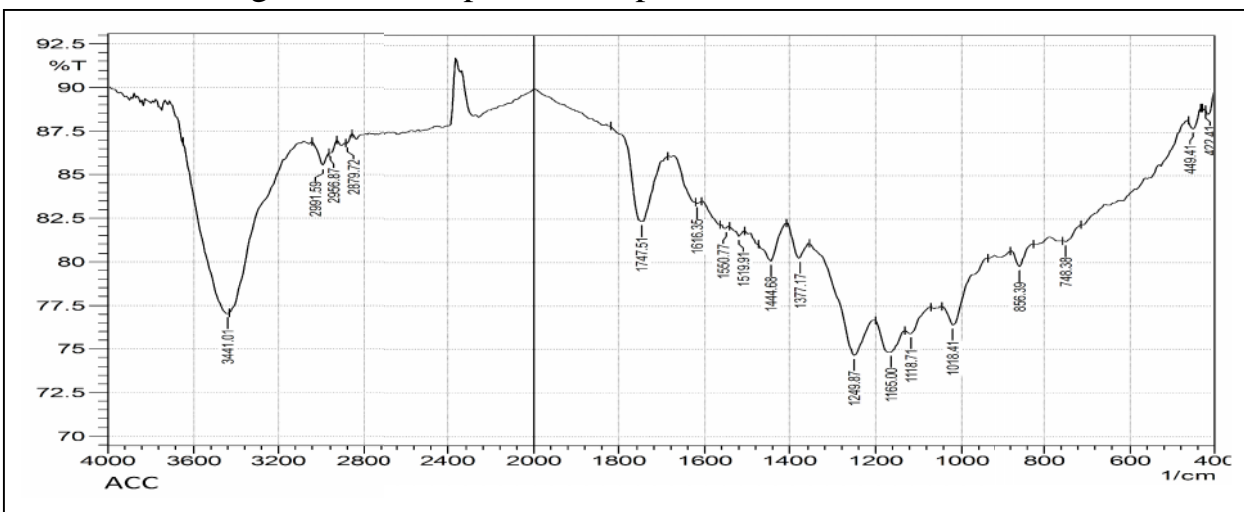
Figure 4.2 : IR spectrum of carboxylic activated carbon
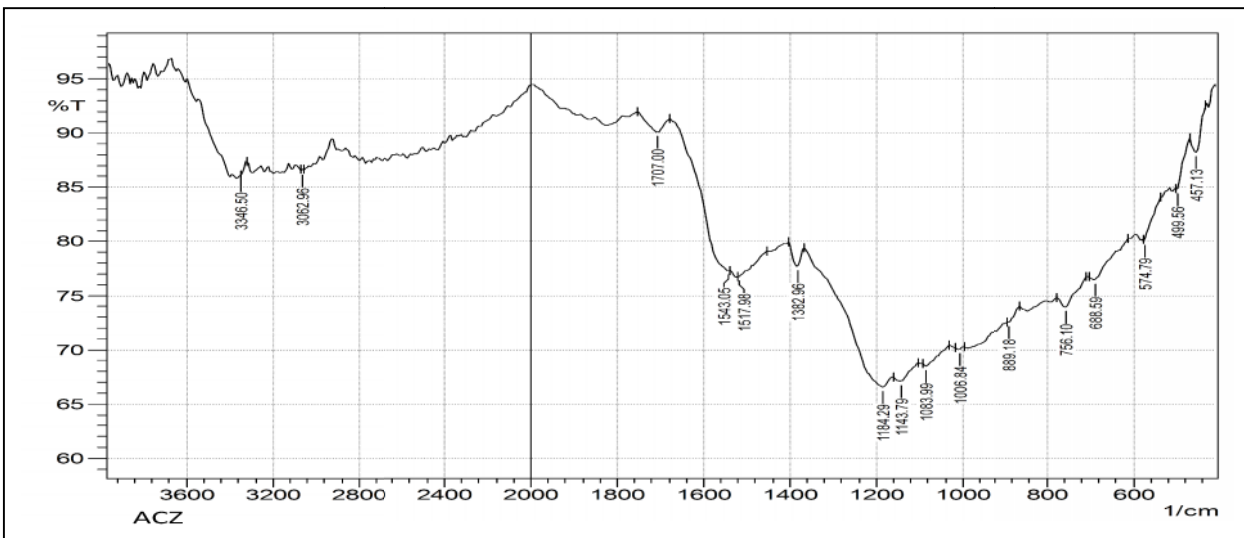
Figure 4.3 : IR spectrum of ACZ
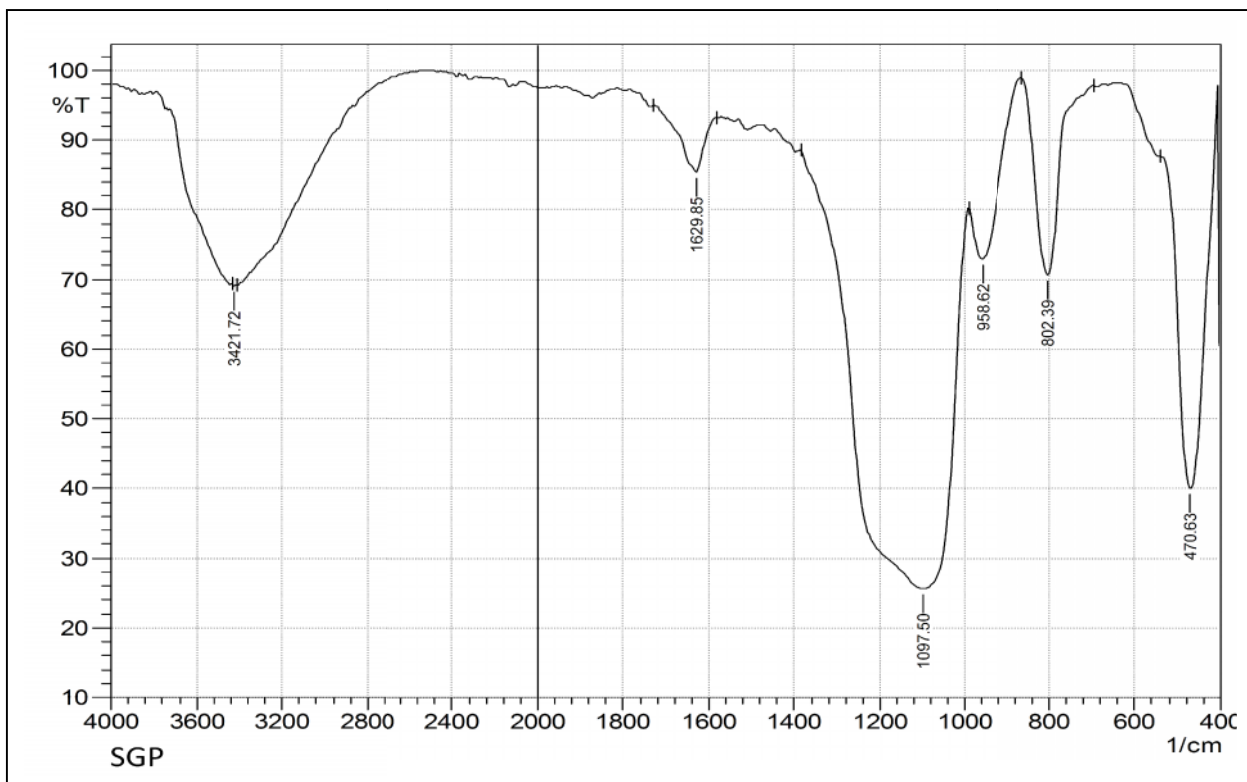
Figure 4.4 : IR spectrum of pure silica gel
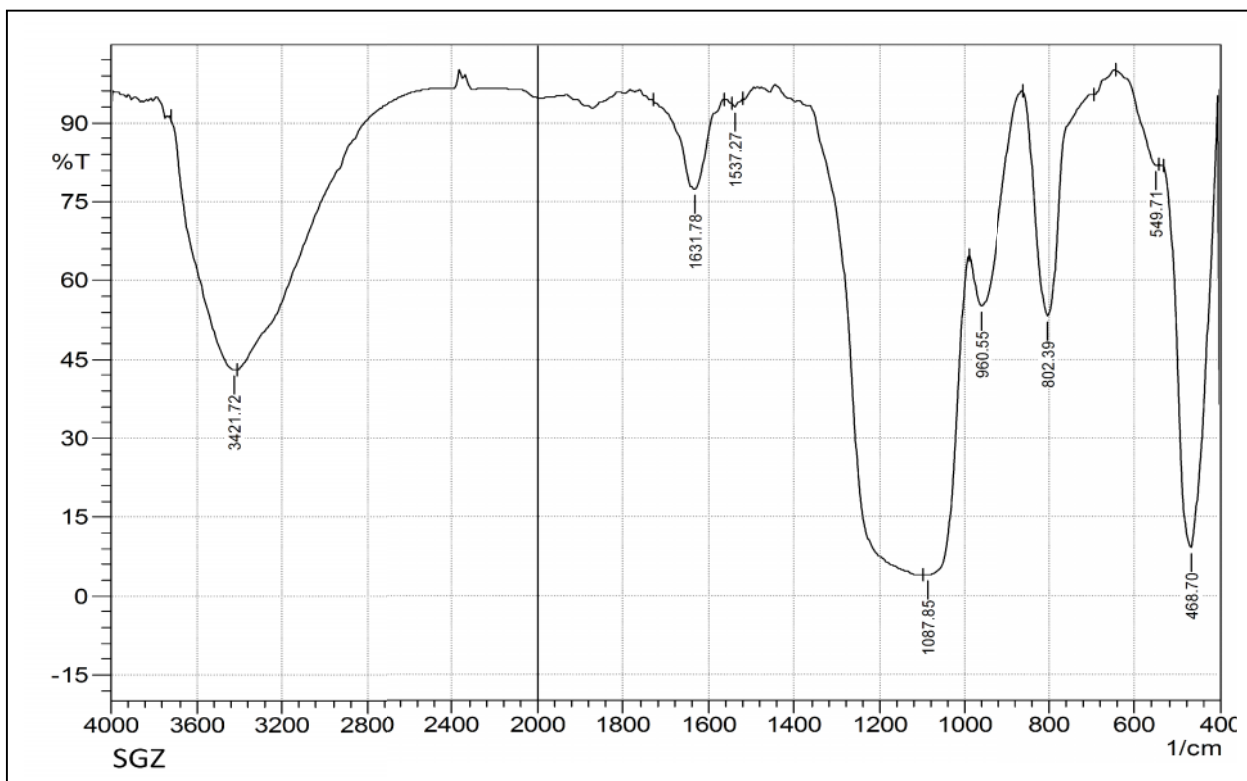
Figure 4.5 : IR spectrum of SGZ
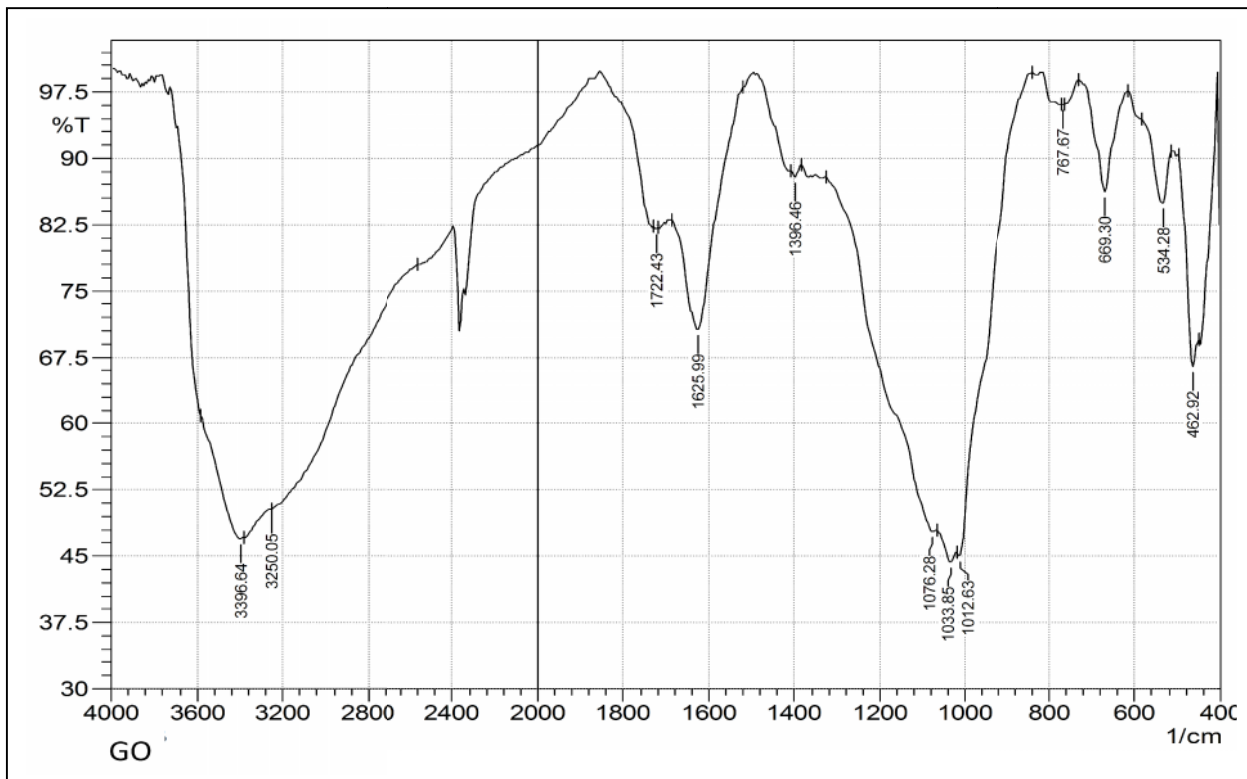
Figure 4.6 : IR spectrum of GO
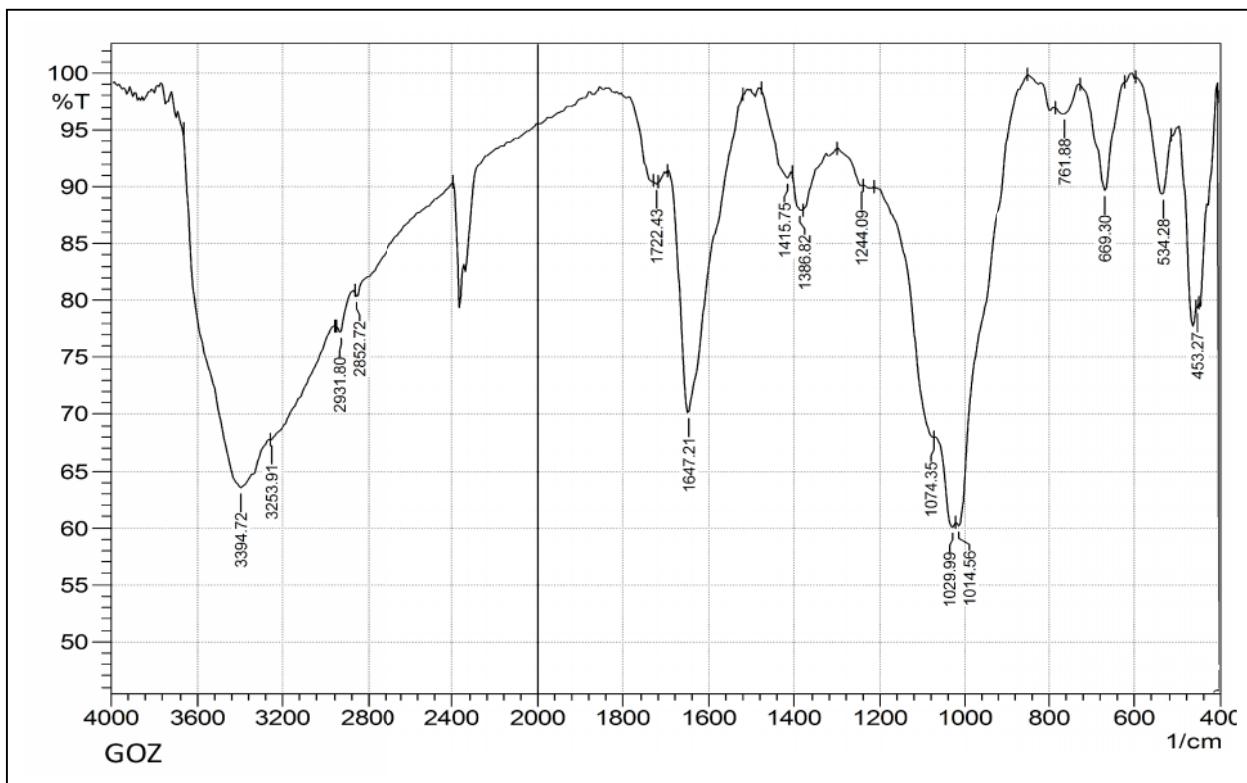
Figure 4.7 : IR spectrum of GOZ

The separated product (sGO) from the soot waste was explained briefly in chapter two. FT-IR spectrum, showed many main peaks at 3383 , 3128 , 2954-2887 , 1741 , 1624 , 1149 - 1101 and 1006 cm^{-1} which were attributed to hydroxyl stretching vibration , aromatic C-H group , aliphatic C-H group , carbonyl group , streching vibration of C=C group and also may dut to the streching vibration of H-O-H , asymmetrical and symmetrical stretching vibration of C-O-C groups and out of plan the bending vibration of C-H groups respectively [135-138] . These data of IR spectrum (Figure 4.8) suggests that the sGO product is a graphitic oxide [139,140] . The structural formula of graphitic oxide is shown in Figure 4.9 [141].
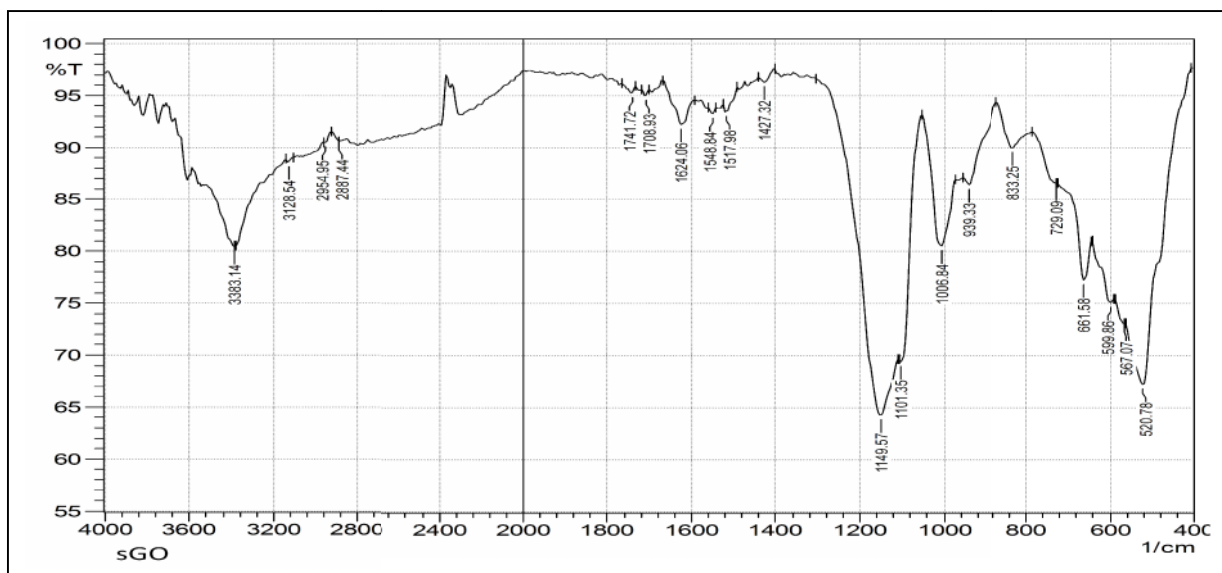
Figure 4.8 : IR spectrum of sGO
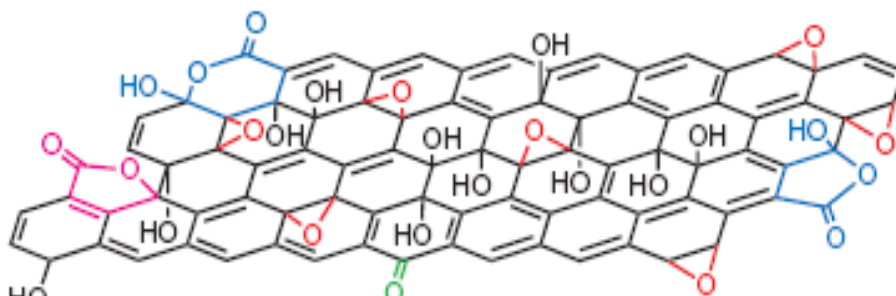
Figure 4.9 : The structural formula of graphitic oxide [130]

The infrared spectrum of sFe adsorbent has demonstrated several peaks like strong and broad peak at 3425 cm^{-1}, which was attributed to hydroxyl stretching vibration and the stretching vibration of H-O-H appeared at 1633 cm^{-1}. The strong peaks revealed a wave number, 1153 ,1114cm^{-1} which took place due to the asymmetrical and symmetrical stretching vibration of C-O-C groups [135 ,142]. Other peaks also appeared at 983-790 and 596 - 462 that pointed to FeO(OH) bending vibration and stretching vibration of Fe-O group respectively [35 ,142,143]. These results of IR spectrum of sFe adsorbent (Figure 4.10) refer to the existence of Iron oxide polluted with some carbon atoms.
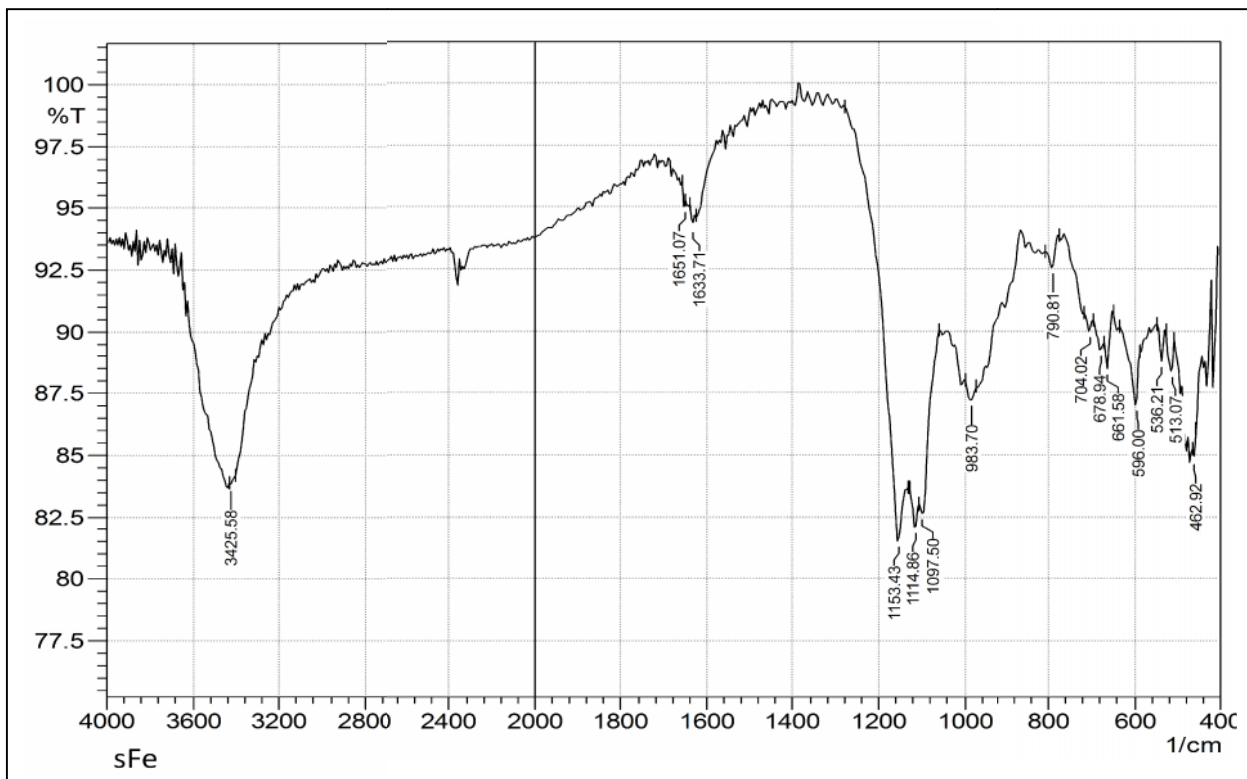
Figure 4.10 : IR spectrum of sFe adsorbent

4.2. Ultraviolet-Visible Spectroscopy

Some adsorbents were analyzed by utilizing UV-Vis spectrophotometer in order to characterize the functional groups that exist in the structural formula of

adsorbents. UV-Vis spectrum of GO in water solution demonstrated two bands. The first is a strong band that shows 233nm is correspondent to π-π^* transitions for aromatic C=C and C=O groups while , the other band is a shoulder band that appears at 310 nm and is correspondent to n-π^* transitions for carbonyl and hydroxyl groups [144-146], this result confirms the completion synthesis of GO where, the spectra of graphite powder and GO are shown in the Figures 4.11 and 4.12, respectively. The spectrum of UV-Vis for GO after modification with selenazone ligand (GOZ) was recorded in it's aqueous solution (Figure 4.13) that showed the strong band at 195 nm after the shift from 233 nm . This is due to the π-π^* transitions of the groups as aromatic C=C , C=O and C=N. The blue shift indicates to complement of modification process with selenazone ligand, on the other hand , very weak band was observed at 306 nm pointed to n-π^* transition.

The adsorbent of sFe in the dispersed water (Figure 4.14) was analyzed by using UV-Vis spectrophotometer where , the spectral data of UV-Vis revealed two bands as a shoulder band at 252 and 320 nm . The broad band at 320 nm may due to the remnants of Plasmon vibration of Iron nano particles [147,148].
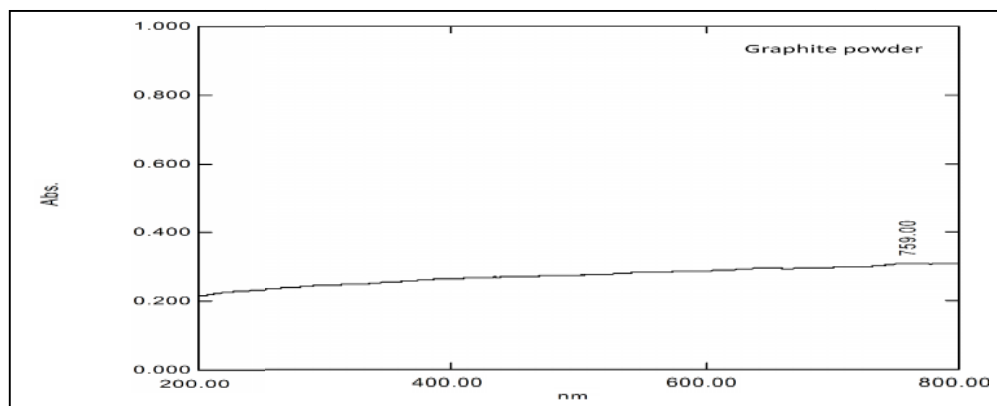
Figure 4.11 : Uv-vis spectrum of graphite powder
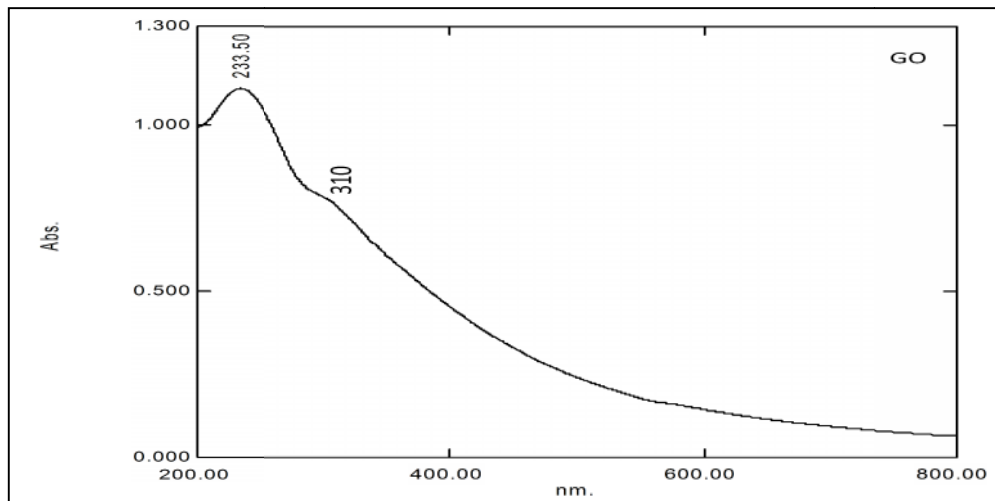
Figure 4.12 : Uv-vis spectrum of GO
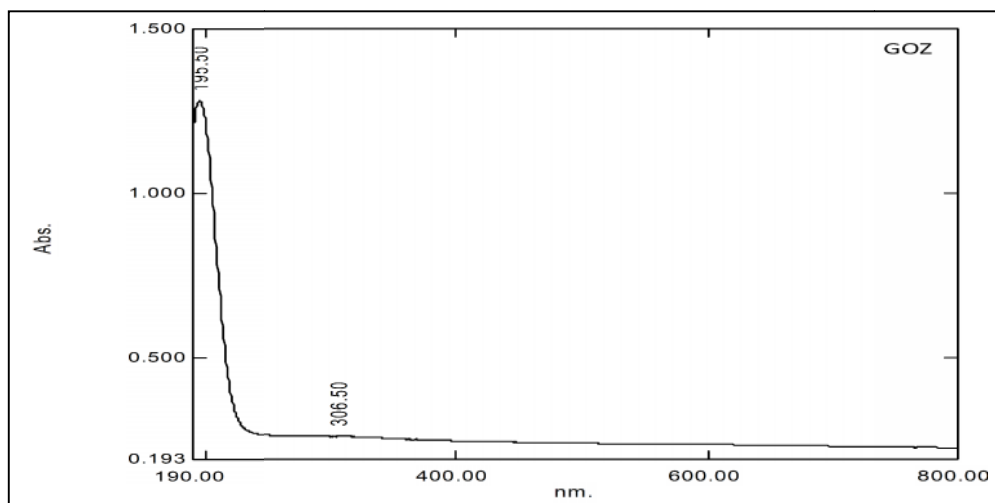
Figure 4.13 : Uv-vis spectrum of GOZ
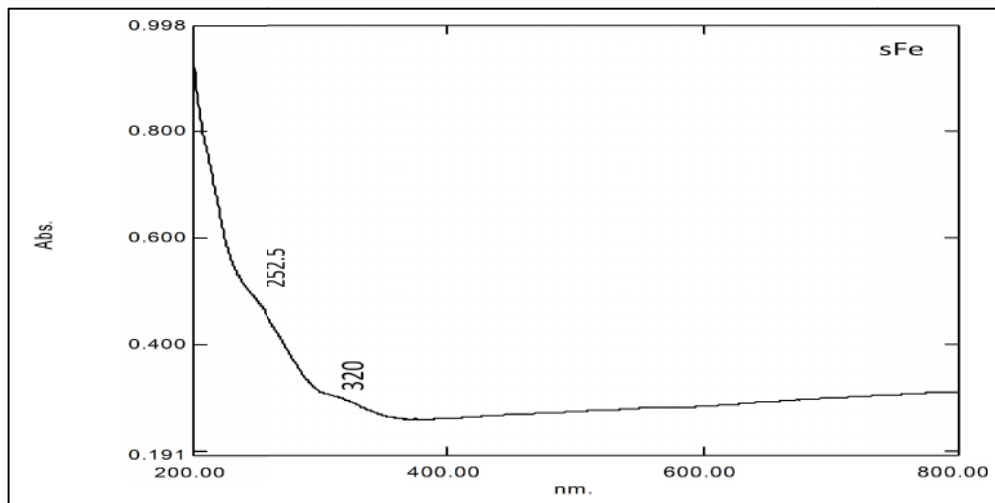
Figure 4.14 : Uv-vis spectrum of sFe

4.3. EDX data analysis

The energy dispersive X-ray technique has been used for the elemental analysis at a room temperature in 0-80 KeV ranging. EDX analysis was applied on some adsorbents samples in order to prove the composition chemical of adsorbents [25].

The EDX data of ACZ adsorbent (Figure 4.15) refer to the existence of carbon and oxygen atoms by using ratio 13.66 (C/O) [149,150]. Moreover , selenium signal appeared and clearly confirmed the selenazone ligand which is joined with activated carbon. The signals of carbon and selenium are presented in EDX spectrum of the modified silica gel (Figure 4.16) indicating that the modification process is completed with selenazone ligand. In addition, the strong signal shows that it belongs to silicon in silica gel structure . The ratio of carbon to oxygen is 16.24, which was calculated depending on EDX spectrum of GO (Figure 4.17) corresponds with previous studies data [136] indicating confirmation of synthesis graphene oxide while, the C/O ratio (2.33) was also calculated from EDX spectrum of sGO (Figure 4.18) that is consistent with C/O ratio of graphitic oxide in previously literature [136,139]. The signal of Iron (Figure 4.19) was revealed in EDX data of sFe adsorbent that confirmed tht Iron present in the structural formula of sFe adsorbent, while the existence of carbon signal pointed to polluted the adsorbent with carbon atoms. The EDX data of all adsorbents are listed in Table 4.1.

Table 4.1 : Elemental analysis ratio by using EDX data

Adsorbent	Element ratio %							C/O ratio	Total ratio %
	C	O	Si	Fe	S	Se	V		
ACZ	92.9	6.8	-	-	-	0.3	-	13.66	100
SGZ	29.9	30.0	40.0	-		0.1	-	0.99	100
GO	94.2	5.8	-	-	-	-	-	16.24	100
sGO	57.3	24.5	-	-	8.6	-	9.6	2.33	100
sFe	5.45	61.36	5.72	24.87	-	-	2.6	0.088	100
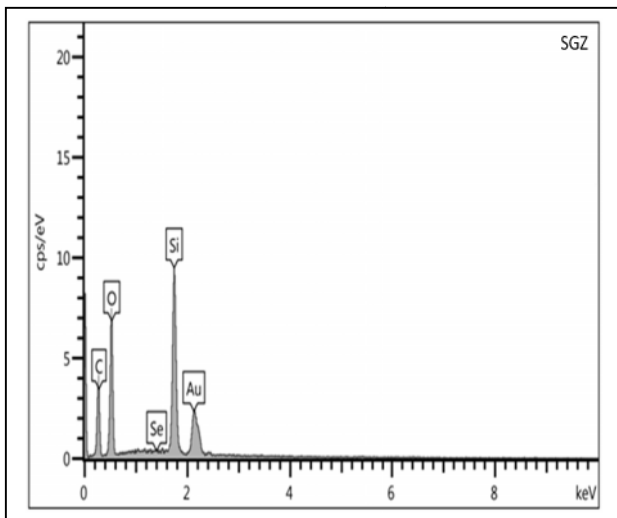
Figure 4.16 : EDX spectrum of SGZ
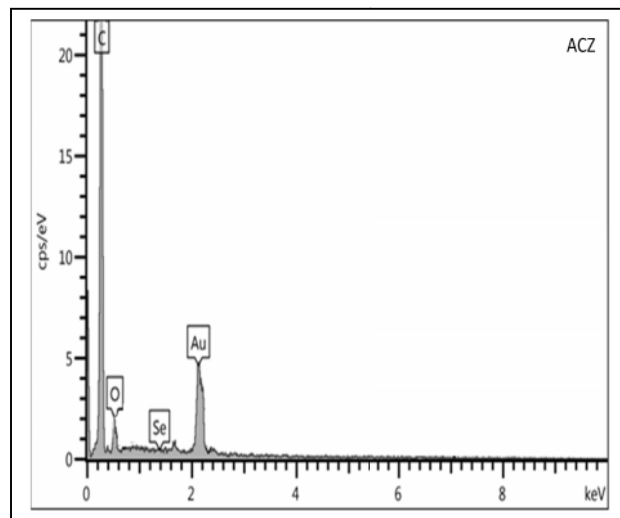
Figure 4.15 : EDX spectrum of ACZ
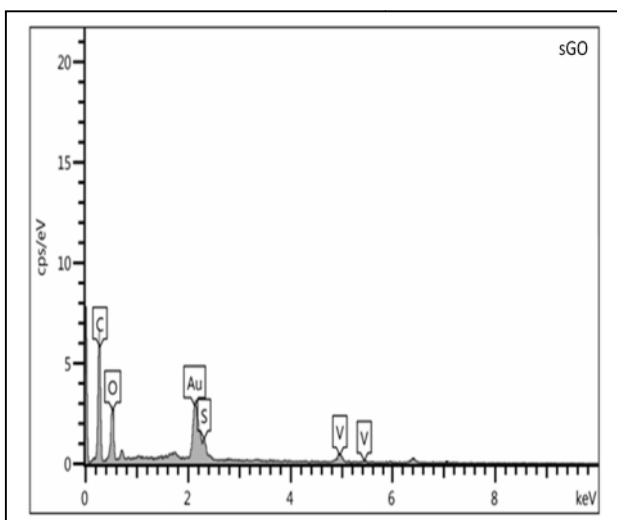
Figure 4.18 : EDX spectrum of sGO
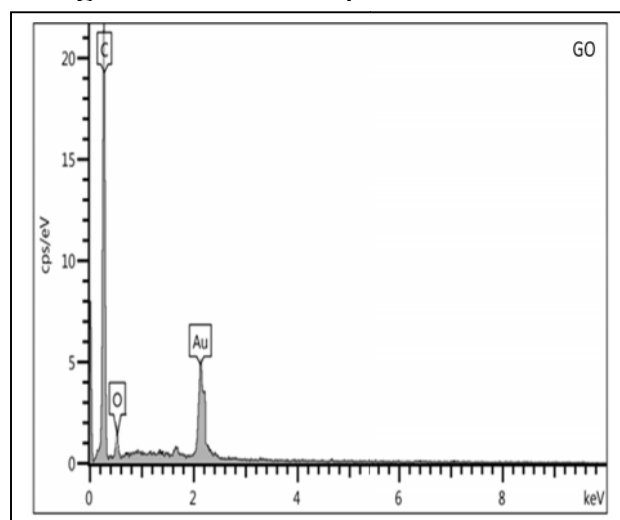
Figure 4.17 : EDX spectrum of GO
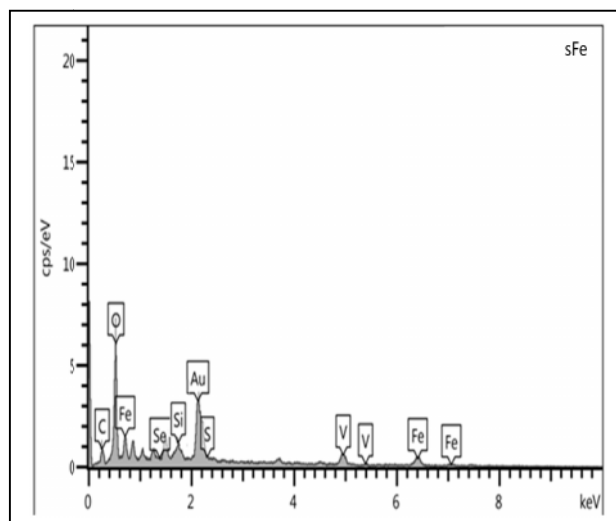
Figure 4.19 : EDX spectrum of sFe

4.4. Field emission Scanning Electron Microscopy

The field emission scanning electron microscopy (FeSEM) technique provided useful information about the characterization of adsorbents such as the topology natural of outer surface , homogeneity factor and particles size [56,67]. The images of adsorbent surfaces using FeSEM technique were obtained at 60.00KX magnification and work distance at 5.8 mm by using voltage accelerated 10.00kV.

The images of ACZ and SGZ (Figures 4.20 and 4.21 respectively) revealed the properties of outer surfaces that are nonhomogeneous. Many grooves and channels that gives a good adsorbent surface . The particles size are measured in the range 18-37nm and 22.3-33.5nm, respectively that attributed to the existence of selenazone ligand nanoparticle.

The data of SEM of graphene oxide (Figure 4.22) was appeared their particles size within the nanoparticles class ranging between 28.16 and 85.6nm. Several channels and grooves appeared on the outer surface while , the topology of the outer surface of GOZ   (Figure 4.23) shows different properties when compared with SEM data of GO because the selenazone ligand which joined with the graphene oxide. Many channels appeared with decreased their particles size in the extent, 20.47 - 48.38 nm that can used in more efficiency as adsorbent surface.

The properties of the outer surface of sGO (Figure 4.24) adsorbent was shown as a nonhomogeneous, various channels and has a low particles size while, the image of sFe (Figure 4.25) appears many grooves and nonhomogeneous surface that can be utilized as a good adsorbent to remove the pollutants from their aqueous solutions . In general , some properties can help to give a good adsorbent such as the existence of channels and grooves , nonhomogeneous distribution and the increase of surface area .
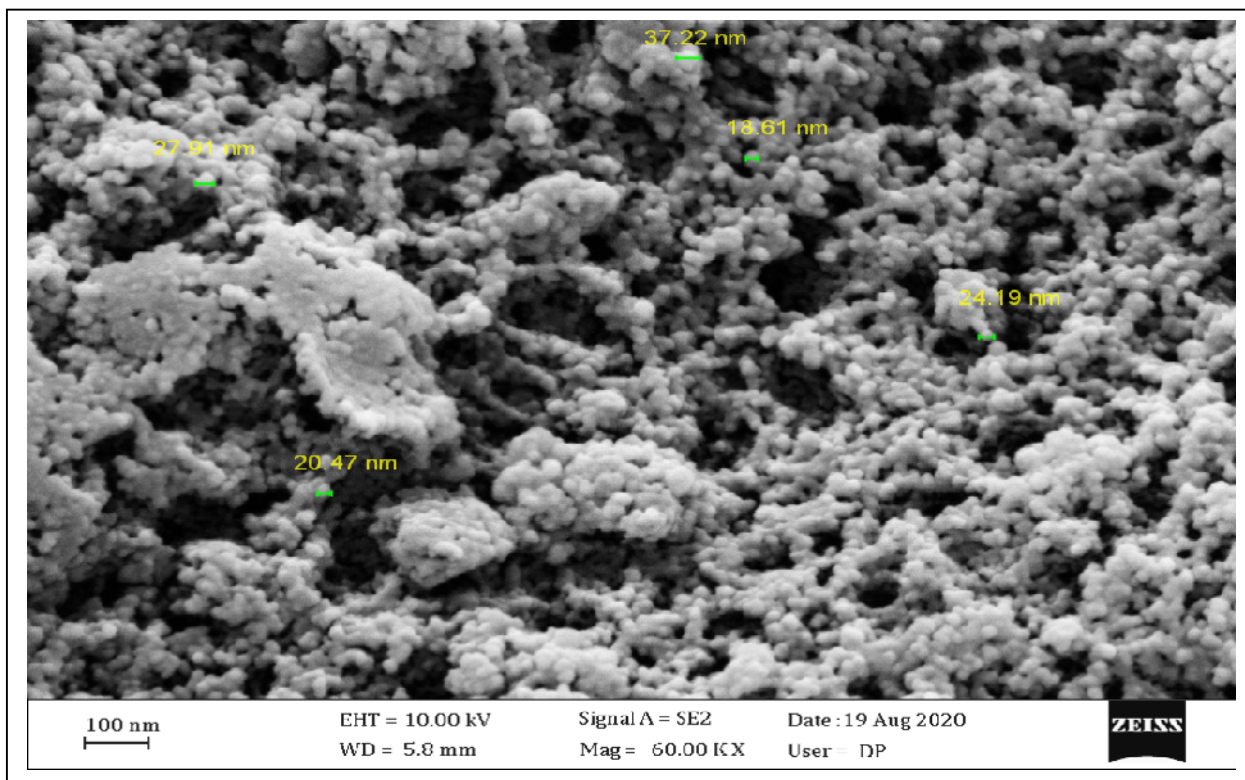
Figure 4.20 : SEM image of ACZ
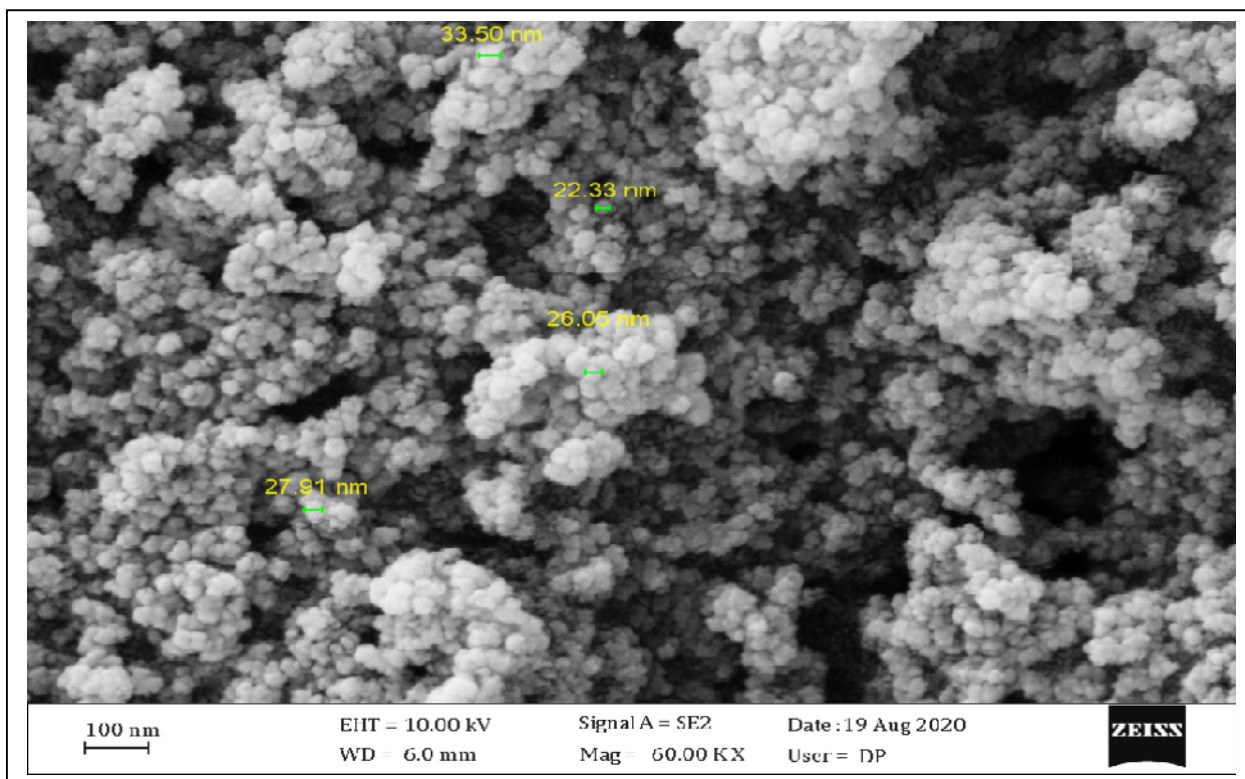
Figure 4.21 : SEM image of SGZ
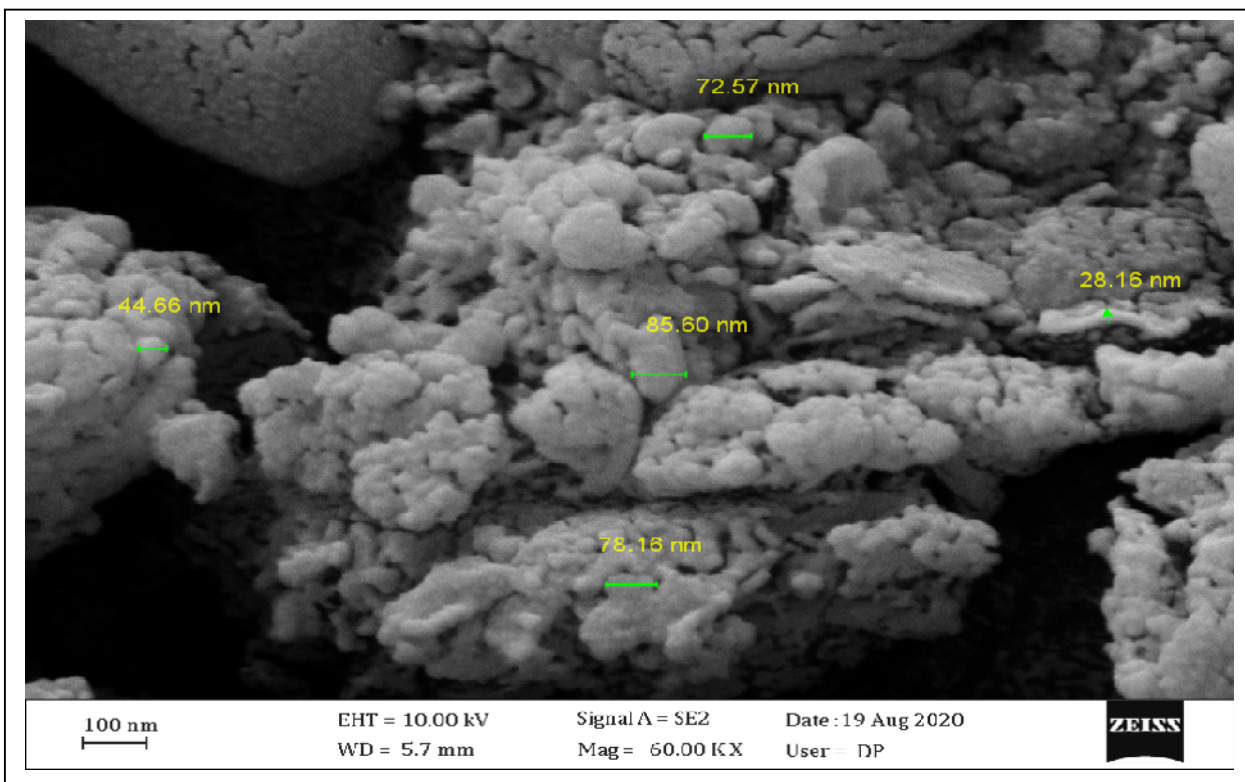
Figure 4.22 : SEM image of GO
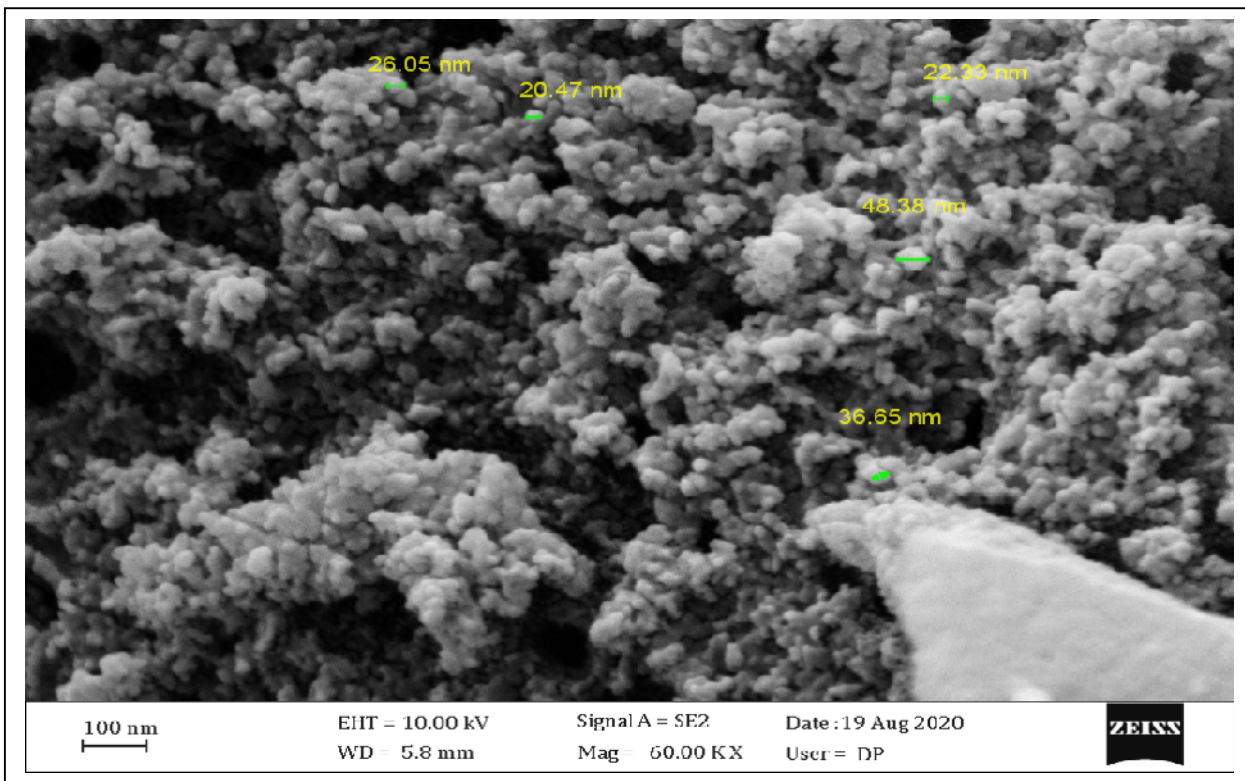
Figure 4.23 : SEM image of GOZ
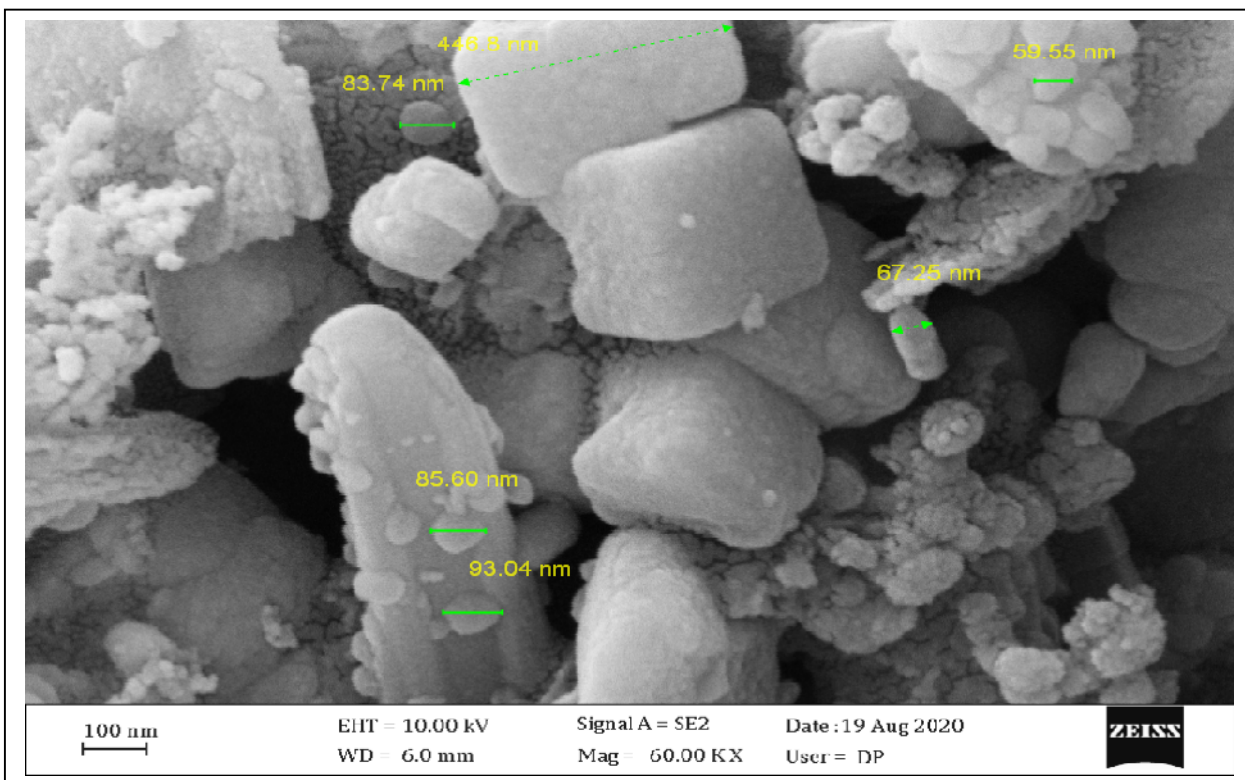
Figure 4.24 : SEM image of sGO
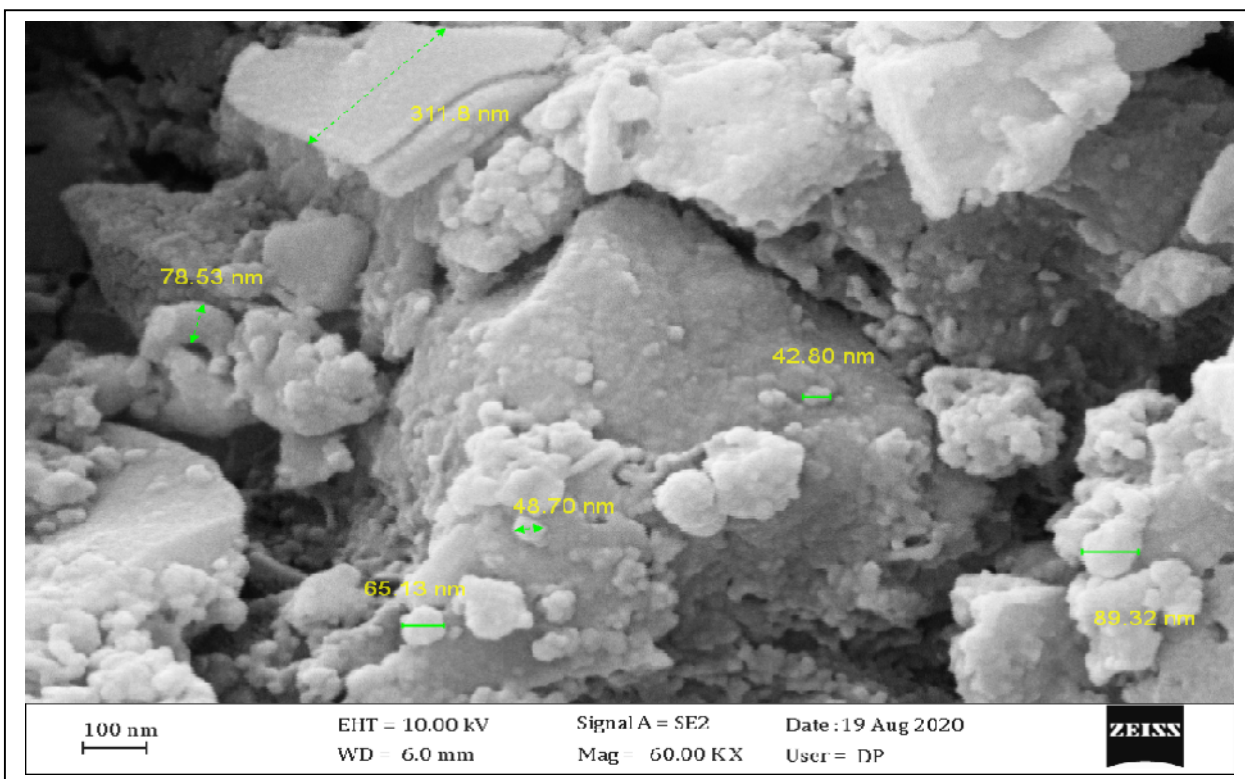
Figure 4.25 : SEM image of sFe

4.5. X-ray Diffraction Spectroscopy

X-ray spectroscopy is employed in this study to characterize the structural formula of adsorbent surface. Additionally, it can be used to confirm a complete modification process that is applied on some adsorbent surfaces. The pattern of ACZ spectrum shows several bands at position 2θ (23.4º , 29.7º , 41.2º , 43.7º , 45.3º , 51.7º , 55.7º , 61.5º ,56.1º and 71.8º). These bands refer to a present of selenazone ligand in the structural formula of ACZ, while the amorphous band obviously appeared as a broad band due to the existence of activated carbon [70 ,151,152]. These data clearly indicat the success of modification process of the activated carbon with selenazone ligand (Z).

The X-ray spectrum of SGZ appears the amorphous structure that corresponds with silica gel pattren in the previous literature[153,154], the characteristic bands showed at position 2θ(22.53º and (23.01º and 29.63º)) which is attributed to silica gel and selenazone ligand respectively. Also , it proves the complete modification process of silica gel with selenazone .

X-ray pattren of GO appears a singl band at around 2θ (11.28º), also, it has the interplaner spacing about 7.83Aº, which is consistent with the characteristic band of graphene oxide spectrum in all the previous studies, [84,85,144,145] . This result refers to the successful preparation of graphene oxide. The well-known, graphene oxide has many functional groups like carboxylic, hydroxyl and epoxy. So, the graphene oxide was also modified with selenazone legand in order to form a new adsorbent surface where , the X-ray spectrum of GOZ reveals the multi bands at around 2θ (12.51º , 18.60º , 23.23º , 26.42º , 29.66º , 43.32º , 44.95º and 56.82º) where , the band at 2θ(12.51º) is attributed to graphene oxide, while the other bands are consistent with the XRD spectrum of selenazone ligand, which is explained

briefly in chapter three. This data confirms the successful modification of graphene oxide into GOZ .

The pattern of sGO XRD spectrum views a different positions at around 2θ (11.90º , 18.47º, 26.20º , 28.97º , 33.01º   and 41.31º) where, these data are corresponding with the graphitic oxide data comparing with previous literature [136,155].

The XRD pattern results of sFe adsorbent demonstrated many characteristic bands at position 2θ (30.0º , 35.92º , 43.61º , 54.44º , 57.43º and 62.75º), they have also interplaner spacing values at (2.97 , 2.49 , 2.07 , 1.68 , 1.60 and 1.48 Aº), respectively. The diffraction bands are consistent with the (220 , 311 , 400 , 422 , 511 and 440) crystal planes respectively. These crystal planes are attributed to the existence Iron oxide [142 ,147 ,156,157] within the sructural formula of sFe adsorbent that is correspondent with all the spectroscopic data which were previously mentioned. Furthermore, the crystals size were calculated through utilizing the highest band (311) by using Debye Scherrer's equation which is 42.2 nm. According to the obtained results of FeSEM and XRD all the adsorbent surfaces are within the nanomaterial class [158,159]. The XRD data of the highest bands of all adsorbent surfaces are listed in Table 4.2 and their spectra are depicted in Figures 4.26 - 4.31 .

Table 4.2 : The XRD data of characteristic bands in all adsorbents

adsorbent	Pos. [°2Th.]	FWHM Left [°2Th.]	d-spacing [Å]	Rel. Int. [%]	Crystal size (D nm)	crystallinity index (CI)
ACZ	29.7763	0.3444	3.0005	100	23.9	79.51
SGZ	22.5337	1.8189	3.9458	100	4.5	11.59
GO	11.2879	0.2952	7.8389	100	27.1	85.79
GOZ	12.1503	0.2460	7.28445	100	32.5	90.80

sGO	12.0930	0.1476	7.31885	89.07	54.1	56.27
	28.9730	0.3936	3.08	100	20.8	61.05
sFe	35.927	0.1968	2.4997	100	42.2	94.78
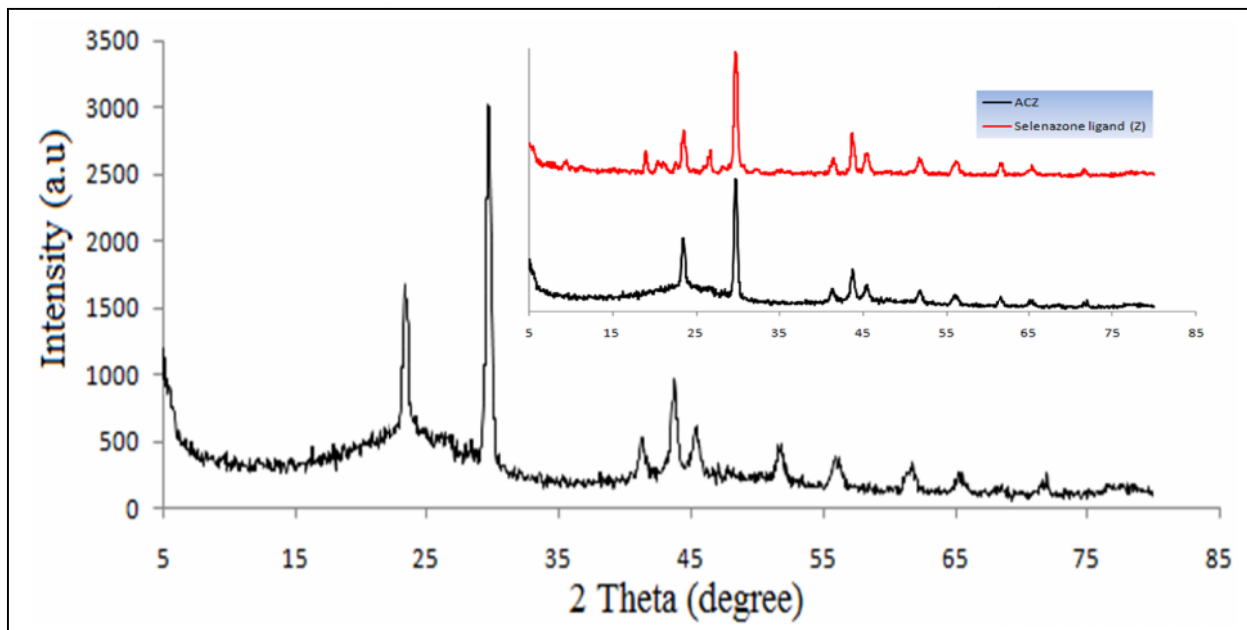
Figure 4.26 : XRD pattren of ACZ
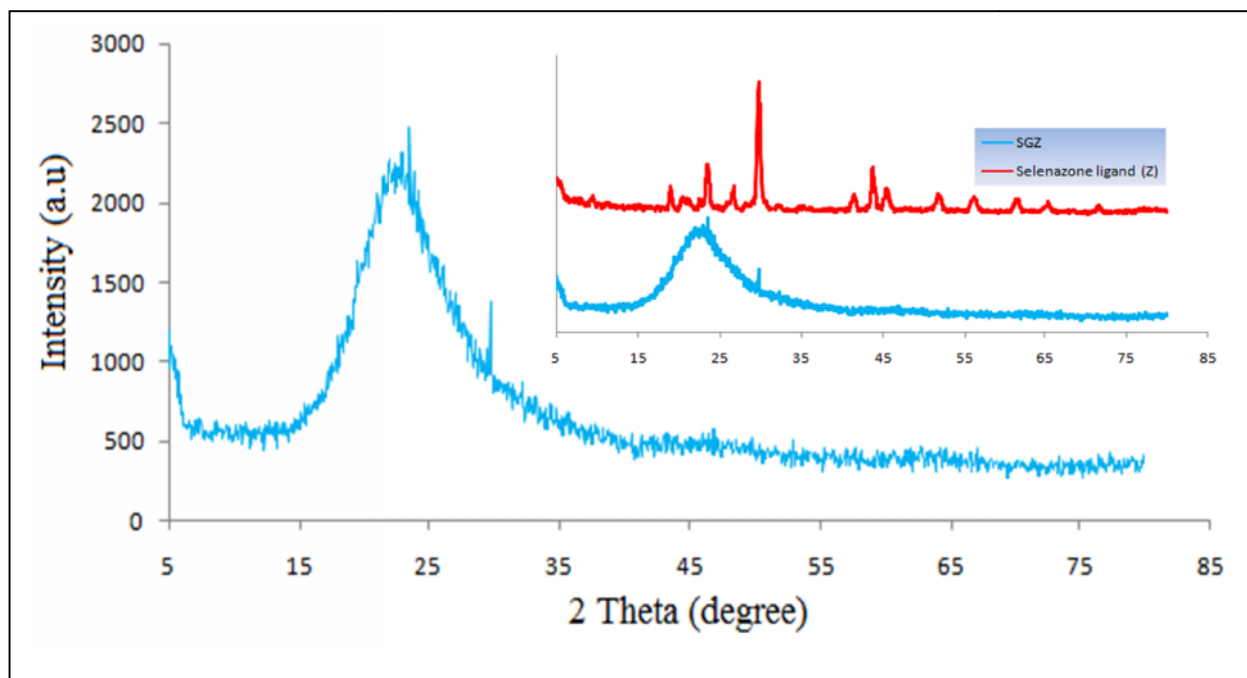
Figure 4.27 : XRD pattren of SGZ
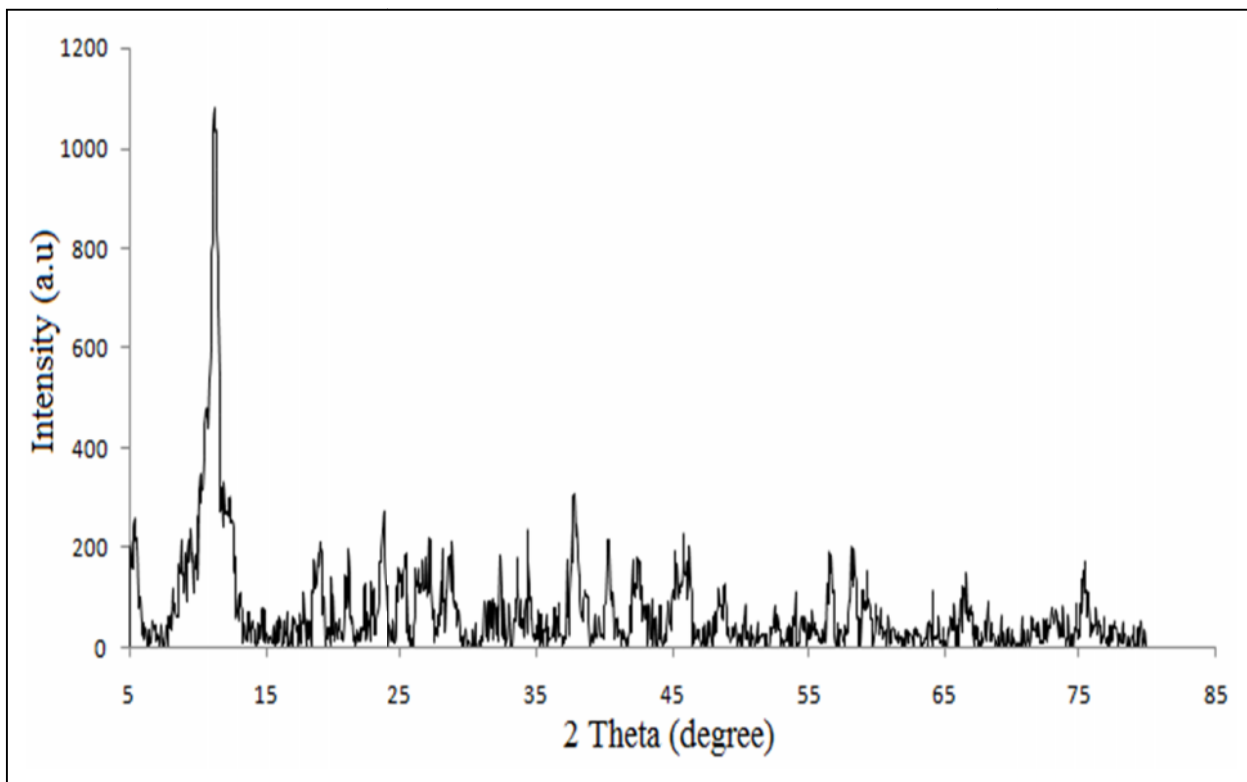
Figure 4.28 : XRD pattren of GO
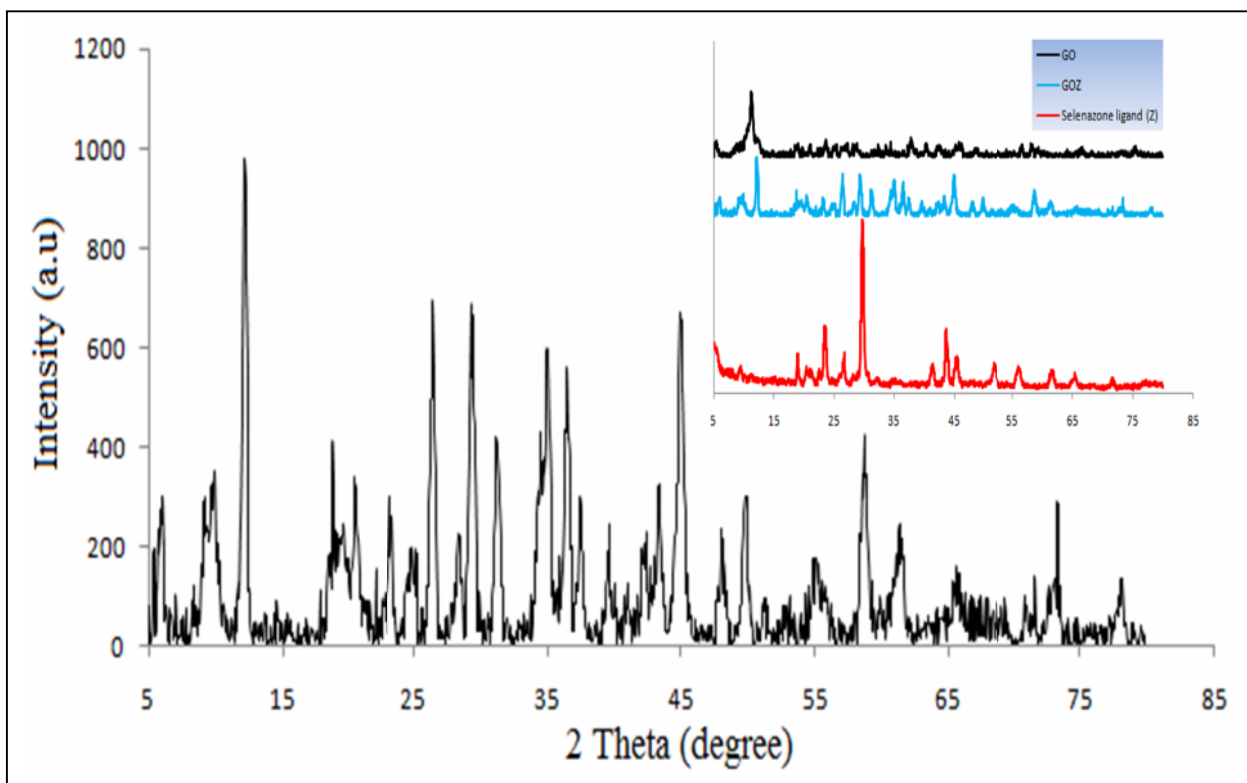
Figure 4.29 : XRD pattren of GOZ
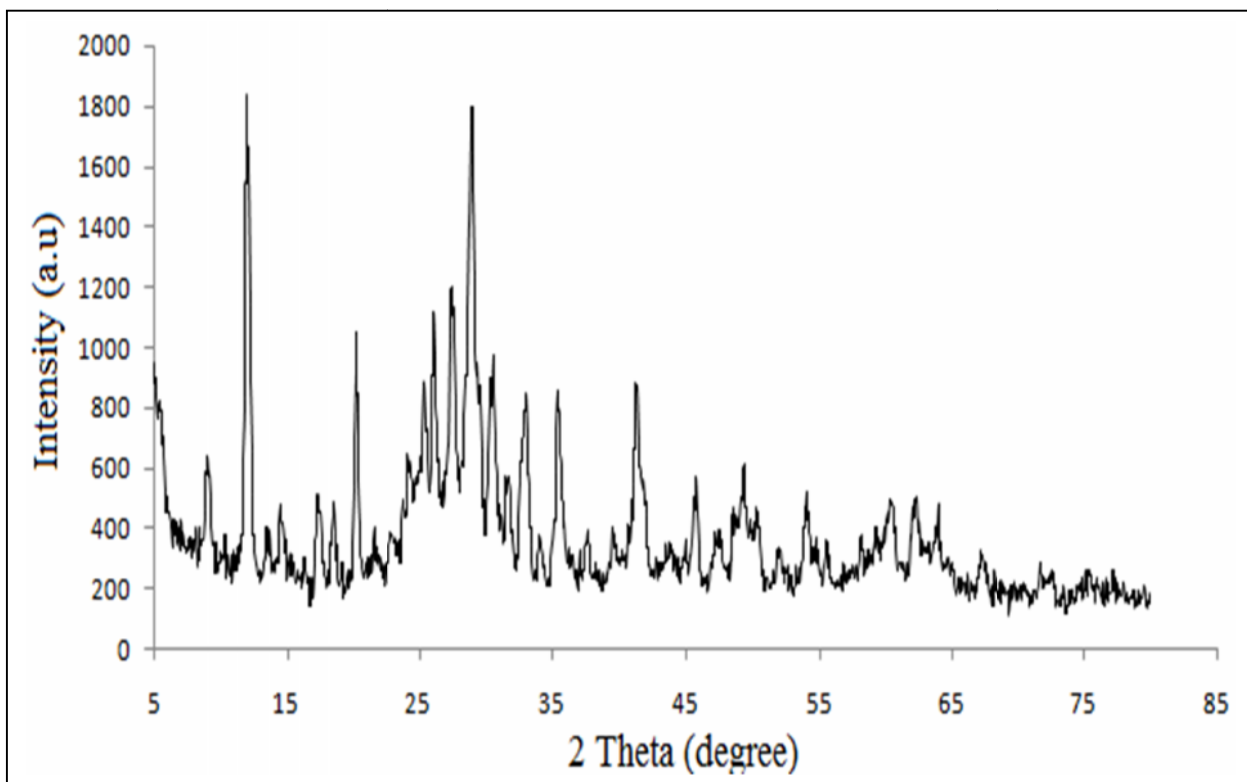
Figure 4.30 : XRD pattren of sGO
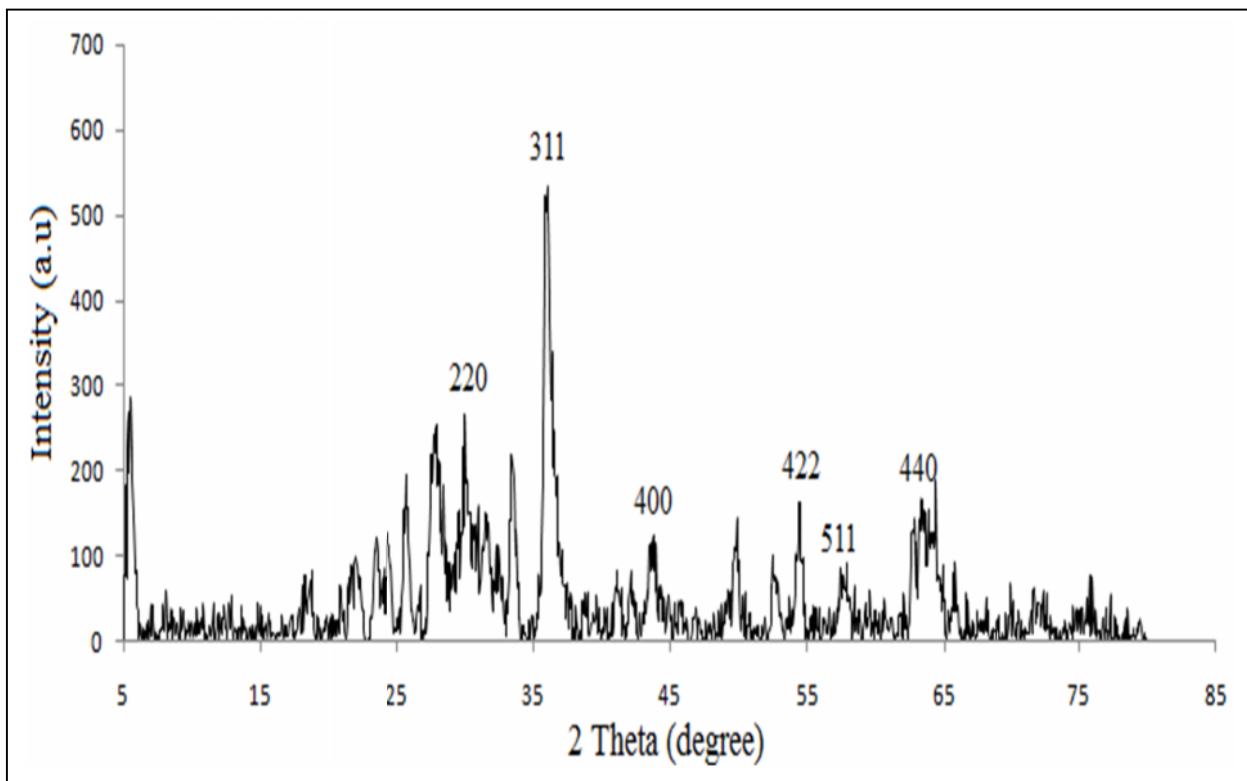
Figure 4.31 : XRD pattren of sFe

4.6. Determination of porosity and surface area for adsorbents

The pore structure plays an important role in the adsorption process and can be defined as a one of the cavity type that exists in the outer surface of a solid material which allows the movement of fluids into , out of , or through the materials [160]. In general , the porosity can be classified into three categories that depend on a pore diameter according to the IUPAC definition that is given as follows [46, 160]:

- Micropores : when a diameter value of pore is less than 2 nm (D <2 nm) .

- Mesopores : when the pore diameter is located within the range from 2 to50nm (2 < D <50 nm) .

- Macropores: when a diameter value of pore is larger than 50nm (D >50 nm).

Basically , the surface area of material depends on the pores structure where the micropores type gives the highest surface area and porosity when compared with other types , the surface area is a main factor which determine the adsorption process efficiency [160]. There are many methods that can determine the surface area for materials such as Brunauer Emmett Teller (BET) , Barrett Joyner Halenda (BJH) , t-plot and Langmuir methods by applying inert gas as N_2 at 77 K onto outer surface of materials and thus , the adsorption-desorption system occurs for nitrogen molecules where the number of the adsorbed nitrogen gas molecules points to the surface area [161,162]. The current work employs BET method to calculate the surface area for the adsorbents while, the pore size and pore volume are provided by using BJH method .

The data of the surface area recorded the highest value in ACZ adsorbent because the activated carbon has three types of pore structure like micropores , mesopores and macropores [46, 160]. The GO adsorbent recorded a higher surface area than their derived adsorbent GOZ, this result may be attributed to the increase of pore volume in GOZ adsorbent than in GO adsorbent [56]. The silica gel

modified (SGZ) also recorded a high surface area , this result may be referred to as good adsorbent to remove some pollutants from their aqueous solutions. The BET results of sGO and sFe demonstrated that the surface area of sGO was higher than the surface area of sFe . All adsorbents revealed pore structures of the micropore type, except for the SGZ and sFe adsorbents, which showed the mesopores type [153] .The BET and BJH data of all adsorbents are depicted in Table 4.3.

Table 4.3 : The porosity and surface area data

adsorbent	Surface area (m^2/g)	Pore volume (cm^3/g)	Pore diameter (nm)	Type of pore
ACZ	170.03	0.1979	1.21	Micropores
SGZ	108.56	1.3585	39.01	Mesopores
GO	5.004	0.0216	1.64	Micropores
GOZ	1.4819	0.0559	1.64	Micropores
sGO	5.6824	0.03588	1.85	Micropores
sFe	1.4915	0.01591	7.99	Mesopores

4.7. Thermal analysis

4.7.1. Differential scanning calorimetry

   DSC curve (Figure 4.32) of the modified activated carbon ACZ indicated two endothermic weak peaks at 122.77 and 668.90 ℃ which is attributed to the starting decomosition of molecules ligand loaded. The weak peaks may be due to the decrease of heat transfer that is attributed to the porosity nature of the activated carbon [163,164] . The DSC of the modified silica gel (Figure 4.33) observed indicated two endothermic weak peaks at 48.24 and 95.93 ℃, which may attributed to the loss of water molecules and decomposition of molecules ligand loaded on the outer surface of silica gel .

Two exothermic peaks at 207.79 and 592.26 ºC and endothermic peak at 110ºC are demonstrated in DSC curve of graphene oxide (GO), which shown in Figure 4.34. This is due to the loss of unstable oxygen existing in the functional groups of graphene oxide to form CO and CO_2 . Therefore the exothermic peaks appeared. The endothermic peak is attributed to the loss of water molecules that were adsorbed by graphene oxide [165,166]. The modified garphene oxide GOZ appeared in three endothermic peaks in DSC curve at 108.64 , 308.57 and 771.12 ºC which were attributed to the loss of water molecules which exist in the structural origin of graphene oxide and decomposition of ligand loaded on GO surface respectively . The DSC data of GOZ adsorbent is shown in Figure 4.35.

 Figure 4.36 of DSC curve to sGO adsorbent appears three endothermic peaks at around 90.68 ºC that may be attributed to water molecules in the structure of sGO adsorbent while the remain materials are lost at 701.96 and 818.62 ºC .

  The DSC curve (Figure 4.37) of sFe adsorbent was revealed in three endothermic peaks, the first peak shows 77.94ºC that may due to loss molecules of lattice water while the second appears at 140.89 ºC that may due to loss of coordinated molecules of water or to loss dehydroxylation. On other hand, in the final step of pyrolysis shows a peak at 770.60ºC which may be attributed to Iron oxide formation after removing the impurities [167]. The DSC data are listed in Table 4.4.
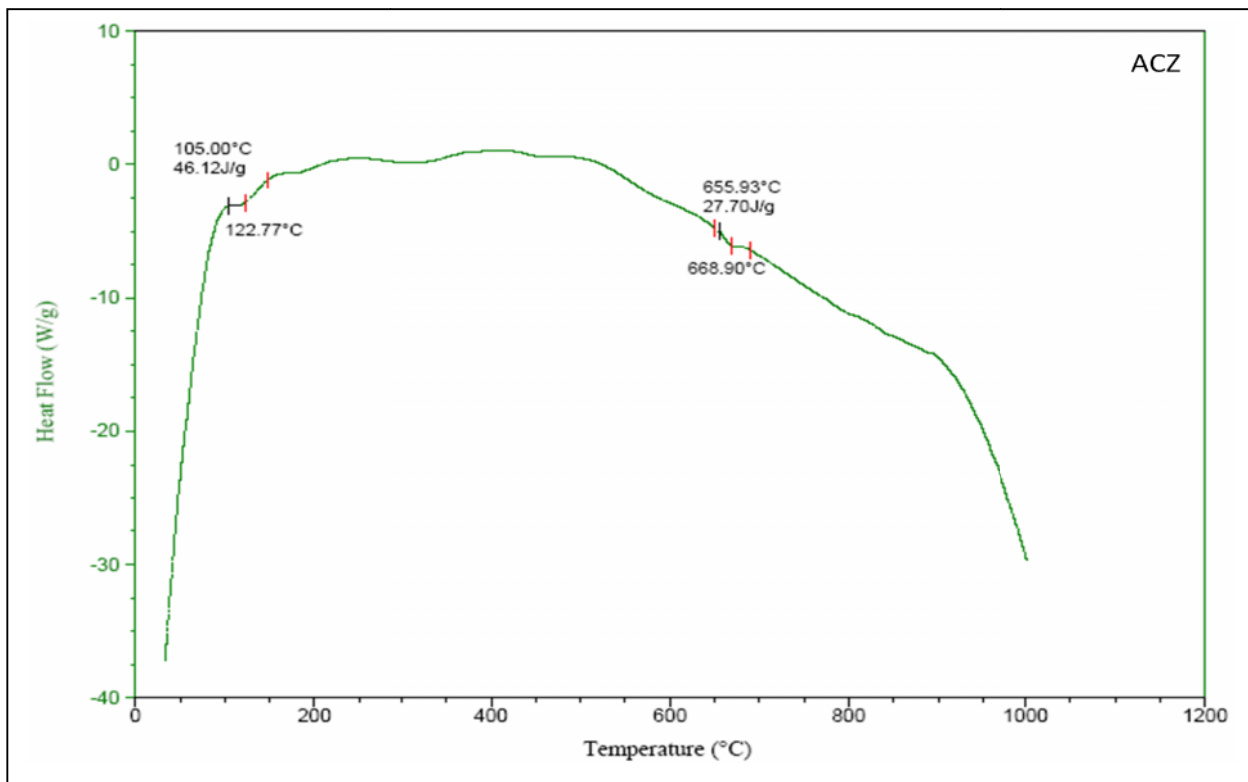
Figure 4.32 : The DSC curve of ACZ
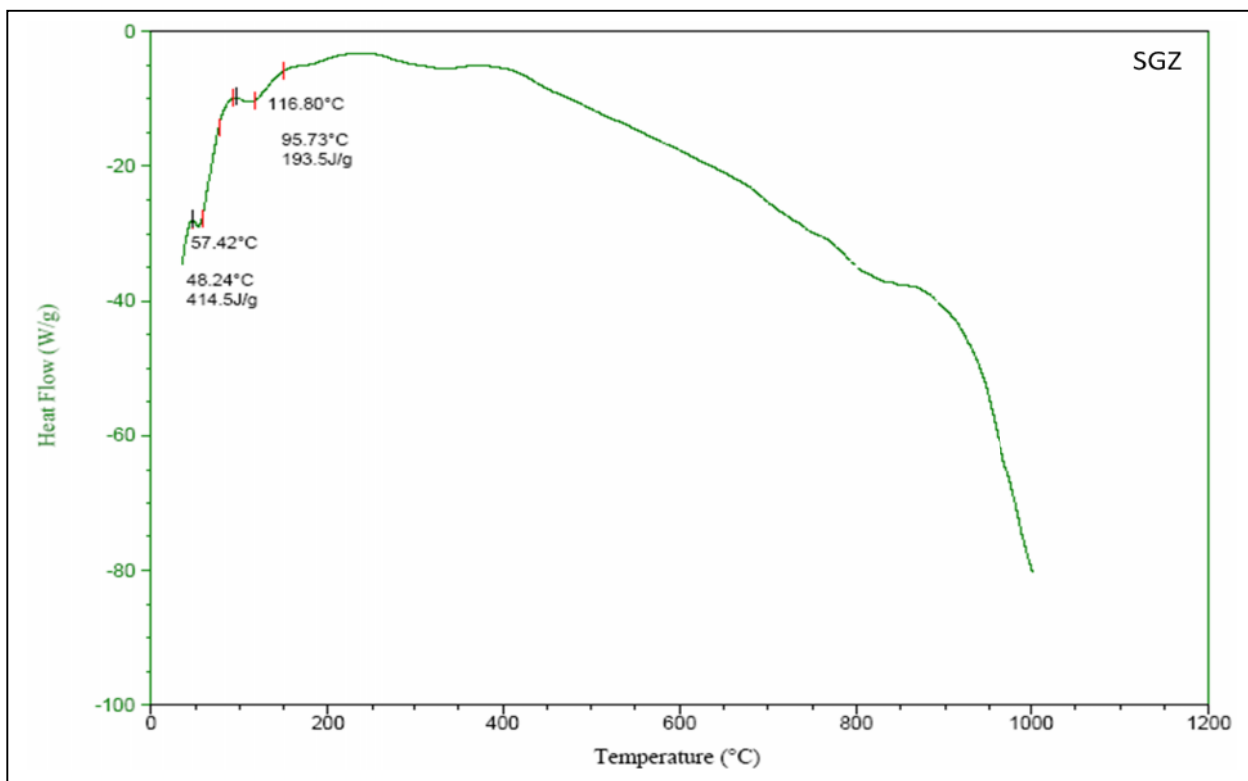
Figure 4.33 : DSC curve of SGZ
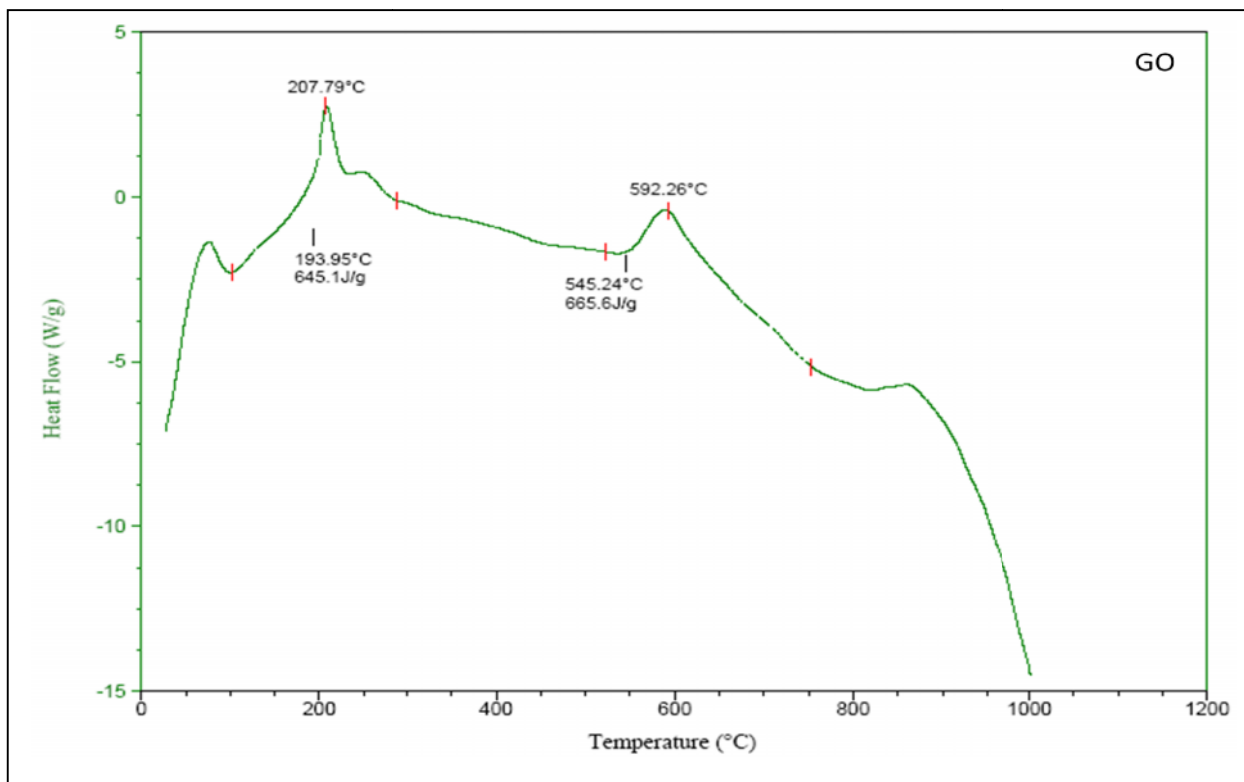
Figure 4.34 : The DSC curve of GO
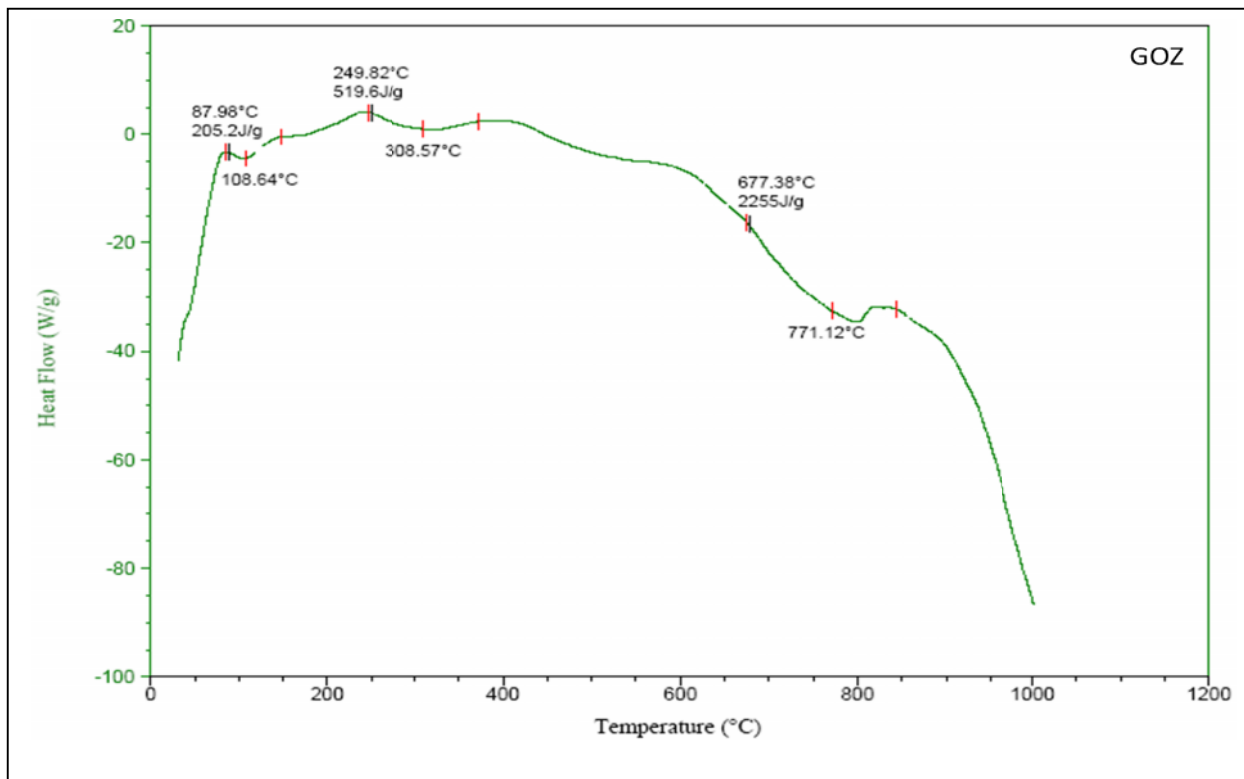
Figure 4.35 : DSC curve of GOZ
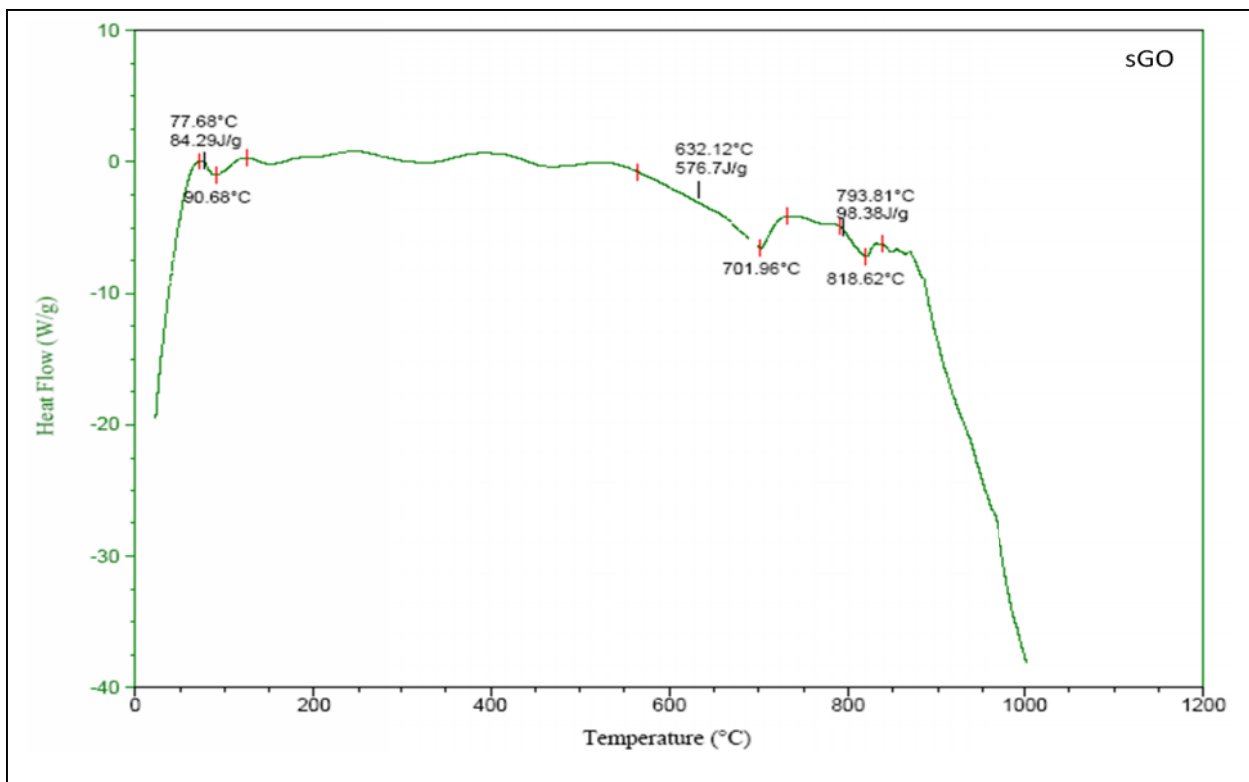
Figure 4.36 : The DSC curve of sGO
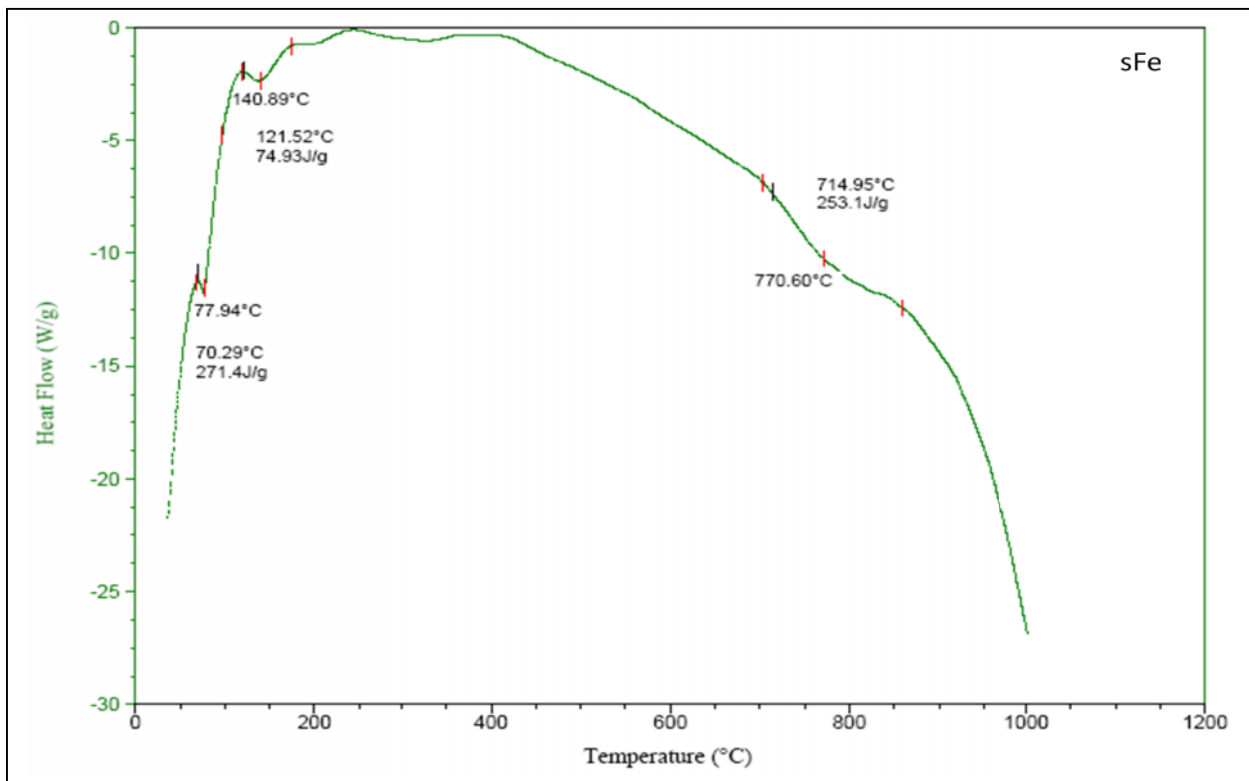
Figure 4.37 : DSC curve of sFe

Table 4.4 : The results of DSC analysis

adsorbent	1st Peak				2nd Peak				3rd Peak			
	T_iºC	T_{max}ºC	T_fºC	ΔH J/g	T_iºC	T_{max}ºC	T_fºC	ΔH J/g	T_iºC	T_{max}ºC	T_fºC	ΔH J/g
ACZ	100	122.77	155	46.12	650	655.93	700	27.70	-	-	-	-
SGZ	45	48.24	60	414.5	95	116	150	193.5	-	-	-	-
GO	75	110	150	-	155	207.79	290	645.1	545	592.2	785	665.6
GOZ	85	108.64	155	205.2	249	308.57	375	519.6	677	771	840	2255
sGO	75	90.86	125	84.29	565	701.96	785	576.7	790	818.62	840	98.38
sFe	70	77.94	85	271.4	121	140.89	175	74.93	705	770.60	860	253.1

4.7.2. Thermogravimtric analysis (TG/DTG)

Thermal analysis (TG/DTG) can provide an important information about the adsorbent materials such as thermal stability , behavior of thermal decomposition for materials , knowning of the lost amount of each pyrolysis stage. The kinetic and thermodynamic parameters can be calculated from thermal analysis data[94 , 108]. Six adsorbent surfaces were measured under the heating rate at 10 ºC/min and inert gas of nitrogen .

The thermogram of ACZ adsorbent revealed three thermal degradation steps , the first step recorded in the range of 35-355ºC (DTG_{max}218ºC) with a weight loss ratio 7.70% , which was attributed to start the loss of some ligand loaded molecules. The second and third steps of the thermal decomposition were recorded in ranges at 360-550ºC (DTG_{max}502ºC) and 555-1000ºC (DTG_{max}845ºC) with loss weight ratio of 6.45% and 33.41% respectively that may be attributed to the loss of residual ligand molecules, the third step was attributed to the decomposition of carbonaceous material [168,169]. The total wight loss ratio is 47.68% and the result of TG/DTG curve was appeared in Figure 4.38.

There were four steps of thermal decomposition demonstrated for the modified silica gel SGZ (Figure 4.39). The first step starts at an extent of 35-160ºC (DTG$_{max}$ 55ºC) with a loss weight ratio of about 8.07% that was attributed to the molecules of lattice water that exists within silica gel structure, while the second pyrolysis step which recorded the range of 165-380ºC (DTG$_{max}$ 331.8ºC) with a loss weight ratio 7.41% may be attributed to the loss ligand loaded molecules that was linked onto SGZ adsorbent surface. The third and fourth steps of pyrolysis recorded the range of 385-735ºC (DTG$_{max}$551ºC) and 740-1000ºC (DTG$_{max}$ 800ºC) with a loss mass ratio of 10.22 and 7.03 %, respectively which referred the occurrence of the dehydroxylation process from the structural formula of SGZ adsorbent [170, 171].

The TG/DTG curve of graphene oxide GO (Figure 4.40) was measured in the range of 25-1000ºC, in which three thermal degredation steps were observed in the range of 25-165ºC (DTG$_{max}$ 94.6ºC) and with a mass loss ratio of 8.61% that was attributed to the molecules of lattice water, while the other steps began with the range of 170-290ºC (DTG$_{max}$ 200.7ºC) and 295-1000ºC (DTG$_{max}$ 565ºC) that corresponded with the percentage of lost mass, 78.04 and 6.55 % respectively which indicated the removal of CO and CO_2 molecules from the structural formula of GO adsorbent . This result of TG/DTG analysis of graphene oxide is consistent with the previous studies [165,166] .

Figure 4.41 refers to TG/DTG thermal analysis of GOZ adsorbent, with three steps appearing in the range of 30-285ºC (DTG$_{max}$220.6ºC) , 290 -745ºC (DTG$_{max}$591.5ºC) and 750-1000ºC (DTG$_{max}$ 887.8ºC), that is consistent with the percentage of a weight loss at 21.15 , 30.46 and 19.56 %, respectively, which may be attributed to loss of lattice water molecules, molecules of ligand loaded, and the removal of CO and CO_2 molecules [172,173].

Five thermal degradtion steps are dipicted in Figure 4.42 and were recorded in TG/DTG curve of sGO adsorbent, the first step appeared with an extent of 20-190ºC (DTG_{max} 93.2ºC) the lost weight ratio corresponds to 2.56 % which is attributed to the occurrence of the dehydration process by removing the water molecules that are linked via weak forces. The other steps were recorded by the range 195-430ºC (DTG_{max}390.2ºC) , 435-595ºC (DTG_{max} 508.7ºC) , 600-835ºC (DTG_{max}656ºC) and 840-1000 ºC (DTG_{max}923.3ºC), this result corresponds with the loss mass percentage at 4.56 , 10.23 , 15.34 and 3.03 % respectively which is consistent with the lost of hydroxyl groups by using the dehydroxylation process and carbon mono oxide and carbon dioxide [140,165 , 166].

The result of TG/DTG analysis of sFe adsorbent (Figure 4.43) exhibted three steps of the thermal decomposition that were recorded with the extent 35-195 ºC (DTG_{max}90ºC) , 200-635ºC (DTG_{max}531ºC) and 640-1000ºC (DTG_{max}945.2ºC) and with a loss weight ratio of 1.18 , 3.39 and 5.68 %, respectively. This result may be attributed to the removal of physical adsorbed molecules of water and dehydroxylation process [148 ,174]. The total the loss weight ratio via all of the pyrolysis steps is 10.2% , where the decrease in loss mass ratio of sFe adsorbent with the increase in temperatures indicates that the sFe adsorbent is Iron oxide nanoparticles, which corresponds with the obtained results for all techniques that were used . Kinetic and thermodynamic parameters are calculated by using Coast-Redfern equation of all the adsorbent surfaces that are listed in Table 4.5 .
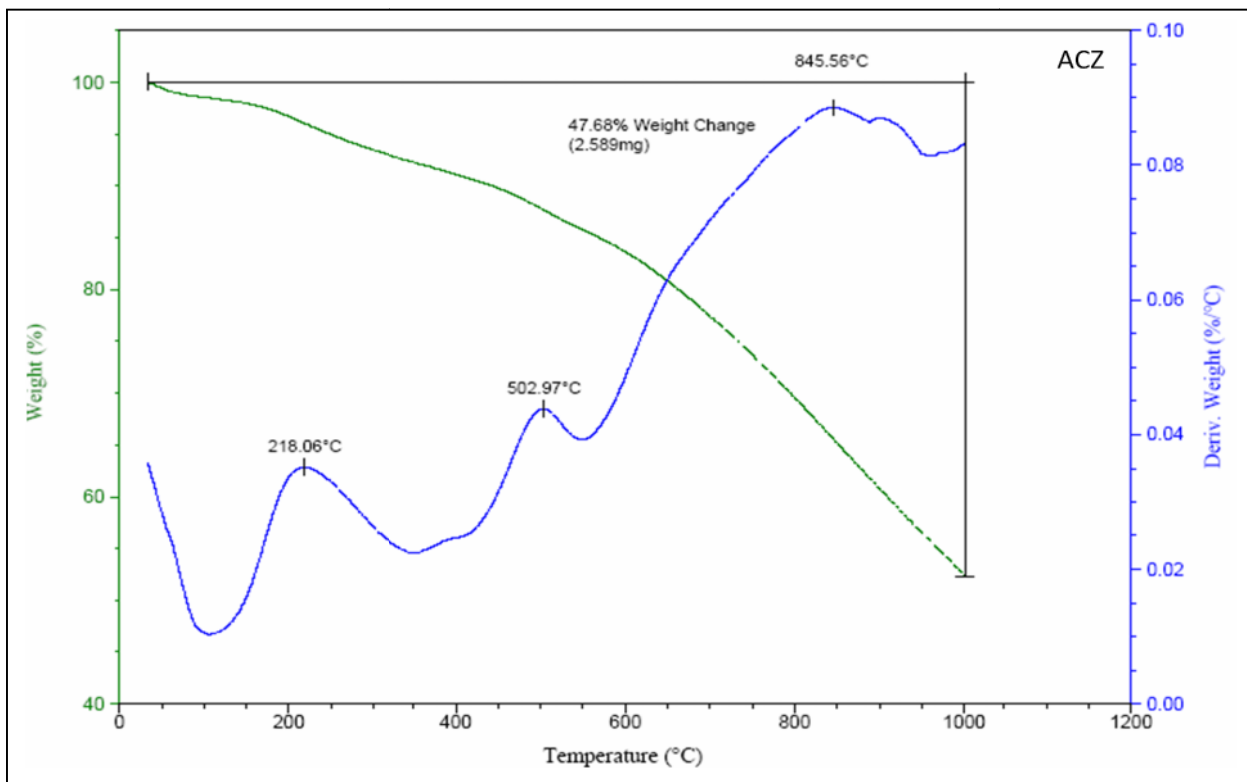
Figure 4.38 : The TG/DTG curve of ACZ
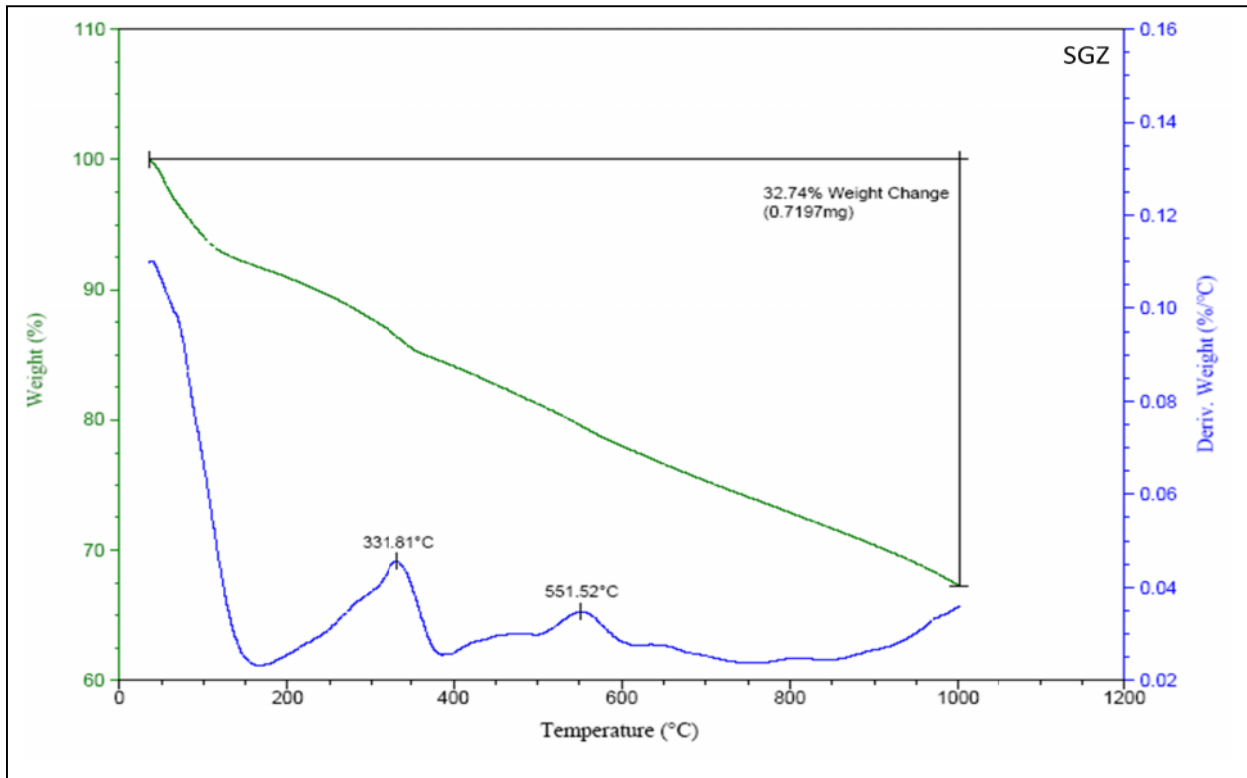
Figure 4.39 : The TG/DTG curve of SGZ
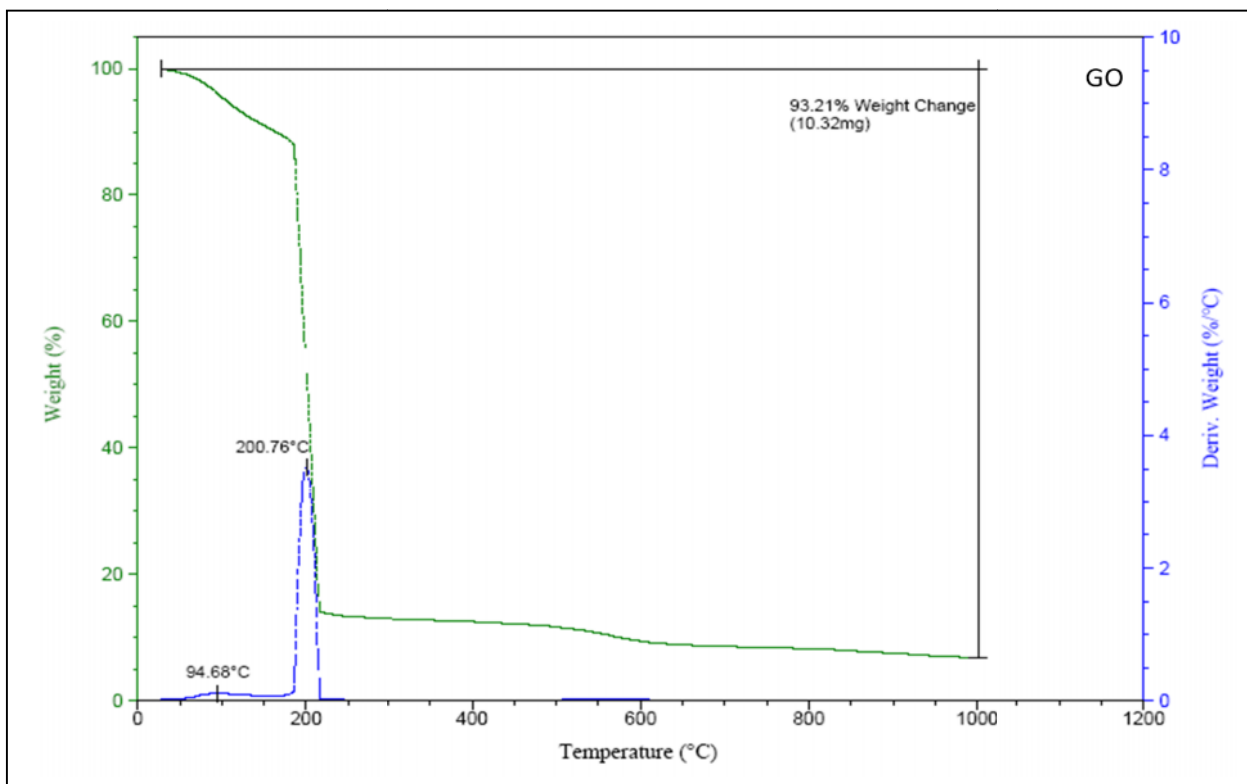
Figure 4.40 : The TG/DTG curve of GO
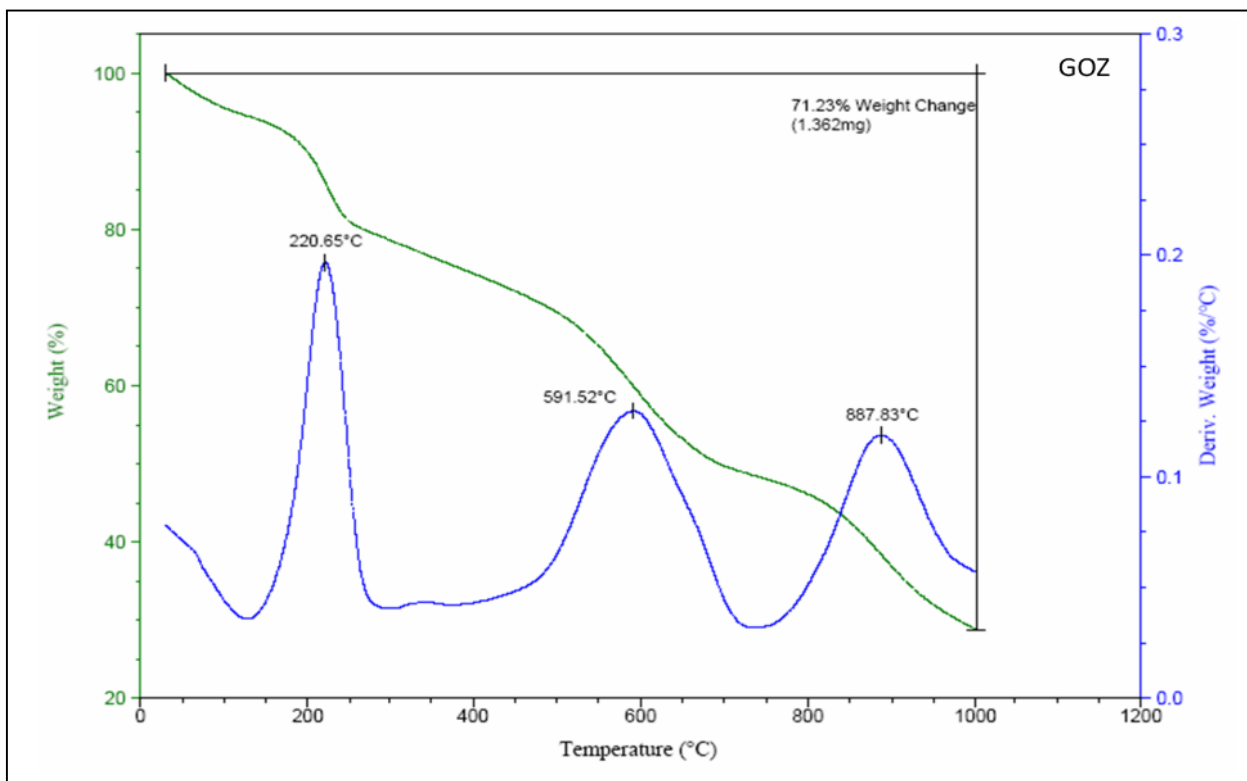
Figure 4.41 : The TG/DTG curve of GOZ
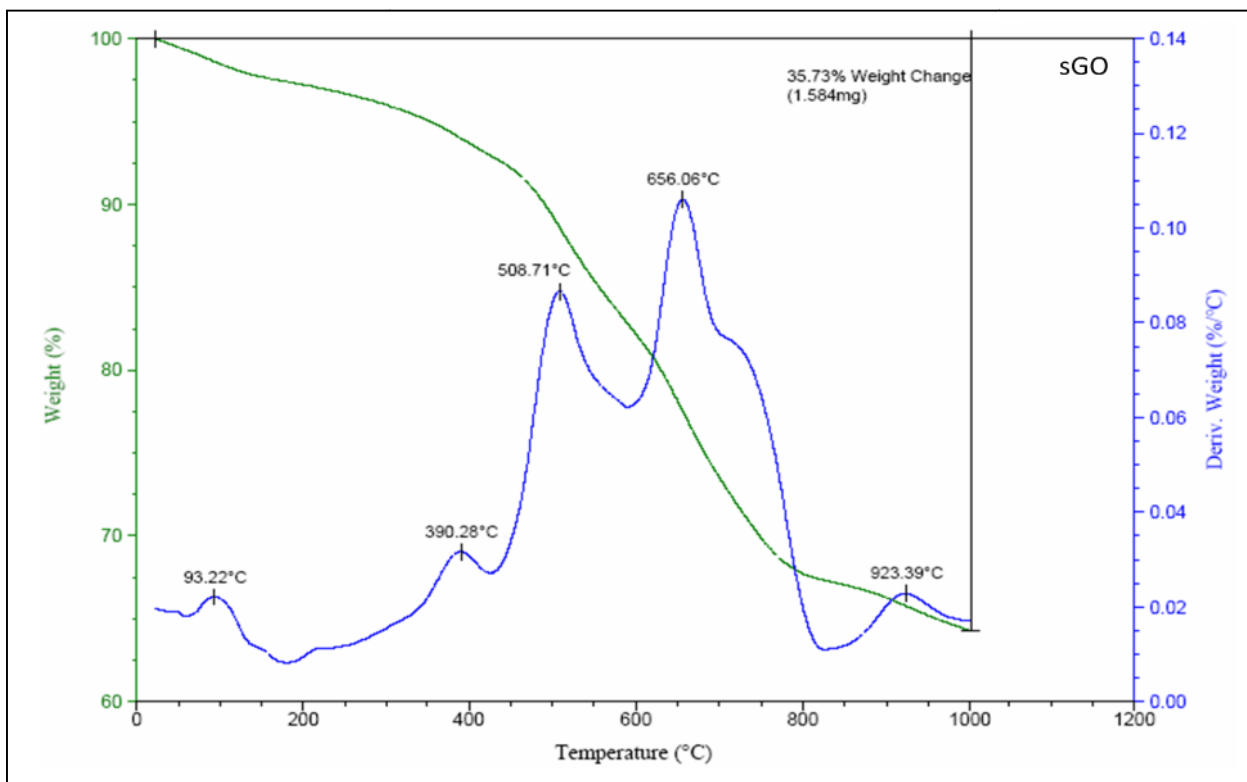
Figure 4.42 : The TG/DTG curve of sGO
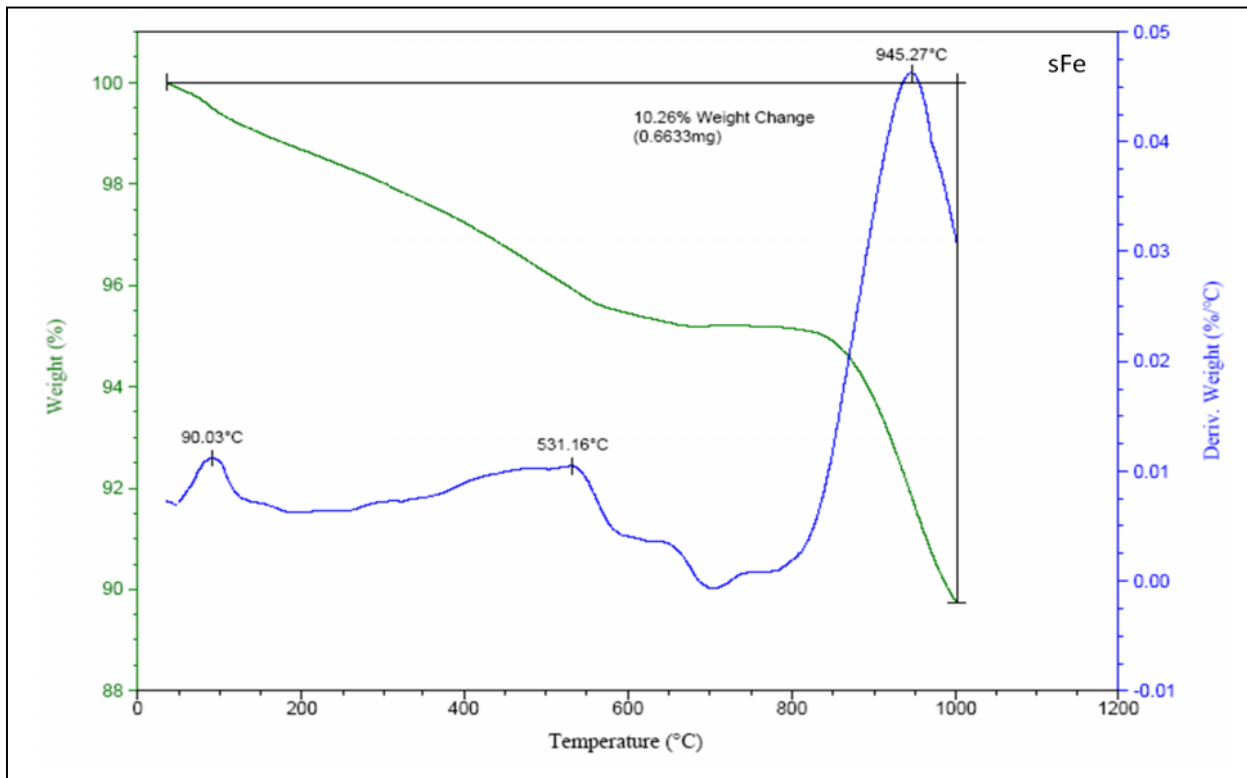
Figure 4.43 : The TG/DTG curve of sFe

Table 4.5: Kinetic – Thermodynamic parameters of all adsorbent surfaces

Complex	Step	A (S^{-1})	E (KJmol^{-1})	ΔH (KJmol^{-1})	ΔS (KJmol^{-1}K^{-1})	ΔG (KJmol^{-1})	R^2
ACZ	1st	0.012132	13.874	9.792	-0.2857	150.089	0.849
	2nd	1156.981	86.831	80.388	-0.1942	230.899	0.957
	3rd	2.293374	77.734	68.439	-0.2490	346.819	0.937
SGZ	1st	1252.725	40.662	37.935	-0.1864	99.074	0.724
	2nd	6.377369	41.664	36.642	-0.2353	178.809	0.955
	3rd	1.257715	54.820	47.969	-0.2514	255.168	0.927
	4th	2536.067	146.272	137.351	-0.1903	341.638	0.928
GO	1st	448.1706	39.723	36.663	-0.1959	108.755	0.96
	2nd	1.19×10^9	108.547	104.614	-0.0750	140.105	0.711
	3rd	0.0157	31.987	25.020	-0.2880	266.397	0.918
GOZ	1st	0.053248	17.235	13.136	-0.2734	147.959	0.866
	2nd	0.17243	41.491	34.308	-0.2683	266.180	0.955
	3rd	2322953	209.944	200.3	-0.1343	356.129	0.965
sGO	1st	1.961083	23.390	20.347	-0.2410	108.559	0.905
	2nd	3.748363	43.949	38.437	-0.2405	197.934	0.952
	3rd	2408746	141.780	135.287	-0.1307	237.399	0.954
	4th	21808.99	137.980	130.256	-0.1713	289.395	0.93
	5th	4.2×10^{10}	311.359	301.415	-0.0530	364.904	0.956
sFe	1st	3.031629	25.660	22.642	-0.2373	108.791	0.948
	2nd	0.05285	28.627	21.942	-0.2776	245.135	0.947
	3rd	531.335	140.786	130.659	-0.2044	379.664	0.829

The ΔG values recorded positive results that referred to the nonspontaneous reaction in all decomposition steps of adsorbents, while the enthalpy (ΔH) in all decomposition steps of adsorbents appeared to be positive values, which indicated that all decomposition steps were endothermic. The negative values of entropy referred to the decomposition reactions process which occurred at a very low rate [94, 108] . The activation energy appeared for adsorbents as a function of the thermal stability where all the adsorbents were ordered according to their thermal stability as : SGZ > GO > sFe > sGO > GOZ > ACZ .

Chapter Five

Results and Discussion

Adsorption and Desorption study

5. Adsorption and Desorption study

5.1. Adsorption study

This section of this chapter aims to remove four different types of dyes (Mordant Red 3 , Congo Red , Basic Brown and Rhodamine B) and two heavy metals (mercury and lead) from their aqueous solutions by using batch adsorption experiments .

5.1.1. Selection of optimum conditions

5.1.1.1. Effect of contact time

The contact time between the adsorbate solution and the adsorbent was studied for a period of time ranged from 5min to 240 min and it continued for 24h at a room temperature by utilizing a fixed concentration about 50 ppm for the dyes solution and 14 ppm for the lead solution of all adsorbent surfaces excepted for SGZ adsorbent that utilized 4ppm , while the concentration of mercury solution was 1000 ppb. The percentage of adsorption amount can be calculated by using the relation as is shown in following[25,67,175] :

$$\% Ad = [(C_o - C_e) / C_o] \times 100$$

Where : C_o , C_e are initial and residual concentration (mg/l) of adsorbate solution .

The contact time of Mordant Red 3 dye (Figure 5.1) was examined for all the adsorbent surface. The results indicated the highest value of the adsorbed amount percentage which is 92.58% by using ACZ adsorbent for 120 mins because the activated carbon has many active sites like grooves , channals and functional groups [160], the lowest value of adsorbed amount percentage is 13.81% that was recorded for 120 mins by SGZ adsorbent. Moreover , the other adsorbent surfaces were recorded the percentage of adsorbed amount at 44.76 , 30.98 and 23.36 % for 120 , 20 and 60 min to GO , sGO and GOZ adsorbent, respectively. On the other hand the adsorbent of sFe has not recorded any reaction with the dye solution of

Mordant Red 3. In general, the adsorption process depended on the chemical and physical properties of each adsorbent and adsorbate materials [24,25] .

For Congo Red, the shortest contact time was recorded in sFe adsorbent for 20 mins with the removal percentage solution of 65.84 % (Figure 5.2), while the highest value was recorded at the contact time for 180 mins with a removal percentage of 63.98% to the sGO adsorbent . In order to reach the equilibrium time that is needed to reach the saturation state of all active sites on adsorbent surfaces by adsorbate [24 , 175] . The other adsorbents recorded different periods of time to contact time for 30 , 60 and120 mins with the removal percentage at 43.64 , 88.75 , 61.58 and 86.89% to GOZ , ACZ , SGZ and GO adsorbents respectively .

For Basic Brown dye, Figure 5.3 appears the increase of the removal percentage to reach of 89.91% for 90 mins by using GOZ adsorbent. On the other hand, the graphene oxide GO adsorbent was recorded rapidly adsorption for a short time around 30 mins with the adsorbed percentage of 88.86%, this may be attributed to the decrease of particles size of GO adsorbent rather than with GOZ . The remained adsorbents recorded various periods of time to reach the equilibrium time at 60,90 and 120 mins with the adsorbed percent of 63.52 , 71.71 , 74.09 and 85.55% to adsorbent of sGO , sFe , SGZ and ACZ respectively .

For Rhodamine B dye, the adsorbent surfaces have been examined, where the three adsorbent surfaces only appeared high efficiency towards the removal of dye from their aqueous solution . contact time was recorded at a period of time for 60-90 mins with the adsorbed percentage at 95.66 , 80.81 and 63.68 to adsorbent of ACZ , GO and GOZ (Figure 5.4), respectively.These results may attributed to the increase of surface area when compared among them [176] .

Heavy metals are faster than the dyes in the adsorption process this is attributed to the small size of heavy metals rather than to the size of dyes molecules. The

ACZ adsorbent recorded the highest removal percentage of mercury from their aqueous solution around 98.18% within a shorter period of time for 30mins, while the longer period of time was recorded by GO and GOZ adsorbents for 90mins with a removal percentage of mercury at 81.32 and 82.57 % respectively. The removal percentage of mercury was recorded by the other adsorbent surfaces at 93.34 , 83.27 and 36.36 % to agitation time for 50 , 30 and 60 min to SGZ , sFe and sGO adsorbents (Figure 5.5), respectively.

The sFe adsorbent was recorded the highest level to remove the lead ions from their aqueous solution at 93.33 % within a short contact time for 30 mins whilst ,the shortest period of contact time was recorded by GO adsorbent for 10mins with the adsorbed percentage of lead ions around 87.46% , this may be attributed to the capability of lead ions to combine with in adsorption sites that leads to fast occupied of adsorption sites in short time [177]. The remained adsorbents were recorded at periods of time in order to reach the equilibirium time for 20 , 40 , 50 and 60 mins with the removal percentage of lead ions from their aqueous solutions at 78.06 , 26.72 , 38.73 and 59.19 % that belong to GOZ , SGZ , ACZ and sGO adsorbents respectively. The results of contact time to remove lead ions are depicted in Figure 5.6 .
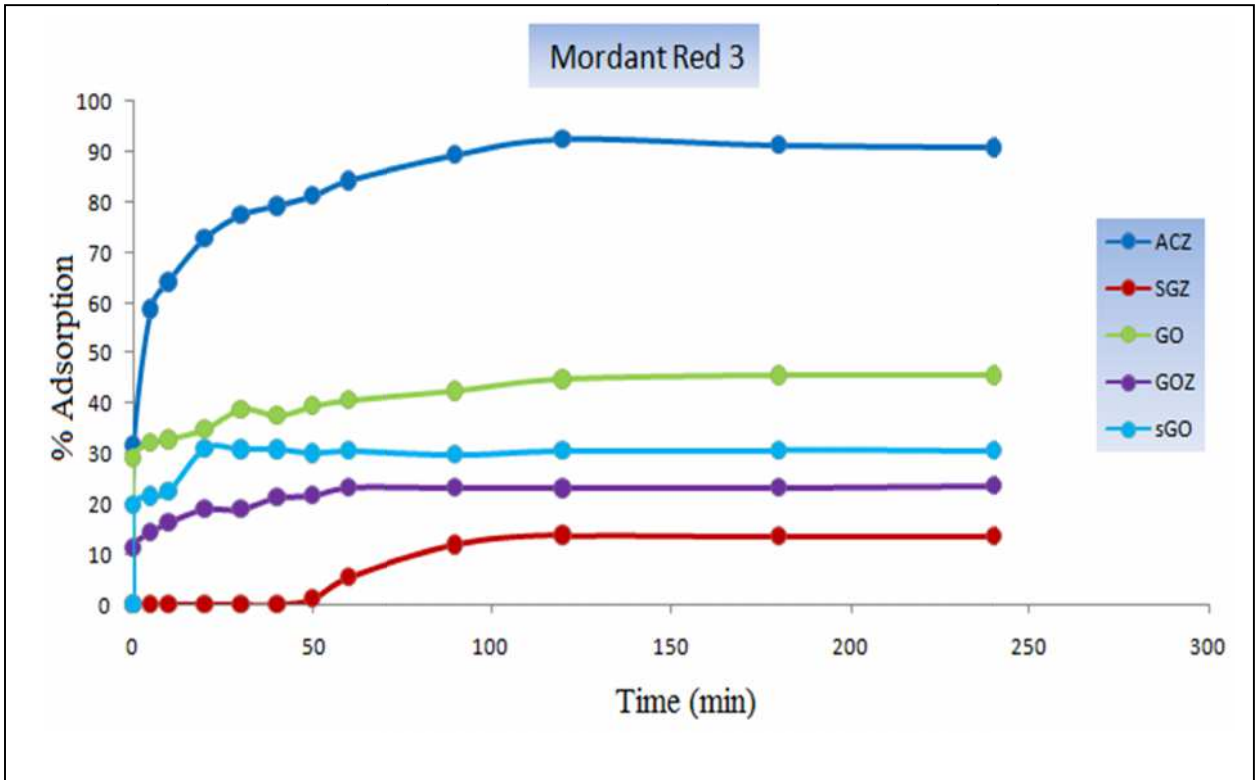
Figure 5.1 : Equilibrium time to adsorbed of Mordant Red 3
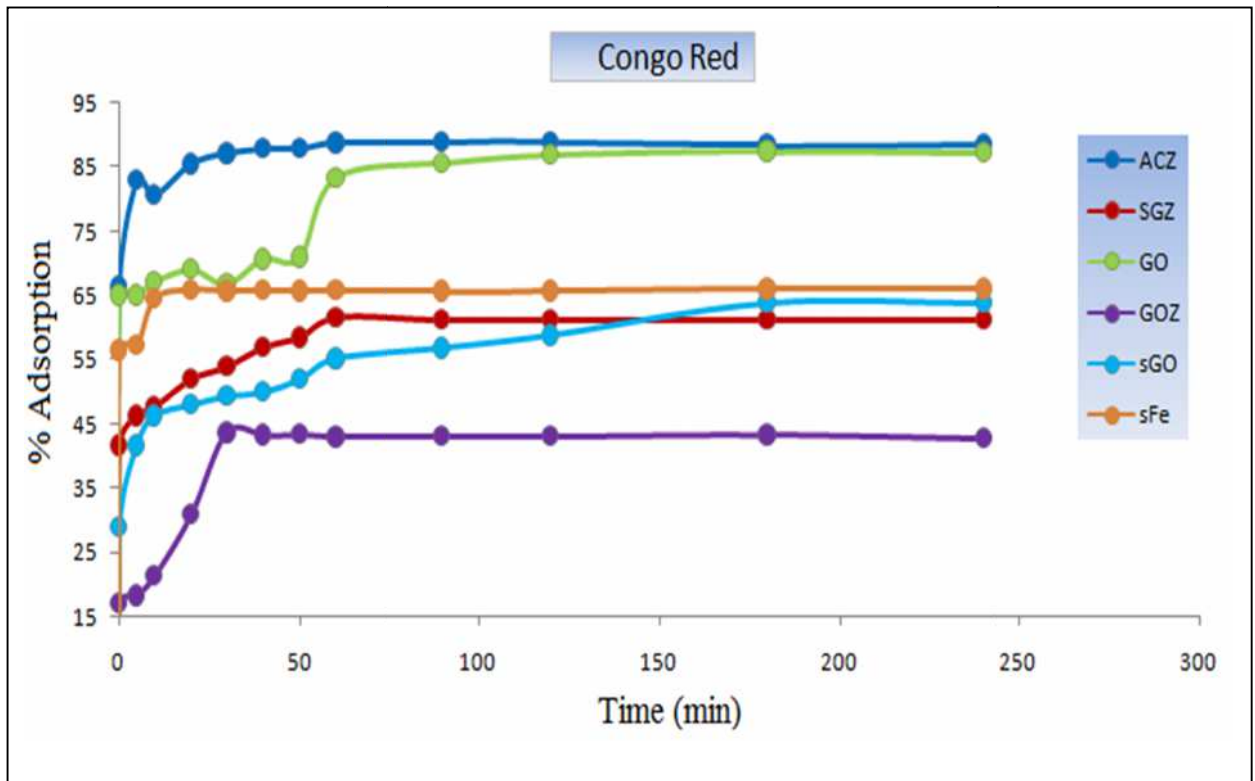
Figure 5.2 : Equilibrium time to adsorbed of Congo Red
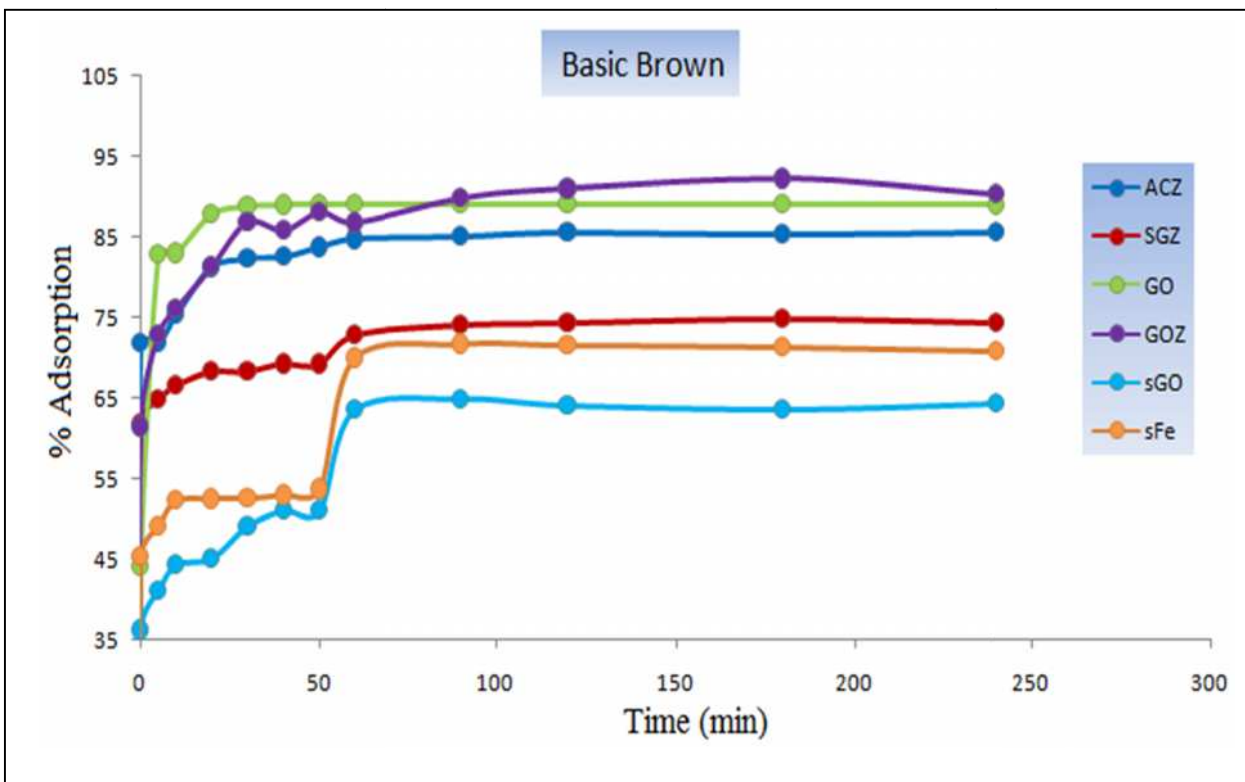
Figure 5.3 : Equilibrium time to adsorbed of Basic Brown
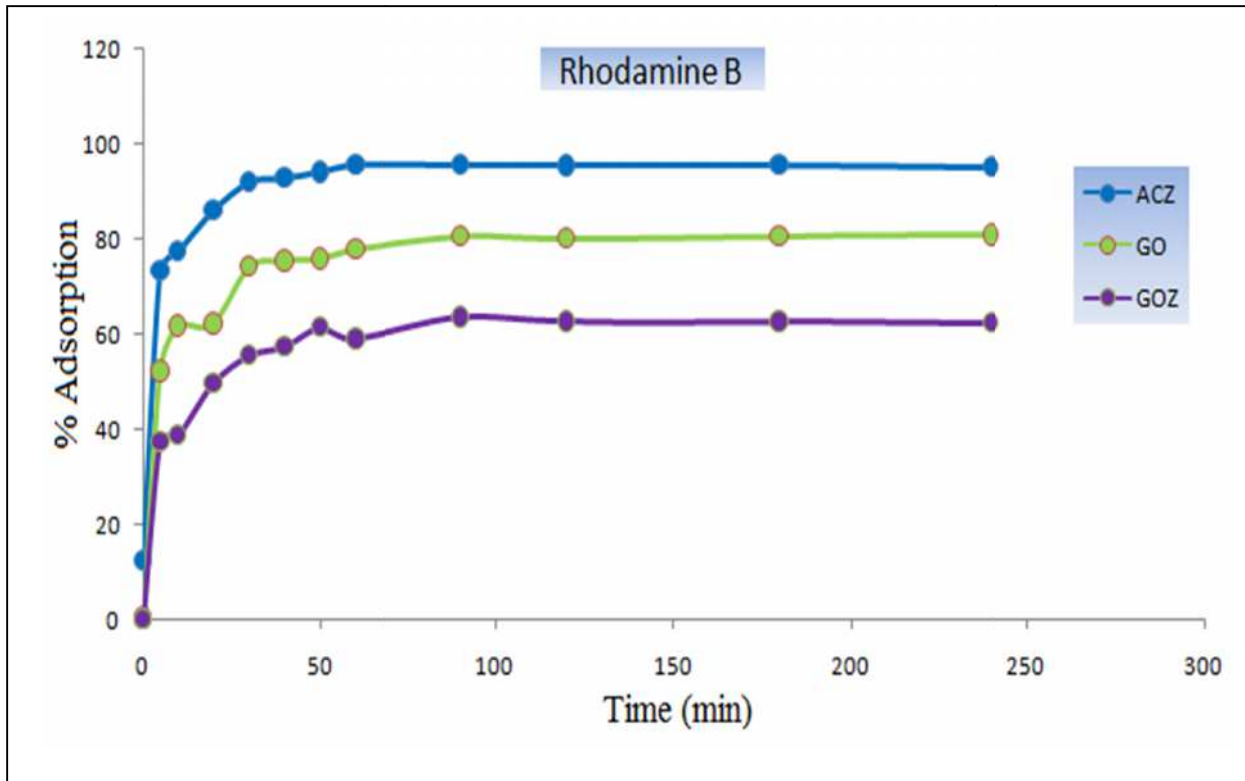
Figure 5.4 : Equilibrium time to adsorbed of Rhodamine B
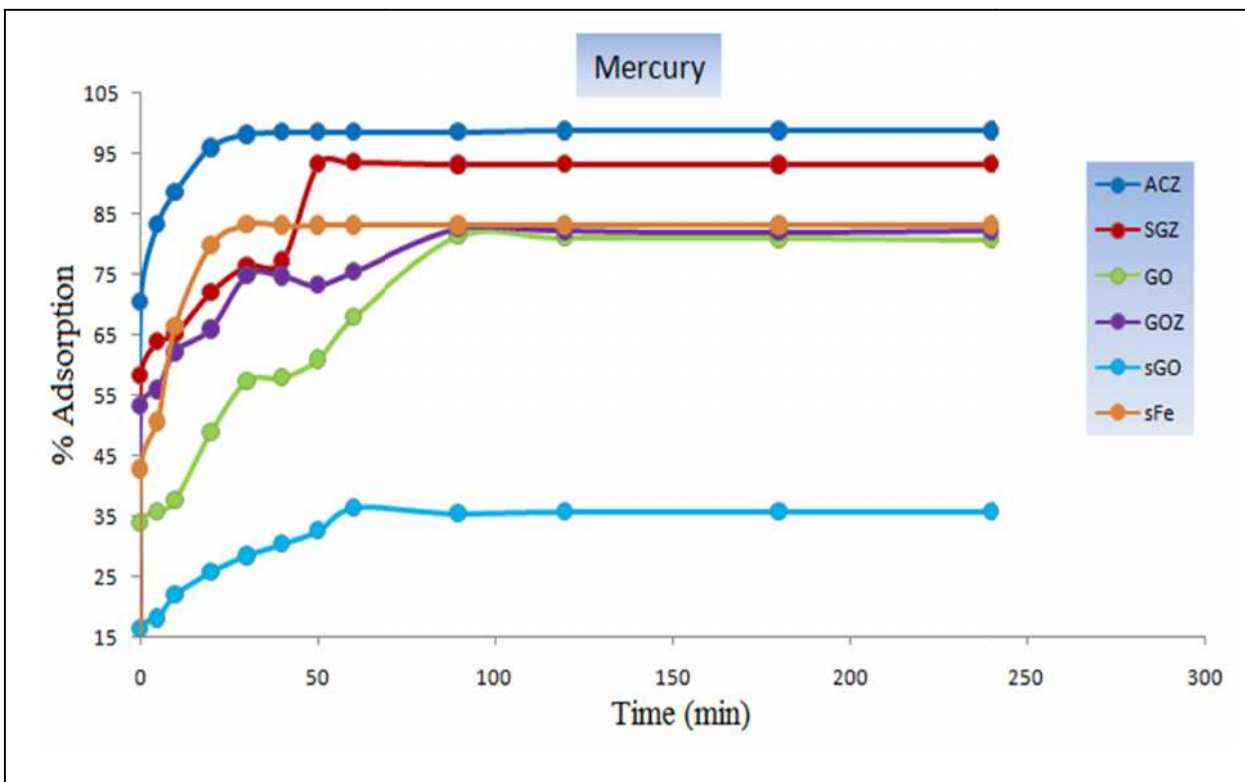
Figure 5.5 : Equilibrium time to adsorbed of Mercury ions
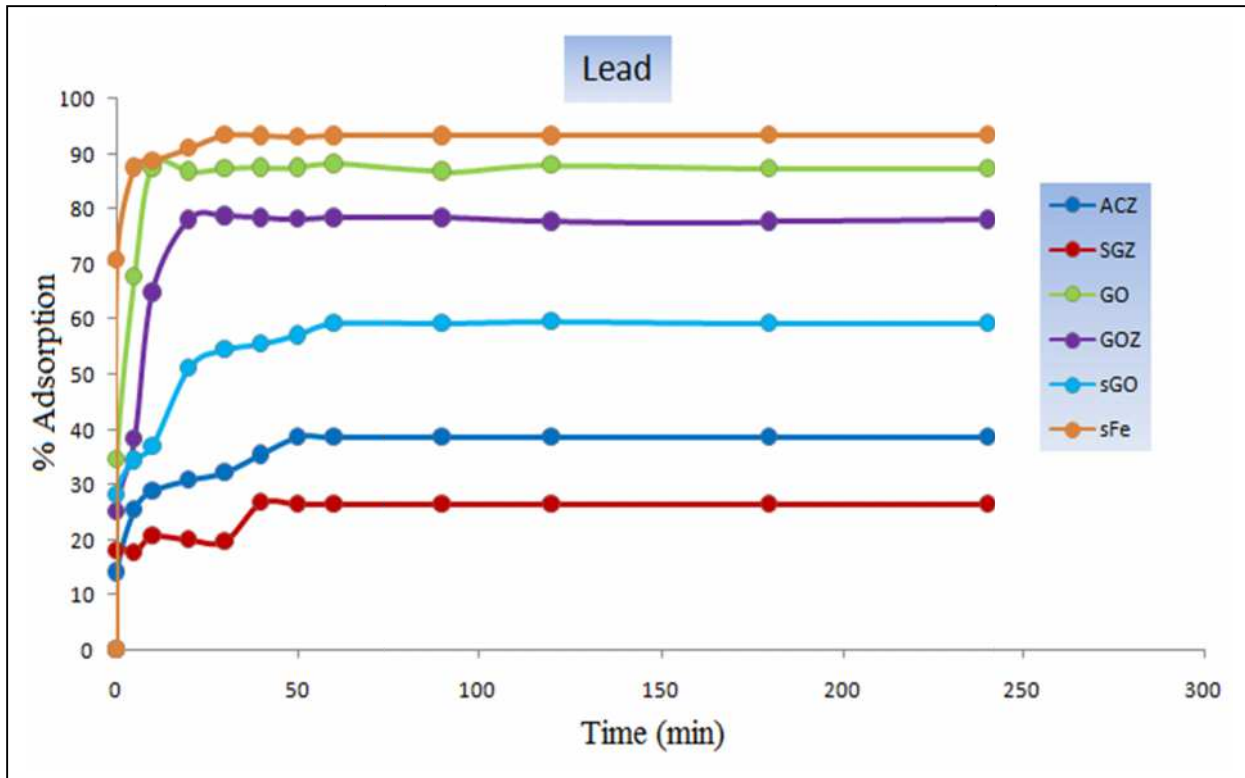
Figure 5.6 : Equilibrium time to adsorbed of Lead ions

5.1.1.2. Effect of temperature (ºC)

The nature of adsorption process depended on the change of temperature, so, the physisorption occurs when the temperature is decreased whilst the increasing temperature can lead to other types of adsorption that is named chemisorption [44,45, 178]. In order to select the best temperature that affects on the adsorption process, the adsorption experiment was carried out under different temperatures with the ranging 25-75ºC .

For Mordant Red 3 dye, the highest level is the removal percentage using ACZ adsoebent at 94.55% (Figure 5.7), it is the best temperature at 35ºC. Moreover , all the adsorbent surfaces recorded their special adsorbed percentage with the decrease in the temperature which refers to the occurrence of the physisorption [179, 180], where the removal percentage of the Mordant Red 3 dye for the other adsorbent surfaces is 14.07 , 47.79 , 28.95 and 30.88 % , it recorded the best temperature in the range of 25-35ºC of the adsorbents of SGZ , GO , GOZ and sGO respectively .

For Congo Red,The data of the removal percentage as a function to the change of temperature are depicted in Figure 5.8 , where these data demonstrated the high adsorbed percentage to congo red dye by using ACZ adsorbent at a low temperture 25ºC was 95.34%, while the highest adsorbed percentage was recorded by using GO adsorbent in which the best special temperature is 55ºC , and the percentage is 99.84% . In general , the other adsorbent surfaces recorded the adsorbed percentage at 69.98 , 56.83 , 85.81and 75.92 % in the temperature 55 ,65 and 75ºC to adsorbent of SGZ , GOZ , sGO and sFe respectively .

For the Basic Brown, three of the adsorbent surfaces (GO , sGO and sFe) recorded a good percentage to remove the basic brown dye from their aqueous solution at room temperature of 89.15 , 79.90 and 74.43%, respectively that refer to the exothermic adsorption process while , the highest removal percentage is

recorded by using ACZ adsorbent is 99.52% in the best temperature of 45ºC. Furthermore , the remained adsorbents (SGZ and GOZ) also recorded a high percent of the removal of the dye which were 79.25 and 95.55% at temperature 55 and 65ºC, respectively. The results of the removal of Basic Brown dye from their aqueous solutions by varying the adsorbents are shown in the Figure 5.9.

For Rhodamine B dye, the adsorption process increases with the increasing temperature, which leads to increase the movement of molecules in the adsorbent and adsorbate and thus increasing the bind between them[178,180, 181]. ACZ adsorbent has recorded the highest percentage to remove the dye (Figure 5.10) is 98.21% with the highst temperature at 75ºC that refer to the endothermic adsorption process [181]. Also, the lowest removal percentage recorded a temperature of 75ºC by GOZ adsorbent around 70.44% , finally the GO adsorbent also recorded the highest removal percent of Rhodamine B dye around 82,22% at 55ºC .

For the heavy metals, Figures 5.11 and 5.12 demonstrated the removal of the mercury and lead ions from their aqueous solutions, respectively. The maximum of the removal percentage of mercury ions was recorded by ACZ and SGZ adsorbents around 99.75 and 97.45% at 55 and 65ºC, respectively. The other adsorbent surfaces were measured to remove mercury ions that gave a good data of the removal percentage around 82.11 , 83.95 , 58.05 and 84.54% with different temperature at 55 , 65 and 25ºC for GO , GOZ , sGO and sFe respectively. On the other hand, the maximum of the removal percentage of lead ions from its aqueous solution was recorded by sFe and GO adsorbent about 93.31 and 91.15 % with the optimum temperature at 35 and 25ºC respectively whereas , the minimum of the removal percentage of lead ions was measured by SGZ adsorbent around 27.51% with an increased temperature at 75ºC. Furthermore , the remained adsorbents (

ACZ , GOZ and sGO) recorded the percentage of the removal of lead ions around 68.65 , 89.25 and 74.06% with the temperatures at 25,35 and 55 ℃, respectively.
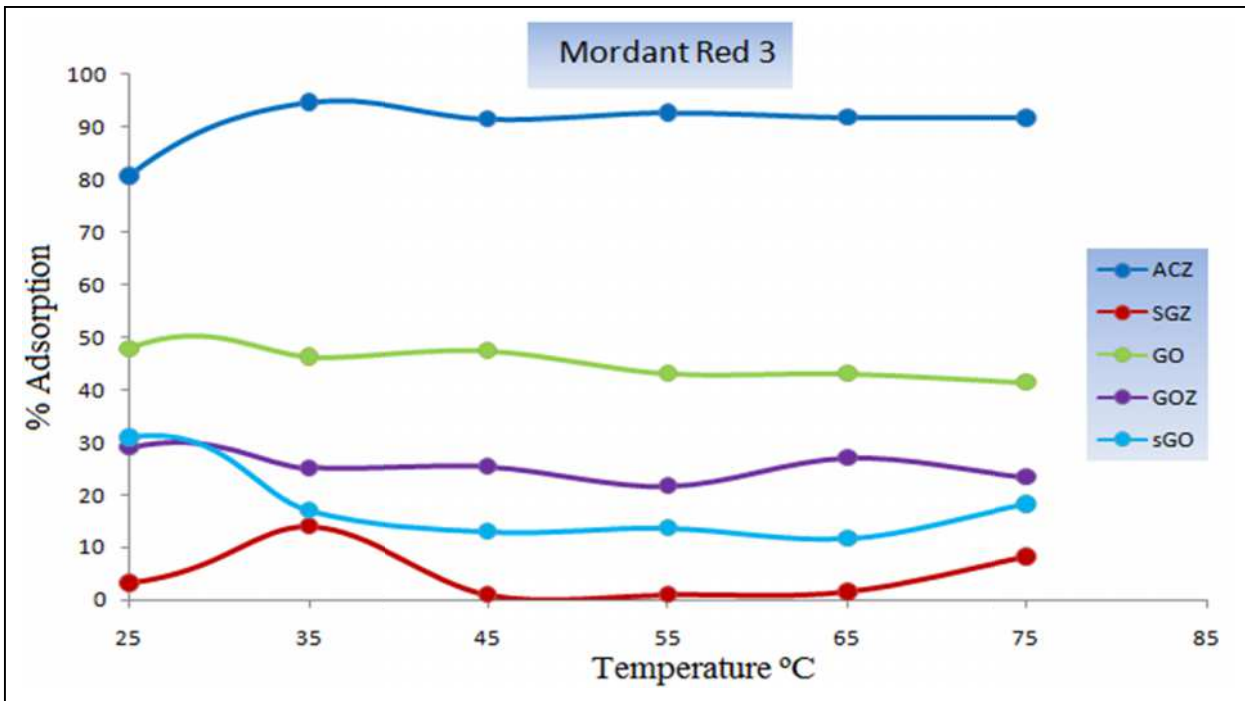
Figure 5.7 : Temperature test to remove of Mordant Red 3
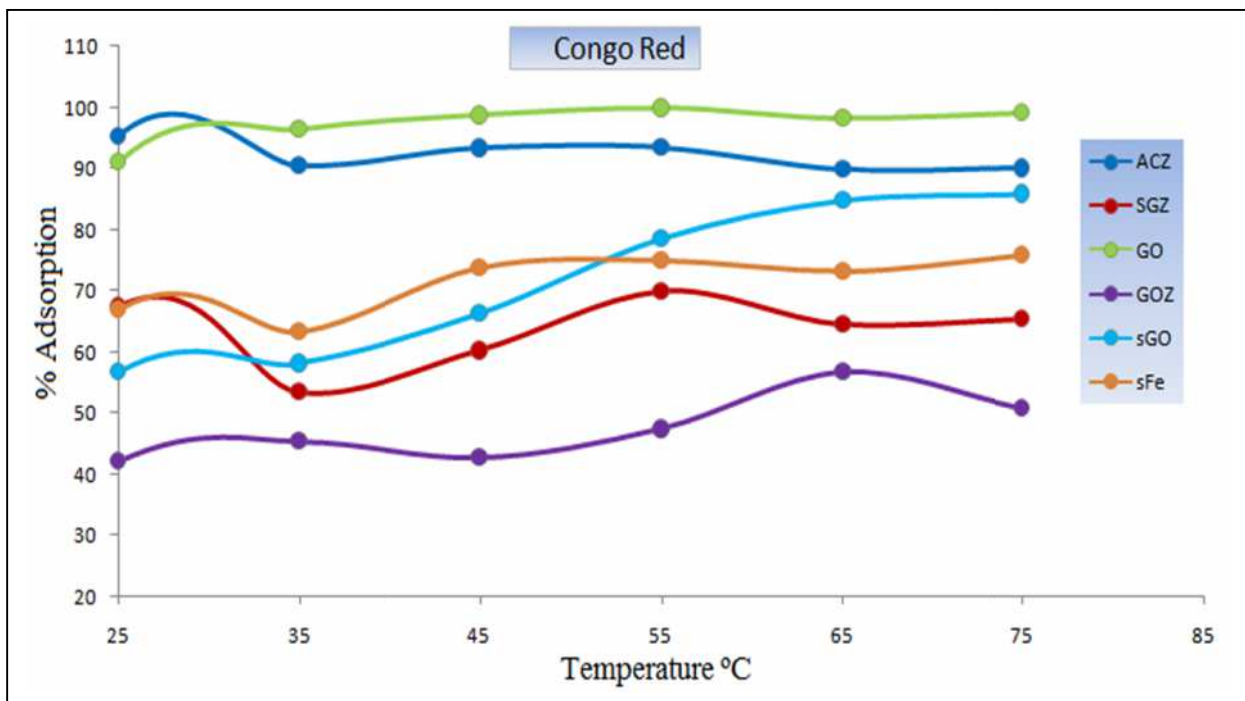
Figure 5.8 : Temperature test to remove of Congo Red
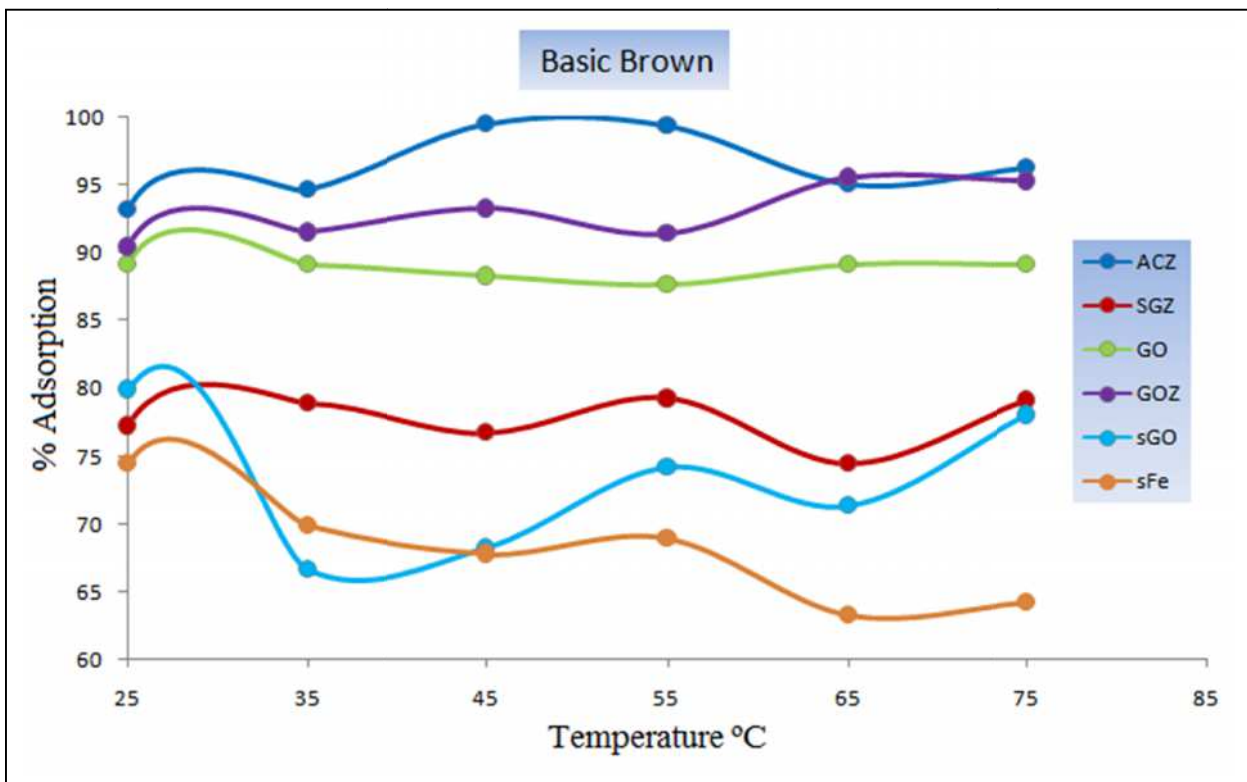
Figure 5.9 : Temperature test to remove of Basic Brown
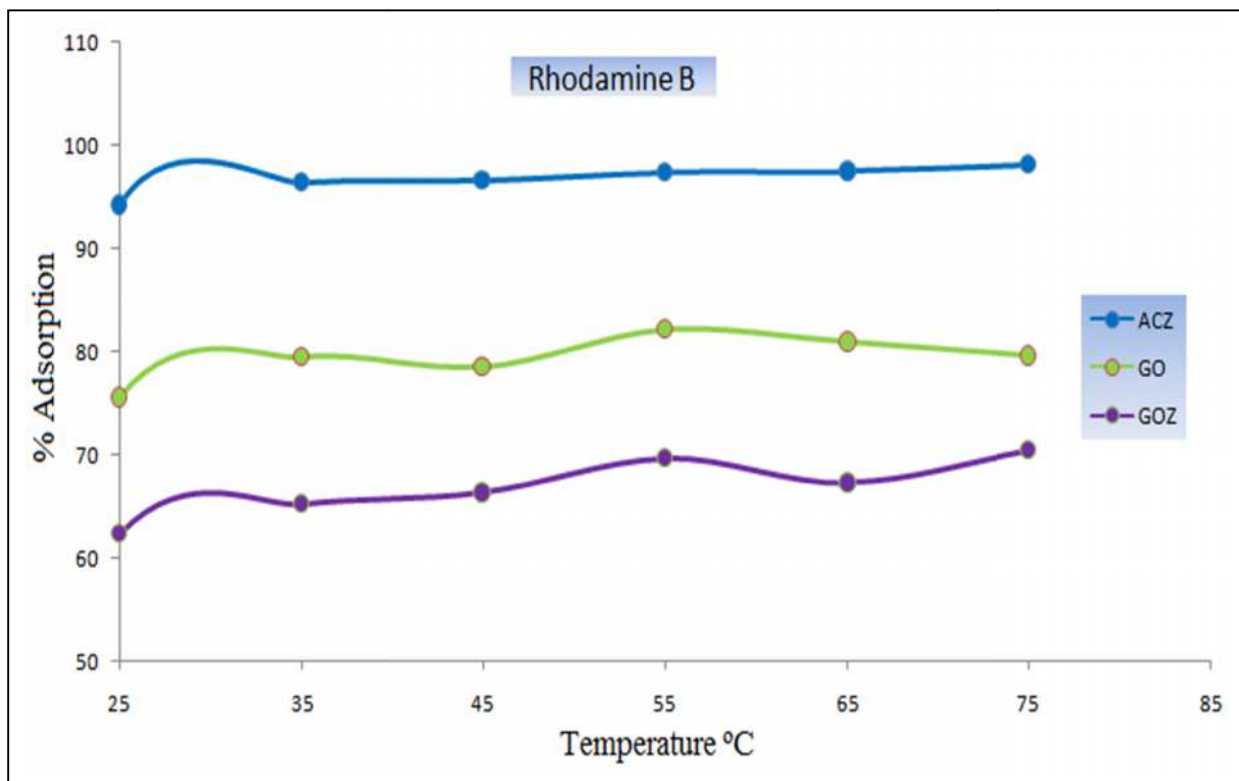
Figure 5.10 : Temperature test to remove of Rhodamine B
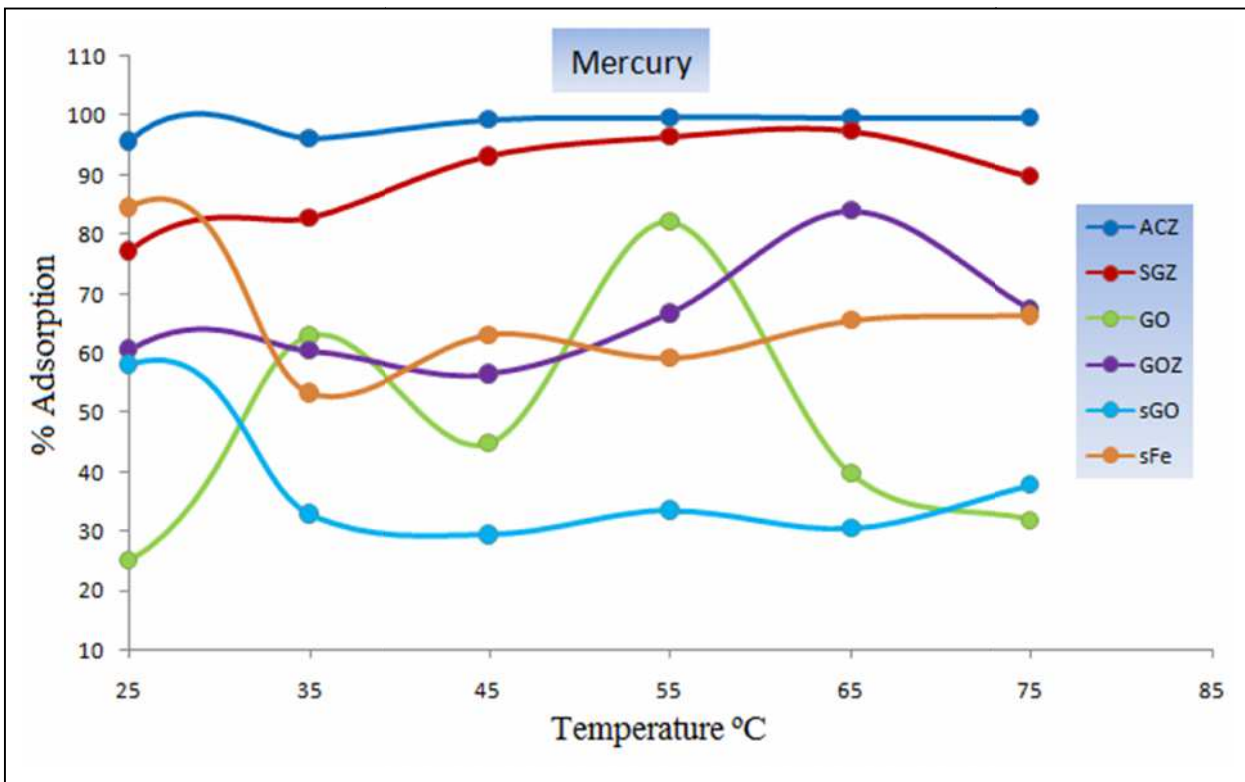
Figure 5.11 : Temperature test to remove of Mercury ions
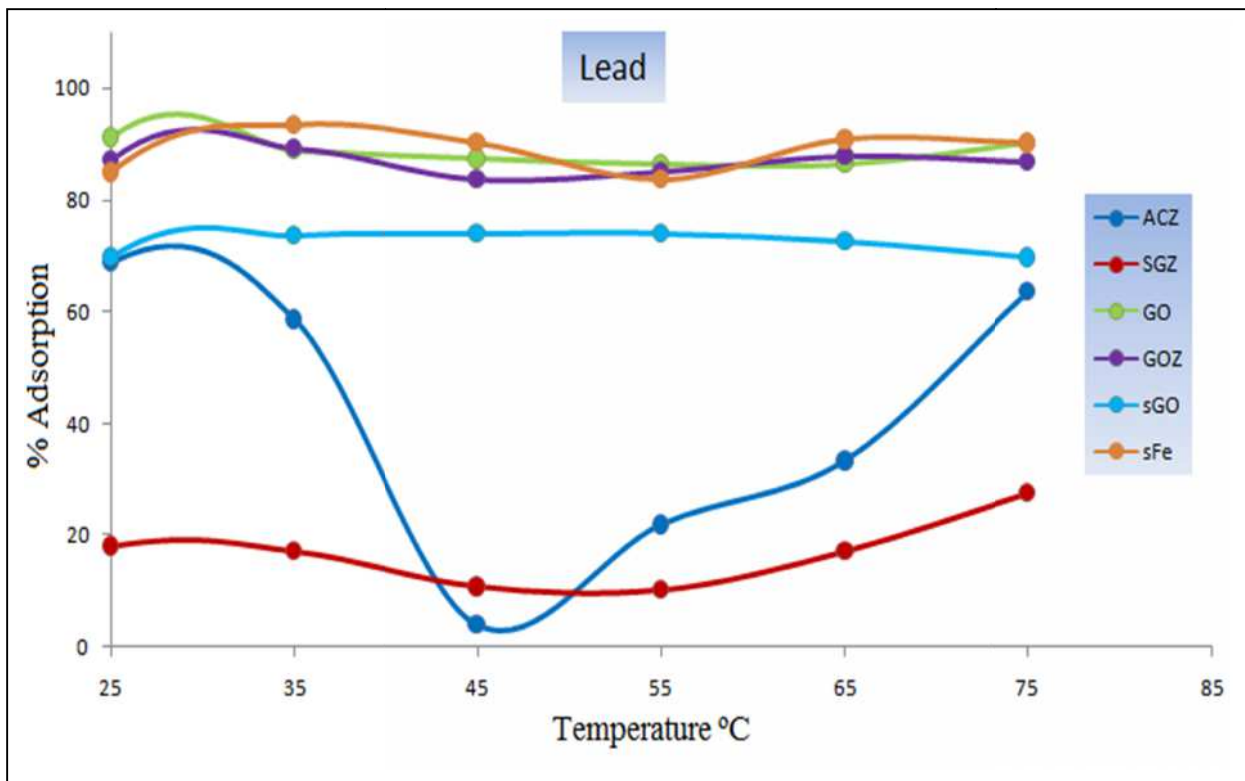
Figure 5.12 : Temperature test to remove of Lead ions

5.1.1.3. Effect of agitation speed

For the Mordant Red 3 dye, The best agitation speed was examined for all adsorbent surfaces (Figure 5.13) ,where by fixing of the adsorption parameters such as the dosage of adsorbent , volume of adsorbate solution , pH solution , temperature and concentration of adsorbate solution, the best agitation speed for SGZ , GOZ and sGO adsorbent is 50 rpm with the removal percent around 15.62 , 29.23 and 31.96 % respectively. The increase of agitation speed to 200 and 150 rpm using ACZ and GO adsorbent recorded the removal percent around 95.11 and 48.15%, respectively .

For Congo Red dye, Figure 5.14 points to the removal of the dye from their aqueous solutions by applying various agitation speeds for all adsorbent surfaces that were used in the current study in which the highest removal percent was recorded by GO and ACZ adsorbent around 95.18 and 92.53 through the agitation speed about 200 and 50 rpm respectively. The other adsorbent surfaces also recorded high levels to remove congo red dye which were around 69.03 , 77.58 , 65.71 and 66 % with agitation speeds at 200 , 50 and 100 rpm for SGZ , GOZ , sGO and sFe, respectively.

For Basic Brown dye (Figure 5.15), the maximum of agitation speeds are recorded in the range 150 to 200 rpm with the removal percentage around 70.38 , 99.98 , 90.38 and 77.55 % by sGO , GO , GOZ and SGZ adsorbents respectively. Besides, the minimum of agitation speeds was determined by ACZ and sFe adsorbents at 50 rpm with an adsorption percent about 92.95 and 72.94 % respectively. The increase of the adsorption amount with the decreases of agitation speed may be attributed to the type of grooves , channels and functional groups that exist in the outer surface of adsorbent materials.

For Rhodamine B dye, the increase of adsorption percentage with the increases of the agitation speed was recorded by GO , GOZ and ACZ adsorbents in order to remove the dye from its aqueous solution with the percentage of 80.16 , 67.91 and 96.09 % in the range of agitation speeds around 150-200 rpm respectively . The results are shown in Figure 5.16 .

For the heavy metals, the removal of Hg and Pb from their aqueous solutions is considered one of the challenges facing the ecosystem. So, the agitation speed as an influencer on adsorption process of mercury and lead was measured for its solutions that appeared the maximum of the removal percentage of mercury and lead around 99.31, 93.28 and 98.70, 93.69 % in the agitation speed at 100 ,50 and 100 ,150 rpm by ACZ ,SGZ and GOZ , sFe respectively . The remains of the adsorbent surfaces recorded the increase of the percentage removal of mercury ions by adsorbents using GO (81.68%) , GOZ (84.79%) , sGO (41.26%) and sFe (83.97%) in the range of the agitation speeds 100, 150 and 200 . On the other hand , the percentage removal of lead ions from their solution recorded various levels as a function to the agitation speeds around 30.86 (200 rpm) , 58.02 (100 rpm) , 74.70 (150 rpm) and 87.93% (100 rpm) by adsorbents for SGZ ,ACZ , sGO and GO respectively . The data of the removal percentage for mercury and lead ions from their aqueous solutions as a function to the agitation speed are depicted in the Figures 5.17 and 5.18 respectively.

The increase in the removal percentage of adsorbate solution with increases in the agitation speed that is attributed to the increase in the rate of adsorbate diffusion from the bulk solution towards the boundry layer solution that surrounds the particles of adsorbent by supporting the turbulence which leads to the decline the thikness of the boundary layer solution [181-184].
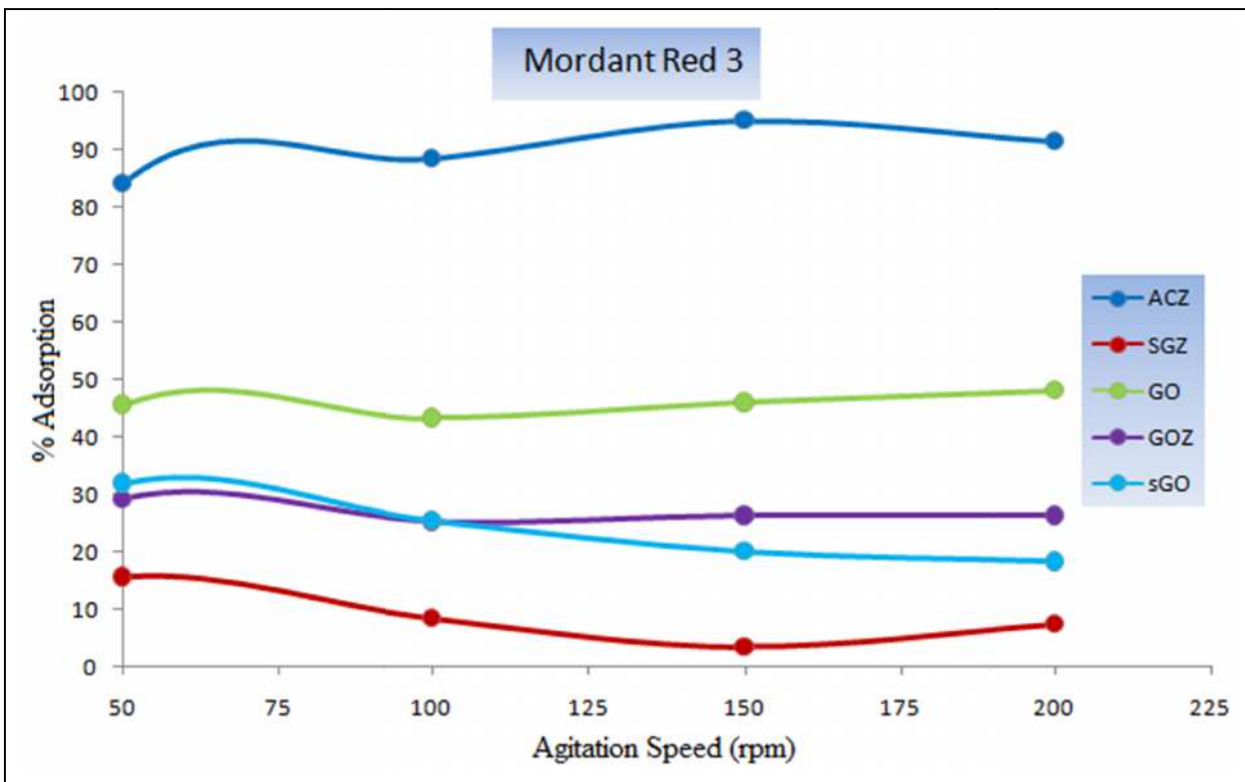
Figure 5.13 :Agitation speed test to remove of Mordant Red 3
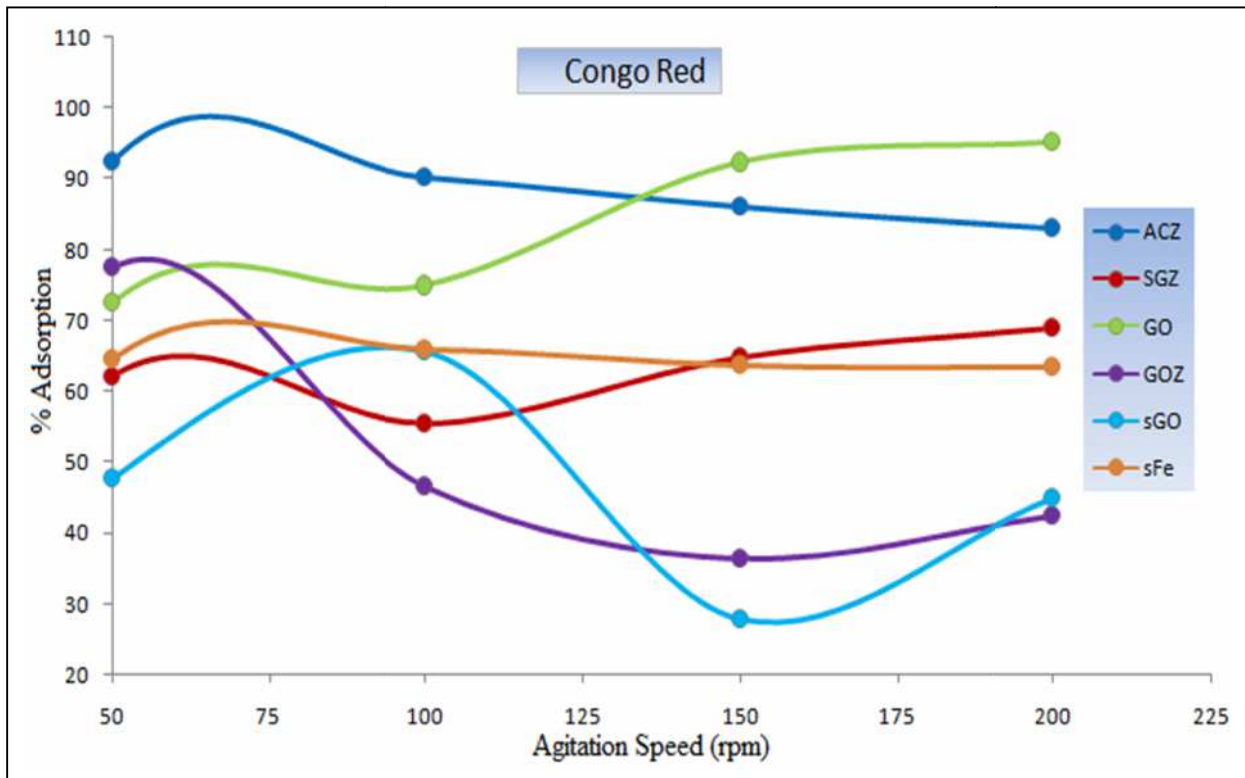
Figure 5.14 : Agitation speed test to remove of Congo Red
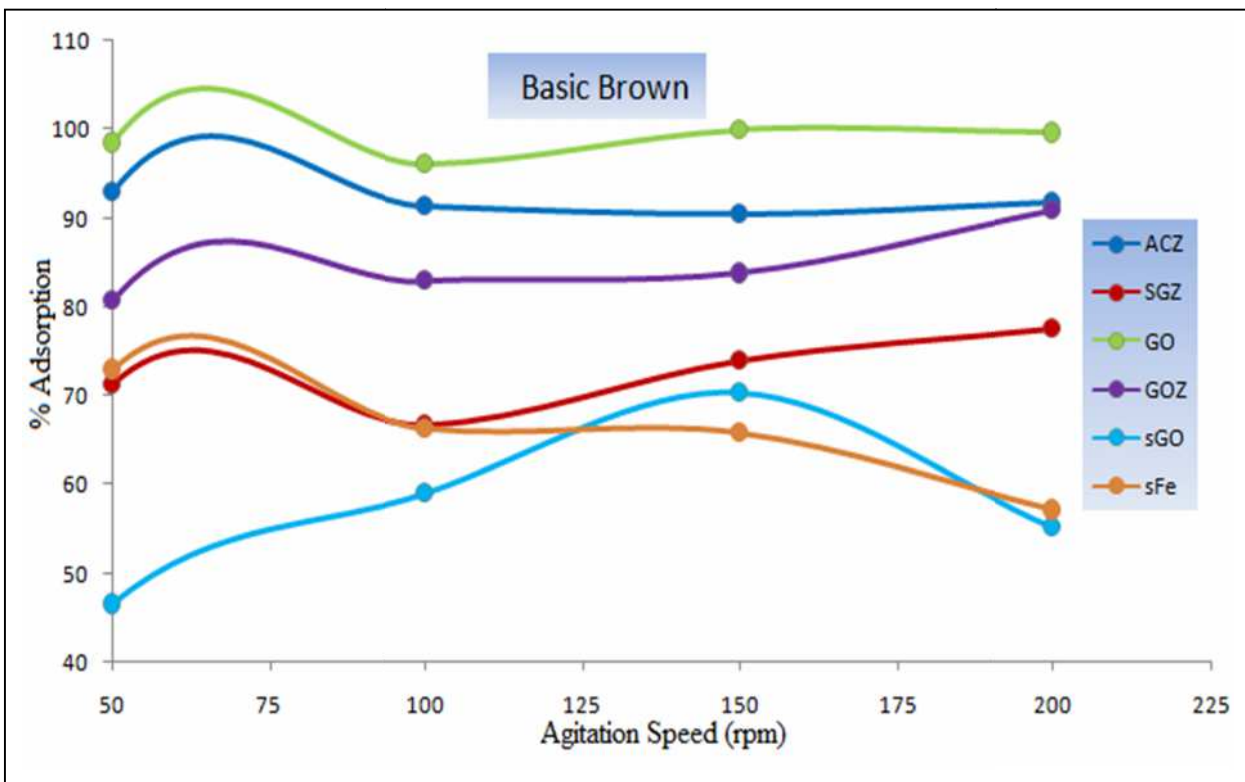
Figure 5.15 :Agitation speed test to remove of Basic Brown
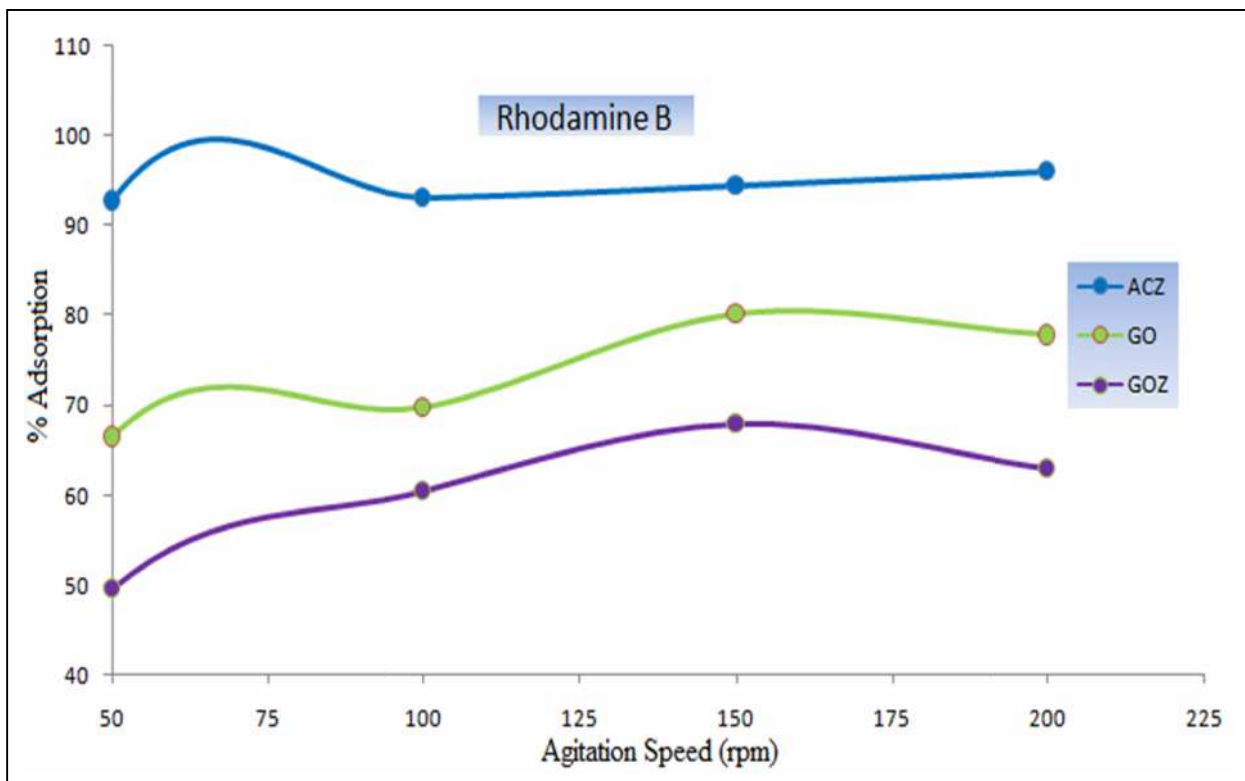
Figure 5.16 : Agitation speed test to remove of Rhodamine B
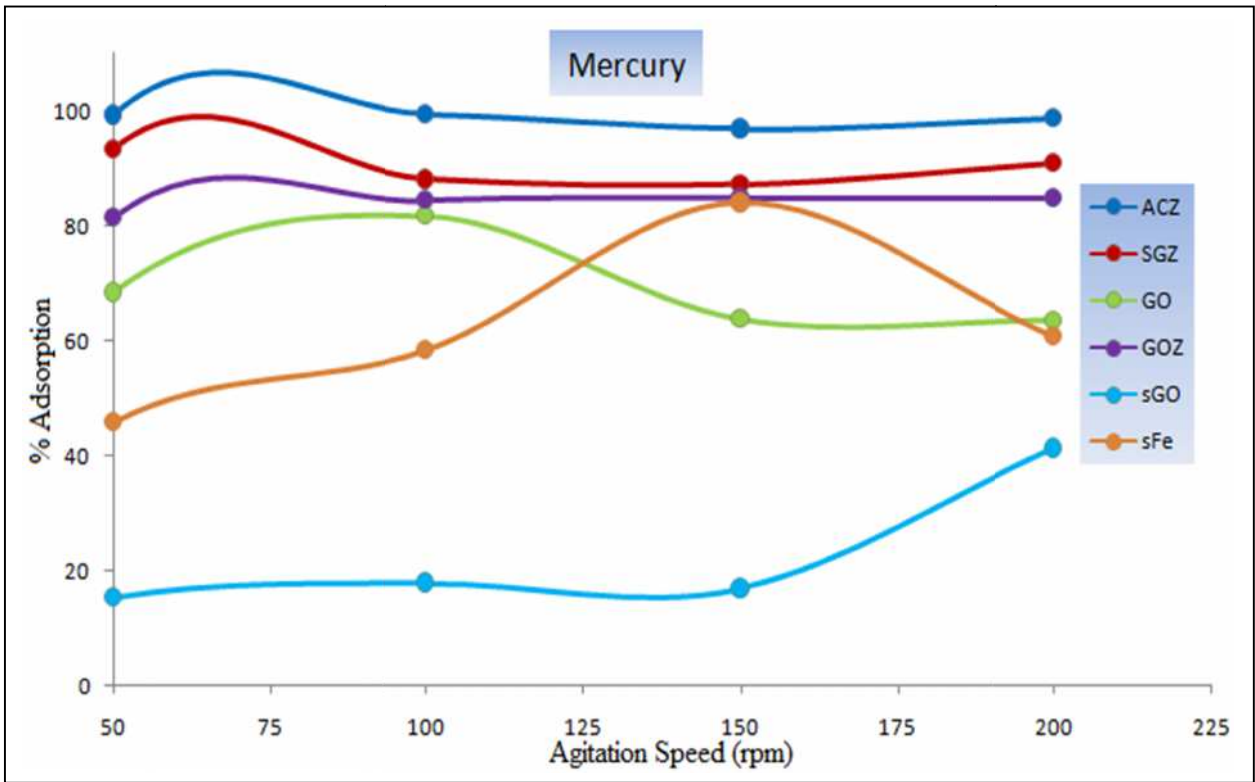
Figure 5.17 :Agitation speed test to remove of Mercury ions
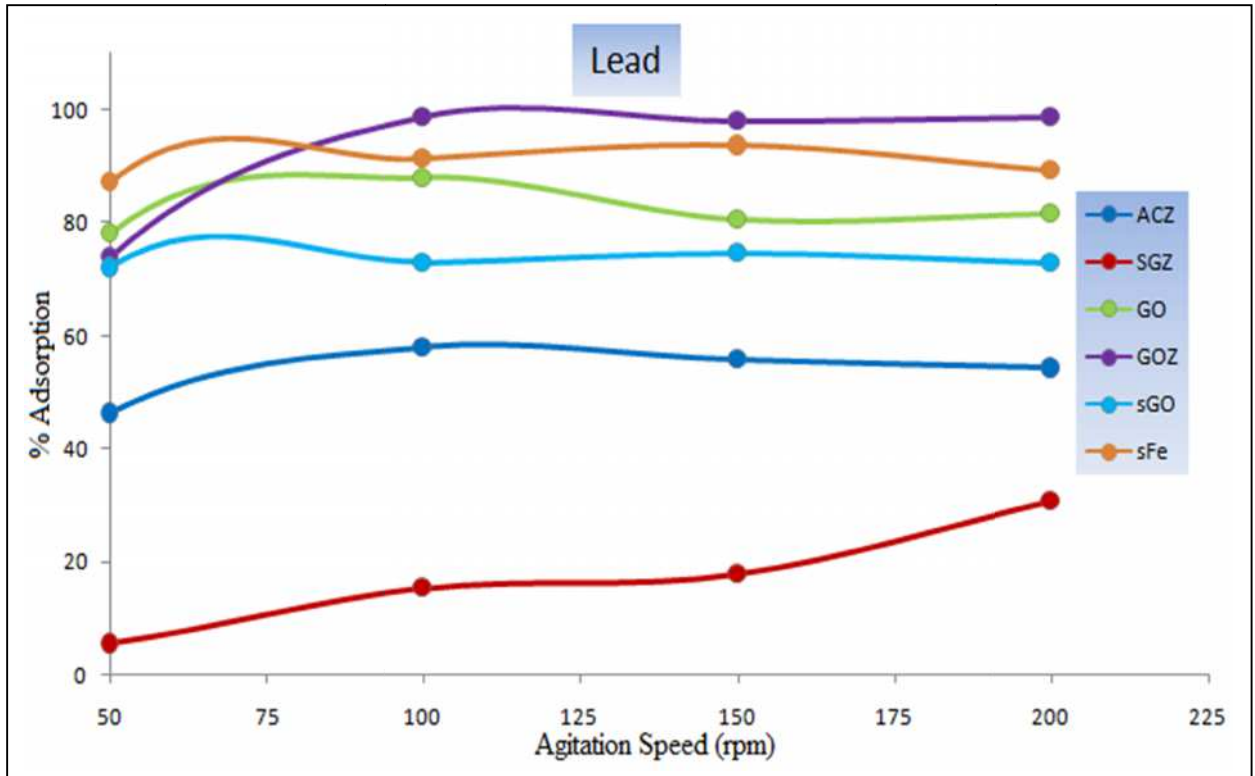
Figure 5.18 : Agitation speed test to remove of Lead ions

5.1.1.4. Effect of pH on adsorption process

   pH levels are considered one of the main important parameters that affect on the adsorption process through their influence on the active sites that lead to change the surface charge for the adsorbents that are responsible for adsorption efficiency [183,184]. The dye of Modrant Red 3 belongs to anionic class dyes, the pH level plays an important role for reaching the adsorption maximum. Therefore , the adsorption process was carried out to remove the dye from its aqueous solution under different pH levels of ranging 3-9. The maximum of adsorption for all adsorbent surfaces (Figure 5.19) were recorded in acidic medium at pH 3 with the removal percentage around 98.10 , 34.34 , 61.13 and 57.08% which belong to ACZ, SGZ, GO and GOZ adsorbents respectively, because the adsorbents have hydroxyl groups in their structural formula that affect changing the pH levels. So, the increase in pH level towards the basic medium leads to the occurrence of an electrostatic repulsion process with anionic adsorbate molecules, which lead to the decrease of adsorption process [100,184]. Moreover , the maximum of adsorption amount was recorded at pH 7 to sGO adsorbent to be 37.06% .

   For Congo Red dye, the increase of adsorption amount with the decreased of pH levels towards acidic medium was recorded to remove the dye as anionic dye (Figure 5.20) from its aqueous solution, where the removal percentage recorded by all adsorbents (SGZ , GO , GOZ , sGO and sFe) were around 72.88 , 99.78 , 82.07 , 89.21 and 76.85 % under the pH level of the range 4-6 . Furthermore , the ACZ adsorbent was recorded the maximum of adsorption amount to be 96.23% under pH level 7. It was also observed, that the congo red dye solution was partial precipitated under pH 3 [185,186].

   For Basic Brown dye, Figure 5.21 appears the removal percentage of the dye from its aqueous solution as a function for varying in pH level, where the results indicated that maximum adsorption amounts by using adsorbents SGZ , GO , GOZ

and sFe in pH level range of 4-6 were 81.76 , 99.91 , 99.53 and 80.74%, respectively. The maximum adsorption was recorded at 99.29 and 82.66% by adsorbents ACZ and sGO in pH level at 7 and 8 respectively . In general , the Basic Brown dye is suffers from the precipitation process when the increase of pH level towards the basic medium is especially at pH 9.

For Rhodamine B dye, the adsorption process was applied in order to remove the dye from its aqueous solution by changing the pH levels for fixing the other parameters under the optimum conditions for each adsorbent . The maximum adsorption for all adsorbents recorded the best removal percentage to remove rhodamine B dye (Figure 5.22) around 98.71, 86.68 and 91.35% and under the pH level for the range 3-7 for ACZ, GO and GOZ adsorbents respectively.

For the heavy metals, the Figures 5.23 and 5.24 refer to the removal of the mercury and lead ions from their aqueous solutions in which, the increase of adsorption amounts of mercury ions (99.79, 99.27 and 98.10 %) were recorded under pH 7 by ACZ, SGZ and sFe adsorbent, respectively. On the other hand , the GO adsorbent recorded the maximum adsorption amount of mercury ions at pH 6 while, the maximum of adsorption to remove the mercury ions was recorded under the basic medium at pH 9 through GOZ and sGO adsorbents , which were 98.44 and 91.34 % respectively. The maximum removal percentage of all adsorbents for removing the lead ions from their aqueous solution was measured under the acidic weak medium for the range of pH levels at 5-6, it was found to be 76, 74.15, 95.86, 99.22, 79.01 and 97.76% that belong to ACZ, SGZ, GO, GOZ, sGO and sFe adsorbents, respectively . The lead ions solution suffers from the deposition process that is above pH 6 which was attributed to lead hydroxide formation [187,188]. In general, pH level changed lead to increase the competition to occupy the active sites of the adsorbent surfaces between the hydrogen ions and hydroxyl ions with

adsorbate molecules. The change in pH levels also leads to change of surface charge of adsorbent into negative or positive charge and thus leads to increase or decrease in the adsorption efficiency by showing the repulsion or attraction process between the adsorbent surface and adsorbate molecules [24,100,183,189].
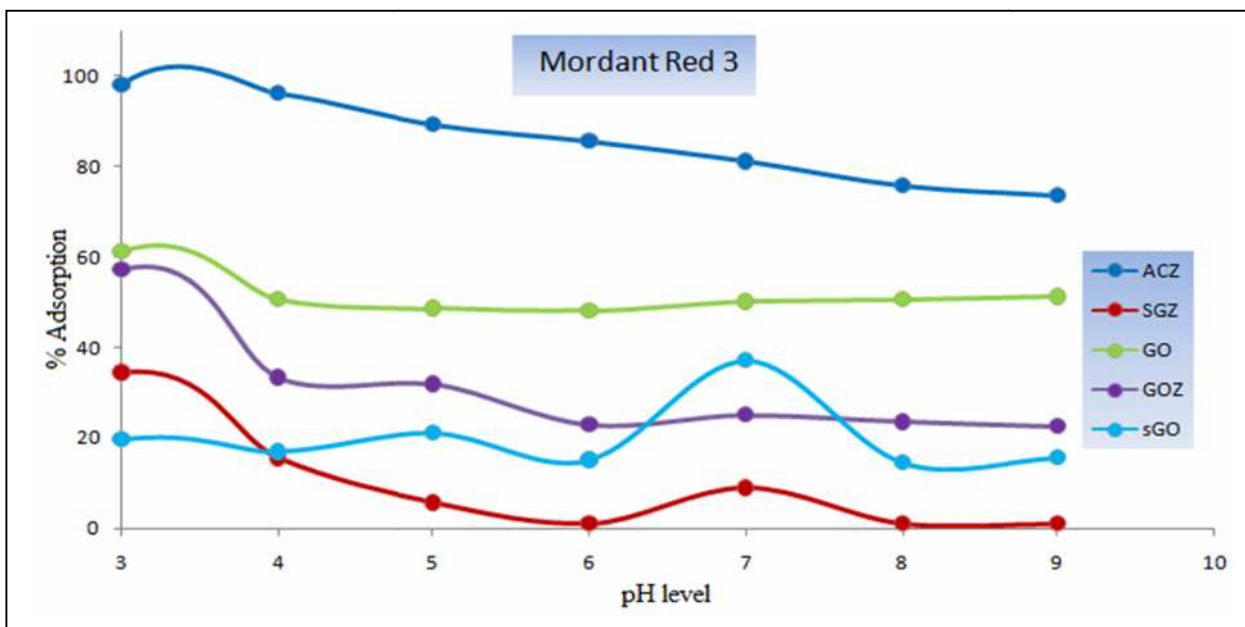
Figure 5.19 :pH level test to remove of Mordant Red 3
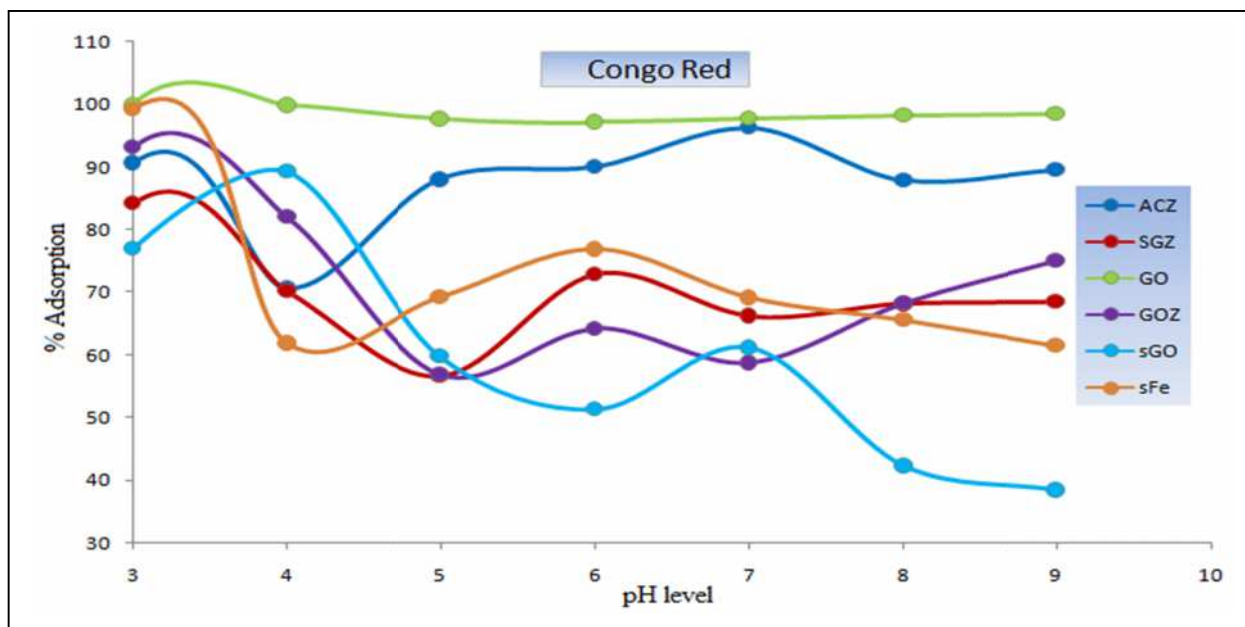
Figure 5.20 : pH level test to remove of Congo Red
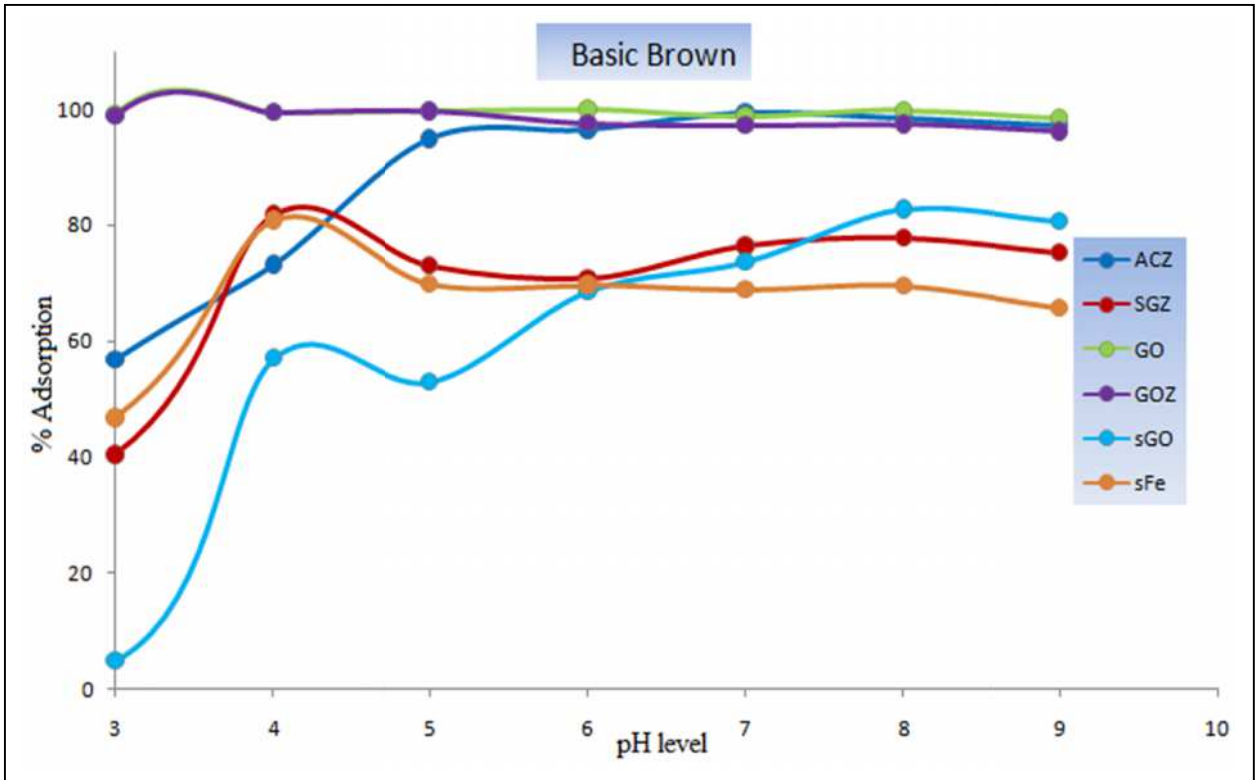
Figure 5.21 :pH level test to remove of Basic Brown
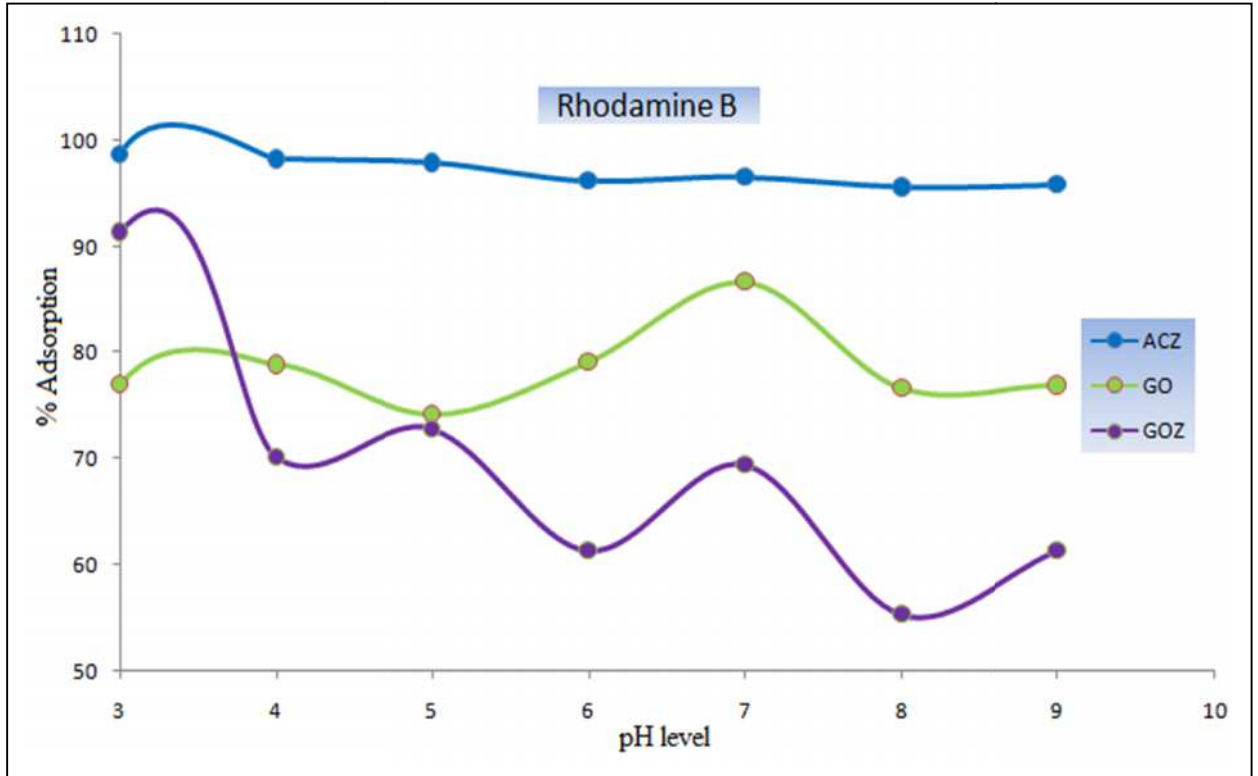
Figure 5.22 : pH level test to remove of Rhodamine B
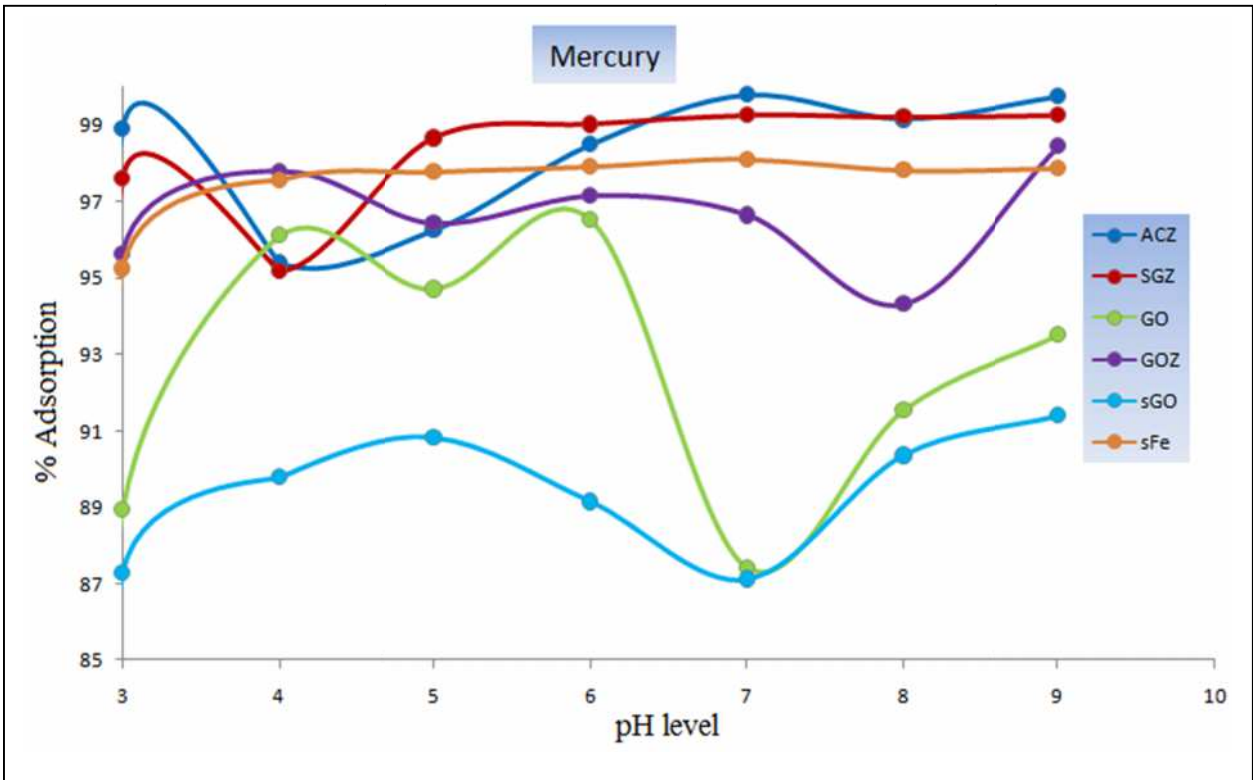
Figure 5.23 :pH level test to remove of Mercury ions
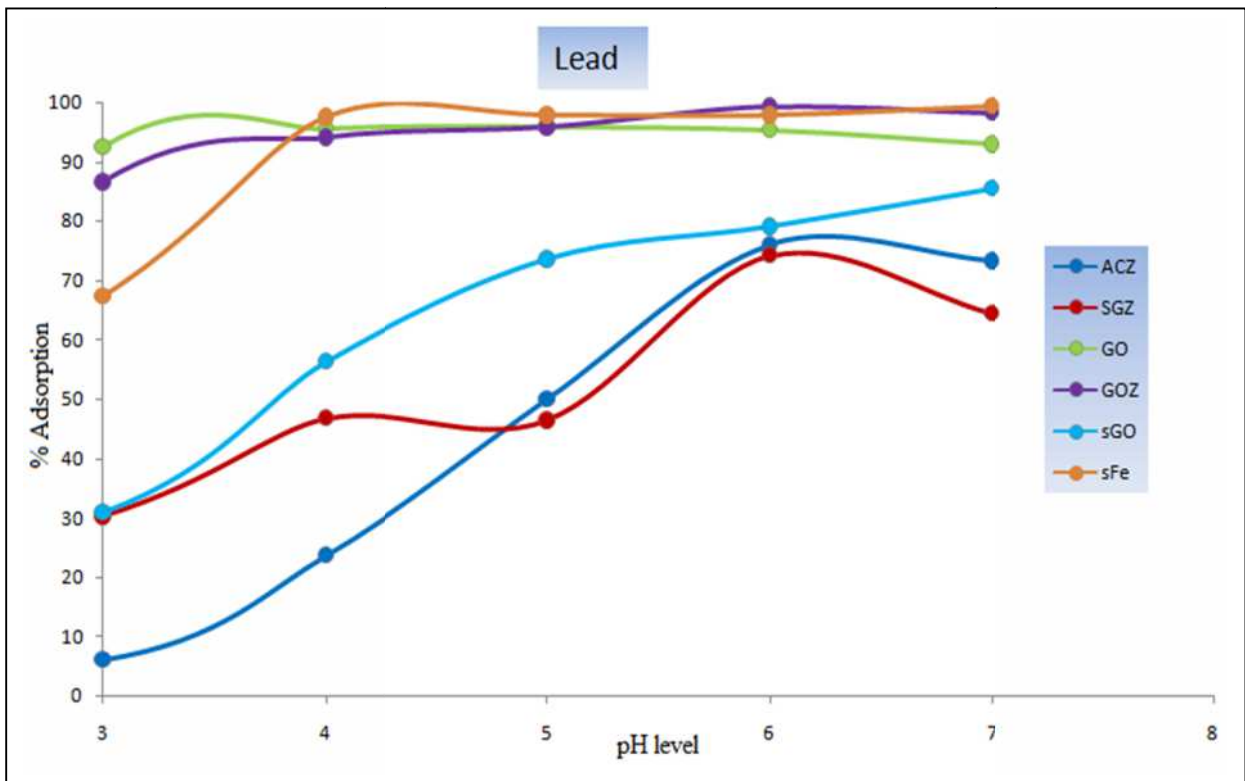
Figure 5.24 : pH level test to remove of Lead ions

The adsorption capacity at the equilibrium state can be defined as a number of milligrams of adsorbate material amount that were adsorbed on one gram of adsorbent surface by fixing the adsorbate volume (10ml) , initial concentration of adsorbate (50 , (4,14) mg/l and 1000 µg/l to solution of dyes , lead and mercury, respectively) and weight of adsorbent material (0.01g) . In addition, the adsorption capacity at the equilibrium (Q_e) has been calculated according to the relation of the following [25,67,190] :

$$Q_e \text{ (mg/g)} = [V \, (C_o - C_e)] / W$$

Where : Q_e is the adsorption capacity at the equilibrium state (mg/g) , C_o is the initial concentration (mg/l) of adsorbate solution , C_e is the concentration of the adsorbate solution (mg/l) at the equilibrium state , V is the volume of adsobate solution (L) and W is the weight of adsorbent material. The optimum conditions of adsorption experiment were used in order to obtain the maximum amount for removing the adsorbate materials from their aqueous solutions .

The data of adsorption capacity of Mordant Red 3 and Rhoadmine B dyes were calculated and recorded for the maximum of adsorption capacity by using ACZ adsorbent because the adsorbent of ACZ has a higher surface area , many of functional groups, several of grooves and channels and positive surface charge. All these reasons help to increase the adsorption capacity. Moreover, the GO adsorbent recorded the highest adsorption capacity which is attributed to hydroxyl, epoxy and carboxyl groups that exist in their structural formula which gives the ability to adsorb congo red dye from its aqueous solution in the low acidic medium. The maximum of adsorption capacity of basic brown dye was recorded by GO and GOZ adsorbent that attributed to the distribution of the functional groups on outer surface , surface area of each adsorbent and distribution of surface charge of adsorbent. All the adsorbents recorded high levels of adsorption capacity of

mercury ions while, the GOZ, sFe and GO adsorbents are recorded the highest value of adsorption capacity of lead ions from their aqueous solution when compared with the remained adsorbents that were attributed to have many functional groups such as hydroxyl, epoxy and selenazone ligand moiety in GOZ adsorbent while the oxygen groups are dominated in sFe adsorbent . The results of the optimum conditions and the calculation of the adsorption capacity are listed in the Table 5.1-5.6 .

Table 5.1 : The optimum conditions of adsorption process of Mordant red 3 dye on all adsorbent surfaces

Adsorbent	Contact Time (min)	Temperature (ºC)	Agitation speed (rpm)	pH level	% Adsorption	Adsorption capacity (mg/g)
ACZ	120	35	150	3	98.1	49.05
SGZ	120	35	50	3	34.34	17.17
GO	120	25	200	3	61.13	30.56
GOZ	60	25	50	3	57.08	28.54
sGO	20	25	50	7	37.06	18.53

Table 5.2 : The optimum conditions of adsorption process of Congo red dye on all adsorbent surfaces

Adsorbent	Contact Time (min)	Temperature (ºC)	Agitation speed (rpm)	pH level	% Adsorption	Adsorption capacity (mg/g)
ACZ	60	25	50	7	96.23	48.115
SGZ	60	55	200	6	72.88	36.44
GO	120	55	200	4	99.78	49.89
GOZ	30	65	50	4	82.07	41.03
sGO	180	75	50	4	89.21	44.60
sFe	20	75	100	6	76.85	38.42

Table 5.3 : The optimum conditions of adsorption process of Basic brown dye on all adsorbent surfaces

Adsorbent	Contact Time (min)	Temperature (⁰C)	Agitation speed (rpm)	pH level	% Adsorption	Adsorption capacity (mg/g)
ACZ	120	45	50	7	99.29	49.64
SGZ	90	55	200	4	81.76	40.88
GO	30	25	150	6	99.91	49.95
GOZ	90	65	200	5	99.53	49.76
sGO	60	25	150	8	82.66	41.33
sFe	90	25	50	4	80.74	40.37

Table 5.4 : The optimum conditions of adsorption process of Rhodamine dye on all adsorbent surfaces

Adsorbent	Contact Time (min)	Temperature (⁰C)	Agitation speed (rpm)	pH level	% Adsorption	Adsorption capacity (mg/g)
ACZ	60	75	200	3	98.71	49.355
GO	90	55	150	7	86.68	43.34
GOZ	90	75	150	3	91.35	45.675

Table 5.5 : The optimum conditions of adsorption process of mercury ions on all adsorbent surfaces

Adsorbent	Contact Time (min)	Temperature (⁰C)	Agitation speed (rpm)	pH level	% Adsorption	Adsorption capacity (µg/g)
ACZ	30	55	100	7	99.79	997.9
SGZ	50	65	50	7	99.27	992.7

GO	90	55	100	6	96.51	965.1
GOZ	90	65	150	9	98.44	984.4
sGO	60	25	200	9	91.34	913.4
sFe	30	25	150	7	98.10	981

Table 5.6 : The optimum conditions of adsorption process of Lead ions on all adsorbent surfaces

Adsorbent	Contact Time (min)	Temperature (⁰C)	Agitation speed (rpm)	pH level	% Adsorption	Adsorption capacity (mg/g)
ACZ	50	25	100	6	76	10.64
SGZ	40	75	200	6	74.15	2.991
GO	10	25	100	5	95.86	13.42
GOZ	20	35	100	6	99.22	13.89
sGO	60	55	150	6	79.01	11.06
sFe	30	35	150	6	97.76	13.68

5.1.2. Adsorption isothermes

The adsorption isotherm shapes revealed two types, L and S of Mordant Red 3 dye for all adsorbents according to the Giles classification, where ACZ and sGO adsorbent recorded L type that referred to the orientation of adsorbate molecules which are horizontal with the adsorbent surface, this type refers to the occurrence of adsorption by using relative weak forces, like van der Waals forces while the other adsorbents recorded S type which pointed to the orientation of adsorbate molecules that are vertical or tilted on adsorbent surface, it also referred to high attraction for the adsorbate molecules towards adsorption layer .

Basic brown dye that was adsorbed onto all adsorbents surface have been recorded as L type by GO and sGO adsorbent while the other adsorbents recorded S type.

Congo Red dye recorded three types S, L and H according to Giles classification where L type was recorded by ACZ adsorbent whilst , H type was recorded by GO adsorbent that tends to record high affinity adsorption towards the adsorbate molecules, this type can occur in the diluted solution of adsorbate molecules. The H type refers to the chemical adsorption type which occurs by employing electrostatic forces finally , the other adsorbents were recorded S type.

The Rhodamine B dye also recorded S type by GO adsorbent while the L type was recorded by ACZ and GOZ adsorbents .

Mercury ions that are adsorbed onto all adsorbents are recorded by S type for all adsorbents, excepted for sFe adsorbent which was recorded by L type. The adsorption of lead ions onto all adsorbents recorded two types S and L where S type was recorded by SGZ , sGO and sFe whilst , the other adsorbents were recorded L type. The results of adsorption shapes according to Giles classification are depicted in Figures 5.25 to 5.28 .
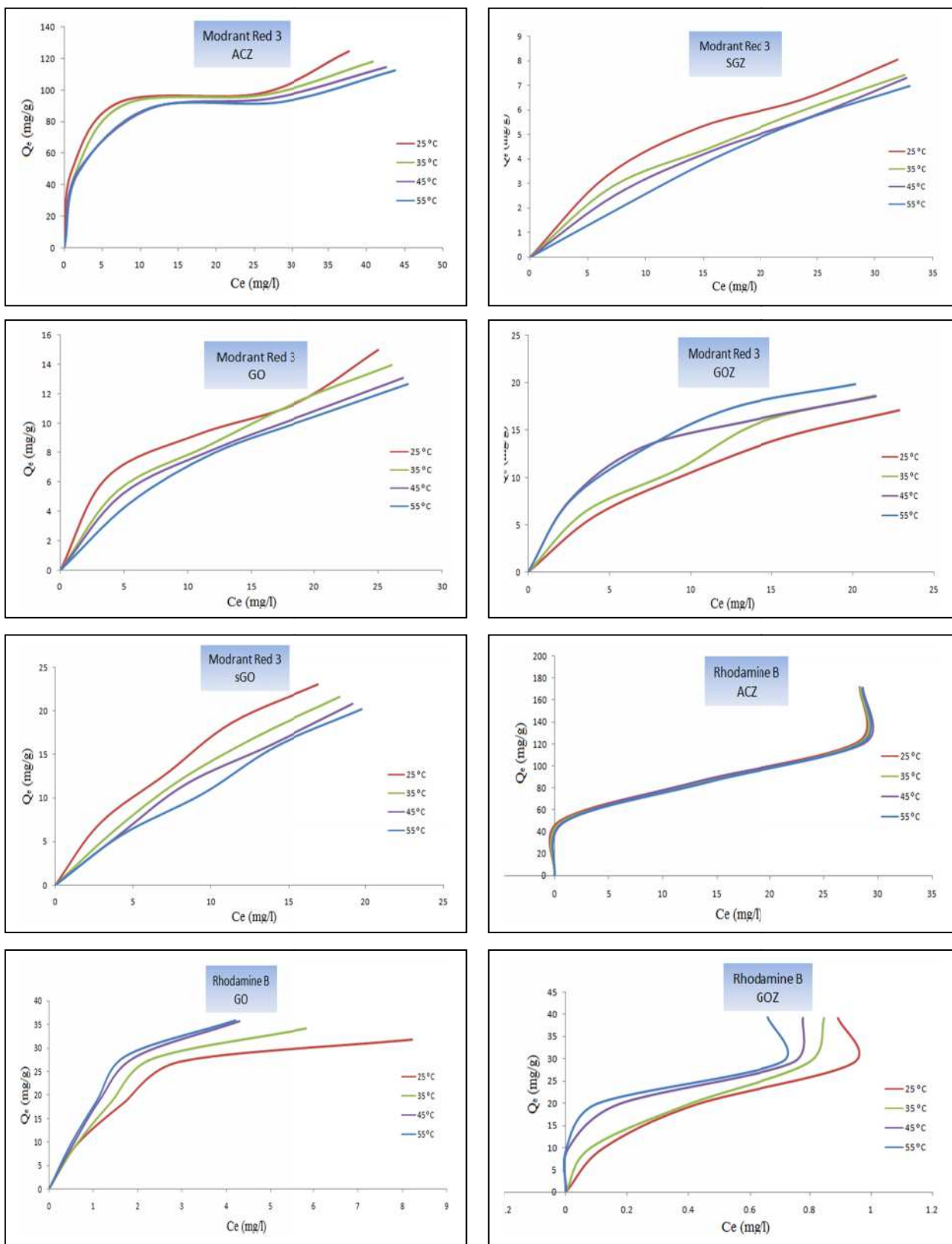
Figure 5.25 : Adsorption isotherm of Mordant red 3 and Rhodamine B dyes
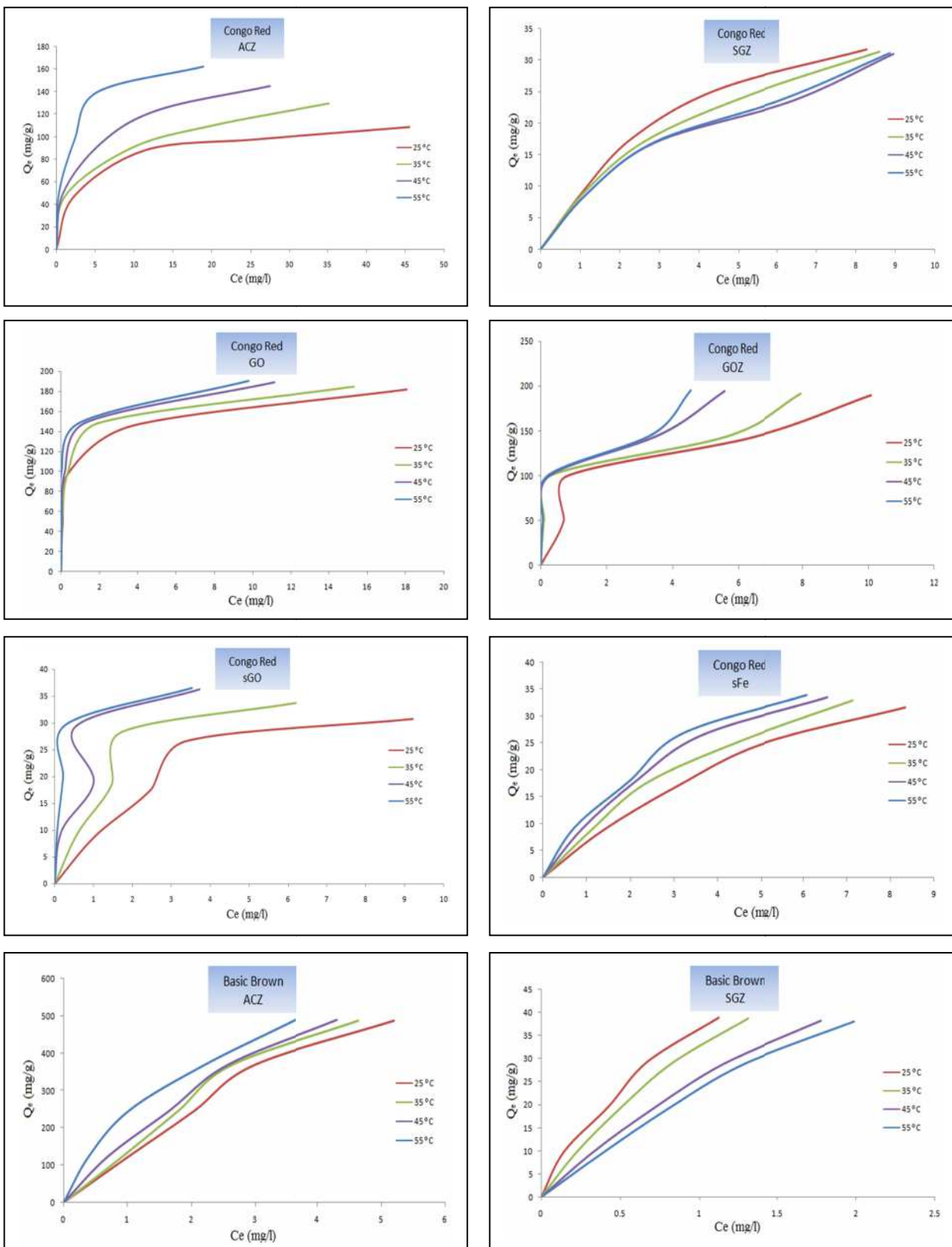
Figure 5.26 : Adsorption isotherm of Congo Red and Basic Brown dyes
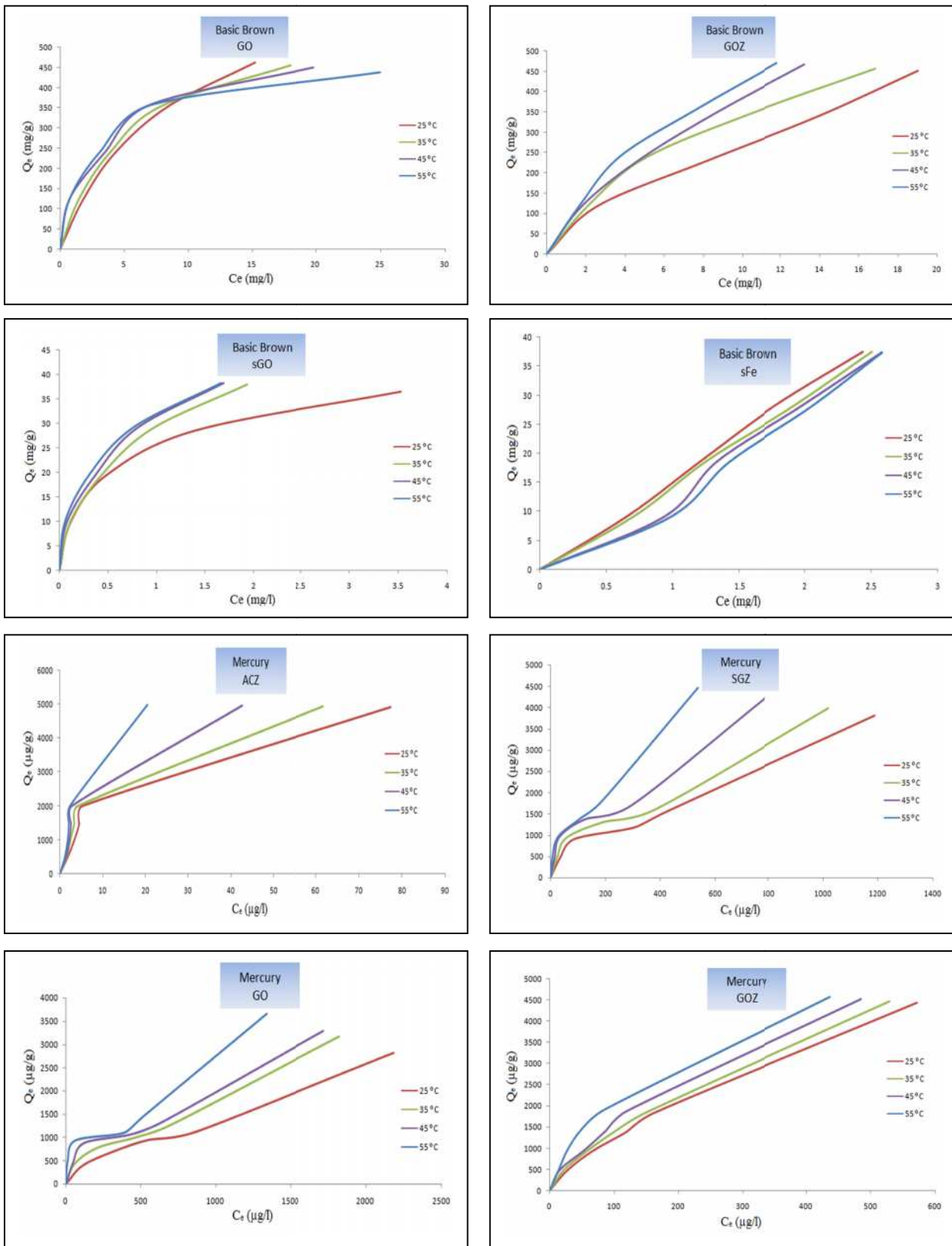
Figure 5.27 : Adsorption isotherm of Basic Brown dyes and Mercury ions
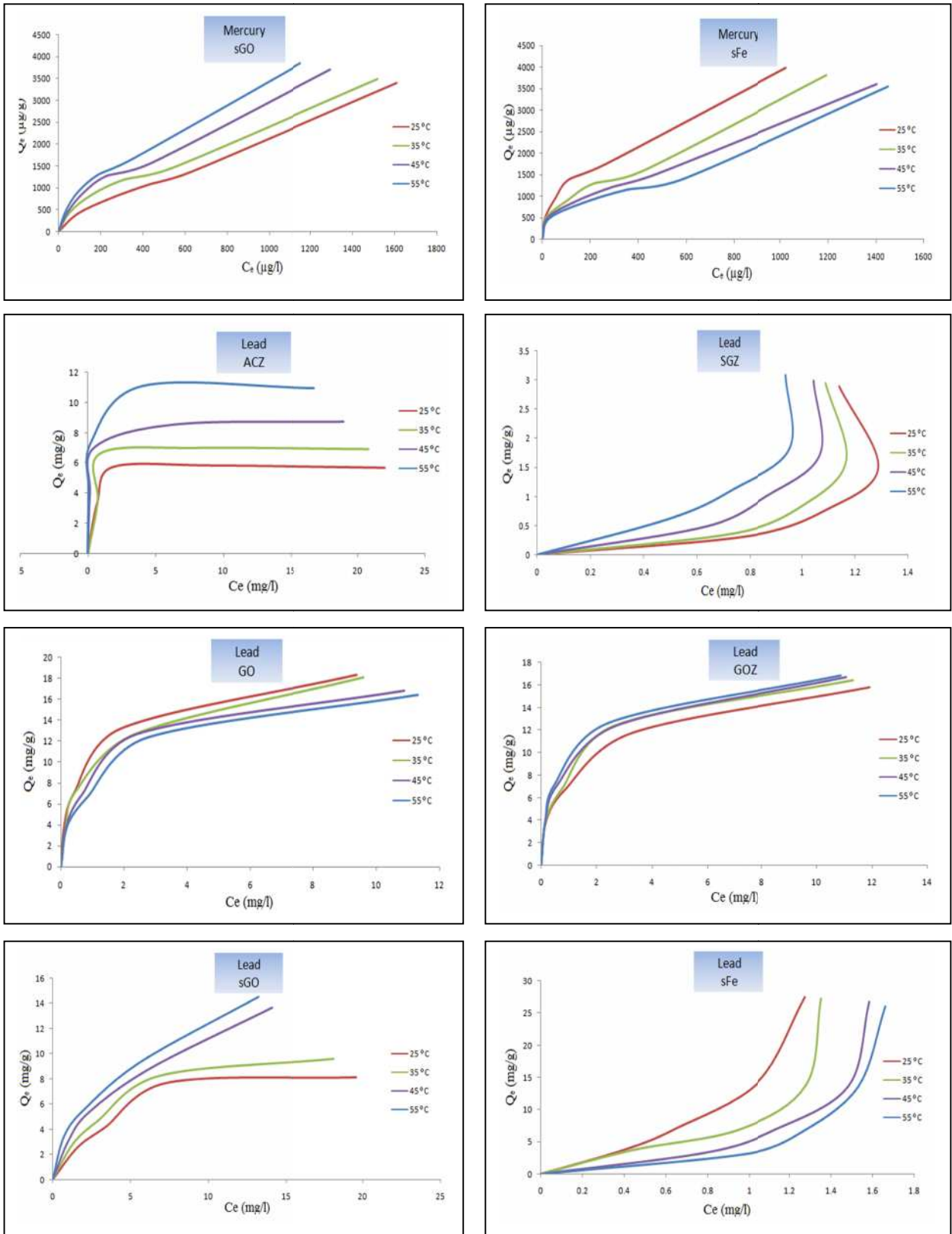
Figure 5.28 : Adsorption isotherm of Mercury and Lead ions

The optimum conditions were applied under four different temperatures (25 , 35 , 45 and 55 ºC) at 0.01g of adsorbent weight in order to study the adsorption isotherm , where a variety of adsorbate concentrations for the range 50-200 mg/l of Mordant Red 3 dye were used and adsorbed (10ml) onto ACZ adsorbent while the other concentration for the remained adsorbents used 10-50 mg/l (10ml) of Mordant Red 3. The same range of concentration to adsorb the Rhodamine B dye was used, while the concentration of Basic Brown dye was 50 -200 mg/l (25 ml). It was adsorbed onto ACZ , GO and GOZ adsorbents. On the other hand, the other concentration was used from the same dye for the rang of 10-50mg/l (10ml) which was adsorbed on SGZ , sGO and sFe adsorbents . The same range of Basic Brown concentration was used to adsorb Congo Red dye on the surface for all adsorbents, but it was 10ml for the adsorbate volume . The mercury concentration is 500 - 5000µg/l with 10 ml for the adsorbate volume, whilst the lead concentration for the range of 4-28 mg/l (10ml) was adsorbed onto all adsorbent surfaces except for the SGZ adsorbent that used a concentration of lead ions in the range of 1-4 mg/l with 10ml for the adsorbate volume .

5.1.2.1. Adsorption isotherme models

In the current study , there are four models of adsorption isotherms that have been utilized in order to describe the adsorption process like Langmuir , Freundlich , Temkin and Dubinin-Radushkevich .

The isotherm for Langmuir and Freundlich were studied for all the adsorbate solutions that were adsorbed onto all adsorbents, where the results of Mordant Red 3 dye that adsorbed onto all adsorbents appeared to show that the maximum value of the adsorption capacity was 124.3 mg/g, which was recorded by ACZ adsorbent because the surface area is higher than the other adsorbents, while the adsorption capacity of the remaining adsorbents in order to remove Mordant Red 3 dye at 28.4 , 22.2 , 31.73 and 44.69 mg/g that was recorded by SGZ , GO , GOZ

and sGO adsorbent, respectively. The adsorption mechanism of ACZ , GO and GOZ adsorbents tends to give monolayer adsorption by fitting with Langmuir isotherm , the Freundlich model was more consistent than the Langmuir isotherm for SGZ and sGO adsorbents when compared with the relationship coefficient values . The adsorption process is favorable when observed in values of the separation factor and heterogeneity factor .

The adsorption process of Congo Red dye onto all adsorbents are favorable and fitted with Langmuir model that refers to form the monolayer adsorption which recorded the highest adsorption capacity at 209.3 mg/g by GOZ adsorbent. This result is attributed to the existence of many functional groups such as the selenazone ligand loaded and the oxygen groups found onto their surface . On the other hand , the adsorption mechanism of the Basic Brown dye that is adsorbed onto all adsorbents is corresponding with Freundlich model which refers to form the multilayer adsorption, so, the GOZ adsorbent recorded a maximum value of adsorption capacity at 883.7 mg/g .

The maximum capacity to adsorb Rhodamine B dye according to Langmuir isotherm was recorded by ACZ adsorbent which was 135.3 mg/g, all the adsorbents are fitted with Langmuir model excepted for the GOZ adsorbent that tends to give multilayer adsorption that agrees with Freundlich isotherm .

Multilayer adsorption dominated to adsorb the mercury ions from their aqueous solution which is more consistent with Freundlich model than with Langmuir isotherm furthermore, the maximum value of adsorption capacity was recorded by GOZ adsorbent where was 8419.2 µg/g .

The maximum value of the adsorption capacity for adsorbing the lead ions from its aqueous solution was recorded by GO and sGO adsorbent, where the values

were 19.94 and 18.94 mg/g, the behavior of the adsorption process was done by all adsorbent surfaces corresponding with Langmuir isotherm except for the SGZ , sGO and sFe adsorbents that tended towards Freundlich isotherm model . All the data of Langmuir and Freundlich isotherms are depicted in the Tables shown from 5.7 to 5.12 and Figures from 5.29 to 5.32 .

.
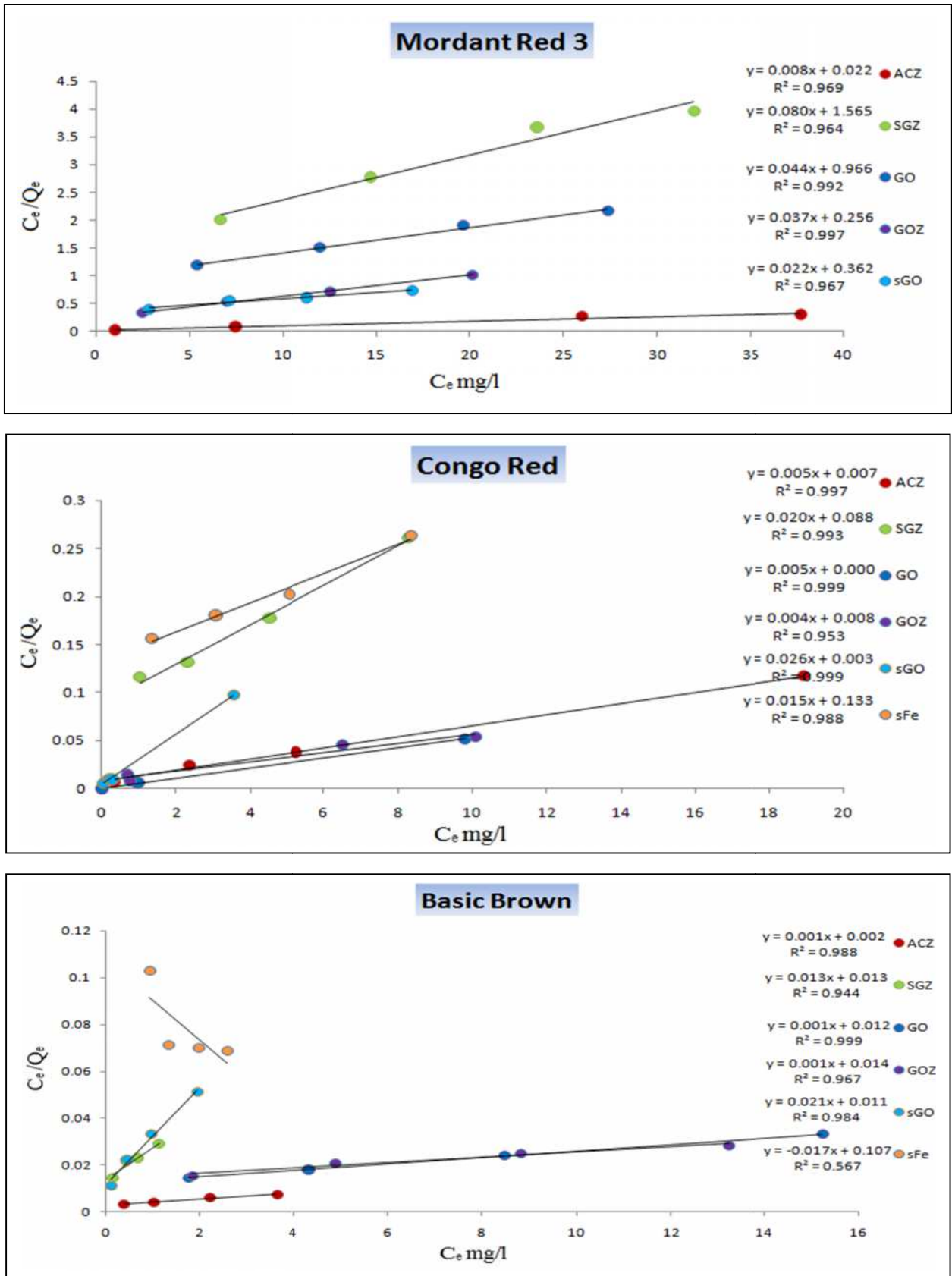
Figure 5.29 : Langmuir model of Mordant red 3, Congo red and Basic brown dyes
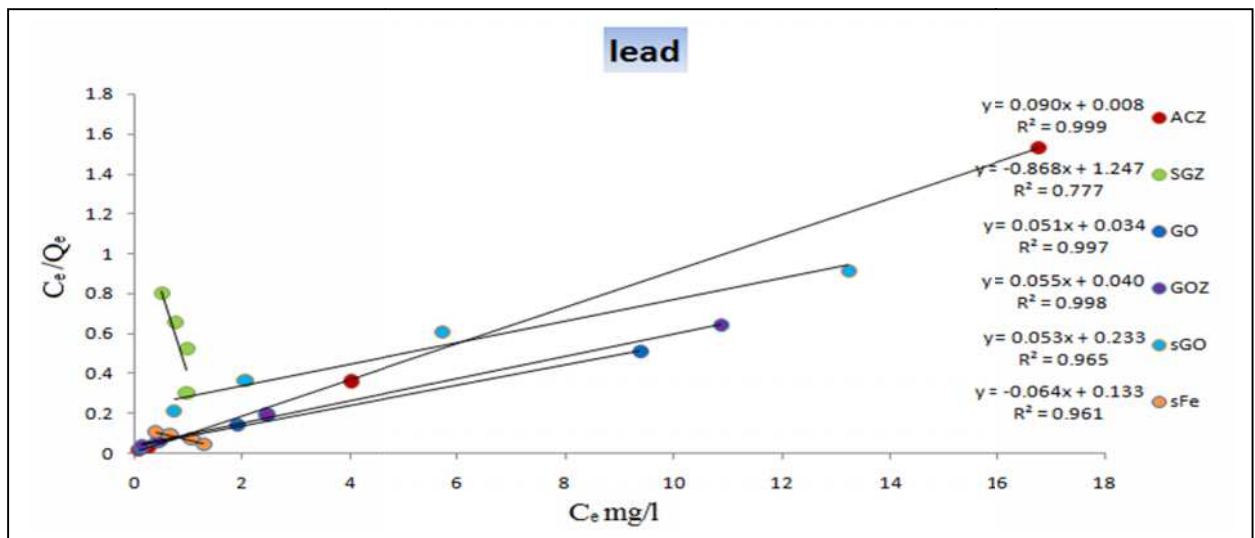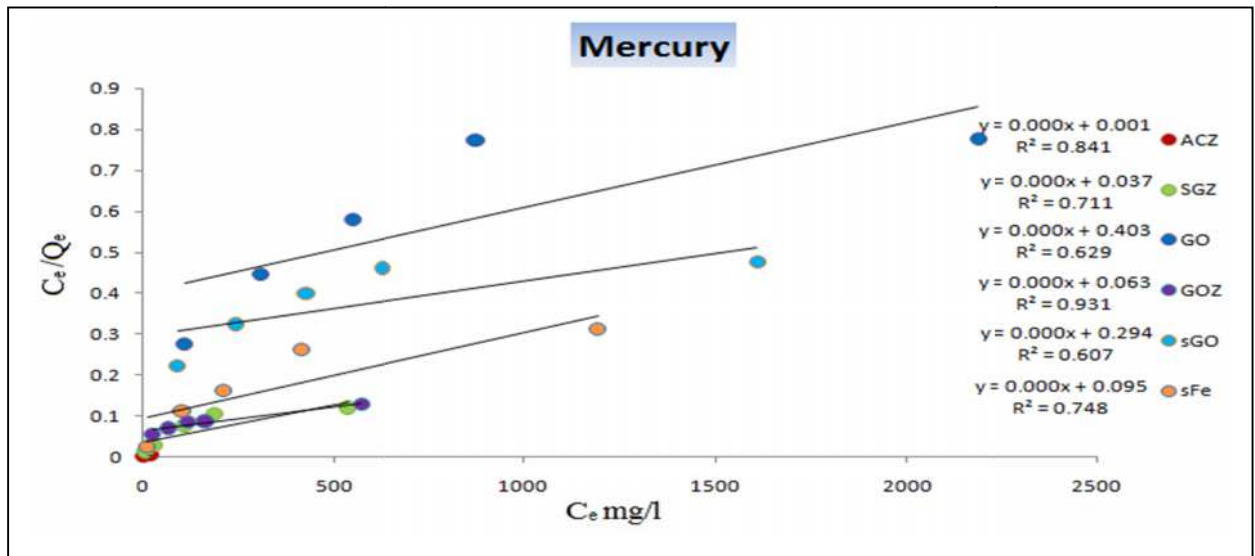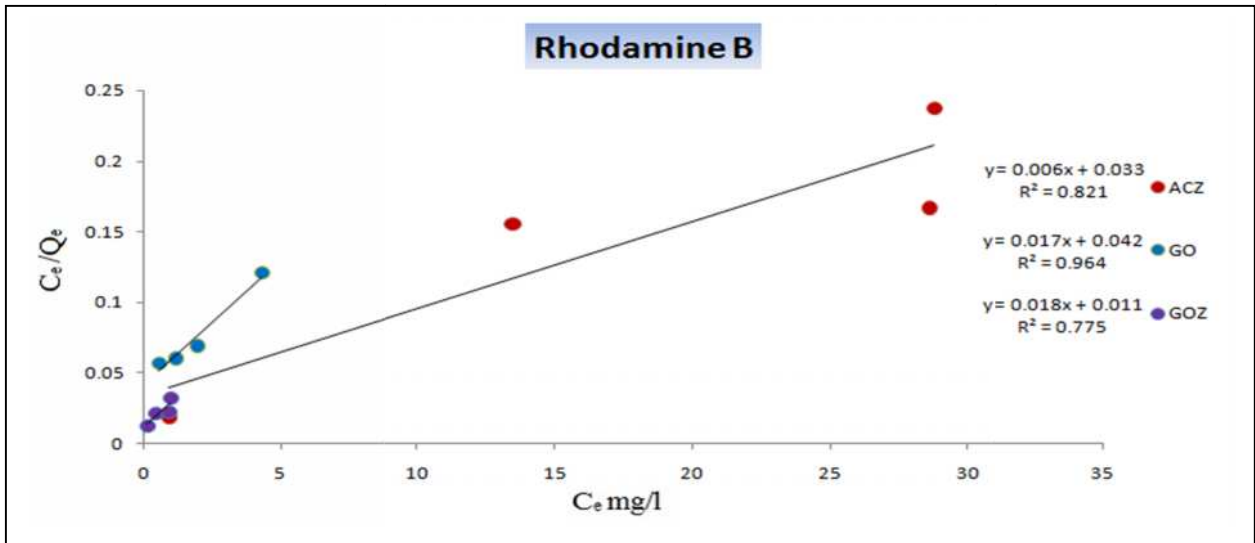
Figure 5.30 : Langmuir model of Rhodamine B dye, Mercury and lead ions
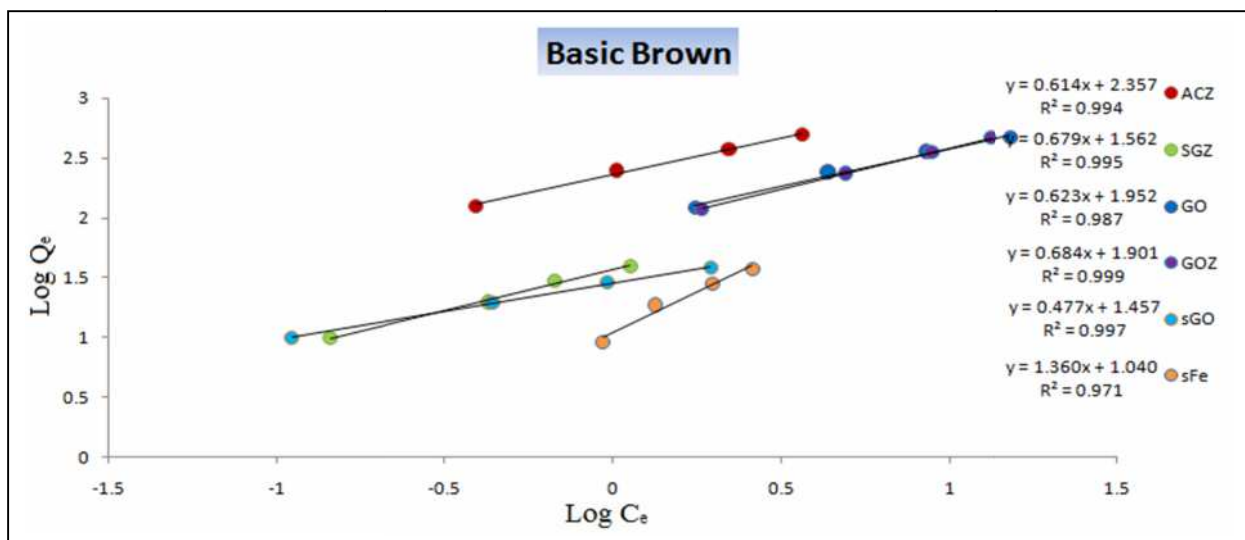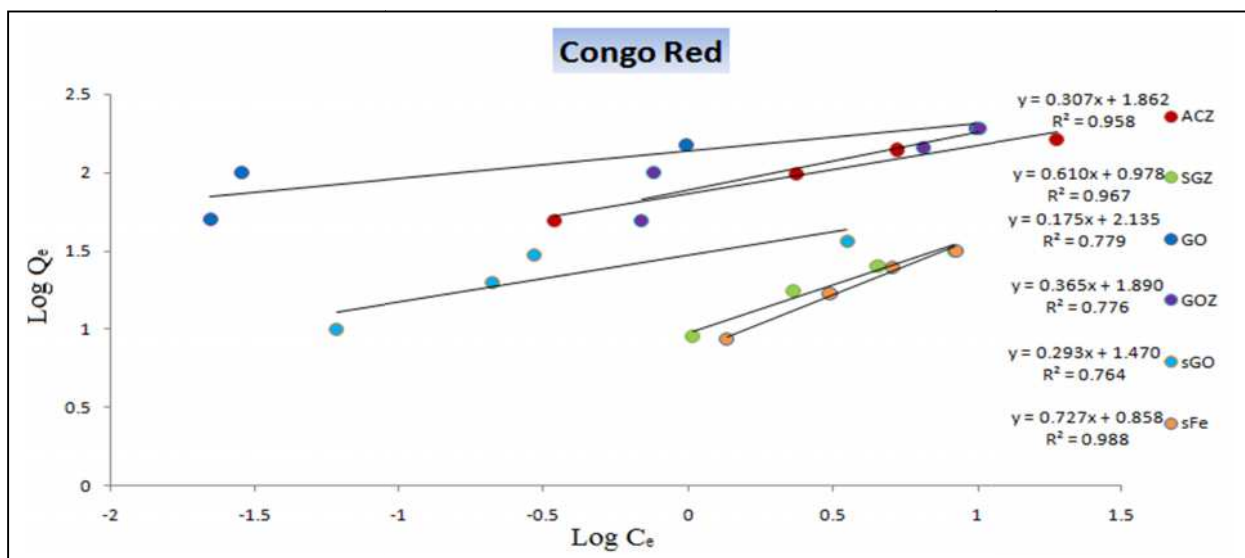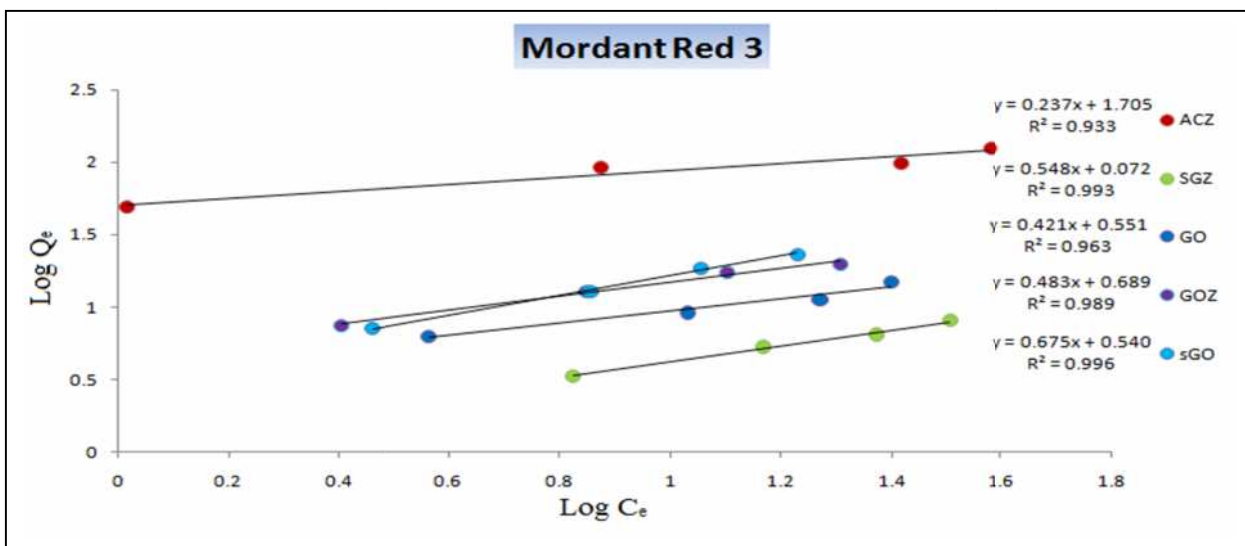
Figure 5.31 : Freundlich model of Mordant red 3, Congo red and Basic brown dyes
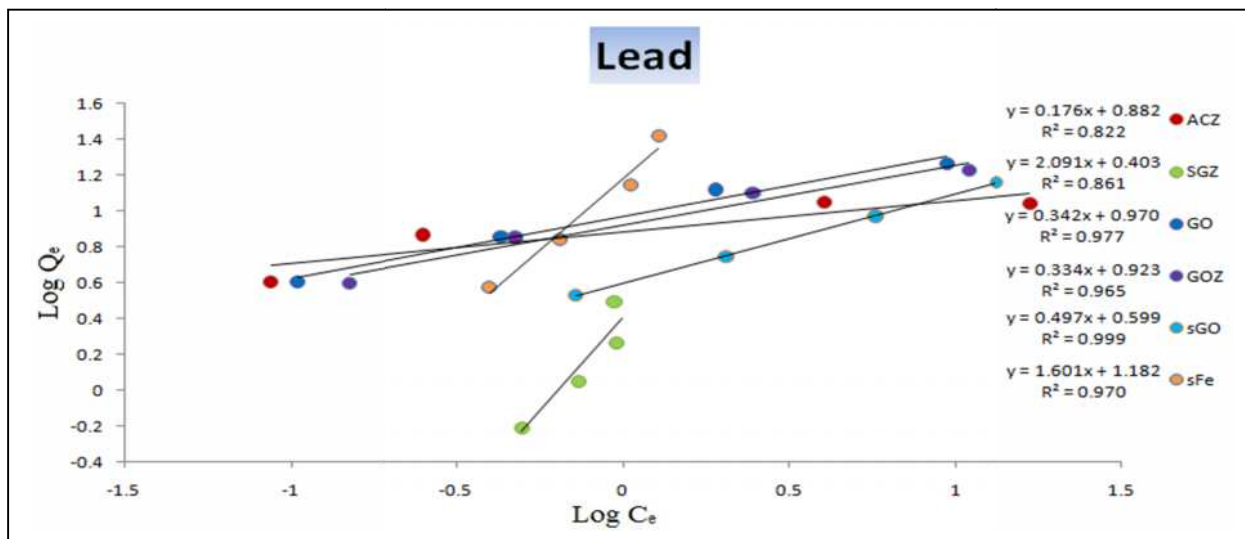
Figure 5.32 : Freundlich model of Rhodamine B dye, Mercury and lead ions

Table 5.7 : The results of Langmuir and Freundlich

isotherms of Mordant Red 3 dye

Adsorbent	C_o mg/l	C_e mg/l	C_e/Q_e g/l	Q_{max} mg/g	K_L L/mg	R_L	R^2	Log C_e	$LogQ_e$	n	K_f	R^2
				Langmuir					**Freundlich**			
ACZ	50	1.035	0.021			0.0392		0.0149	1.689			
	100	7.453	0.080	124.3	0.361	0.0200	0.969	0.8723	1.966	4.21	50.74	0.933
	150	25.99	0.265			0.0134		1.4149	1.991			
	200	37.74	0.303			0.0101		1.5768	2.095			
SGZ	10	6.674	2.006			0.6614		0.8243	0.521			
	20	14.702	2.775	28.4	0.051	0.4941	0.964	1.1673	0.724	1.82	1.18	0.993
	30	23.587	3.677			0.3943		1.3726	0.807			
	50	31.95	3.968			0.3281		1.5044	0.905			
GO	10	3.662	0.577			0.4881		0.5637	0.801			
	20	10.753	1.162	22.2	0.104	0.3228	0.992	1.0315	0.966	2.37	3.55	0.963
	30	18.605	1.632			0.2412		1.2696	1.0564			
	50	18.673	0.596			0.1925		1.2712	1.495			
GOZ	10	2.536	0.339			0.4049		0.4041	0.872			
	20	7.05	0.544	31.73	0.065	0.2538	0.997	0.8481	1.112	2.07	4.88	0.989
	30	12.613	0.725			0.1849		1.1008	1.240			
	50	20.621	0.701			0.1454		1.3143	1.468			
sGO	10	2.883	0.405			0.6180		0.4598	0.852			
	20	7.162	0.557	44.69	0.061	0.4472	0.967	0.8550	1.108	1.48	3.47	0.996
	30	11.342	0.607			0.3504		1.0546	1.270			
	50	30.24	1.530			0.2880		1.48058	1.295			

Table 5.8 : The results of Langmuir and Freundlich

isotherms of Congo Red dye

Adsorbent	C_o mg/l	C_e mg/l	C_e/Q_e g/l	Q_{max} mg/g	K_L L/mg	R_L	R^2	Log C_e	$LogQ_e$	n	K_f	R^2
				Langmuir					**Freundlich**			
ACZ	50	0.346	0.006			0.0253		-0.460	1.695			
	100	2.37	0.024	172.8	0.7697	0.0128	0.997	0.3747	1.989	3.24	72.92	0.958
	150	5.257	0.037			0.0085		0.7207	2.144			
	200	18.92	0.116			0.0064		1.2770	2.209			
SGZ	10	1.039	0.115			0.4808		0.0166	0.952			
	20	2.316	0.130	85.46	0.1079	0.3165	0.993	0.3647	1.247	1.38	8.97	0.967
	30	4.515	0.177			0.2359		0.6546	1.406			
	50	7.421	0.831			0.1880		0.8704	0.950			
GO	50	0.022	0.0004			0.0023		-1.657	1.698			
	100	0.028	0.0002	192.1	8.428	0.0011	0.999	-1.552	1.999	5.70	136.5	0.779
	150	0.979	0.0065			0.0007		-0.009	2.173			
	200	9.801	0.0515			0.0005		0.9912	2.279			

Adsorbent	C_o mg/l	C_e mg/l	C_e/Q_e g/l	Q_{max} mg/g	K_L L/mg	R_L	R^2	Log C_e	LogQ_e	n	K_f	R^2
GOZ	50	0.68	0.013	209.3	0.5636	0.0342	0.953	-0.161	1.692	2.73	77.78	0.776
	100	0.76	0.007			0.0174		-0.119	1.996			
	150	6.49	0.045			0.0116		0.8128	2.156			
	200	10.07	0.053			0.0087		1.0033	2.278			
sGO	10	0.06	0.006	43.79	6.6799	0.0147	0.999	-1.221	0.997	3.40	29.54	0.764
	20	0.21	0.010			0.00743		-0.675	1.296			
	30	0.29	0.009			0.0049		-0.533	1.472			
	50	2.95	0.062			0.00379		0.4701	1.672			
sFe	10	1.35	0.156	65.93	0.1138	0.4677	0.988	0.1316	0.936	1.37	7.21	0.988
	20	3.05	0.180			0.3052		0.4854	1.228			
	30	5.05	0.202			0.2265		0.7036	1.397			
	50	6.33	0.145			0.1801		0.8017	1.640			

Table 5.9 : The results of Langmuir and Freundlich isotherms of Basic Brown dye

Adsorbent	Langmuir							Freundlich				
	C_o mg/l	C_e mg/l	C_e/Q_e g/l	Q_{max} mg/g	K_L L/mg	R_L	R^2	Log C_e	LogQ_e	n	K_f	R^2
ACZ	50	0.39	0.003	761.7	0.4702	0.0407	0.988	-0.404	2.093	1.62	227.97	0.994
	100	1.02	0.004			0.0208		0.0115	2.393			
	150	2.20	0.005			0.0139		0.3434	2.567			
	200	3.63	0.007			0.0105		0.5606	2.691			
SGZ	10	0.14	0.014	72.92	0.9845	0.0922	0.944	-0.841	0.993	1.47	36.51	0.995
	20	0.42	0.021			0.0483		-0.371	1.291			
	30	0.67	0.022			0.0327		-0.172	1.467			
	50	1.68	0.034			0.0247		0.2266	1.684			
GO	50	1.75	0.0145	728.9	0.1129	0.1504	0.999	0.2430	2.081	1.60	89.64	0.987
	100	4.30	0.0180			0.0813		0.6342	2.378			
	150	8.45	0.0239			0.0557		0.9273	2.548			
	200	15.23	0.0329			0.0423		1.1827	2.664			
GOZ	50	1.83	0.0152	883.7	0.0799	0.5556	0.967	0.2633	2.080	1.46	79.68	0.999
	100	4.89	0.0205			0.3846		0.6894	2.376			
	150	8.83	0.0250			0.2941		0.9460	2.547			
	200	13.23	0.0283			0.2381		1.1216	2.669			
sGO	10	0.11	0.0112	47.60	1.8607	0.0510	0.984	-0.954	0.995	2.09	28.64	0.997
	20	0.43	0.0223			0.0261		-0.359	1.291			
	30	0.96	0.0330			0.0175		-0.017	1.462			
	50	1.60	0.0331			0.0132		0.2046	1.684			
sFe	10	0.93	0.1027	58.64	0.1588	0.3862	0.567	-0.030	0.957	0.73	10.97	0.971
	20	1.33	0.0714			0.2393		0.1248	1.271			
	30	1.96	0.0701			0.1734		0.2935	1.447			
	50	1.78	0.0369			0.1359		0.2504	1.683			

Table 5.10 : The results of Langmuir and Freundlich

isotherms of Rhodamine B dye

Adsorbent	Langmuir							Freundlich				
	C_o mg/l	C_e mg/l	C_e/Q_e g/l	Q_{max} mg/g	K_L L/mg	R_L	R^2	Log C_e	$LogQ_e$	n	K_f	R^2
ACZ	50	0.91	0.0186	135.3	0.5078	0.0378	0.821	-0.038	1.690	2.97	50.20	0.741
	100	13.45	0.1554			0.0193		1.1289	1.937			
	150	14.39	0.1187			0.0129		1.1581	2.083			
	200	14.31	0.0835			0.0097		1.1557	2.233			
GO	10	0.54	0.0573	56.93	0.4176	0.1931	0.964	-0.266	0.975	1.54	15.77	0.941
	20	1.14	0.0604			0.1069		0.0569	1.275			
	30	1.94	0.0692			0.0739		0.2884	1.448			
	50	1.90	0.0395			0.0564		0.2789	1.682			
GOZ	10	0.12	0.0123	54.33	1.6261	0.0579	0.775	-0.913	0.994	1.64	34.92	0.945
	20	0.41	0.0213			0.0298		-0.377	1.291			
	30	0.94	0.0324			0.0200		-0.025	1.463			
	50	1.23	0.0253			0.0151		0.0916	1.688			

Table 5.11 : The results of Langmuir and Freundlich

isotherms of Mercury ions

Adsorbent	Langmuir							Freundlich				
	C_o µg/l	C_e µg/l	C_e/Q_e g/l	Q_{max} µg/g	K_L L/µg	R_L	R^2	$LogC_e$	$LogQ_e$	n	K_f	R^2
ACZ	500	1.11	0.002	7782.9	0.089	0.029	0.841	0.046	2.698	1.44	712.5	0.841
	1000	1.85	0.001			0.010		0.269	2.999			
	1500	2.08	0.001			0.007		0.319	3.175			
	2000	2.36	0.001			0.005		0.373	3.300			
	5000	20.5	0.004			0.002		1.312	3.697			
SGZ	500	6.81	0.013	5512.6	0.0048	0.291	0.771	0.833	2.693	2.15	190.6	0.95
	1000	27.99	0.028			0.170		1.447	2.987			
	1500	107.5	0.077			0.120		2.031	3.143			
	2000	188.3	0.103			0.093		2.275	3.258			
	5000	536.6	0.120			0.039		2.729	3.649			
GO	500	108.2	0.276	4815.2	0.0005	0.795	0.629	2.034	2.593	1.58	18.55	0.968
	1000	308.4	0.445			0.659		2.489	2.839			
	1500	550.4	0.579			0.564		2.740	2.977			
	2000	871.6	0.772			0.492		2.940	3.052			
	5000	2185	0.776			0.279		3.339	3.449			
GOZ	500	26.87	0.056	8419.2	0.0018	0.517	0.931	1.429	2.674	1.36	42.77	0.999
	1000	66.45	0.071			0.349		1.822	2.970			
	1500	118.5	0.085			0.263		2.073	3.140			
	2000	162.3	0.088			0.211		2.210	3.264			
	5000	571.3	0.129			0.096		2.756	3.646			

	500	91.16	0.222			0.812		1.959	2.611			
	1000	244.3	0.323			0.684		2.387	2.878			
sGO	1500	426.9	0.397	7367.3	0.0004	0.591	0.607	2.630	3.030	1.38	14.7	0.984
	2000	630.3	0.460			0.520		2.799	3.136			
	5000	1608	0.474			0.302		3.206	3.530			
	500	13.03	0.026			0.476		1.115	2.687			
	1000	102.4	0.114			0.312		2.010	2.953			
sFe	1500	210.9	0.163	4779.6	0.002	0.232	0.748	2.324	3.110	2.3	138.3	0.939
	2000	416.9	0.263			0.185		2.620	3.199			
	5000	1191	0.312			0.083		3.075	3.580			

Table 5.12 : The results of Langmuir and Freundlich

isotherms of Lead ions

Adsorbent	Langmuir							Freundlich				
	C_o mg/l	C_e mg/l	C_e/Q_e g/l	Q_{max} mg/g	K_L L/mg	R_L	R^2	Log C_e	$LogQ_e$	n	K_f	R^2
ACZ	4	0.087	0.021			0.022		-1.059	0.6082			
	8	0.251	0.034	11.35	10.724	0.012	0.999	-0.600	0.8672	5.66	7.63	0.822
	14	4.021	0.362			0.006		0.604	1.0454			
	28	16.77	1.529			0.003		1.224	1.0399			
SGZ	1	0.49	0.798			0.561		-0.303	-0.205			
	2	0.73	0.653	1.151	0.696	0.435	0.777	-0.132	0.052	0.478	2.53	0.861
	3	0.95	0.521			0.340		-0.020	0.262			
	4	0.93	0.303			0.262		-0.027	0.490			
GO	4	0.10	0.025			0.138		-0.981	0.606			
	8	0.43	0.059	19.94	1.50	0.080	0.997	-0.366	0.856	2.92	9.34	0.977
	14	1.89	0.143			0.042		0.2778	1.121			
	28	9.38	0.511			0.023		0.9723	1.263			
GOZ	4	0.14	0.037			0.149		-0.824	0.601			
	8	0.47	0.066	18.28	1.3706	0.087	0.998	-0.323	0.853	2.98	8.37	0.965
	14	2.45	0.193			0.046		0.3891	1.102			
	28	10.86	0.644			0.025		1.0361	1.226			
sGO	4	0.723	0.211			0.512		-0.140	0.534			
	8	2.033	0.364	18.94	0.2291	0.364	0.965	0.3081	0.746	2.0	3.97	0.999
	14	5.719	0.608			0.223		0.7573	0.973			
	28	13.22	0.911			0.135		1.1212	1.161			
sFe	4	0.397	0.106			0.339		-0.400	0.573			
	8	0.647	0.092	16.14	0.4687	0.2187	0.961	-0.188	0.843	0.624	15.21	0.970
	14	1.048	0.074			0.123		0.0206	1.148			
	28	1.275	0.048			0.071		0.1058	1.422			

The adsorption isotherm of Mordant Red 3 dye was studied using the Temkin and D-R isotherms, the results of Mordant Red 3 dye was adsorbed onto all adsorbents which appeared the maximum of adsorption capacity according to D-R isotherm which was 105.3 mg/g, it was recorded by ACZ adsorbent, that was attributed to having a higher surface area than the other adsorbents, while the adsorption energy (E) values of Mordant Red 3 dye, which adsorbed onto all adsorbent surfaces indicate the occurrence of the physisorption process . The constant of Temkin isotherm (b_T) was calculated by slope from Temkin equation when it was plotted between the ln C_e on x axis versus adsorption capacity at equilibrium state Q_e on y axis , the lowest value of Temkin constant b_T was 0.133 J/mol to the ACZ adsorbent, that refers to increase in the surface coverage of adsorbate molecules onto adsorben surface [44,53] . The adsorption process of mordant red 3 dye onto all adsorbents surface is more fitted with Temkin isotherm than with D-R isotherm .

The adsorption process of Congo Red dye onto all adsorbents surface are more fitted with Temkin model than with D-R isotherm except for their adsorbed onto sGO surface that is consistent with D-R isotherm when is carried out, find out the comparison with the correlation coefficient (R^2) values. The adsorption capacity was calculated by utilizing the D-R isotherm and it showed 134.7 , 24.4 , 174.7 , 171.5 , 37.2 and 28.5 mg/g to the ACZ , SGZ , GO , GOZ , sGO and sFe adsorbents, respectively. On the other hand, the adsorption process of Congo Red dye onto all adsorbents surface tends towards the physical adsorption through using the adsorption energy values that were recorded in the range 0.86 to 7.46 KJ/mol .

The adsorption isotherm of the Basic Brown dye was studied onto all adsorbents surface that appeared corresponding with Temkin isotherm , except for the sFe adsorbent which is consistent with both D-R and Temkin isotherms . The

adsorption energy was calculated and shows the range from 0.71 to 3.70 KJ/mol which denotes the occurrence of the physisorption process . The highest adsorption capacity was recorded according to D-R isotherm where it was 432.2 for the activated carbon modified with selenazone ligand . Whilst , the Temkin constant b_T and A_T were computed and exhibited values in the range 0.015 -0.261 J/mol and 0.988- 21.51 L/g respectively .

The adsorption capacity for adsorbing the Rhodamine B dye onto three adsorbents surface (ACZ , GO and GOZ) was calculated by extracting the intercept from D-R equation when plotting the square of Polanyi potential versus lnQ_e , the valus were 122.5 , 34.6 and 36.02 mg/g, respectively. The adsorption nature of Rhodamine B dye onto three adsorbents surface can be described as physical adsorption . The surface coverage of adsorbate molecules increases with decrease of heat adsorption onto adsorbent surface that is consistent with Temkin constant value b_T . The adsorption process of all adsorbents is corresponding with D-R isotherm more than with Temkin isotherm except for the adsorption of dye onto GO adsorbent that suitable with Temkin isotherm .

The adsorption energy (E) results denotes the occurrence of physical adsorption by interacting the mercury ions with the molecules of adsorbent surfaces, the adsorption capacity was computed by D-R isotherm where recorded at 3905.3 , 1882.6 , 1294.3 , 2036.6 , 1531.8 and 1640.9 µg/g to the ACZ , SGZ , GO , GOZ , sGO and sFe respectively, these results are consistent with Temkin constant (b_T) data which denoted the decline of heat adsorbtion with the increases of the surface coverage by adsorbate molecules . The correlation coefficient data were compared between Temkin and D-R isotherms and then showed the adsorption process of mercury ions onto all adsorbents surface that were more fitted with Temkin model

than with D-R model except for their adsorbed onto ACZ adsorbent which its behavior was fit with D-R isotherm .

The series of the concentrations of lead ions (4 ,8 ,14 and 28 mg/l) were adsorbed onto all adsorbents surface under different temperatures at (25 , 35 , 45 and 55 ℃), except for the SGZ adsorbent which used the less of lead ions concentration at (1 ,2 ,3 and 4 mg/l). In order to study the adsorption isotherm models . The values of adsorption energy denoted to the occurrence of the physisorption process by adsorbing the lead ions onto all adsorbent surfaces , the highest of the adsorption capacity was recorded by sFe adsorbent according to D-R isotherm which was 31.1 mg/g that was consistent with the data of Temkin isotherm constant (b_T) . On other hand , the adsorption process of lead ions onto ACZ , SGZ and sFe adsorbents surface is more corresponding with D-R isotherm than with Temkin isotherm whilst , the others of adsorbents surface are concurring to adsorb for lead ions with Temkin isotherm . The all data of Temkin and D-R isotherms are depicted in the Tables listed from 5.13 to 5.18 and Figures from 5.33 to 5.36 .
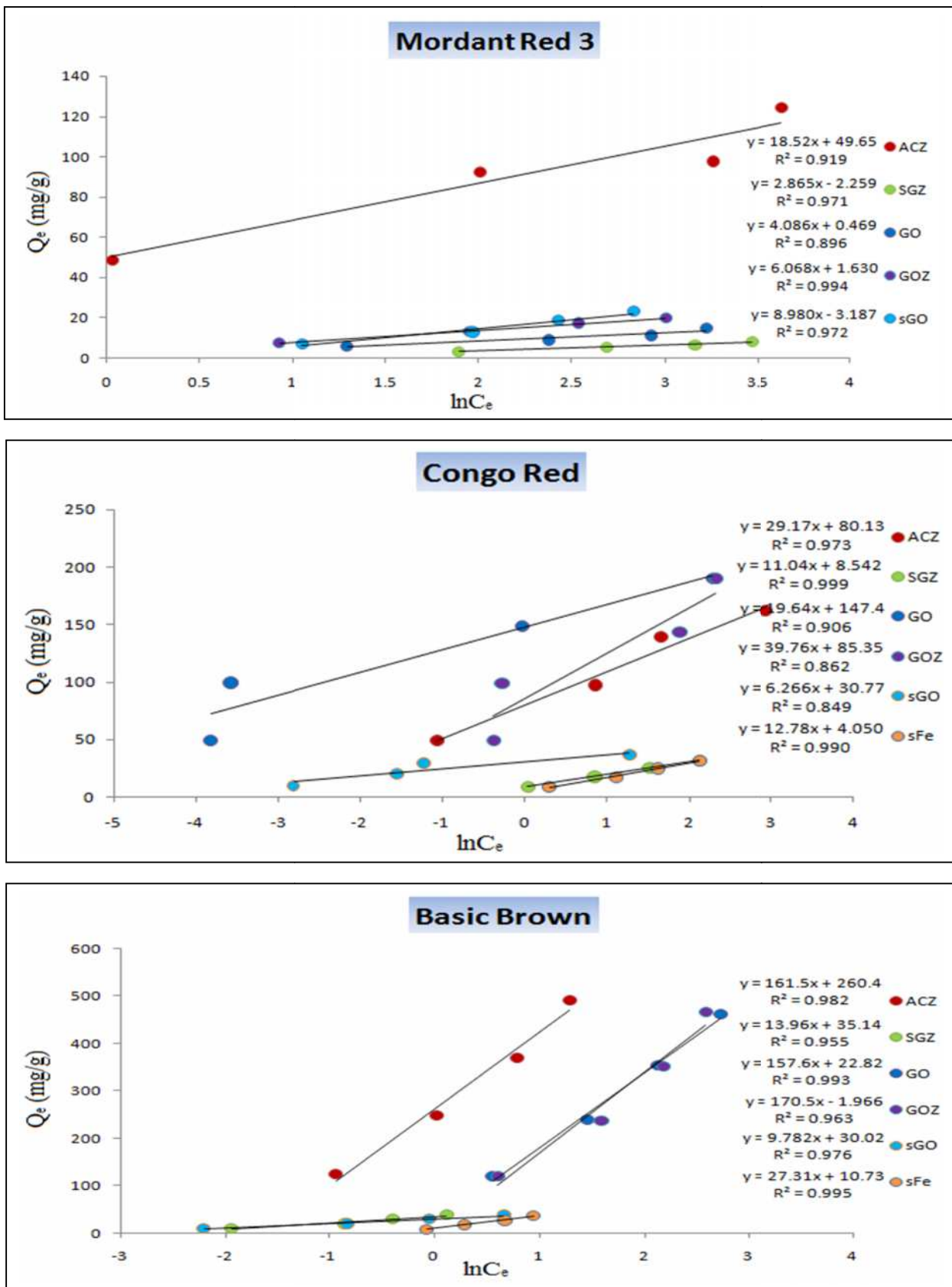
Figure 5.33 : Temkin model of Mordant red 3, Congo red and Basic brown dyes

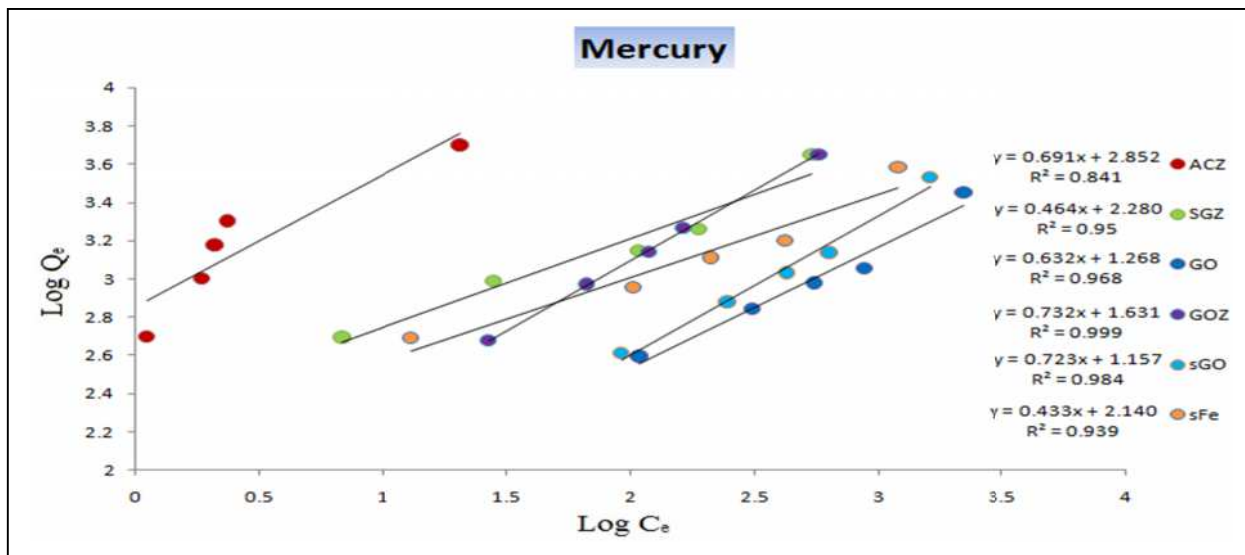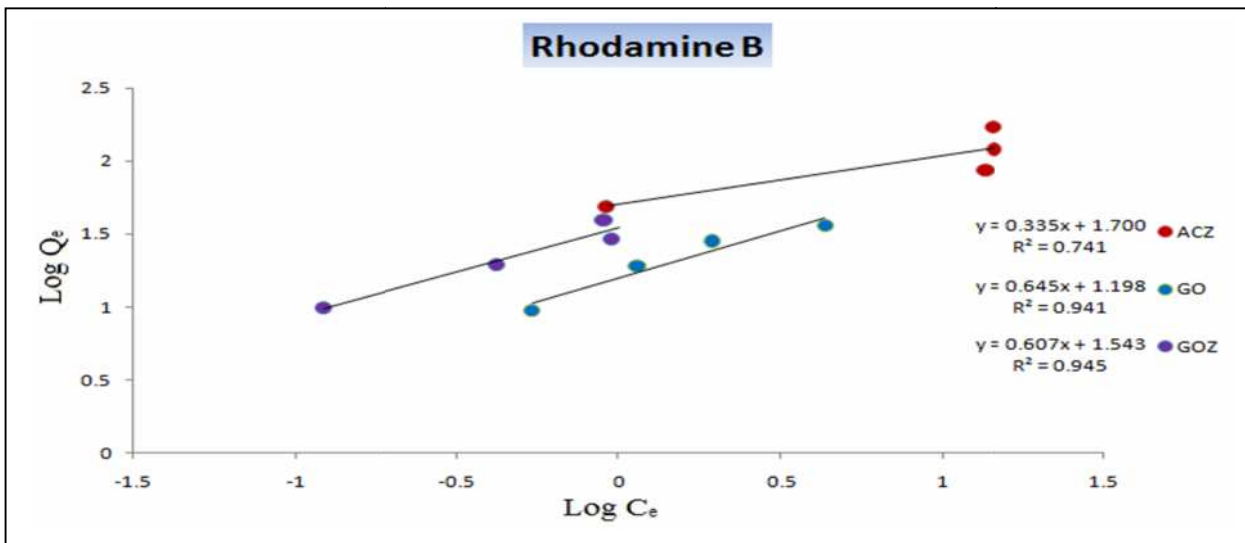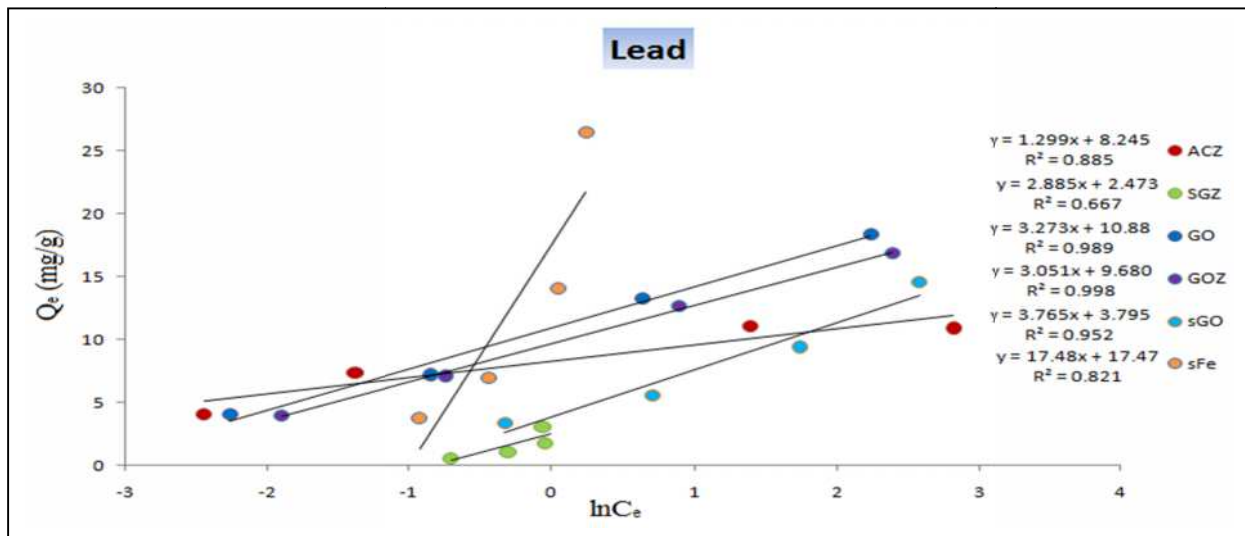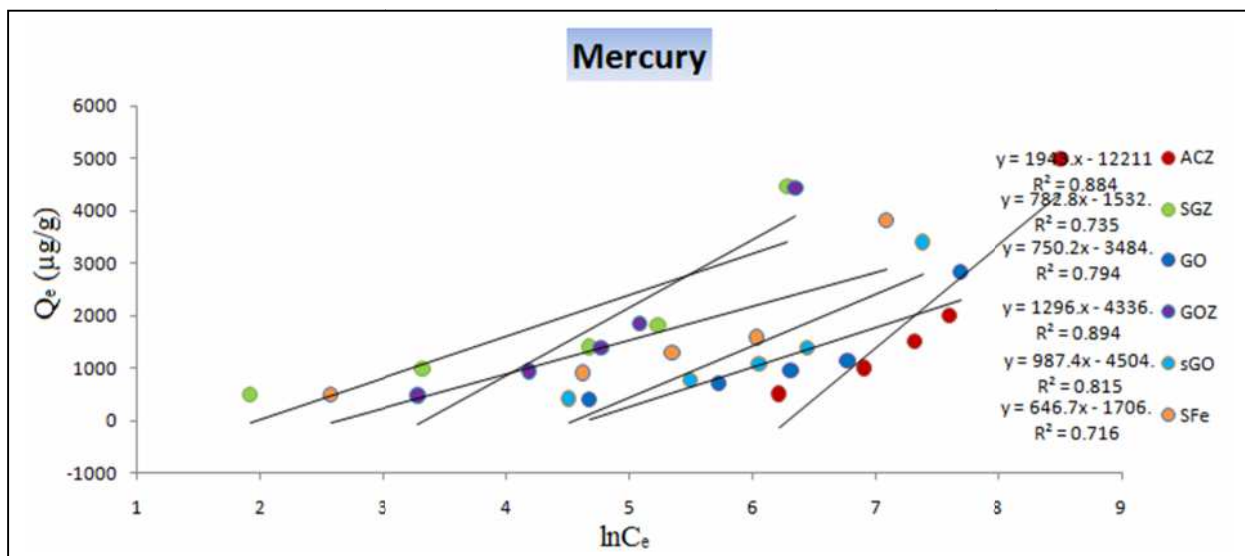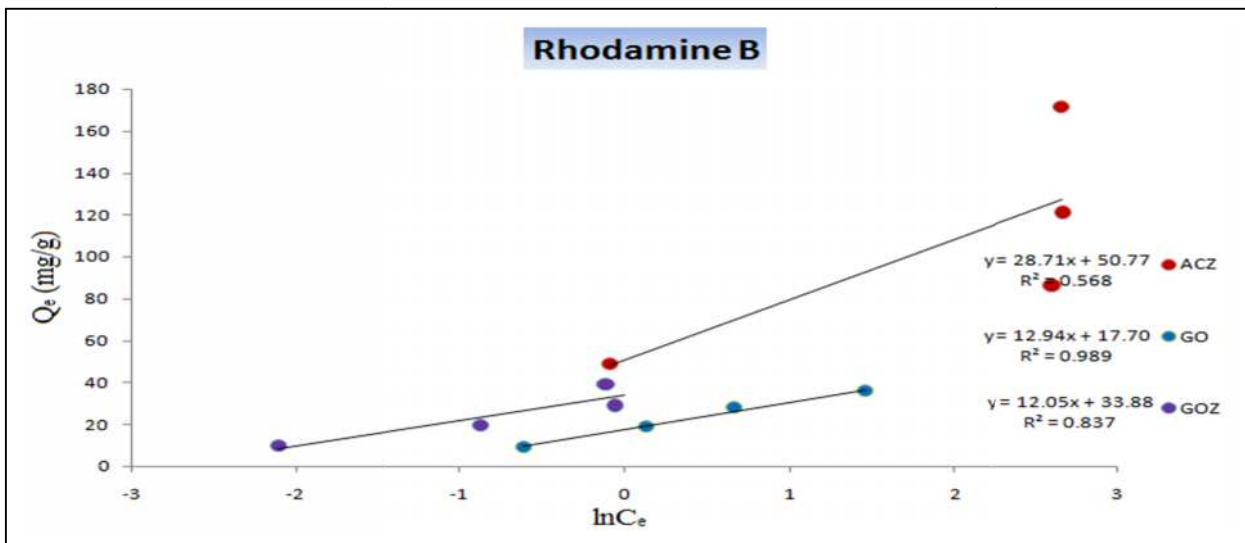Figure 5.34 : Temkin model of Rhodamine B dye, Mercury and lead ions
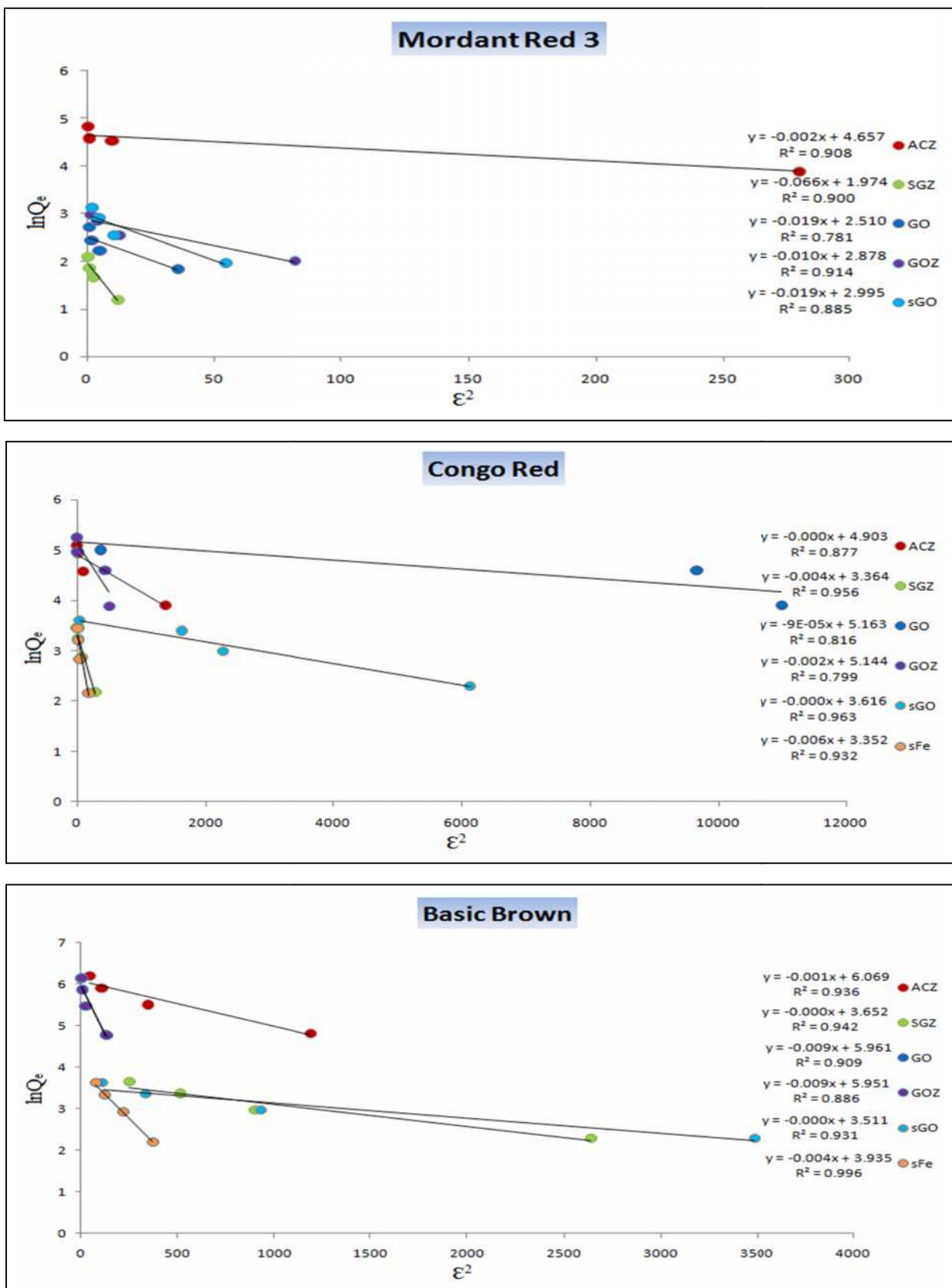
Figure 5.35 : D-R model of Mordant red 3, Congo red and Basic brown dyes
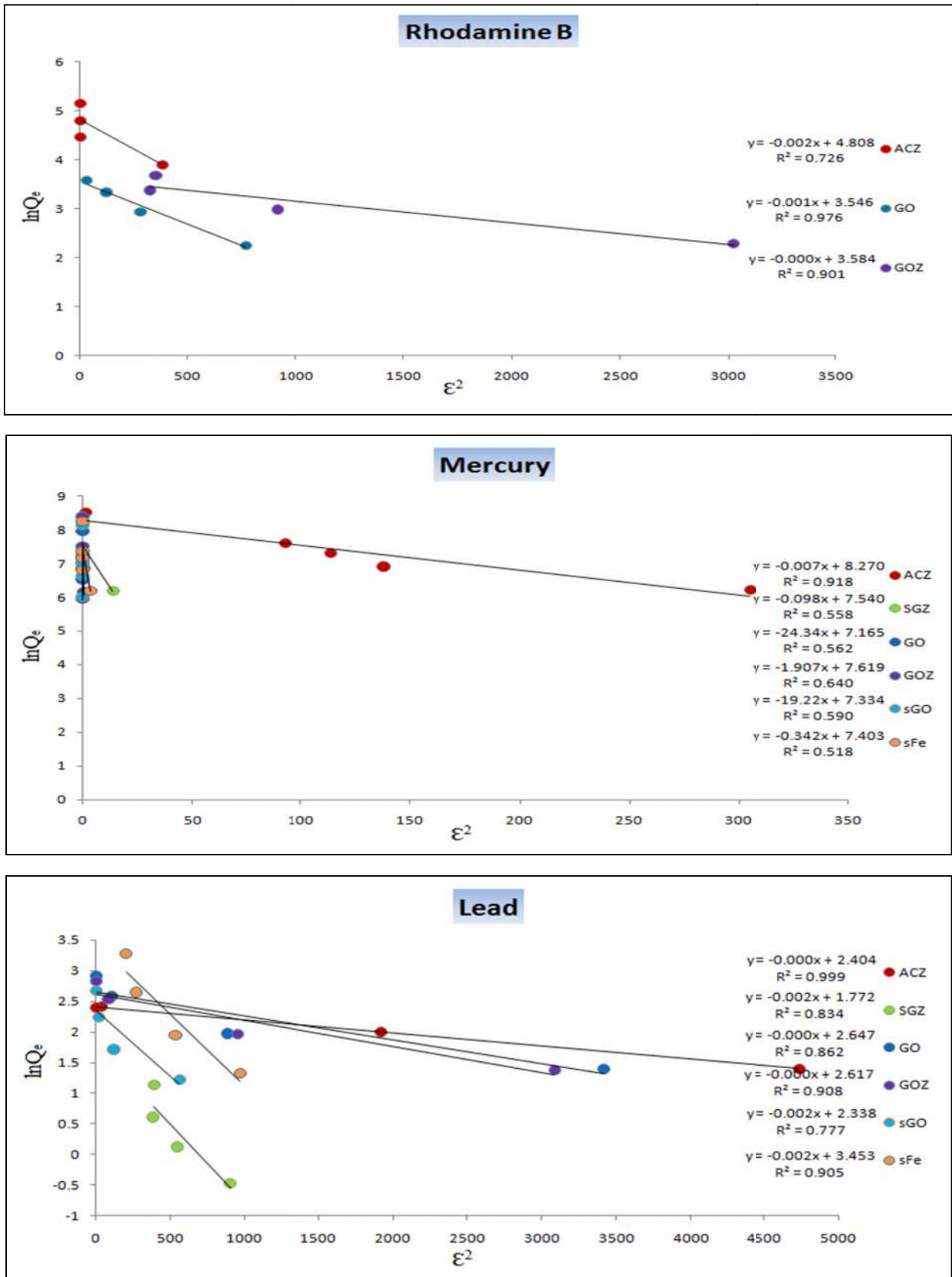
Figure 5.36 : D-R model of Rhodamine B dye, Mercury and lead ions

Table 5.13 : The results of Temkin and D-R isotherms
of Mordant Red 3 dye

Adsorbent	C_o mg/l	lnQ_e	2		Q_{max} mg/g	E KJ/mol	R^2	Q_e mg/g	LnC_e	b_T	A_T	R^2
	50	3.89	28058					48.96	0.034			
ACZ	100	4.52	97305	2.7×10^{-7}	105.3	1.35	0.908	92.54	2.008	0.133	14.6	0.919
	150	4.58	8743					98	3.258			
	200	4.82	4198					124.51	3.630			
	10	1.20	119657					3.32	1.898			
SGZ	20	1.66	26580	6.6×10^{-6}	7.20	0.27	0.90	5.29	2.687	0.864	0.454	0.971
	30	1.85	10583					6.41	3.160			
	50	2.91	5830					18.45	3.451			
	10	1.84	357810					6.338	1.298			
GO	20	2.22	48538	1.9×10^{-6}	12.3	0.51	0.781	9.247	2.375	0.606	1.121	0.896
	30	2.43	16825					11.395	2.923			
	50	3.44	9446.8					31.327	2.927			
	10	2.01	821695					7.464	0.930			
GOZ	20	2.56	130841	1.1×10^{-6}	17.7	0.67	0.914	12.95	1.953	0.449	1.308	0.994
	30	2.85	43289					17.38	2.534			
	50	3.38	17420					29.37	3.026			
	10	1.96	544294					7.117	1.058			
sGO	20	2.55	104858	2×10^{-6}	19.9	0.504	0.885	12.838	1.968	0.275	0.701	0.972
	30	2.92	43824					18.658	2.428			
	50	2.98	20169					19.76	3.409			

Table 5.14 : The results of Temkin and D-R isotherms
of Congo Red dye

Adsorbent	C_o mg/l	lnQ_e	2		Q_{max} mg/g	E KJ/mol	R^2	Q_e mg/g	LnC_e	b_T	A_T	R^2
	50	3.90	13.7×10^6					49.65	-1.06			
ACZ	100	4.58	921529	7.3×10^{-8}	134.7	2.60	0.877	97.63	0.86	0.093	15.59	0.973
	150	4.93	225510					139.48	1.65			
	200	5.08	19718					162.15	2.94			
	10	2.19	2790173					8.96	0.03			
SGZ	20	2.87	790755	3.7×10^{-7}	24.4	1.17	0.956	17.68	0.83	0.359	4.71	0.999
	30	3.23	245697					25.48	1.50			
	50	2.18	79891					41.72	2.00			
	50	3.91	1.1×10^8					49.97	-3.81			
GO	100	4.60	96.5×10^6	9×10^{-9}	174.7	7.46	0.816	99.97	-3.57	0.138	1825	0.906
	150	5.00	3683708					149.02	-0.02			
	200	5.24	70192.67					190.19	2.282			

Adsorbent	C_o mg/l	$\ln Q_e$	ε^2		Q_{max} mg/g	E KJ/mol	R^2	Q_e mg/g	LnC_e	b_T	A_T	R^2
GOZ	50	3.89	4935136	1.9×10^{-7}	171.5	1.58	0.799	49.31	-0.37	0.062	8.55	0.862
	100	4.59	4328658					99.24	-0.27			
	150	4.96	125736					143.5	1.87			
	200	5.24	54950					189.9	2.31			
sGO	10	2.29	613.2×10^5	2.2×10^{-8}	37.2	4.79	0.963	9.94	-2.81	0.435	135.6	0.849
	20	2.98	22705149					19.78	-1.55			
	30	3.39	16389137					29.70	-1.22			
	50	3.85	462873					47.04	1.08			
sFe	10	2.15	1877525	6.6×10^{-7}	28.5	0.86	0.932	8.64	0.30	0.193	1.37	0.990
	20	2.82	491369					16.94	1.11			
	30	3.21	200076					24.94	1.62			
	50	3.77	78718					43.66	1.84			

Table 5.15 : The results of Temkin and D-R isotherms

of Basic Brown dye

Adsorbent	C_o mg/l	$\ln Q_e$	ε^2	D-R	Q_{max} mg/g	E KJ/mol	R^2	Q_e mg/g	LnC_e	b_T	A_T	R^2
ACZ	50	4.82	11.8×10^6	1×10^{-7}	432.2	2.13	0.936	124.0	-0.93	0.016	5.01	0.982
	100	5.51	34.3×10^5					247.4	0.026			
	150	5.91	10.4×10^5					369.4	0.790			
	200	6.19	43.9×10^4					490.9	1.290			
SGZ	10	2.28	26.3×10^6	5.3×10^{-8}	38.5	3.04	0.942	9.856	-1.93	0.177	12.38	0.995
	20	2.97	89.8×10^5					19.57	-0.85			
	30	3.37	51×10^5					29.32	-0.39			
	50	3.87	24.8×10^5					48.31	0.521			
GO	50	4.79	12.5×10^5	9.6×10^{-7}	388.1	0.71	0.909	120.6	0.559	0.015	1.155	0.993
	100	5.47	26.7×10^4					239.2	1.460			
	150	5.86	76.6×10^3					353.8	2.135			
	200	6.13	24.8×10^3					461.9	2.723			
GOZ	50	4.79	13.2×10^5	9×10^{-7}	383.9	0.74	0.882	120.4	0.606	0.015	0.988	0.963
	100	5.47	24.1×10^4					237.7	1.587			
	150	5.86	80.4×10^3					352.9	2.178			
	200	6.14	37×10^3					466.9	2.582			
sGO	10	2.29	34.7×10^6	3.6×10^{-8}	33.4	3.70	0.931	9.889	-2.198	0.261	21.51	0.976
	20	2.97	92.9×10^5					19.56	-0.827			
	30	3.36	33.4×10^5					29.04	-0.040			
	50	3.87	11.3×10^5					48.39	0.471			
sFe	10	2.20	37.1×10^5	4.7×10^{-7}	51.1	1.03	0.996	9.06	-0.07	0.096	1.48	0.995
	20	2.92	21.8×10^5					18.66	0.287			
	30	3.33	11.8×10^5					28.03	0.676			
	50	3.87	75.1×10^4					48.22	0.576			

Table 5.16 : The results of Temkin and D-R isotherms

of Rhodamine B dye

Adsorbent	C_o mg/l	lnQ_e	2		Q_{max} mg/g	E KJ/mol	R^2	Q_e mg/g	LnC_e	b_T	A_T	R^2
			D-R						**Temkin**			
ACZ	50	3.89	38.1×10^5	2.4×10^{-7}	122.5	1.44	0.726	49.08	-0.088	0.092	5.85	0.568
	100	4.46	35.9×10^3					86.54	2.599			
	150	4.79	31.5×10^3					121.2	2.666			
	200	5.14	31.8×10^3					171.3	2.661			
GO	10	2.24	76.4×10^5	1.7×10^{-7}	34.6	1.68	0.976	9.458	-0.612	0.204	3.927	0.989
	20	2.93	27.7×10^5					18.86	0.131			
	30	3.33	12×10^5					28.05	0.664			
	50	3.87	30.5×10^4					48.09	0.642			
GOZ	10	2.29	30.2×10^6	4.4×10^{-8}	36.02	3.36	0.901	9.878	-2.103	0.205	16.64	0.837
	20	2.97	91.3×10^5					19.58	-0.869			
	30	3.36	32.1×10^5					29.05	-0.059			
	50	3.88	34.7×10^5					48.76	0.211			

Table 5.17 : The results of Temkin and D-R isotherms

of Mercury ions

Adsorbent	C_o mg/l	lnQ_e	2		Q_{max} µg/g	E KJ/mol	R^2	Q_e µg/g	LnC_e	b_T	A_T	R^2
			D-R						**Temkin**			
ACZ	500	6.21	30.5×10^5	7.4×10^{-7}	3905.3	0.82	0.918	498.8	0.10	0.001	1.24	0.884
	1000	6.90	13.7×10^5					998.1	0.61			
	1500	7.31	11.3×10^5					1497.9	0.73			
	2000	7.59	92.6×10^4					1997.6	0.85			
	5000	8.51	16.8×10^3					4979.4	3.02			
SGZ	500	6.20	13.9×10^4	9.9×10^{-5}	1882.6	0.22	0.558	493.1	1.91	0.003	0.14	0.735
	1000	6.87	9161					972	3.33			
	1500	7.23	637.4					1392	4.67			
	2000	7.50	208.4					1811	5.23			
	5000	8.40	25.77					4463	6.28			
GO	500	5.97	519	0.002	1294.3	0.014	0.562	391.7	4.68	0.003	0.01	0.794
	1000	6.53	64.32					691.5	5.73			
	1500	6.85	20.22					949.5	6.31			
	2000	7.02	8.069					1128	6.77			
	5000	7.94	1.284					2814	7.68			
GOZ	500	6.15	8191.7	0.0001	2036.6	0.05	0.640	473.1	3.29	0.001	0.03	0.894
	1000	6.83	1369.4					933.5	4.19			
	1500	7.23	433.07					1381	4.77			
	2000	7.51	231.4					1837	5.08			
	5000	8.39	18.77					4428	6.34			

Adsorbent	C_o	$\ln Q_e$	ε^2		Q_{max}	E	R^2	Q_e	$\ln C_e$	b_T	A_T	R^2
sGO	500	6.01	730.62					408.8	4.51			
	1000	6.62	102.4					755.6	5.49			
	1500	6.97	33.60	0.001	1531.8	0.01	0.590	1073.089	6.05	0.002	0.01	0.815
	2000	7.22	15.42					1369	6.44			
	5000	8.12	2.370					3391	7.38			
sFe	500	6.18	35808					486.9	2.56			
	1000	6.79	619.1					897.5	4.62			
	1500	7.16	146.6	3.4×10^{-5}	1640.9	0.12	0.518	1289	5.35	0.003	0.07	0.716
	2000	7.36	37.62					1583	6.03			
	5000	8.24	4.617					3808	7.08			

Table 5.18 : The results of Temkin and D-R isotherms

of Lead ions

Adsorbent	D-R C_o mg/l	$\ln Q_e$	ε^2		Q_{max} mg/g	E KJ/mol	R^2	Temkin Q_e mg/g	$\ln C_e$	b_T	A_T	R^2
ACZ	4	1.36	47.3×10^6					3.91	-2.44			
	8	2.04	19.1×10^6	2.1×10^{-8}	10.8	4.88	0.999	7.74	-1.38	2.18	659	0.885
	14	2.30	36.6×10^4					9.97	1.39			
	28	2.41	24.9×10^3					11.2	2.81			
SGZ	1	-0.4	90.3×10^5					0.62	-0.69			
	2	0.11	54.7×10^5	2.5×10^{-7}	5.88	1.39	0.834	1.12	-0.30	0.945	2.35	0.667
	3	0.60	38.2×10^5					1.82	-0.04			
	4	1.12	39.1×10^5					3.09	-0.06			
GO	4	1.35	34.1×10^6					3.89	-2.26			
	8	2.02	88.6×10^5	2.5×10^{-7}	13.9	3.56	0.862	7.56	-0.84	0.760	26.8	0.989
	14	2.49	11×10^5					12.1	0.63			
	28	2.92	62.9×10^3					18.6	2.23			
GOZ	4	1.34	30.8×10^6					3.85	-1.89			
	8	2.01	95.4×10^5	4.3×10^{-8}	13.5	3.42	0.908	7.52	-0.74	0.90	23.3	0.998
	14	2.44	87.1×10^4					11.5	0.89			
	28	2.84	57.6×10^3					17.1	2.38			
sGO	4	1.18	56×10^5					3.27	-0.32			
	8	1.78	11.8×10^5	2.1×10^{-7}	10.1	1.53	0.777	5.96	0.70	0.733	2.70	0.952
	14	2.11	19.3×10^4					8.28	1.74			
	28	2.69	39.5×10^3					14.7	2.58			
sFe	4	1.28	96.9×10^5					3.60	-0.92			
	8	1.99	53.5×10^5	2.3×10^{-7}	31.1	1.46	0.901	7.35	-0.43	0.143	2.73	0.821
	14	2.56	27.5×10^5					12.9	0.04			
	28	3.28	20.5×10^5					26.7	0.24			

5.1.3. Thermodynamic parameters of adsorption

The impact of temperature on adsorption process was studied in order to understand the adsorption operation behavior in the solid –liquid system . On the other hand , it helps also to estimate the values of thermodynamic functions such as the change of the standard functions states for enthalpy H^o , Gipps free energy G^o and entropy S^o . The thermodynamic parameters can be calculated by depending firstly on equilibrium constant (K) that denote the distribution and diffusion of the molecules of adsorbate between the solid phase and the liquid phase after applied the optimal conditions for the adsorption process , the equilibrium constant can be calculated by the following relation [35 ,72, 176 ,191] :

$$K = C_{solid} / C_{liquid}$$

Where C_{solid} represents the equilubrium concentration of adsorbate molecules after their adsorbed onto the adsorbent surface (mg/l) while , the C_{liquid} (mg/l) is the concentration of adsorbate molecules in the solution at equilibrium state (C_e) . The change of standard free energy G^o was calculated using the following relation [191 -193] :

$$G^o = - RT \ln K$$

Where R is the universal gas constant (8.314 J .mol^{-1}.K^{-1}) and T (^{o}K) is the absolute temperature . The G^o is an important thermodynamic parameter that refers to the spontaneous or nonspontaneous adsorption reaction by the interaction between the adsorbate molecules with adsorbent surface, the negative G^o value is denots to the spontaneous adsorption reaction while , the positive value refers to the nonspontaneous reaction. the adsorption nature can be provided information by utilizing the G^o values , physisorption occurs in the range of G^o values from -20 to 0 KJ/mol while , the range between -80 to -400 points to the occurrence of the

chemosorption process [72,74] . The data of equilibrium constant (K) are shown in the Table 5.19 - 5.24 .

Table 5.19 : The results of equilibrium constant to adsorb of Mordant red 3 dye (50 mg/l) under different temperature

Adsorbent	T ^{0}K	1/T	K Equilibrium constant	lnK	R^2
ACZ	298	0.003356	47.30918	3.856704	
	308	0.003247	31.93808	3.463799	0.891
	318	0.003145	26.76235	3.286996	
	328	0.003049	25.49709	3.238564	
SGZ	298	0.003356	0.251956	-1.3785	
	308	0.003247	0.228086	-1.47803	0.940
	318	0.003145	0.222868	-1.50118	
	328	0.003049	0.21157	-1.5532	
GO	298	0.003356	0.600384	-0.51019	
	308	0.003247	0.536807	-0.62212	0.978
	318	0.003145	0.484726	-0.72417	
	328	0.003049	0.46279	-0.77048	
GOZ	298	0.003356	0.748328	-0.28991	
	308	0.003247	0.872046	-0.13691	0.887
	318	0.003145	0.867414	-0.14224	
	328	0.003049	0.983635	-0.0165	
sGO	298	0.003356	1.359882	0.307398	
	308	0.003247	1.179124	0.164772	0.972
	318	0.003145	1.085941	0.082447	
	328	0.003049	1.021325	0.021101	

Table 5.20 : The results of equilibrium constant to adsorb of Congo red dye (50 mg/l) under different temperature

Adsorbent	T ^{0}K	1/T	K Equilibrium constant	lnK	R^2
ACZ	298	0.003356	20.54244	3.022493	
	308	0.003247	38.87241	3.660285	0.977
	318	0.003145	59.97561	4.093938	
	328	0.003049	143.5087	4.966395	
SGZ	298	0.003356	3.833837	1.343866	
	308	0.003247	3.651163	1.295046	0.826
	318	0.003145	3.46628	1.243082	
	328	0.003049	3.511617	1.256077	

Adsorbent	T °K	1/T	K Equilibrium constant	lnK	R²
GO	298	0.003356	601.4096	6.399276	0.996
	308	0.003247	960.5385	6.867494	
	318	0.003145	1611.903	7.385171	
	328	0.003049	2271.727	7.728296	
GOZ	298	0.003356	71.56894	4.270661	0.804
	308	0.003247	514.4639	6.243125	
	318	0.003145	942.3962	6.848426	
	328	0.003049	960.5385	6.867494	
sGO	298	0.003356	3.343105	1.2069	0.934
	308	0.003247	5.442261	1.694195	
	318	0.003145	9.775862	2.279916	
	328	0.003049	10.33466	2.335503	
sFe	298	0.003356	3.796163	1.333991	0.971
	308	0.003247	4.610098	1.528249	
	318	0.003145	5.107803	1.630769	
	328	0.003049	5.571382	1.717643	

Table 5.21 : The results of equilibrium constant to adsorb of Basic Brown dye (50 mg/l) under different temperature

Adsorbent	T °K	1/T	K Equilibrium constant	lnK	R²
ACZ	298	0.003356	48.45598	3.880656	0.880
	308	0.003247	53.64481	3.982385	
	318	0.003145	71.04611	4.263329	
	328	0.003049	125.9036	4.835516	
SGZ	298	0.003356	34.61888	3.544399	0.970
	308	0.003247	29.60444	3.387924	
	318	0.003145	21.52252	3.0691	
	328	0.003049	19.1005	2.949715	
GO	298	0.003356	27.57143	3.31678	0.880
	308	0.003247	34.31073	3.535458	
	318	0.003145	69.62147	4.243073	
	328	0.003049	68.93007	4.233093	
GOZ	298	0.003356	18.34236	2.909213	0.972
	308	0.003247	22.69668	3.122219	
	318	0.003145	26.26281	3.268154	
	328	0.003049	28.55083	3.351686	
sGO	298	0.003356	10.35074	2.337058	0.777
	308	0.003247	19.63983	2.97756	
	318	0.003145	22.61275	3.118514	
	328	0.003049	22.98082	3.13466	
sFe	298	0.003356	15.40016	2.734378	0.921
	308	0.003247	14.96169	2.705493	
	318	0.003145	14.5159	2.675245	
	328	0.003049	14.49187	2.673588	

Table 5.22 : The results of equilibrium constant to adsorb of Rhodamune B dye (50 mg/l) under different temperature

Adsorbent	T ^{o}K	1/T	K Equilibrium constant	lnK	R^2
ACZ	298	0.003356	121.2494	4.797849	0.833
	308	0.003247	73.8503	4.30204	
	318	0.003145	53.64481	3.982385	
	328	0.003049	56.73672	4.038422	
GO	298	0.003356	3.866772	1.35242	0.914
	308	0.003247	5.858711	1.76793	
	318	0.003145	8.304489	2.116796	
	328	0.003049	8.505703	2.140737	
GOZ	298	0.003356	43.84305	3.780616	0.925
	308	0.003247	46.16981	3.832326	
	318	0.003145	50.41388	3.920267	
	328	0.003049	59.33183	4.083146	

Table 5.23 : The results of equilibrium constant to adsorb of Mercury ions (5000 μg/l) under different temperature

Adsorbent	T ^{o}K	1/T	K Equilibrium constant	lnK	R^2
ACZ	298	0.003356	63.69418	4.154093	0.921
	308	0.003247	80.00341	4.382069	
	318	0.003145	116.3642	4.756725	
	328	0.003049	242.4684	5.490871	
SGZ	298	0.003356	3.212552	1.167066	0.962
	308	0.003247	3.908997	1.363281	
	318	0.003145	5.384254	1.683479	
	328	0.003049	8.316903	2.11829	
GO	298	0.003356	1.288116	0.253181	0.954
	308	0.003247	1.74017	0.553983	
	318	0.003145	1.908952	0.646554	
	328	0.003049	2.734455	1.005932	
GOZ	298	0.003356	7.751456	2.047881	0.991
	308	0.003247	8.44786	2.133913	
	318	0.003145	9.310909	2.231187	
	328	0.003049	10.45146	2.346741	
sGO	298	0.003356	2.108366	0.745913	0.969
	308	0.003247	2.298664	0.832328	
	318	0.003145	2.8689	1.053929	
	328	0.003049	3.350618	1.209145	

	298	0.003356	3.89799	1.360461	
sFe	308	0.003247	3.197737	1.162443	**0.954**
	318	0.003145	2.564653	0.941823	
	328	0.003049	2.448723	0.895567	

Table 5.24 : The results of equilibrium constant to adsorb of lead ions

(4 mg/l) under different temperature

Adsorbent	T ⁰K	1/T	K Equilibrium constant	lnK	R^2
ACZ	298	0.003356	4.801904	1.56901	**0.881**
	308	0.003247	4.838687	1.57664	
	318	0.003145	24.44076	3.19625	
	328	0.003049	46.58094	3.84119	
SGZ	298	0.003356	2.537315	0.93110	**0.940**
	308	0.003247	2.706672	0.99572	
	318	0.003145	2.86879	1.05389	
	328	0.003049	3.298838	1.19357	
GO	298	0.003356	38.73442	3.65672	**0.926**
	308	0.003247	25.58307	3.24193	
	318	0.003145	22.56055	3.11620	
	328	0.003049	19.51634	2.97125	
GOZ	298	0.003356	21.70849	3.07770	**0.965**
	308	0.003247	24.17801	3.18544	
	318	0.003145	25.27964	3.23000	
	328	0.003049	26.6471	3.28268	
sGO	298	0.003356	1.623141	0.48436	**0.986**
	308	0.003247	2.196036	0.78665	
	318	0.003145	3.050728	1.11538	
	328	0.003049	4.729711	1.55386	
sFe	298	0.003356	9.420669	2.24290	**0.925**
	308	0.003247	8.444622	2.13353	
	318	0.003145	4.212956	1.43816	
	328	0.003049	3.184048	1.158153	

The change of enthalpy H and the change of entropy S can be calculated graphically when it is plotted between ln K values versus 1/T (Figures 5.37 and 5.38) by utilizing the following relations [35, 51,76, 194] :

$$G^o = \ H - T \ S$$

$$Ln \ K = (\ S/R) - (\ H / RT)$$
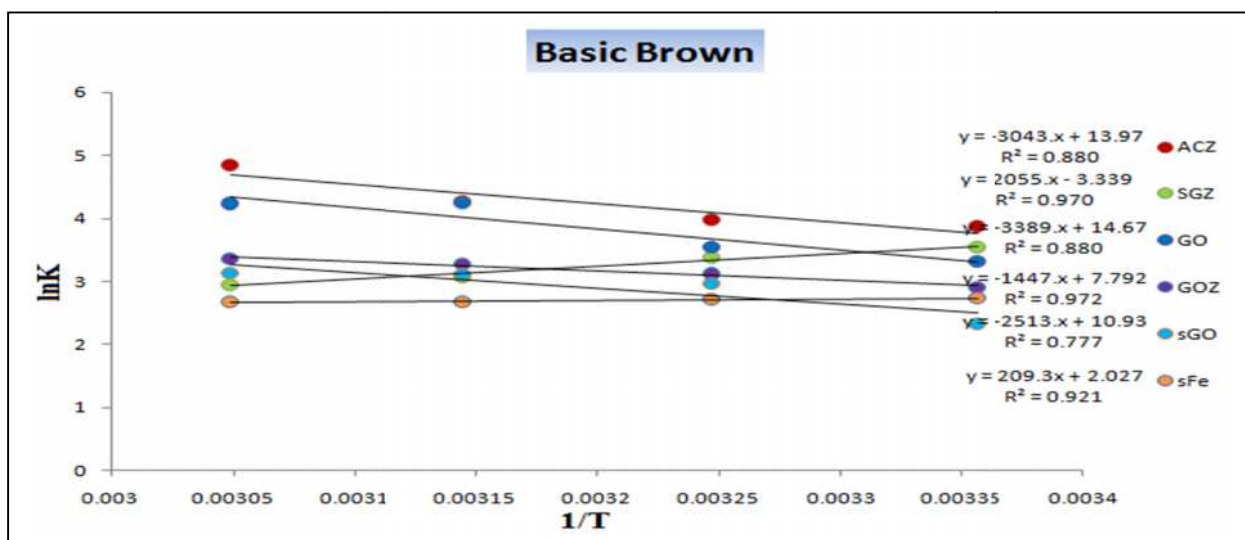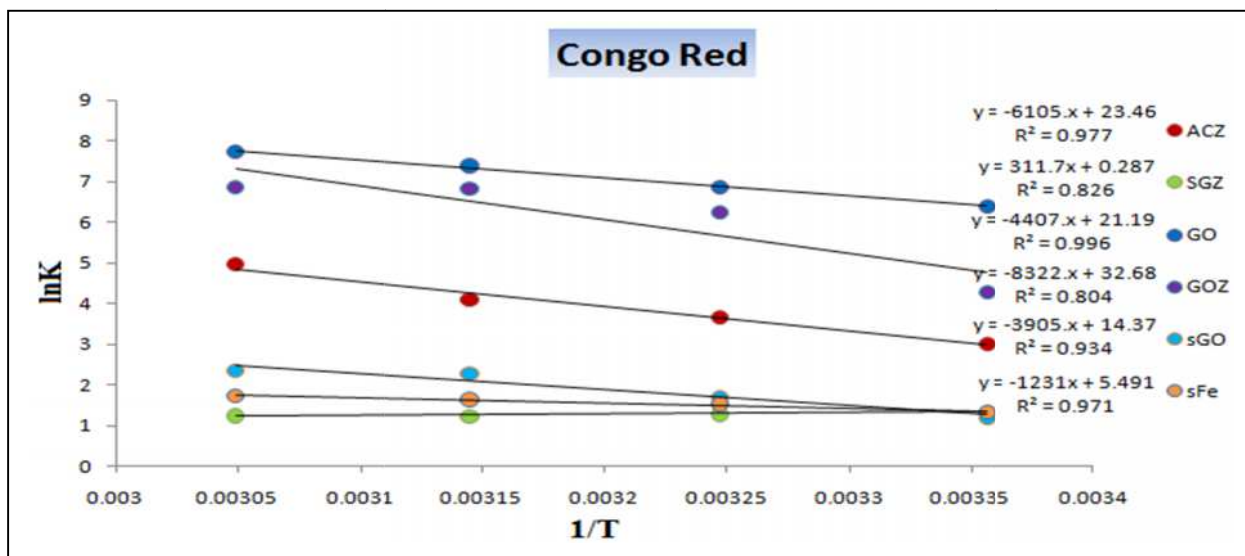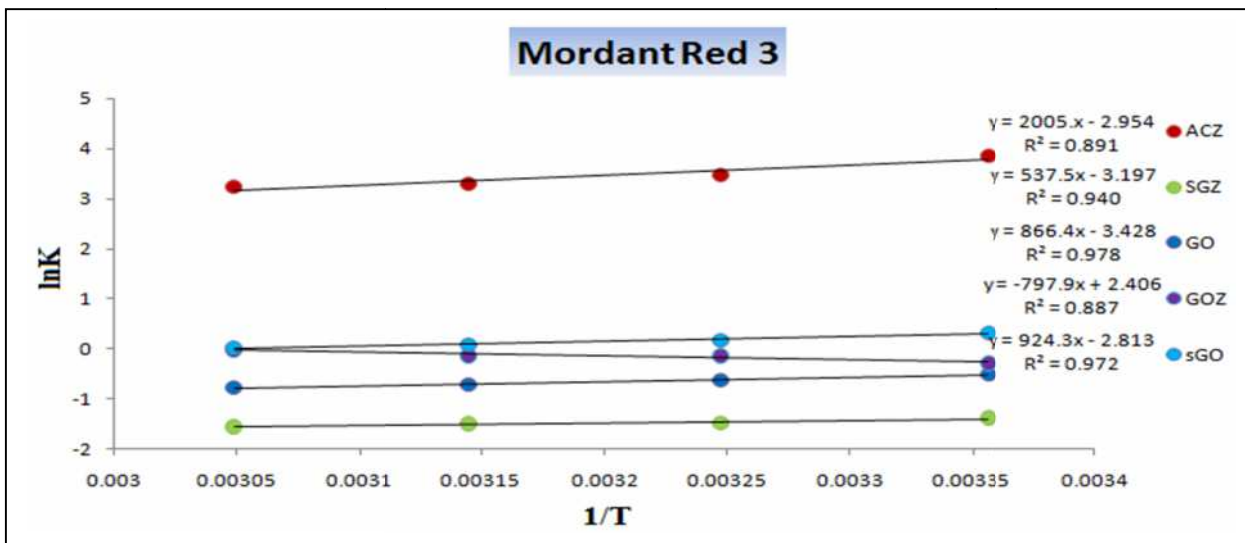
Figure 5.37 : Plot of lnK versus 1/T of Mordant red 3 ,Congo Red and Basic Brown dyes
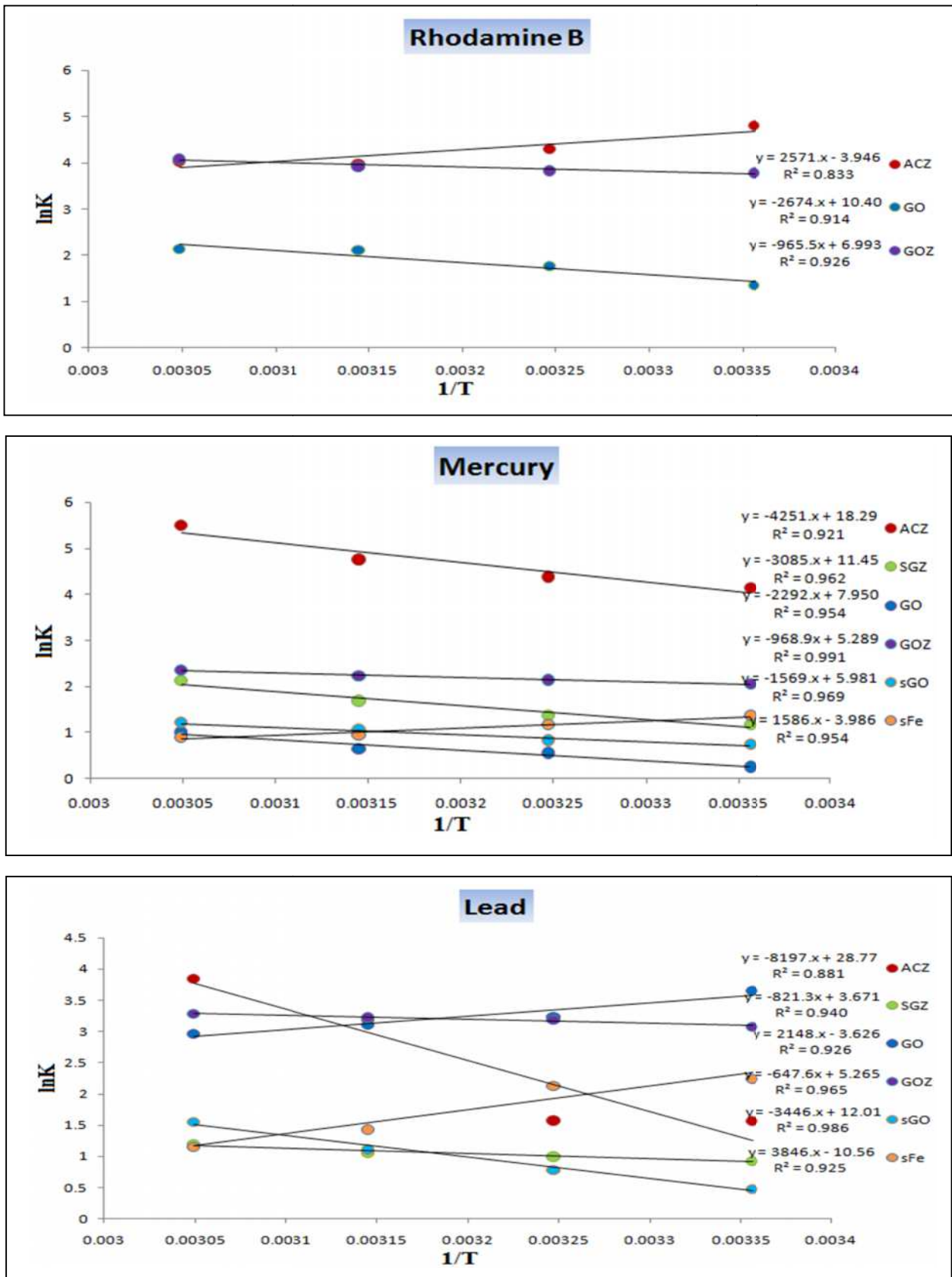
Figure 5.38 : Plot of lnK versus 1/T of Rhodamine B dye , Mercury and Lead ions

The H° (KJ.mol^{-1}) data were extracted from the slope while , the change of standard entropy (KJ.mol^{-1}.K^{-1}) can be calculated from the intercept . The positive H° value indicated the adsorption process is endothermic whilst , the negative value is pointiong to exothermic process , the adsorption nature can describe the physical or chemical adsorption using the H° values, the range of the change of enthalpy between -4 to -40 KJ/mol refers to the physical adsorption , compared to the occurrence of the chemosorption process when the range is located between -40 to -800 KJ/mol [76] . The negative value of S° is pointing to the decrease affinity of adsorbent surface towards the adsorbate molecules while , the positive value refers to the increase in the randomness of adsorbate molecules of the solid - liquid system in order to bind with adsorbent surface [74].

The adsorption process of Mordant Red 3 dye onto all adsorbents surface were appeared the exothermic process by observing the H° values , except their adsorbed on GOZ adsorbent where was an endothermic process , the adsorption reaction between Mordant Red 3 molecules with all adsorbents surface are nonspontaneous except their interacted with ACZ and sGO adsorbents which were a spontaneous reaction moreover , all the adsorbents surface were recorded negative values of S° that refer to decline in the affinity of all adsorbents towards the molecules of Mordant Red 3 dye except for the GOZ adsorbent which increased the affinity towards the dye molecules .

The G° values revealed the negative value when it adsorbed Congo Red dye on all adsorbents surfaces which indicate that the adsorption reaction of Congo Red dye is spontaneous thermodynamically, when the increase of negative value for the G° value with increases of temperature that suggested the adsorption process tended towards more spontaneous at a higher temperature [72]. All the adsorbents adsorbed the dye of Congo Red from their aqueous solution by the endothermic

reaction except for the SGZ adsorbent that can be interacted with dye molecules through the exothermic reaction . In addition , all the adsorbents surfaces show more affinity towards the interaction with Congo Red molecules .

The Basic Brown dye is adsorbed onto all adsorbents surfaces through the spontaneous reaction according to the G° values, while the adsorption reaction was exhibted the endothermic for interacting between Basic Brown dye with all adsorbents surfaces for except the SGZ and sFe adsorbents which were exothermic reaction . All the adsorbents recorded a positive value of the entropy S° when the dye solution was adsorbed except for the SGZ adsorbent which recorded the negative value .

The ACZ adsorbent appeared the exothermic reaction when it adsorbed the solution of Rhodamine B dye while , the GO and GOZ adsorbents have recorded the positive value of the change of enthalpy . All the adsorbents showed a negative value for the change of free energy that referred to the adsorption reaction is spontaneuos and the adsorption nature is physical adsorption . Finally , the ACZ adsorbent recorded the negative value of the S° while , the GO and GOZ adsorbents recorded positive values .

All the adsorbents surfaces were appeared the physisorption and the spontaneous reaction towards the adsorption of the mercury ions from their aqueous solution. Moreover , the adsorption reactions tended to be more spontaneous with the increases of temperature by monitoring the G° values , the positive values were recorded to the H° function for the range 8.05 -35.35 KJ/mol that referred to the endothermic adsorption reactions on all adsorbents surfaces except for the sFe adsorbent which showed the exothermic reaction . The positive values of entropy function denote to the solid – liquid system that suffers more randomness and affinity to adsorb the mercury ions onto all adsorbents surfaces

while , the negative value that was recorded by sFe adsorbent indicates the decline of the affinity towards the adsorption of mercury ions from its solution which leads to the decrease of the adsorption efficiency .

The lead ions are adsorbed spontaneously onto all adsorbents surfaces , the physical adsorption occurs when the values of G^o were located between -20 to 0 KJ/mol [74] where , all adsorbents surfaces recorded the negative values of the G^o for the range -1.2 to -10.4 KJ/mol under four different temperatures (298 , 308 ,318 and 328 °K) . All the adsorbents surfaces gave the endothermic reaction to the adsorption process except for GO and sFe adsorbents, that recorded the exothermic reaction . The increase of the randomness in lead ions solution that was adsorbed on all the adsorbents materials can lead to increase the interaction between the lead ions in the solution with the adsorbents surfaces that reflected positively on the efficiency of the adsorption process but the negative value of the S^o was recorded by the GO and sFe adsorbents . The data of thermodynamic functions are depicted in Table 5.25 .

Table 5.25 : The results of thermodynamic parameters

of adsorption process

Adsorbent	Adsorbate	H	S	G KJ/mol			
		KJ/mol	KJ/mol/K	298 ⁰K	308 ⁰K	318 ⁰K	328 ⁰K
ACZ	Mordant Red 3	-16.675	-0.024	-9.5552	-8.8697	-8.6903	-8.8315
SGZ		-4.469	-0.026	3.41533	3.78481	3.96889	4.23555
GO		-7.204	-0.028	1.2640	1.5930	1.9146	2.1010
GOZ		6.633	0.020	0.71828	0.35059	0.37606	0.04499
sGO		-7.686	-0.023	-0.7616	-0.4219	-0.2179	-0.0575
ACZ	Congo Red	50.765	0.195	-7.4884	-9.3729	-10.823	-13.543
SGZ		-2.592	0.002	-3.3295	-3.3162	-3.2865	-3.4253
GO		36.648	0.176	-15.854	-17.585	-19.525	-21.075

GOZ		69.204	0.271	-10.580	-15.986	-18.106	-18.727
sGO		32.475	0.119	-2.9901	-4.3383	-6.0277	-6.3689
sFe		10.236	0.045	-3.3050	-3.9134	-4.3115	-4.684
ACZ	**Basic Brown**	25.302	0.116	-9.6146	-10.197	-11.271	-13.186
SGZ		-17.095	-0.027	-8.7815	-8.6755	-8.1142	-8.0438
GO		28.184	0.122	-8.2175	-9.0532	-11.218	-11.543
GOZ		12.033	0.064	-7.2077	-7.9951	-8.6405	-9.1400
sGO		20.903	0.090	-5.7902	-7.6246	-8.2448	-8.5481
sFe		-1.740	0.016	-6.7746	-6.9279	-7.0729	-7.2908
ACZ	**Rhodamine B**	-21.384	-0.032	-11.887	-11.016	-10.528	-11.012
GO		22.242	0.086	-3.3507	-4.5271	-5.5965	-5.8377
GOZ		8.027	0.058	-9.3667	-9.8134	-10.364	-11.134
ACZ	**Mercury**	35.350	0.152	-10.292	-11.221	-12.576	-14.973
SGZ		25.652	0.095	-2.8914	-3.4909	-4.4508	-5.7765
GO		19.064	0.066	-0.6272	-1.4185	-1.7093	-2.7431
GOZ		8.056	0.043	-5.0737	-5.4643	-5.8989	-6.3995
sGO		13.049	0.049	-1.8480	-2.1313	-2.7864	-3.2973
sFe		-13.196	-0.033	-3.3706	-2.9766	-2.4900	-2.4422
ACZ	**Lead**	68.17	0.239	-3.8873	-4.0373	-8.4504	-10.474
SGZ		6.628	0.030	-2.3068	-2.5497	-2.7863	-3.2548
GO		-17.863	-0.030	-9.0598	-8.3016	-8.2387	-8.1025
GOZ		5.384	0.043	-7.6252	-8.157	-8.5396	-8.9518
sGO		28.657	0.099	-1.2000	-2.0143	-2.9489	-4.2373
sFe		-31.983	-0.087	-5.5569	-5.4633	-3.8022	-3.1582

5.2. Desorption study

5.2.1. The effect of solvents

The regeneration process was studied in the current work by utilizing three solvents that are different in polarity, such as distilled water , methanol and ethanol for 24h under continuous shaking in order to recover the dyes. Heavy metals can be

recovered from the adsorbent surface after their adsorbed using different concentrations of HCl at (0.5 , 1 and 2N) . The results of the desorption process revealed a good solvent used to recover all dyes after they have been adsorbed onto all adsorbent surfaces it is methanol solvent, which was attributed to its ability to penetrate into the adsorbent molecules that leads to increase the release of dye molecules towards the liquid phase [69]. On the other hand, the best concentration of HCl that was used to recover of the adsorbed mercury ions onto all adsorbent surfaces was 0.5 N except for the SGZ , sGO and sFe adsorbents that used 2N of HCl . The desorption process of lead ions on all adsorbents is favorited to use a low concentration (0.5N) of HCl except for the sGO and SGZ adsorbents, which prefer concentrations of 1 and 2N, respectively . Figures 5.39 and 5.40 show the results of the desorption experiment after 24 hours.
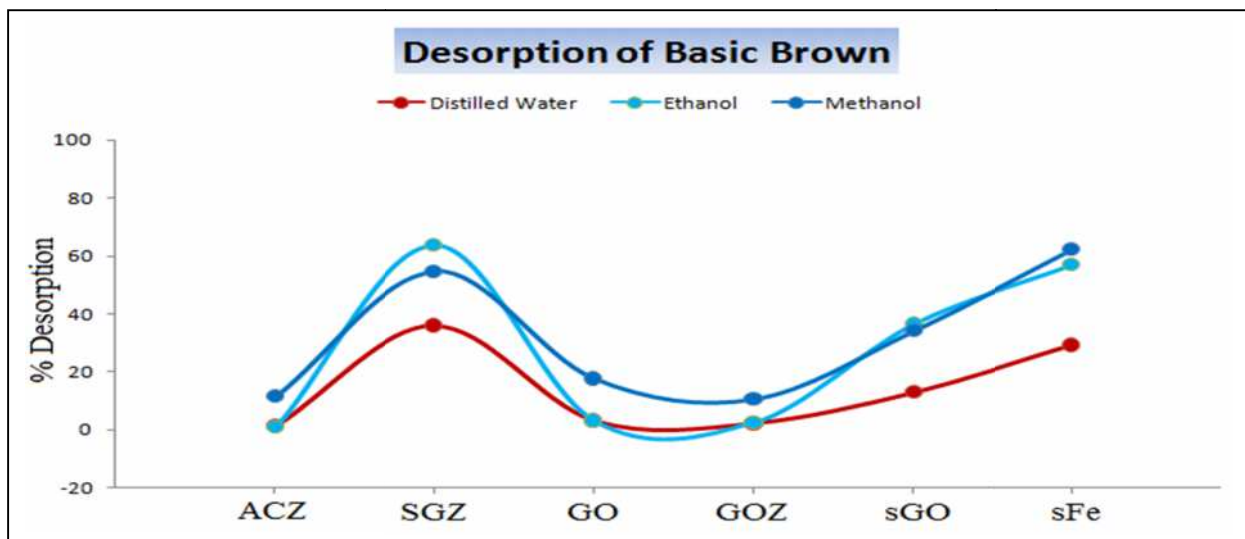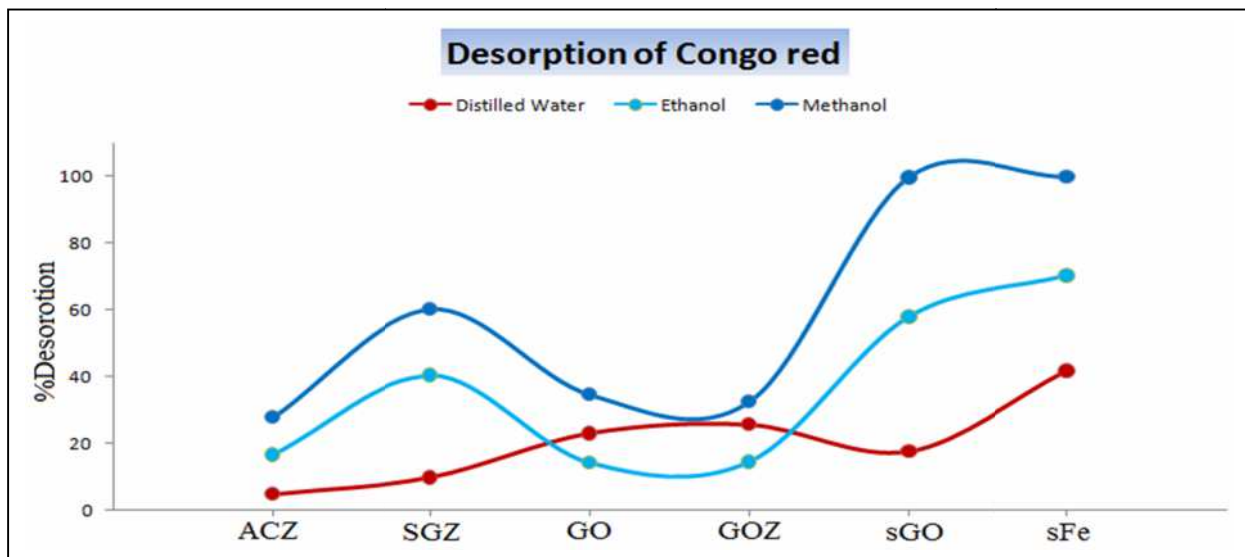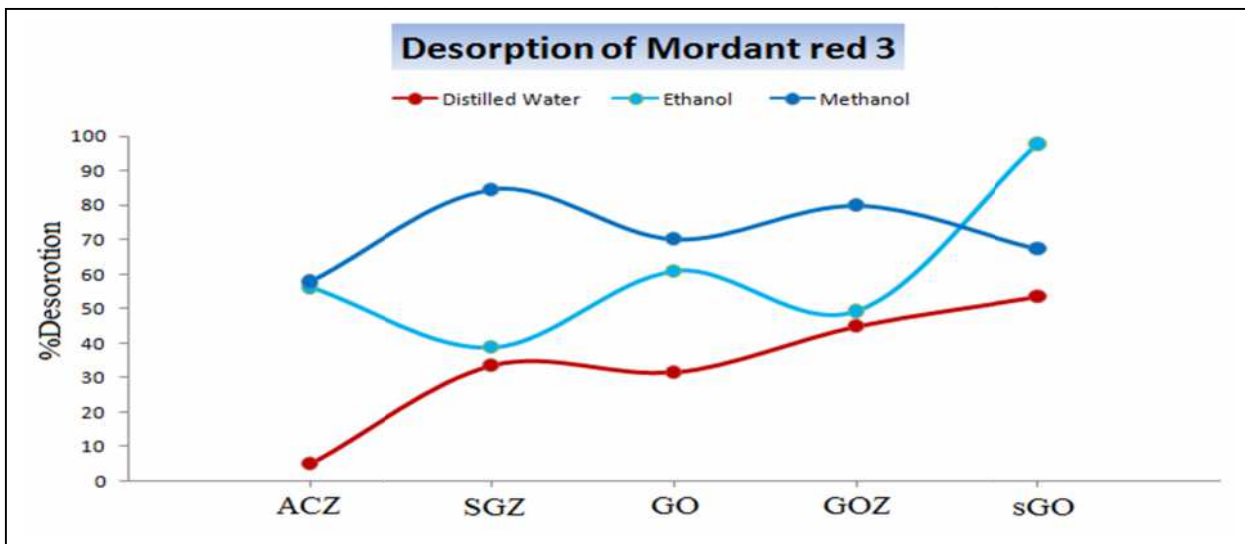
Figure 5.39 :The desorption experiment ofMordant Red 3,Congo Red and Basic Brown dyes
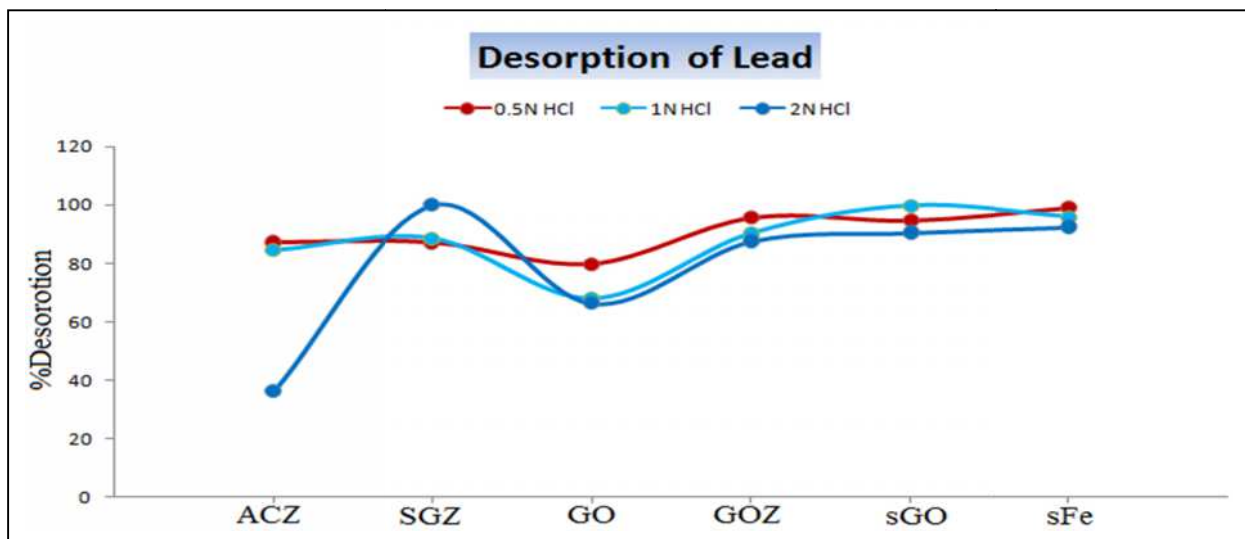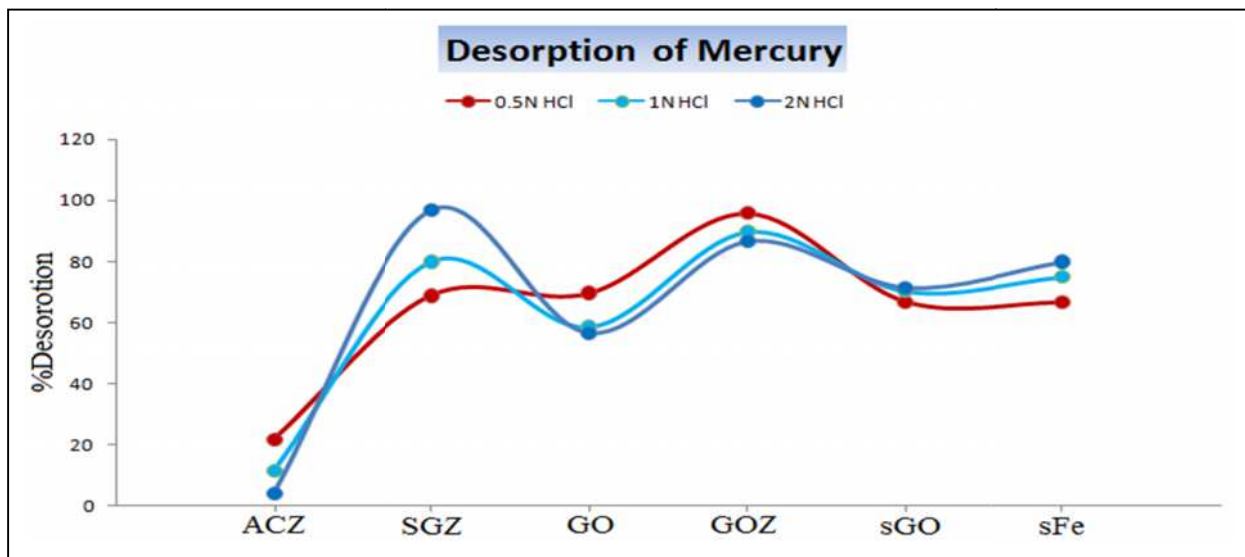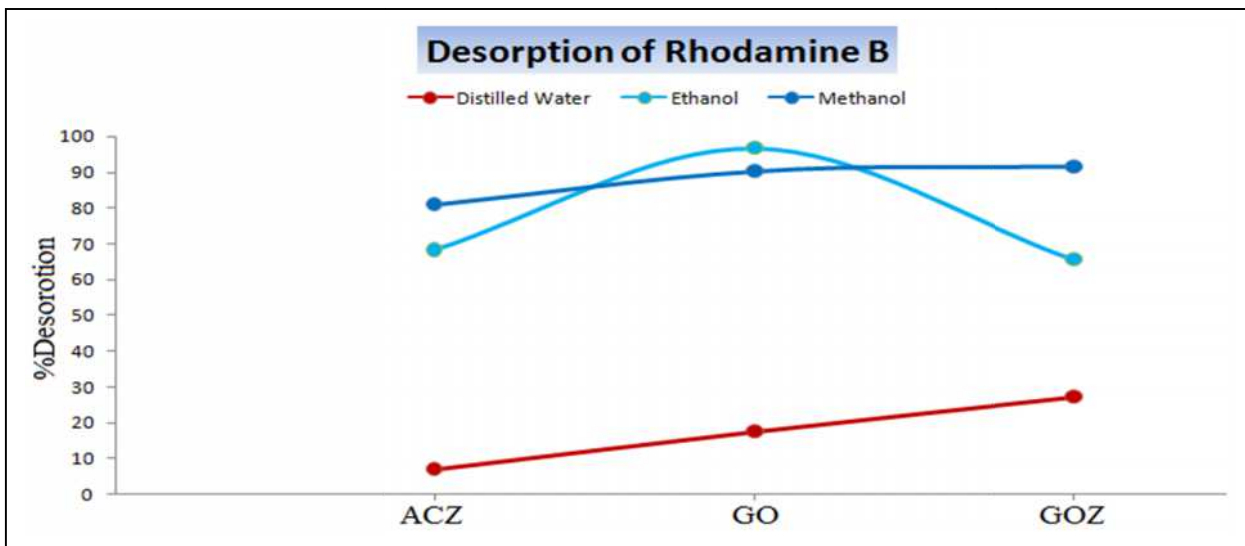
Figure 5.40 : The desorption experiment of Rhodamine B dye , Mercury and Lead ions

5.2.2. The effects of Time

The effect of time on the desorption process was studied by utilizing a period of time for 10 , 30 and 60 mins to recover the dyes molecules after its binding onto adsorbent surface while , the recovery of the heavy metals used different periods of time for 5 , 15 , 30 and 60 mins . The special solvent was used to regenerate all adsorbents after they released the adsorbate molecules towards liquid phase where , a methanolic solution is more appropriate than the other solvents such as the distilled water and ethanol absolute in order to recover the dyes molecules after their adsorbed onto all of the adsorbents surface .

The maximum desorption efficiency of Mordant Red 3 dye was determined by SGZ adsorbent and then followed by GOZ adsorbent more than the other adsorbents. The increase of dye amount that released towards the liquid phase from adsorbent surface may be attributed to the weak binding between the dye molecules with the adsorbent surface that was more allowed to penetrate into adsorbent material by solvent molecules [56] . On the other hand, the ACZ adsorbent was recorded the lowest percent than the other adsorbents to recover the Mordant Red 3 dye this may be attributed to the strong binding found between them which shows that the adsorption reaction of dye molecules onto the adsorbent surface is irreversible type [169,195] . The percent recovery of the Mordant Red 3 dye on all adsorbents surfaces was obeyed to order in the following :   SGZ > GOZ > GO> sGO > ACZ .

The best adsorbents to the release of Congo Red as anionic dye towards the liquid phase after their adsorbed were recorded from the adsorbent that separated from soot waste as it was mentioned previously (sGO and sFe), because the change of adsorbent charge after using methanol as a recovery solvent leads to increase the repulsion between the functional groups on the adsorbent surface such as hydroxyl and carboxylic group with the anionic dye this outcome may be attributed to the

weak electrostatic attraction [69 ,196] between the adsorbate with the adsorbent, so, it was observed the increase of dye recovery ratio from the adsorbents solid material . The recovery percentage of congo red dye from all adsorbents was arranged according to the highest recovery as follows : sGO > sFe > SGZ > GO > GOZ > ACZ .

Methyl alcohol is a good solvent when it is compared with the other solvents as water and ethyl alcohol in order to recover the Basic Brown dye from all adsorbents surface at a room temperature. So, it was observed that the ability of adsorbent surface to release the dye molecules towards the methanolic solution are arranging as follows : sFe > SGZ > sGO > GO > ACZ > GOZ . The structural formula of adsorbent plays an important role in the increase of the adsorption and desorption efficiency [195]. The desorption efficiency increases with the changes of the charge of adsorbent surface and also it weakens the binding between the molecules of adsorbate and adsorbent surface that basically depend on the structural formula in both the adsorbent and the adsorbate .

The maximum level to recover the Rhodamine B dye from the three adsorbents surface (ACZ , GO and GOZ) has been determined ,where the percentage was 91.54% by modifying the graphene oxide with selenazone ligand, may attributed to the weak electrostatic attraction and also , to the increase in the repulsion between the adsorbed molecules of dye with adsorbent surface when the change of pH value of adsorbent surface . The recovery percent of Rhodamine B dye from all adsorbents surface were arranged by the following : GOZ > GO > ACZ .

The desorption process of heavy metals after applied the optimum conditions for their adsorption on the adsorbent surface was studied and examined under three concentrations of HCl at 0.5 , 1 and 2N for 24 hours and then the optimal concentration was applied for different periods of time 5, 15, 30 and 60 minute. The best recovery percent of mercury ions after its adsorbed on the adsorbents

surface where was 96.92 and 95.90 % by adsorbents the silica gel and graphene oxide after their modified with selenazone ligand, the lowest recovery percent was recorded in ACZ adsorbents because the strong binds found between the cationic ions of mercury with ACZ adsorbent as well as , may be attributed to micropores structural [195] for ACZ adsorbent . Besides, all the adsorbents surfaces (ACZ, SGZ, GO, GOZ, sGO and sFe) recorded a good and high recovery percent for the lead ions where they were 87.16 , 99.89 , 79.66 , 95.54 , 99.76 and 98.91 respectively , this may be basically attributed to the weak electrostatic attractions between lead ions with adsorbents surfaces. The results of all desorption experiment are listed in Table 5.26 and 5 .27 and Figures 5.41 and 5.42 .

Table 5.26 : The results of desorption experiment of dyes

under different periods time at 50 mg/l

Adsorbent	Adsorbate	A_o mg/l	10 min		30 min		60 min		24h	
			A_o-A_r mg/l	% De	A_o-A_r mg/l	% De	A_o-A_r mg/l	% De	A_o-A_r mg/l	% De
ACZ	Mordant Red 3	46.846	22.784	48.6	23.539	50	26.762	57.1	27.039	57.7
SGZ		18.451	9.214	49.9	12.562	68	15.584	84.4	15.609	84.5
GO		30.379	14.375	47.3	18.202	59	21.727	71.5	21.349	70.2
GOZ		29.379	18.454	62.8	21.148	71	23.338	79.4	23.464	79.8
sGO		18.837	7.6283	40.4	10.221	54.2	12.613	66.9	12.663	67.2
ACZ	Congo Red	48.115	7.3045	15.1	9.8964	20.5	12.409	25.7	13.313	27.6
SGZ		36.44	19.640	53.8	20.047	55.01	21.542	59.1	21.916	60.1
GO		49.89	13.721	27.5	14.412	28.8	17.472	35.02	17.324	34.7
GOZ		41.03	11.793	28.7	11.865	28.9	13.087	31.8	13.375	32.5
sGO		44.60	42.868	96.1	43.596	97.7	44.486	99.7	44.405	99.5
sFe		38.42	24.069	62.6	29.126	75.8	35.588	92.6	37.929	98.7
ACZ	Basic Brown	49.64	1.7580	3.54	3.0534	6.15	5.3666	10.81	5.73675	11.5
SGZ		40.88	19.385	47.4	19.385	47.4	22.090	54.03	22.3610	54.6
GO		49.95	3.2499	6.5	3.8486	7.70	8.5526	17.12	8.8091	17.6
GOZ		49.76	3.7629	7.56	4.5154	9.07	4.6095	9.263	5.2680	10.5
sGO		41.33	13.042	31.5	13.790	33.3	14.704	35.57	14.205	34.3
sFe		40.37	21.795	53.9	22.487	55.7	24.839	61.53	25.185	62.3
ACZ	Rhodamine B	49.665	39.321	79.1	39.765	80.06	40.209	80.960	40.246	81.03
GO		43.34	35.359	81.5	36.425	84.04	39.041	90.081	39.144	90.31
GOZ		46.386	39.969	86.1	40.912	88.19	42.410	91.428	42.466	91.54
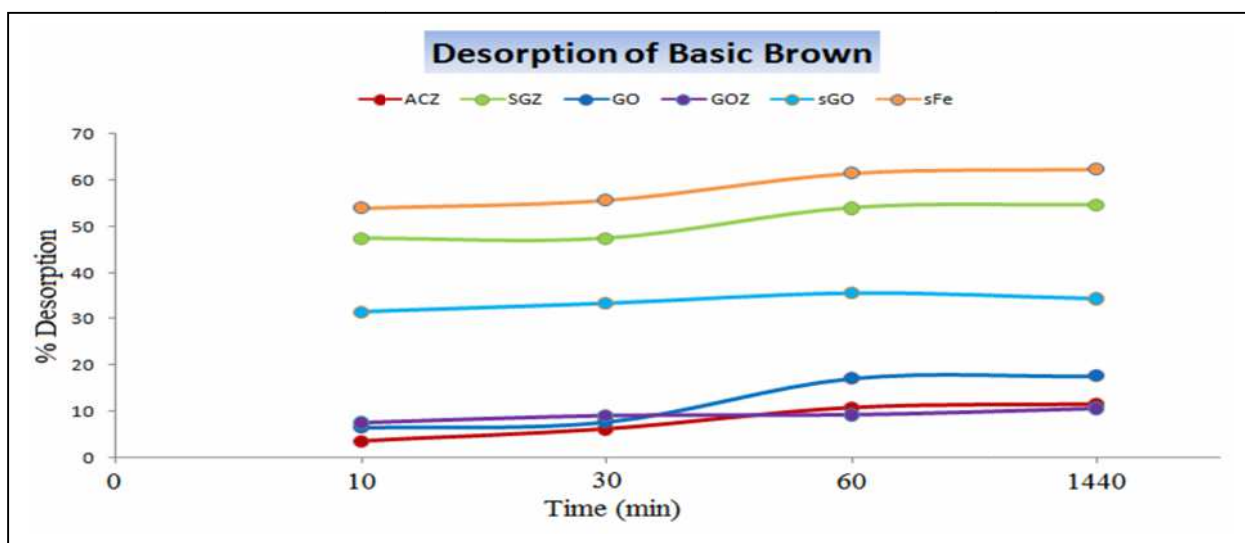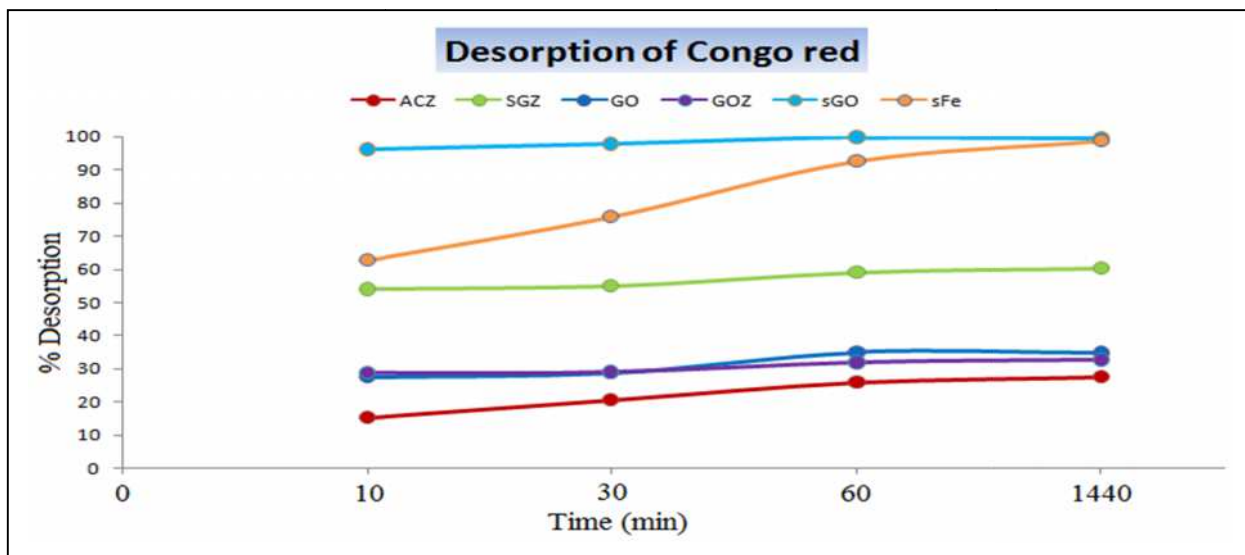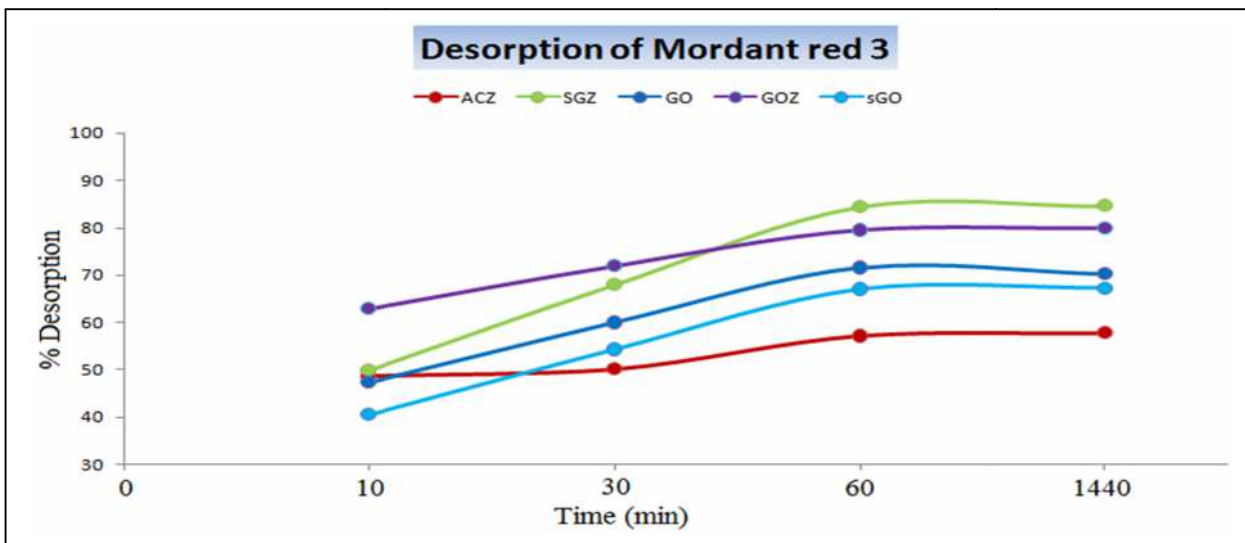
Figure 5.41 : Effect of time on desorption of Mordant Red 3, Congo Red and Basic Brown dyes
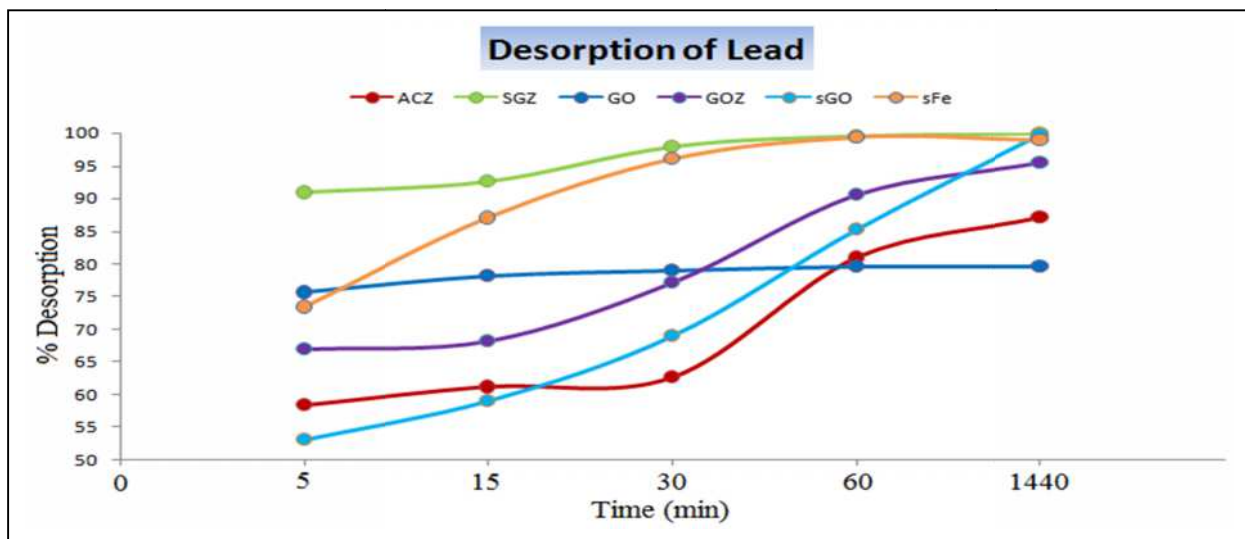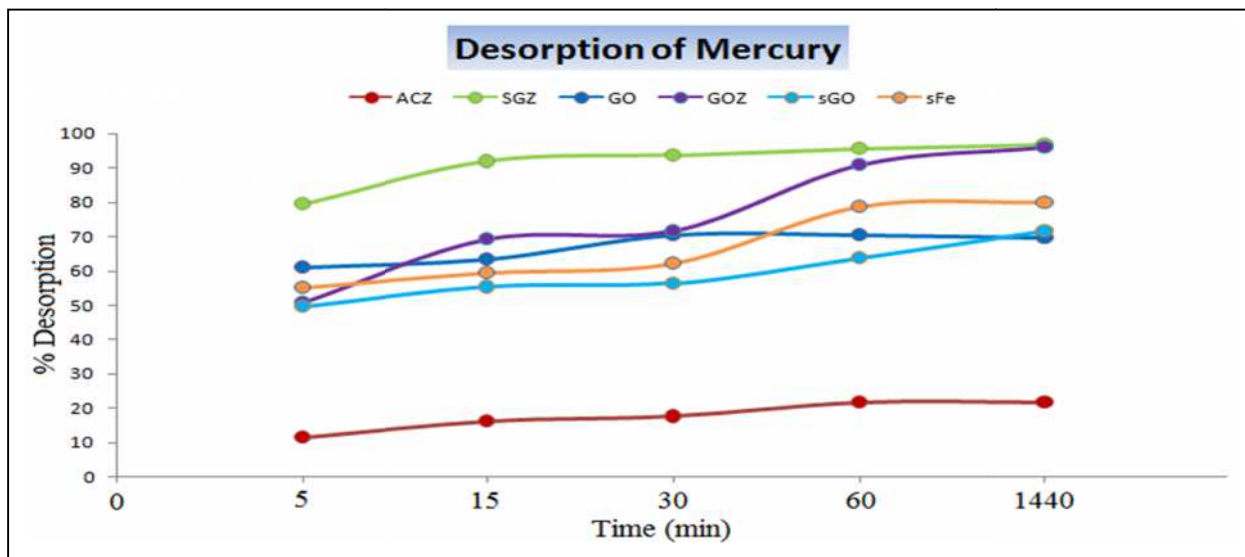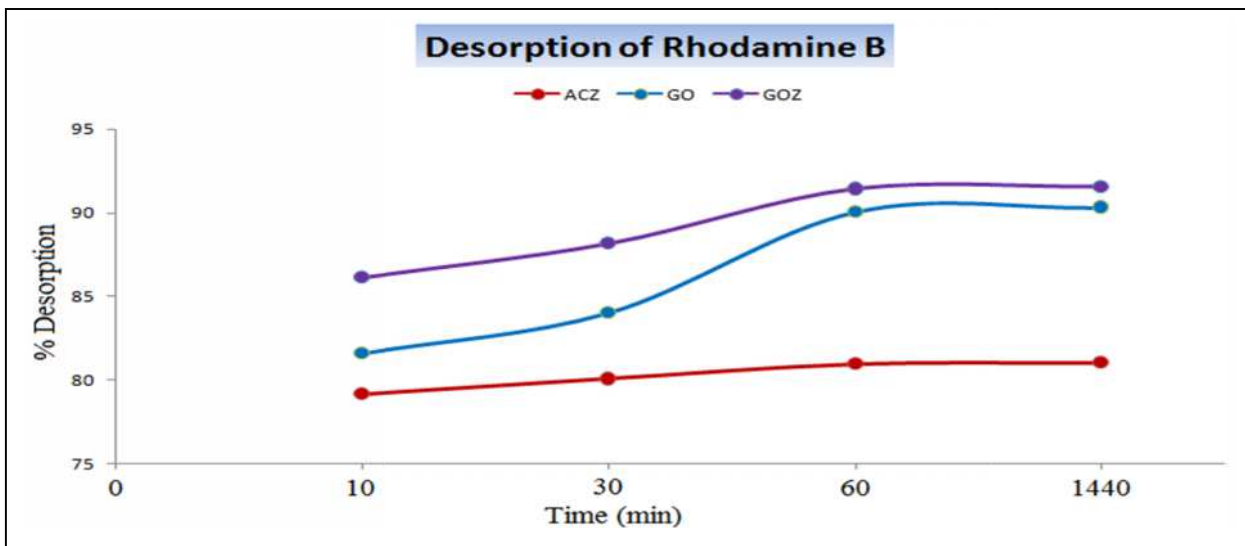
Figure 5.42 : Effect of time on desorption of Rhodamine B dye, Mercury and Lead ions

Table 5.27 : The results of desorption experiment of heavy metals

under different periods time

Adsorbent	Adsorbate	A_o mg/l	15 min		30 min		60 min		24h	
			A_o-A_r mg/l	% De	A_o-A_r mg/l	% De	A_o-A_r mg/l	% De	A_o-A_r mg/l	% De
ACZ	Mercury (2mg/l)	1.9976	0.3250	16.2	0.3524	17.6	0.4352	21.78	0.4362	21.8
SGZ		1.8117	1.6651	91.9	1.6990	93.78	1.7303	95.509	1.7560	96.92
GO		1.1284	0.7168	63.5	0.7945	70.40	0.7945	70.409	0.7864	69.69
GOZ		1.8377	1.2711	69.1	1.3172	71.67	1.6708	90.921	1.7624	95.90
sGO		1.3697	0.7581	55.3	0.7728	56.42	0.8740	63.816	0.9799	71.54
sFe		1.5831	0.9416	59.4	0.9866	62.32	1.2458	78.695	1.2664	80
ACZ	Lead (14mg/l)	10.64	6.5109	61.1	6.6682	62.67	8.6117	80.937	9.2748	87.16
SGZ		3.991	3.6947	92.5	3.9097	97.96	3.9684	99.433	3.9867	99.89
GO		13.42	10.482	78.1	10.603	79.01	10.675	79.551	10.690	79.66
GOZ		13.89	9.4762	68.2	10.713	77.12	12.579	90.568	13.271	95.54
sGO		11.06	6.5336	59.0	7.6262	68.95	9.4423	85.373	11.033	99.76
sFe		13.68	11.908	87.0	13.147	96.10	13.597	99.393	13.531	98.91

Chapter Six

Results and Discussion

Environmental Study

6. Environmental study

   The spills of carcinogenic materials such as the dyes that released into the water environment by increasing the anthropogenic activities can lead to several impacts on the health of organisms and plants in ecosystem . These materials can be accumulated in the tissues of organisms especially the fish and then transported into human via the food chain that caused many risks on the health of human [197,198] . Therefore, the current study focuses on the dyes removal from the water environment by preparing three different types from the polluted water that contain 50 mg/l to each of the dyes type . Where , the dyes solution was prepared for three types of water such as distilled , river and sea waters in order to make the simulation for real polluted water in dyes .

6.1. Collection of real samples and their analysis

   River and sea water samples have been collected in summer season from al-Najebia station that is located on Shatt Al-arab River and the marine region of Iraq which is located the nearby khor Alamaya port by utilizing the water collector insrument at depth 15 cm from the surface water while , the distillation water was obtained by utilizing the distillation process of tap water . Some physico-chemical properties of waters were measured directly in the filed such as acidic function (pH) , electrical conductivity (EC) , salinity and total dissolved solid (TDS) , pH level appears the alkali behavior to distilled and sea waters that was attributed to the existence of high concentration for the sodium carbonate and sodium bicarbonates [2,23] whilst , the pH value of river water recorded the neutral state . The increase of electrical conductivity value indicates the increase of salts concentration in the water samples. Some cations and anions in water samples have been determined and thus showed that the chloride ions are dominate within the anions class while , the sodium , calcium and magnesium ions are dominate within

the cations categories. On other hand, the heavy metals ions did not appear any notable effects like the competition ions to bind with the active sites on the adsorbent surfaces because of their smaller concentration rather than on their concentration of sodium, calcium and magnesium ions. The data of some physico-chemical properties and concentrations of some anions and cations are listed in Table 6.1 .

Table 6.1 : The results of some physico-chemical properties and concentration of some anions and cations in defferent types of water

parameter	Distilled Water	River Water	Sea Water
pH	8.50	7.03	7.81
EC µS/cm	6.8	2590	63900
Salinity g/l	N.D	1.3	43.1
TDS mg/l	4.55	1683.6	38340
SO_4^{-2} mg/l	1.1	265	3032.5
Cl^{-1} mg/l	2.38	719.603	23857.62
CO_3^{-2} mg/l	0.09	1	38.4
HCO_3^{-1} mg/l	0.5	4	68.32
Na^{+1} mg/l	N.D	215	2224
K^{+1} mg/l	N.D	29	370
Ca^{+2} mg/l	0.0417	342.5	2853.75
Mg^{+2} mg/l	N.D	32.5	2808
SiO_2 mg/l	0.605	3.674	1.442
Fe^{+3} mg/l	N.D	0.011	0.0037
Pb^{+2} mg/l	N.D	0.019	0.2020
Cu^{+2} mg/l	N.D	0.0056	0.0006
Ba^{+2} mg/l	N.D	88	751

6.2. Simulation of polluted waters by dyes

A solution containing 50 mg/l of each dye types was prepared in the distilled water and then it was measured using UV-Vis spectrophotometer by scanning the wavelength from 200 to 800 nm , UV-Vis spectrum of dyes mixture was compared with the electronic spectral for four dyes such as Mordant Red 3 , Congo Red , Basic Brown and Rhodamine B (Figure 6.1). Besides, the electronic spectrum of dyes mixture recorded many bands for the range around (260, 422) , (342, 595) , 455 and (351 , 515 and 553) nm that belong to the bands for Mordant Red 3 , Congo Red , Basic Brown and Rhodamine B dyes, respectively.
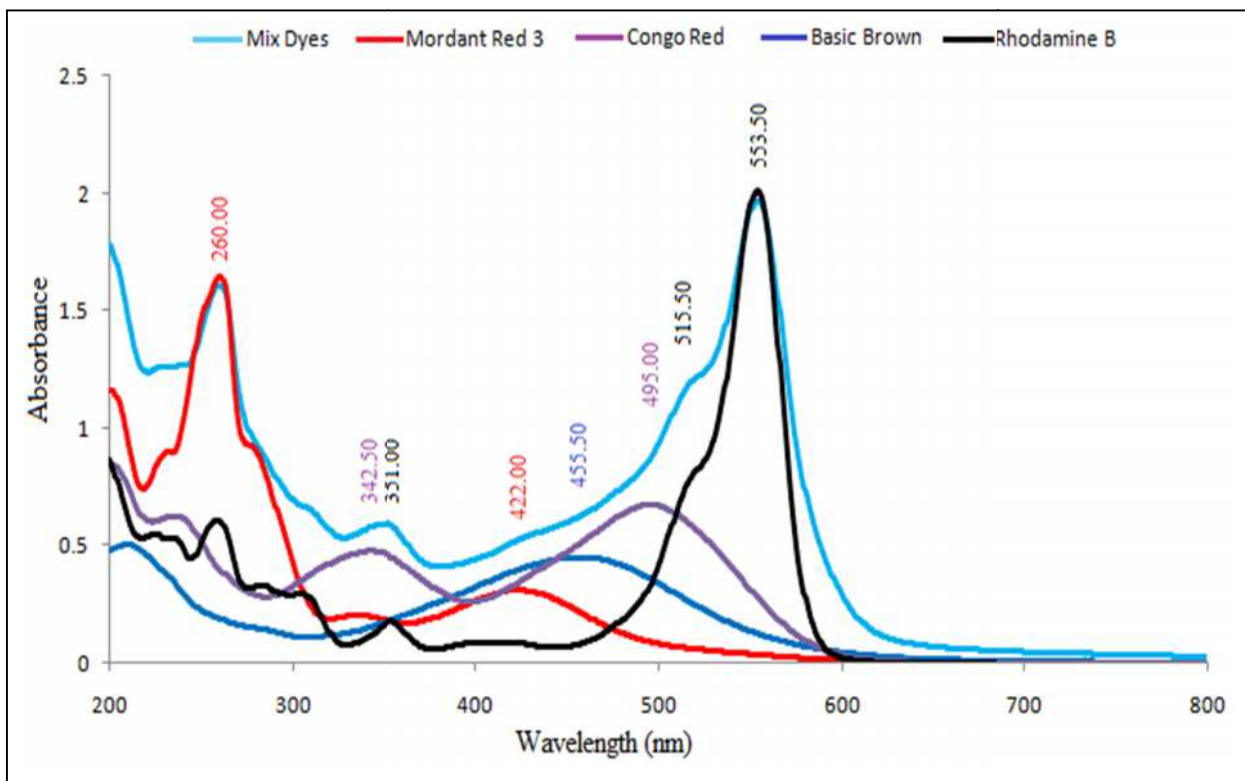
Figure 6. 1 :UV-Vis Spectrum of dyes mixture

The dyes mixture solution was also prepared in river and sea waters in order to keep the same matrix salts in real samples when it is polluted by dyes , the change of bands intensity of dyes mixture was observed in three types of water, this outcome may be attributed to the occurrence of the change in ionic strength among

the mixtures of dyes. The Figure 6.2 showed the preparation of dyes mixture in three types of water .
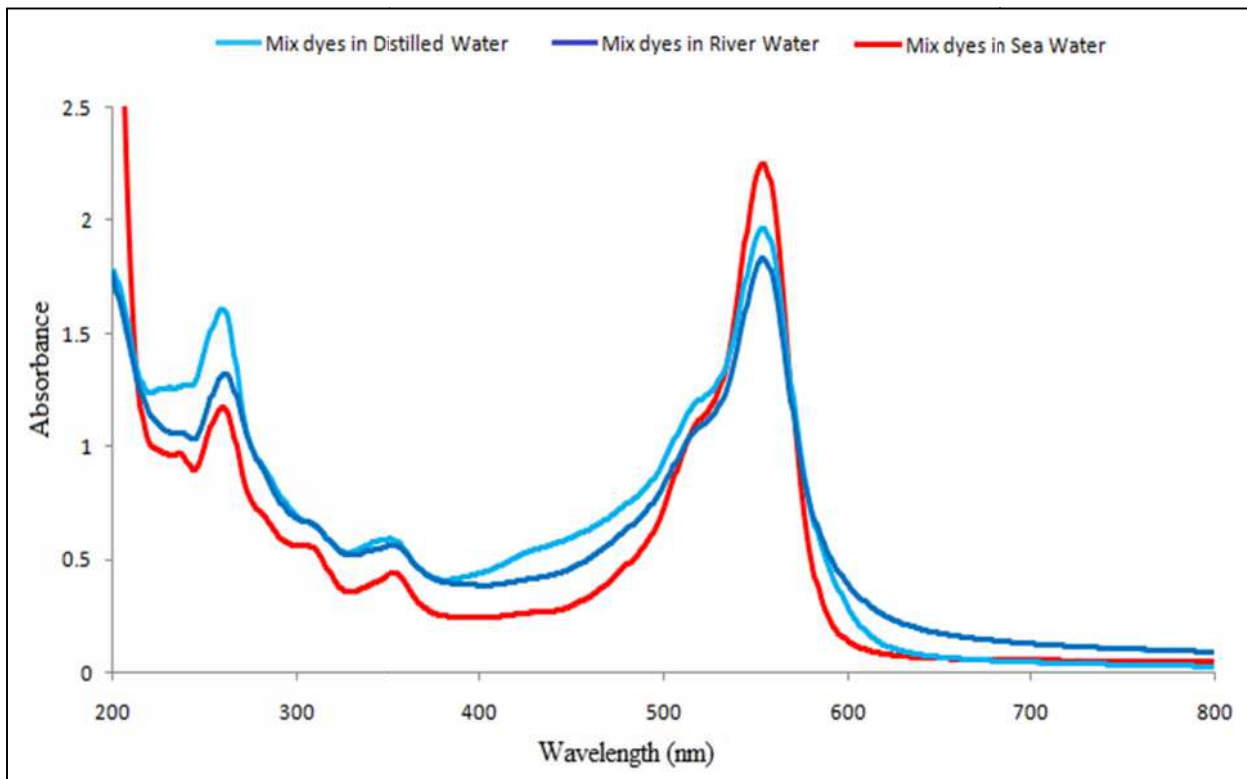
Figure 6. 2 :UV-Vis Spectrum of dyes mixture in three types of water

6.3. Adsorption experiment of dyes mixture

The adsorption experiment was applied on the polluted different type of waters for four dyes (50 mg/l) by utilizing six adsorbent surfaces at a room temperature for 24 hours under natural pH level of each type water .

The maximum value of the removal efficiency for the Mordant Red 3 dye was recorded by percent 70.8 % in distilled water , 73.1% in river water and 78.8% in sea water for sGO and ACZ adsorbents, respectively. The increase of the removal efficiency of Mordant Red 3 dye by using ACZ and SGZ adsorbents with the increases in ionic strength of water was observed, this state may be attributed to the repulsive forces that have been reduced by cations such as Na^+, Ca^{+2} and Mg^{+2}

which neutralized some groups such as the carboxylic, hydroxyl and amine on adsorbents surface [199,200]. On the other hand, The decrease of removal efficiency of Mordant Red 3 dye by utilizing GO , GOZ and sGO adsorbents with the increases in ionic strength of water was also recorded because of the increase of competition to occupy the active sites of adsorbents surface between adsorbate molecules and cations [201,202] .

The adsorption data for Congo Red and Basic Brown dyes from their different aqueous solutions are similar where , the maximum level to adsorb Congo Red and Basic Brown dyes were (80.9 , 84.5 and 81%) and (80.2 , 88.5 and 78%) onto the adsorbents sGO and ACZ in distilled , river and sea waters, respectively. The impact of ionic strength on adsorption process was studied where, it showed that the ability to the adsorption of Congo Red and Basic Brown dyes was increased with the increases in the salts content level on all adsorbents surface except for GO and sGO .

The cationic dye as Rhodamine B was adsorbed onto three adsorbent surfaces such as ACZ , GO and GOZ. The high removal percent was recorded on the adsorbents GO and ACZ at 90.9 , 75.3 and 82 % in distilled , river and sea waters, respectively. While , the effect of salts content on the adsorption process revealed the decreasing ability of adsorbate molecules to bind with the adsorbents surface with increases of salts content that was attributed to the increase of the competition for occupying the vacant active sites onto the adsorbents surface. The results of dyes mixture adsorption are listed in Table 6.2 and Figures 6.3 to 6.6 .

Table 6.2 : The results of Adsorption-desorption experiments of dyes in three types of water

| Adsorbent	Adsorbate (50 mg/l)	Distilled Water				River Water				Sea Water			
		A_o mg/l	A_o-A_r mg/l	% Ad	% De	A_o mg/l	A_o-A_r mg/l	% Ad	% De	A_o mg/l	A_o-A_r mg/l	% Ad	% De
ACZ	Mordant Red 3	31.21	26.43	62.4	84.6	36.5	28.57	73.1	78.0	35.4	24.622	70.8	69.5
SGZ		11.34	11.27	22.6	99.3	21.9	21	43.8	99.7	16.1	16.137	32.3	99.6
GO		31.51	31.29	63	99.3	8.0	8.031	16.1	99.4	12.1	12.059	24.3	99.0
GOZ		17.00	16.84	34	99.0	16.5	16.54	33.0	99.9	12.5	12.487	25.1	99.1
sGO		35.40	35.37	70.8	99.8	13.42	13.41	26.8	98.7	0.85	0.8459	1.70	99.2
ACZ	Congo Red	35.98	35.73	71.9	99.3	42.2	42.13	84.5	99.6	40.5	37.554	81	92.72
SGZ		16.55	16.52	33.1	99.8	28.8	28.75	57.7	99.5	22.2	22.131	44.5	99.27
GO		38.98	38.93	77.9	99.8	24.3	24.20	48.6	99.4	23.7	23.000	47.4	99.44
GOZ		26.41	26.33	52.8	99.6	30.4	30.21	60.9	99.2	26	25.705	52	98.86
sGO		40.48	40.12	80.9	99.1	19.6	19.43	39.3	98.8	16.8	16.771	33.6	99.68
sFe		8.765	8.652	17.5	98.7	25.5	25.32	51.1	99.0	17	16.708	34	98.28
ACZ	Basic Brown	33.34	11.30	66.6	33.8	44.2	14.16	88.5	31.9	39.0	9.0104	78.0	23.08
SGZ		15.39	15.39	30.7	99.9	35.7	35.31	71.5	98.7	31.8	31.666	63.7	99.41
GO		32.45	20.05	64.9	61.7	28.8	24.16	57.7	83.7	24.6	24.600	49.3	99.84
GOZ		19.77	13.12	39.5	66.3	33.6	21.87	67.3	64.9	28.3	22.708	56.6	80.15
sGO		40.11	33.80	80.2	84.2	25.5	25.46	51.1	99.6	20.2	20.028	40.4	98.98
sFe		11.50	11.48	23.0	99.8	31.1	30.98	62.2	99.5	20.4	20.400	40.9	99.99
ACZ	Rhodamine B	41.38	41.15	82.7	99.4	37.6	37.36	75.3	99.1	41.0	40.628	82.0	99.08
GO		45.49	45.37	90.9	99.7	14.8	14.73	29.6	99.4	16.6	16.491	33.2	99.16
GOZ		37.50	37.42	75.0	99.7	21.8	21.80	43.6	99.9	17.2	17.139	34.4	99.63
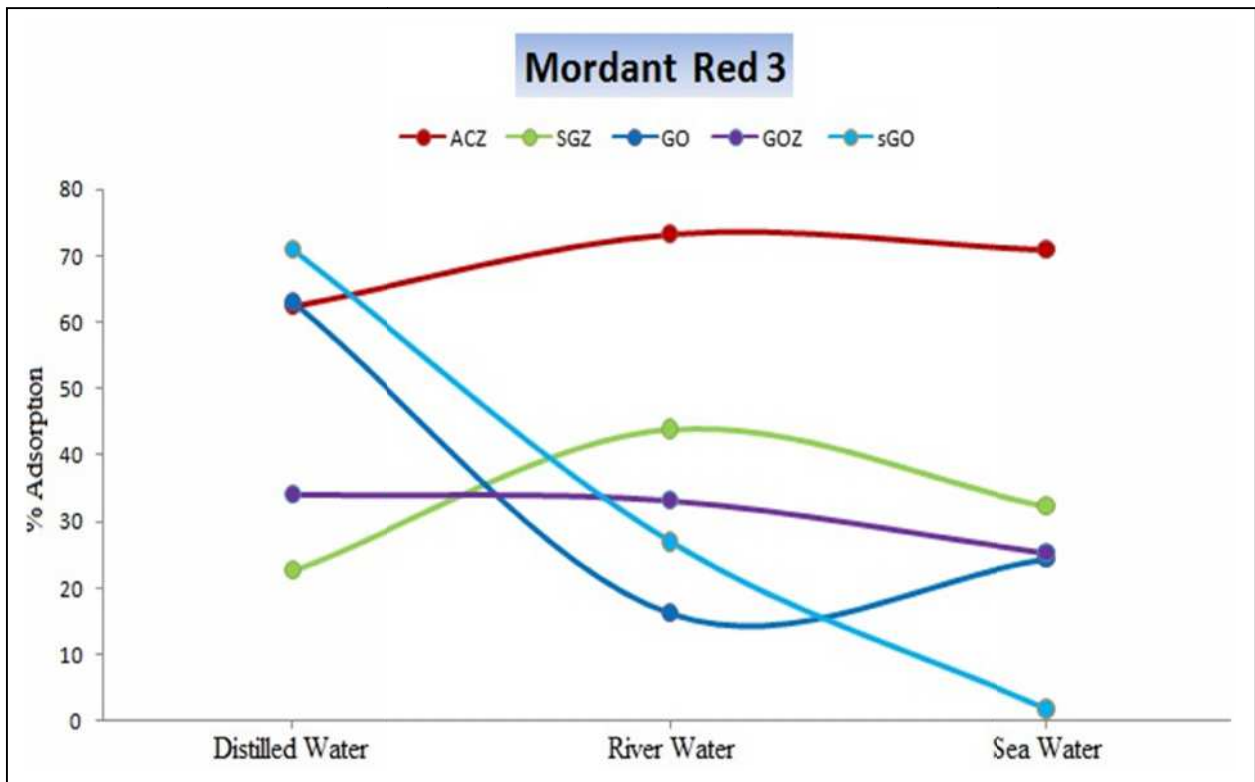
Figure 6.3 :Adsorption of Mordant Red 3 dye

Figure 6.4 :Adsorption of Congo Red dye
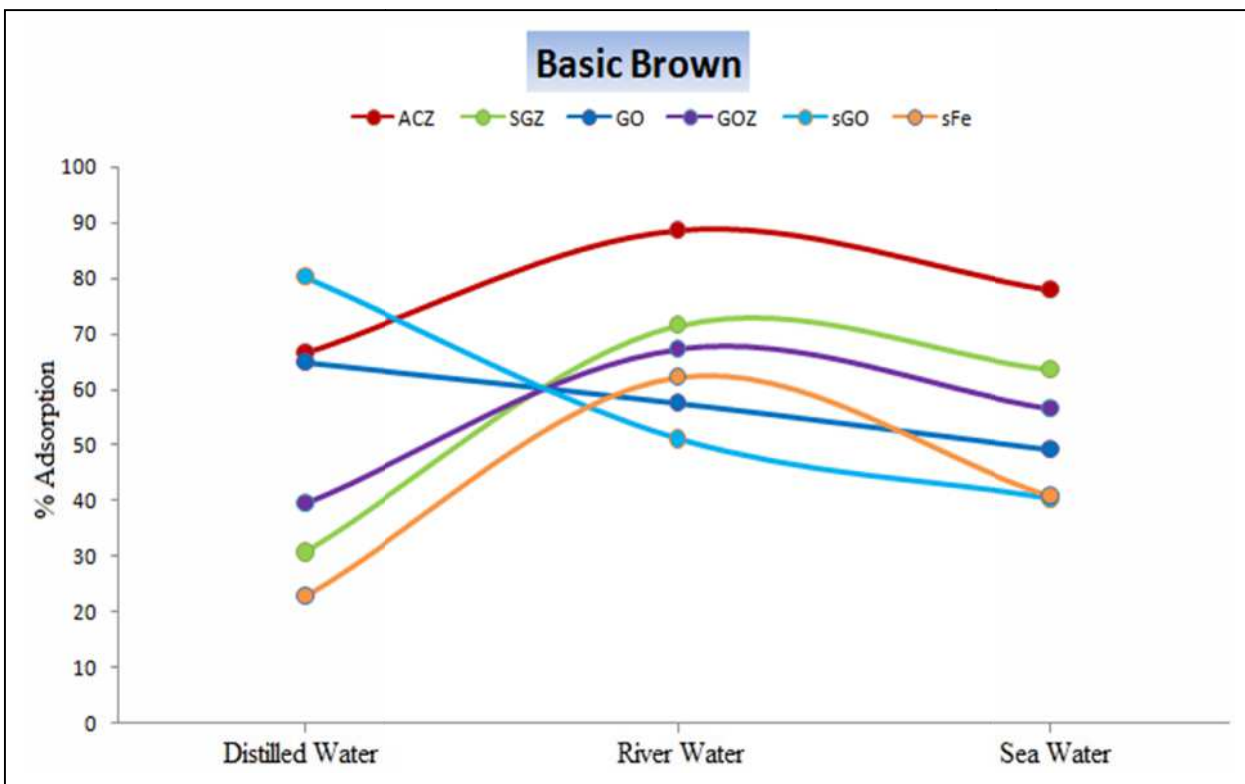
Figure 6.5 :Adsorption of Basic Brown dye

Figure 6.6 :Adsorption of Rhodamine B dye

6.4. Desorption experiment of dyes mixture

The recovery experiment of dyes was carried out onto six adsorbent surfaces after their adsorbed by using methanol as a recovery solvent at a room temperature for one hour under a continuous shaking , then it was separated by utilizing a centrifuge instrument at 2500 rpm for 15min . The filter solution was taken and analyzed by utilizing UV-Vis spectrophotometer at the maximum wavelength ($_{max}$) to each type of dyes.

The regeneration process of adsorbents after their adsorbed of the Mordant Red 3 dye recorded the highest recovery percent from sGO , GOZ and SGZ adsorbents after its adsorbed of the dye in distilled , river and sea waters where the percentage was 99.8 , 99.9 and 99.6%, respectively. All adsorbents after its adsorbed of the Mordant Red 3 dye revealed the ability to release the dye towards the methanolic solution by high a percentage but, the ACZ adsorbent recorded the low ratio in order to recover the dye to liquid phase once again , this result may be attributed to the strong bind found between dye molecules with ACZ adsorbent surface. Also, the activated carbon has structural micropores that prevent the internal solvent movement for releasing the dye to liquid phase [195] .

The desorption process depended on the structure of both the adsorbate molecules and adsorbent surface. So, the anionic dye as Congo Red recorded the high recovery percentage by utilizing methanol solvent for all adsorbents surface that is attributed to the small molecules of solvent that easily internal movement , may due to the weak electrostatic attractions found between the adsorbate molecules with adsorbents surfaces . The effect of salts content is unnoticeable in the desorption effeciencey .

The desorption effeciency of Basic Brown dye from all adsorbents surface was increased with the increases of the ionic strength that due to the weak binding

between the adsorbate and adsorbent molecules with increases of salts content whilst, the ACZ adsorbent showed the decrease of desorption effeciency with the increases of the ionic strength. Besides, the high percentage to the recovery of Basic Brown dye from SGZ and sFe was recorded after their adsorbed in the distilled water at 99.9 and 99.8 %, respectively .

The recovery process of Rhodamine B dye from three adsorbent surfaces (ACZ , GO and GOZ) recorded the high recovery percentage for the range 99.08 to 99.9% after their adsorbed in the three types of water such as distilled , river and sea waters . The desorption efficiency of Rhodamine B dye from all adsorbents surface is unaffected with the increases of the ionic strength of adsorbents, this happens due to the weak attraction between the adsorbate and adsorbent molecules and with the increases of salts concentration . The desorption experiment data of dyes mixture from all adsorbents surface are listed in Table 6.2 and Figures 6.7 to 6.10 .
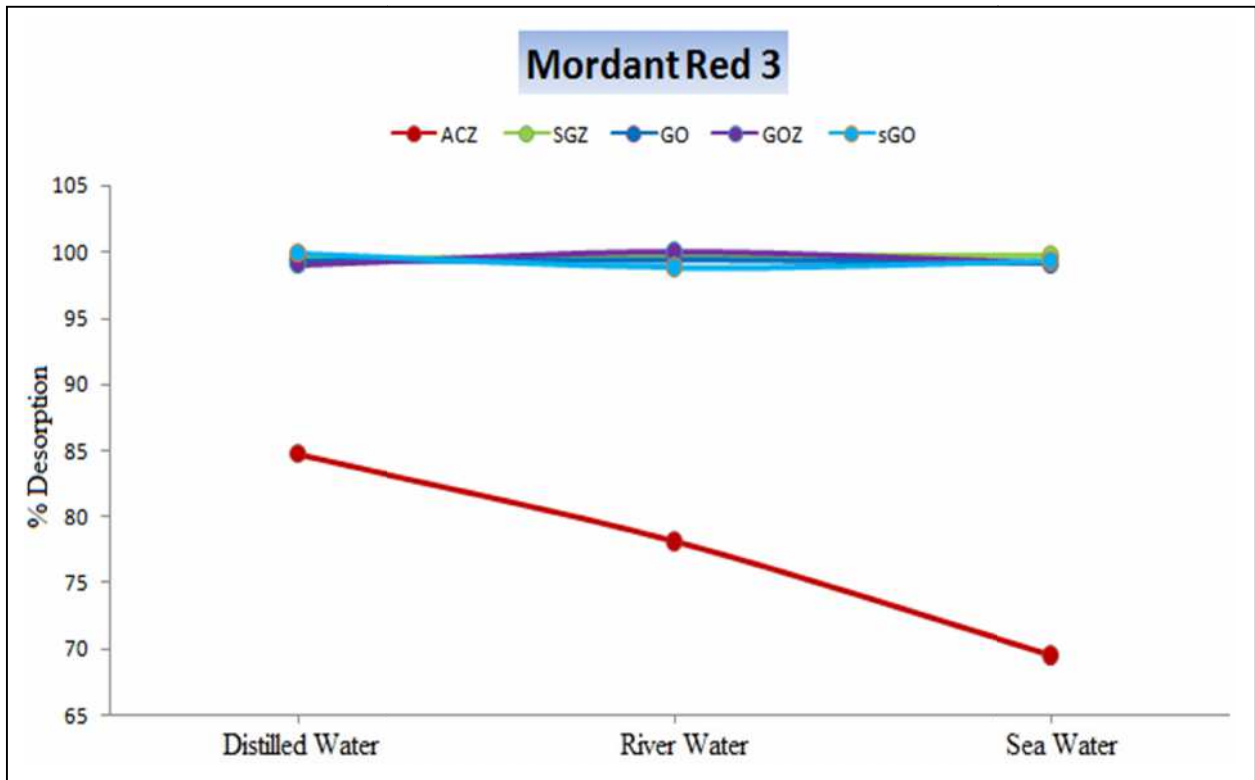
Figure 6.7 :Desorption of Mordant Red 3 dye
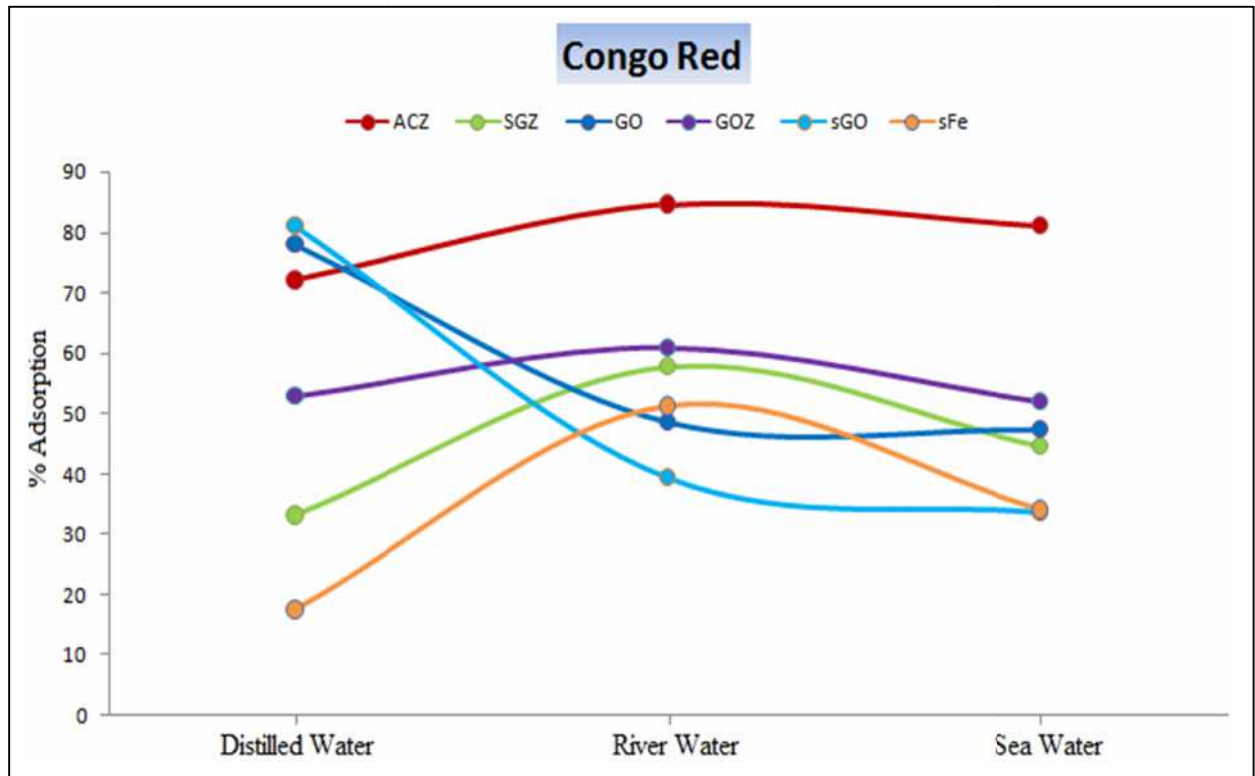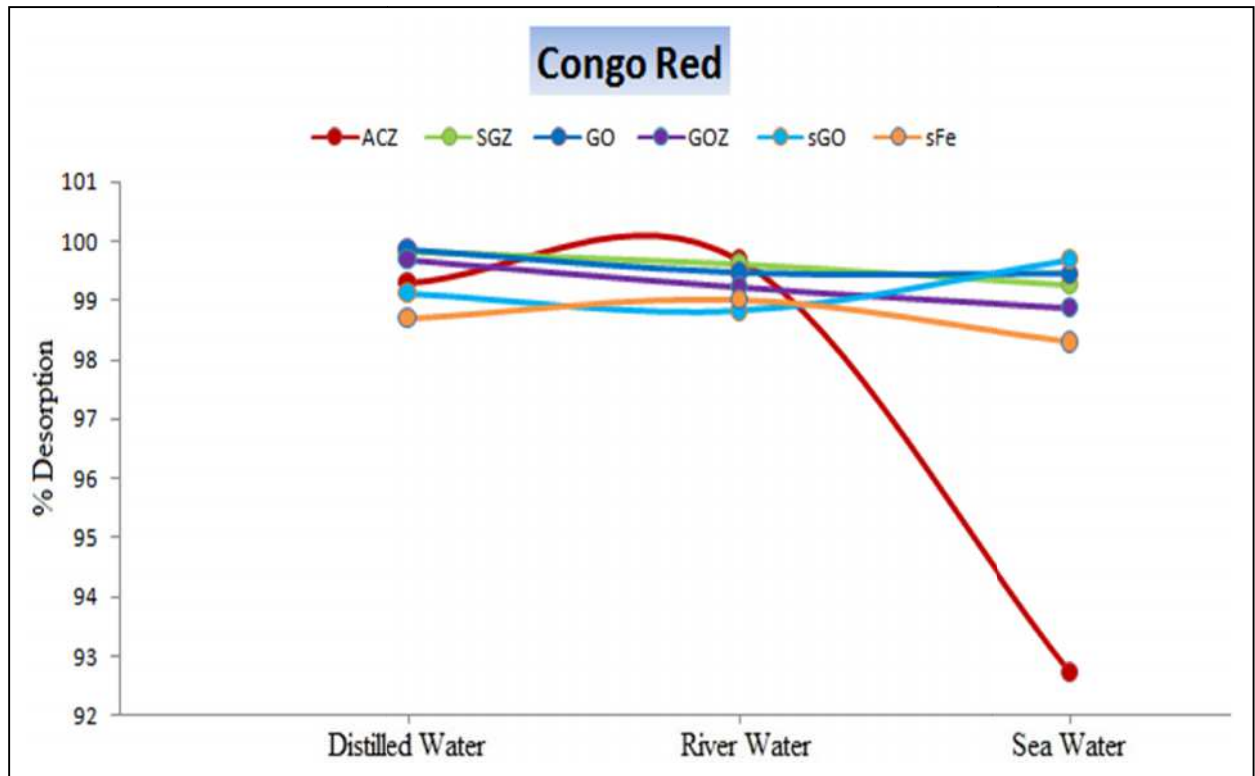

Figure 6.8 :Desorption of Congo Red dye
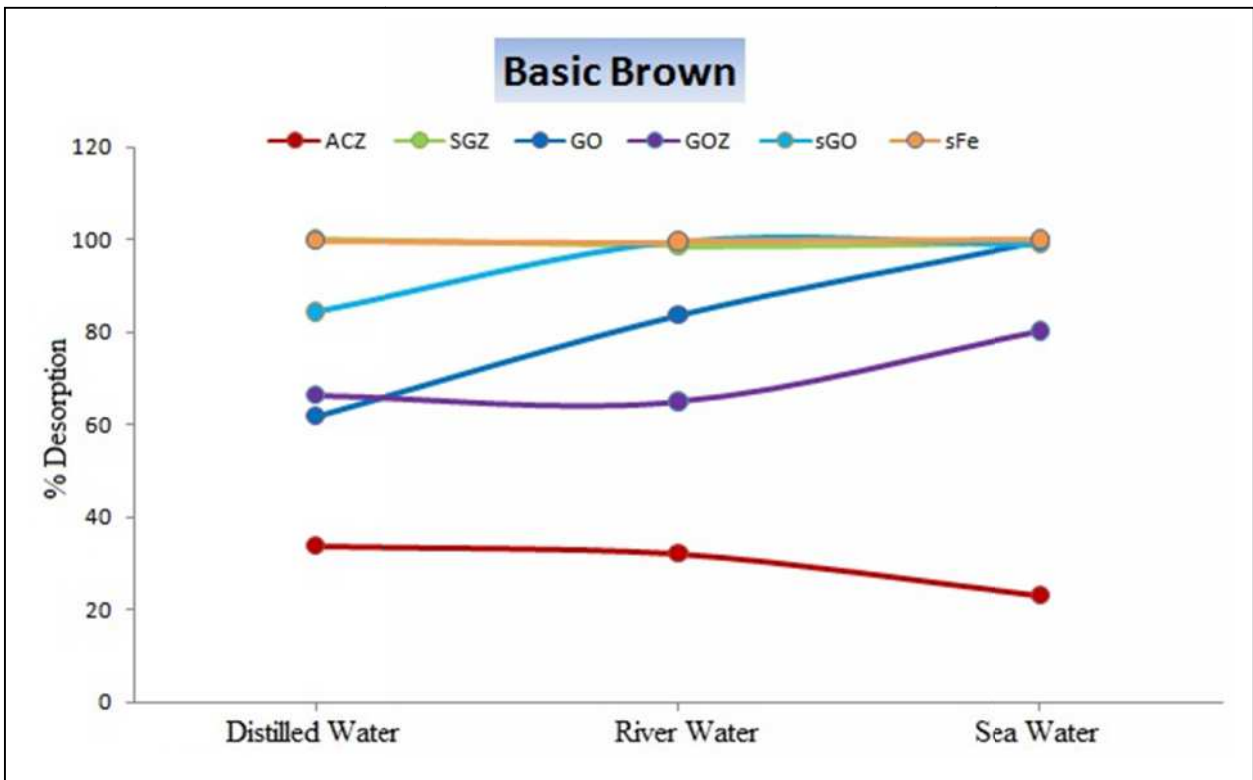
Figure 6.9 :Desorption of Basic Brown dye

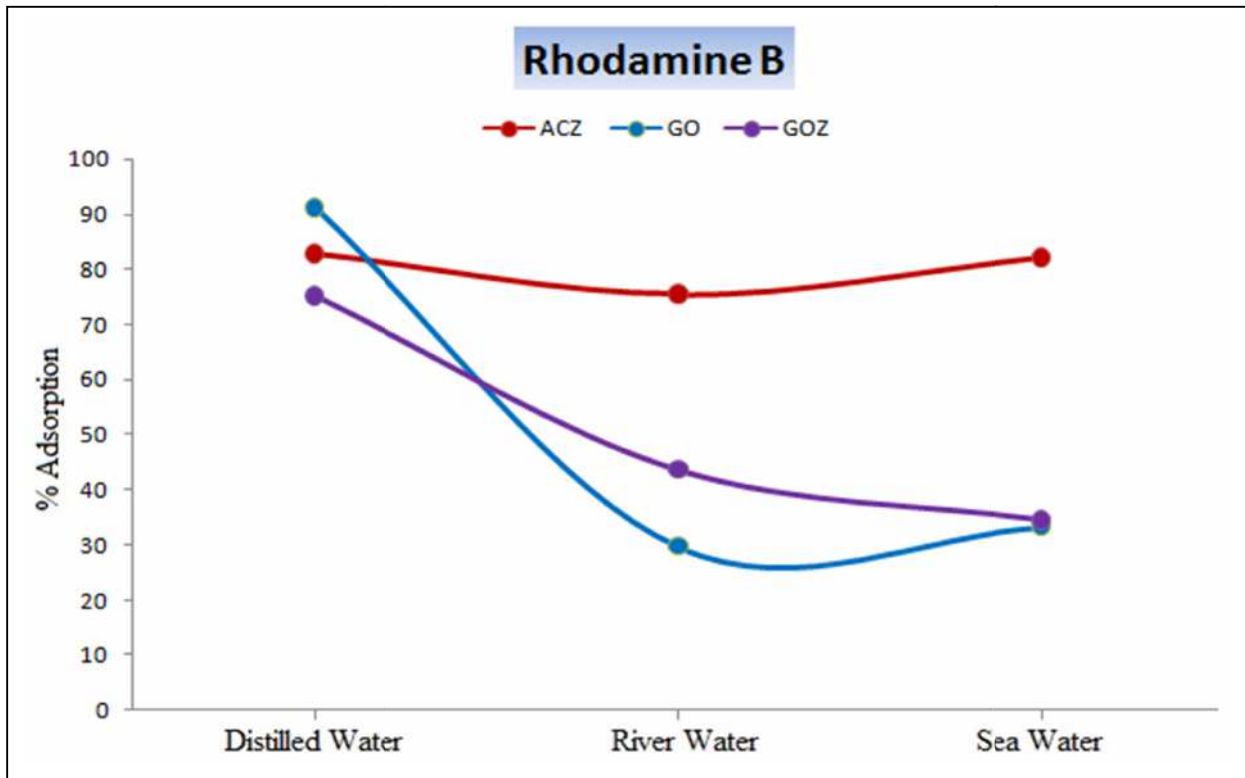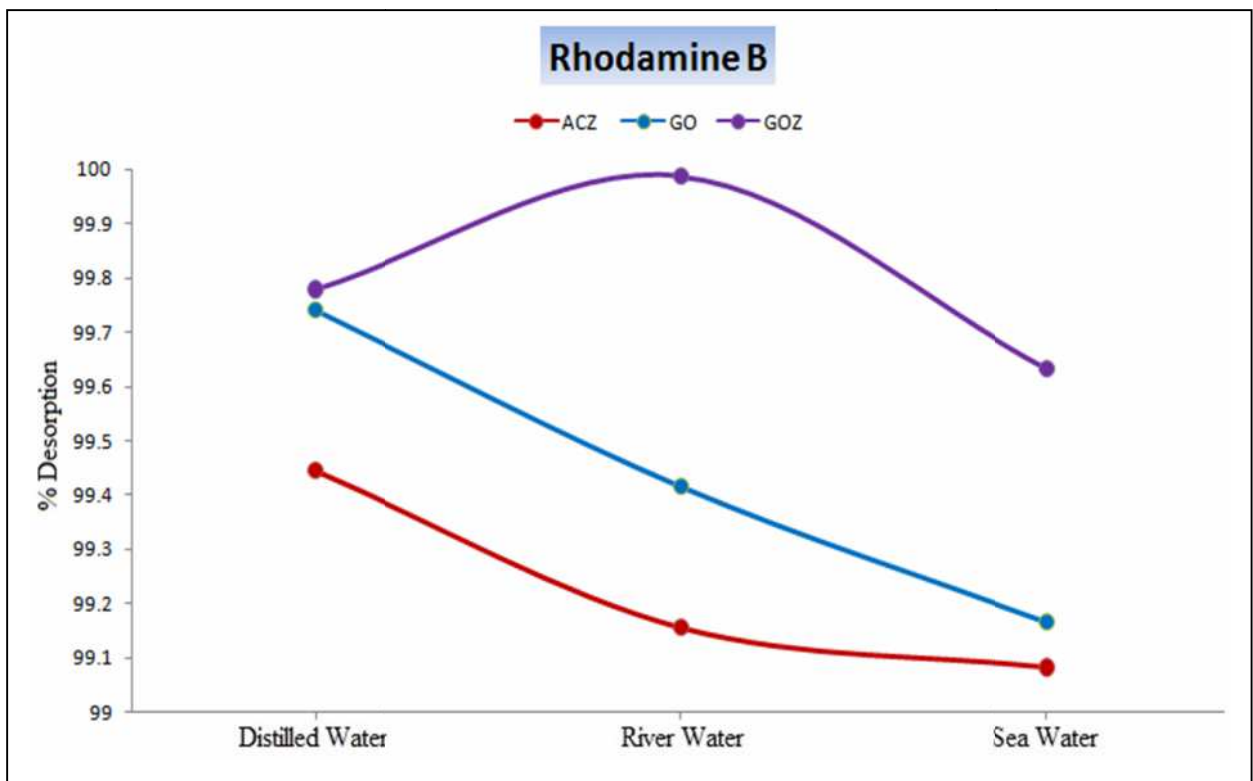Figure 6.10 :Desorption of Rhodamine B dye

Conclusions

Conclusions

The conclusions of current study can be summarized as follows:

1-Selenazone ligand was synthesized by replacing the sulfur atom in the dithiozone molecule to the selenium atom, and four complexes were prepared with divalent ions (Pb^{+2}, Cd^{+2}, Co^{+2} and Ni^{+2}).

2- The XRD and SEM measurements indicated the prepared nanoparticles for selenazone ligand.

3- The results of the thermal study were agreed with data of atomic spectroscopy that suggested from the geometric structure of the complexes.

4- The nickel complex demonstrated the highest value of activation energy which has more thermal stability when it is compared with other complexes. The thermal stability of the complexes was given in the following order : $Ni(Z)_4 > Co(Z)_4 > Cd(Z)_4 > Pb(Z)_4$.

5- Graphene oxide nanoparticles have been successfully prepared from graphite powder under special conditions.

6- Graphene oxide, activated carbon and silica gel were successfully grafted with selenazone ligand.

7- The activation energy was extracted from the thermal analysis data (TG/DTG) for the prepared nanomaterials which were reflected in the thermal stability that was ordered as : $SGZ > GO > sFe > sGO > GOZ > ACZ$.

8- The prepared nanomaterials were used as adsorbents with high efficiency under the optimum conditions (contact time, temperature , pH level and agitation speed)

to remove four dyes such as Mordant red 3 , Congo red , Basic Brown and Rhodamine B as well as, the ions of mercury and lead from their aqueous solutions.

9- The isotherm models of Langmuir and Freundlich were dominated by describing the mechanism of the adsorption process for the adsorbate material onto the prepared adsorbents.

10- The data of free energy G° is appropriate with the adsorption energy (E KJ/mol) which shows the physisorption that occurs for all adsorption process .

11- The solvent of methanol and 0.5N of HCl are more suitable solutions to recover the dye molecules and heavy metals (Hg and Pb) ions from the adsorbents, respectively.

12- The ionic strength for solutions of simulation of polluted water by using four dyes impacted positively and negatively on the adsorption efficiency.

Recommendations

Recommendations

1- The investigation of selenazone ligand ability to chelate with other metals.

2- preparing the activated carbon and graphene oxide from the natural materials and friendly to the environment for using as adsorbent after their grafted with selenazone ligand .

3- Synthesis of new compounds of organoselenium and tullerium that are gafted onto the prepared activated carbon, graphene oxide and graphene for using as a good adsorbent for removing several pollutants such as hydrocarbons, phenols compounds, pesticides, pharmaceutical compounds, carcinogenic dyes and toxic heavy metals.

4- using the separated nanoparticles from the soot waste to remove other toxic heavy metals such as arsenic, cadmium and chromium.

References

References

1- C.H.Latorre , J.B.Garcia , S.G.Martin and R.M.P.Crecente , Solid phase extraction for the speciation and preconcentration of inorganic selenium in water samples: A review,Analytica Chimica Acta,Vol.804 ,pp.37-49, 2013.

2- Z.A. Abdulnabi, W.F. Hassan, D.K.K. Al-Khuzaie , S.M. Saleh , and M.G. Hashim , Evaluation of selenium levels for the water surfaces in southern of Iraq . Journal of Chemical and Pharmaceutical Research. Vol. 7, No.10, pp.495-501, 2015.

3- A.Terol , F.Ardini , A.Basso and M.Grotti , Determination of selenium urinary metabolites by high temperature liquid chromatography-inductively coupled plasma mass spectrometry , Journal of Chromatography A, Vol.1380 , pp. 112-119, 2015 .

4- D. perrone , M. Monteirob and J. C.Rtes nunes , Selenium: Chemistry, Analysis, Function and Effects , Chapter one : the chemistry of selenium , Food and Nutritional Components in Focus No. 9 , The Royal Society of Chemistry ,2015 .

5- T. Wirth , Organoselenium Chemistry modern developments in organic synthesis , Topics in Current Chemistry,Vol. 208 , Springer-Verlag Berlin Heidelberg , 2000 .

6- T. Wirth , Organoselenium Chemistry: Synthesis and Reactions, [1st]Ed. , Wiley-VCH Verlag & Co. KGaA, Boschstr. 12, 69469 Weinheim, Germany , 2012 .

7- R. Guo, L. Liao and X. Zhao , Electrophilic Selenium Catalysis with Electrophilic N-F Reagents as the Oxidants, Molecules , Vol. 22, pp.1-13, 2017.

8- L. H. S. Smith, S. C. Coote, H. F. Sneddon, and D. J. Procter , Beyond the Pummerer Reaction: Recent Developments in Thionium Ion Chemistry, Angew. Chem. Int. Ed., Vol.49, pp.5832 – 5844, 2010.

9- T. Eom and A. Khan, Selenium-Epoxy 'Click' Reaction and Se-Alkylation-Efficient Access to Organo-Selenium and Selenonium Compounds, Chemistry, Vol. 2, pp.827–836, 2020.

10- J. Nakayama , K. Akimoto and M. Hoshino , reaction of sulfur ylides with elemental sulfur and selenium. aspects and mechanistic considerations , J. phys. Org. chem., Vol.1 , pp. 53-57 1988.

11- M. Raghavendra, H. S. B. Naik and B. S. Sherigara , A facile one-pot microwave-induced synthesis of some novel selenolo[2,3-b]quinoline derivatives under solvent-free conditions , Phosphorus, Sulfur, and Silicon, Vol.183, pp.1501–1509, 2008 .

12- C.Narajji , M.D.Karvekar and A.K.Das , Biological importance of organoselenium compounds , Indian J. Pharm. Sci. , Vol.69, No.3 , pp.344-351 , 2007 .

13- C.Cobo-Angel , J.Wichtel and A.Ceballos-Marquez , Selenium in milk and human health, Animal Forntiers , Vol.4 , No.2 , pp.38-43, 2014 .

14- C. V.Rao , I. Cooma, J. G.R. Rodriguez , B. Simi, K. El-Bayoumy and B. S.Reddy , Chemoprevention of familial adenomatous polyposis development in the APC^{min} mouse model by 1,4-phenylene bis(methylene)selenocyanate , Carcinogenesis , vol.21, No.4, pp.617–621, 2000 .

15- S.Nagy, A.Ozsváth, A.Cs. Bényei , E.Farkas and P.Buglyo, Donor Atom Preference of organoruthenium and organorhodium cations on the interaction

with novel ambidentate (N,N) and (O,O) chelating ligands in aqueous solution, Molecules, Vol.26, No.3586, pp.1-23, 2021.

16-B. C. Ranu and B. Banerjee, Organoselenium Chemistry, Walter de Gruyter GmbH, Berlin/Boston, ISBN 978-3-11-062224-9, 2020.

17- R.S. Ramakrishna and H.M.N.H. Irving , Selenazone : the analogue of dithizone , Analytical chimica acta , Vol.48 ,pp.251-266 , 1969 .

18- M. Zec, T. Srdic-Rajic, A. Krivokuca, R. Jankovic, T. Todorovic, K. Andelkovic and S.Radulovic , Novel selenosemicarbazone metal complexes exert anti-tumor effect via alternative, caspase-independent necroptotic cell death , Medicinal Chemistry , Vol.10 , 2014 .

19- T. R. Todorovic´, A. Bacchi , N. O. Juranic´, D. M. Sladic´, G. Pelizzi , T. T. Bozˇic´, N. R. Filipovic´and K. K. And-elkovic´, Synthesis and characterization of novel Cd(II), Zn(II) and Ni(II) complexes with 2-quinolinecarboxaldehyde selenosemicarbazone. Crystal structure of bis(2-quinolinecarboxaldehyde selenosemicarbazonato)nickel(II) , Polyhedron , Vol.26, pp.3428–3436, 2007.

20- H. Shen , H. Zhu , M. Song , Y. Tian , Y. Huang , H. Zheng, R.Cao, J. Lin , Z. Bi1 and W. Zhong , A selenosemicarbazone complex with copper efficiently down-regulates the 90-kDa heat shock protein HSP90AA1 and its client proteins in cancer cells , BMC Cancer, Vol.14, pp.629, 2014.

21- Z. A. Abdulnabi, M. K. Altememi, WF.Hassan, D. K.K.Al-Khuzaie and S. M.Saleh, Assessing of Some Toxic Heavy Metals Levels and Using Geo Accumulation Index in Sediment of Shatt Al-Arab and the Iraqi Marine Region, Bagh. Sci. J., Vol.16, No. 2, pp.323-331, 2019.

22- J. G. Speth , Environmental Pollution, EARTH '88: Changing Geographic, National Geographic Society, ISBN 0-915825-36-8, 1988.

23- Z.A. Abdulnabi, Assessment of some toxic elements levels in Iraqi marine water, Mesopot. J. Mar. Sci., Vol.31, No. 1, pp. 85 - 94 , 2016.

24- A. A.Abdullah, Synthesis of some azo dyes derived from Procaine and study the adsorption of these dyes by activated carbon prepared from local Z.spina-christi fruits pits, M.Sc Thesis ,University of Basrah, 2015.

25- I. K. Radhi, Removing Some Anionic Dyes by Modification of CaO Derived from Eggshell and Study of Adsorption, Kinetic, Thermodynamics and Photocatalytic characteristics, Ph.D Thesis, University of Basrah, 2019.

26- M.K. Hill, Understanding environmental pollution, Cambridge University press , [3th]Ed, 2010.

27- G. Saxena, R. Chandra and R. N. Bharagava, Environmental pollution, toxicity profile and treatment approaches for tannery wastewater and its chemical pollutants, reviews of environmental contamination and toxicology, Springer International Publishing 2016.

28- A. R. LANG, Dyes and pigments: new research, Nova science publishers, Inc. New York, ISBN 978-1-60876-195-1, 2009.

29- K.Hunger, Industrial dyes chemistry, properties, applications , WILEY-VCH Verlag GmbH & Co. KGaA, Weinheim, ISBN 3-527-30426-6, 2003.

30- S. Benkhaya, S. El Harfi and A. El Harfi, Classifications, properties and applications of textile dyes: A review, Appl. J. Env. Eng. Sci., Vol. 3. No.3, pp. 311-320, 2017.

References

31- P. S.Vankar, Chemistry of natural dyes, Resonance , 2000.

32-M.Oves, M.S. Khan, A. H. Qari, M. N. Felemban and T.Almeelbi, Heavy metals: biological importance and detoxification strategies, J. Bioremed.& Biodeg., Vol.7, No. 2, 2016.

33- **A**.Y.H.Alshmery, Estimation of some heavy metals in clams, sediments and water from Shatt Al-Arab and treatment rocks porcellanite, M.Sc Thesis ,University of Basrah, 2013.

34-R. Singh, N. Gautam, A. Mishra and R. Gupta, Heavy metals and living systems: An overview, Ind. J. Pharm., Vol. 43,No. 3,pp.246-253, 2011.

35- A.Y. Hmood and T.E. Jassim, Adsorption of copper(II) and lead(II) ions from aqueous solutions by porcellanite, Mesopot. J. Mar. Sci., Vol.28,No.2,pp. 109 – 120, 2013.

36-H. Zhang ,D. Ma, Q. Xie and X. Chen, An approach to studying heavy metal pollution caused by modern city development in Nanjing, China, Env. Geo.,Vol.38, No.3, pp.223-228, 1999.

37- WHO (World Health Organization) , Health risks of heavy metals from long-range transboundary air pollution, WHO Regional Office for Europe, ISBN 978 92 890 7179 6, 2007.

38- L. K. Wang, Y.Hung and N.K. Shammas, Physicochemical Treatment processes, Vol.3, eISBN 1-59259-820-x, Humana Press Inc., New Jersey, 2005

39- D. Zioui, Z. Tigrine, H. Aburideh , S. Hout, M. Abbas and N. k. Merzouk, Membrane Technology for Water Treatment Applications, Digital Proceeding of ICCES , Istanbul, Turkey , 2015.

40- Z. Mai, Membrane processes for water and wastewater treatment : study and modeling of interactions between membrane and organic matter, Ph.D Thesis, Ecole Centrale Paris, 2014.

41- Z.Hubicki, M.Wawrzkiewicz, G.Wójcik, D.Kołody ska and A. Wołowicz, Ion Exchange - Studies and Applications, Chapter one: Ion Exchange Method for Removal and Separation of Noble Metal Ions, InTech, 2015.

42- A.K.Bajpai and M.Rajpoot, Adsorption techniques-A review, J.Sci.Indus.Res., Vol.58, pp.844-860, 1999.

43- A.Gapelman ,Adsorption Basic Part 1, American institute of chemical engineers, 2017.

44- A.B.-Petriciolet, D.I.M.-Castillo, H.E.R.-Avila, Adsorption Processes for Water Treatment and Purification,ISBN 978-3-319-58135-4, Springer, 2017.

45- D.M.Ruthven, Principles adsorption and adsorption processes, John wliey&Sons, ISBN 0-471-88606-7, 1984.

46- H. S. Kose, The effects of physical factors on the adsorption of synthetic organic compounds by activated carbons and activated carbon fibers, M.Sc Thesis, Clemson University, 2010.

47- S.Iftekhar, D.L.Ramasamy, V.Srivastava, M.B.Asif and M.Sillanpaa, Understanding the factors affecting the adsorption of Lanthanum using different adsorbents: A critical review , Chemosphere, Vol.204,pp. 413-430, 2018.

48- M.B.Desta, Batch Sorption Experiments: Langmuir and Freundlich Isotherm Studies for the Adsorption of Textile Metal Ions onto Teff Straw (Eragrostis tef) Agricultural Waste, J. Thermo., Vol.1, pp.1-6, 2013.

49- N.Ayawei, A.N.Ebelegi and D.Wankasi, Modelling and Interpretation of Adsorption Isotherms, J.Chem., Vol.1, pp.1-11, 2017.

50- A.A.Mizhir, A.A.Abdulwahid and H.S.Al-Lami, Adsorption of carcinogenic dye Congo red onto prepared graphene oxide-based composites, Desalination and Water Treatment, Vol.202, pp.381–395, 2020.

51- D. Lin, F. Wu, Y. Hu, T. Zhang, C. Liu, Q. Hu, Y. Hu, Z. Xue, H. Han, and T.-Hsing Ko, Adsorption of Dye by Waste Black Tea Powder: Parameters, Kinetic, Equilibrium, and Thermodynamic Studies, J.Chem., Vol.1, pp.1-13, 2020.

52- V.O.S.Neto, A.G.Oliveira, R.N.P.Teixeira, M.A.A.Silva, P.T.C.Freire, D.D.Keukeleire and R.F.Nascimento, Use of coconut bagasse as alternative adsorbent for separation of copper (II) ions from aqueous solutions: isotherms, kinetics, and thermodynamic studies, BioResources, Vol.6, No.3, pp.3376-3395, 2011.

53- O. Ali and S. Mohamed, Adsorption of copper ions and alizarin red S from aqueous solutions onto a polymeric nanocomposite in single and binary systems, Turk. J. Chem., Vol.41, pp.967-986, 2017.

54- S.Kaur, S.Rani and R.K.Mahajan, Adsorption kinetics for removal of hazardous dye congo red by biowaste materials as adsorbents, J.Chem., Vol.1, pp.1-12, 2013.

55- W.C.Wanyonyi, J.M.Onyari and P.M.Shiundu, Adsorption of congo red dye from aqueous solutions using roots of *Eichhornia crassipes*: kinetic and equilibrium studies, Energy Procedia, Vol.50, pp.862 – 869, 2014 .

56- A. A. M. Albaheli, Preparation of graphene oxide-grafted polymers and the analytical study of their interaction with congo red and bismark brown dyes, Ph.D Thesis, University of Basrah, 2020.

57- N.A.S.M.Sandollah, S.A.I.S.M.Ghazali, W.N.W.Ibrahim and R.Rusmin, Adsorption-Desorption Profile of Methylene Blue Dye on Raw and Acid Activated Kaolinite, Indones. J. Chem., Vol.20, No. 4, pp.755 - 765, 2020.

58- B.E.M.-Cordero, P.A.-Madrid, C.C.L.-Porras, P.P.-Ruiz and M.M.-Yoshida, Study of the adsorption of arsenic (III and V) by magnetite nanoparticles synthetized via AACVD, Mate. Res., Vol.19, No.1, pp.103-112, 2016.

59- **A.** Kaushal and S.K. Singh**,** Removal of heavy metals by nanoadsorbents: A review, J. . Env. Biotech. Res., Vol. 6, No. 1, pp. 96-104, 2017.

60- M. S. Shafeeyan, W. M. A. W. Daud, A. Houshmand and A. Shamiri, A review on surface modification of activated carbon for carbon dioxide adsorption, J. Anal. Appl. Pyro., Vol. 89, pp.143–151, 2010.

61- K.PYRZYNSKA, Application of Carbon Sorbents for the Concentration and Separation of Metal Ions, ANAL. SCI., Vol. 23, pp.631-637, 2007.

62- I.Khan, K.Saeed and I.Khan, Nanoparticles: Properties, applications and toxicities , Arab. J. Chem., Vol.12, pp.908–931, 2019.

63- A.E.Burakov, E.V.Galunin, I.V.Burakova, A.E.Kucherova, S. Agarwal, A.G.Tkachev and V.K.Gupta, Adsorption of heavy metals on conventional

and nanostructured materials for wastewater treatment purposes: A review, Ecotoxic. Env. Safety, Vol.148, pp.702–712, 2018.

64- A. Nimibofa, E. A. Newton, A. Y. Cyprain and W. Donbebe, Fullerenes: Synthesis and Applications, J.Mate. Sci. Res., Vol.7, No.3, pp.22-36, 2018.

65- K. Atkovska, K. Lisichkov, G. Ruseska, A. T. Dimitrov and A.Grozdanov, removal of heavy metal ions from wastewater using conventional and nanosorbents: A review, J. Chem. Techn. Metall.,Vol. 53, No.2,pp.202-217, 2018.

66- V.Gupta, N.Sharma, U. Singh, M.. Arif and A. Singh, Higher oxidation level in graphene oxide, Optik, Vol.143, pp.115–124, 2017.

67- K.S.Brgaal, Adsorption and biochemical study for the removal of dyes from water using modified organic compounds obtained from scrap ground tyre rubber , Ph.D Thesis , University of Basrah, 2020.

68- C.Namasivayam, D.Kavitha, Removal of Congo Red from water by adsorption onto activated carbon prepared from coir pith, an agricultural solid waste, Dyes and Pigments, Vol.54, pp.47–58, 2002.

69- P.-Jen Lu, H.-Chieh Lin, W.-Te Yu and J.-Ming Chern, Chemical regeneration of activated carbon used for dye adsorption, J. of the Taiwan Inst. Chem. Eng., Vol.42, pp.305–311, 2011.

70- M.Fayazi, M.G.-Motlagh and M.A.Taher, The adsorption of basic dye (AlizarinredS) from aqueous solution onto activate dcarbon/ -Fe2O3 nano-composite: Kinetic and equilibrium studies, Materials Science in Semiconductor Processing, Vol.40, pp.35–43,2015.

71- B.Kamarehie, A.Jafari, M.Ghaderpoori , M. AminKarami, K.Mousavi and A.Ghaderpoury, Data on the alizarin red S adsorption from aqueous solutions on PAC, treated PAC, and PAC/ Fe2O3, Data in Brief,Vol.20, pp.903-908, 2018.

72- T.A. Khan, R.Rahman and E.A.Khan, Decolorization of bismarck brown R and crystal violet in liquid phase using modified pea peels: non-linear isotherm and kinetics modeling, Model.Earth Syst.Env.,Vol.2, pp.141, 2016.

73- Z.Maderova, E.Baldikova, K.Pospiskova, I.Safarik, M.Safarikova, Removal of dyes by adsorption on magnetically modified activated sludge, Int.J. Env.Sci.Technol. Vol.13, pp.1653-1664, 2016.

74- R.Lafi , I.Montasser and A.Hafiane, Adsorption of congo red dye from aqueous solutions by prepared activated carbon with oxygen-containing functional groups and its regeneration, Adsor. Sci. & Techn., Vol.37, No. 1–2,pp.160–181, 2019.

75- N. Abdolrahimi and A. Tadjarodi, Adsorption of Rhodamine-B from Aqueous Solution by Activated Carbon from Almond Shell, Proceedings, Vol.41, pp.51, 2019.

76- D.L.Postai,C.A.Demarchi,F.Zanatta, D.C.C.Melo and C.A.Rodrigues, Adsorption of rhodamine B and methylene blue dyes using waste of seeds of Aleurites Moluccana, a low cost adsorbent, Alexandria Engineering Journal, Vol.55, pp.1713–1723, 2016.

77- D.Mohan, V.K.Gupta, S.K.Srivastava and S.Chander, Kinetics of mercury adsorption from wastewater using activated carbon derived from fertilizer

waste, Colloids and Surfaces A: Physicochem. Eng. Aspects, Vol.177, pp.169-181, 2001.

78- H.S.Silva, S.V.Ruiz, D.L.Granados and J.M.Santángelo, Adsorption of Mercury (II) from Liquid Solutions Using Modified Activated Carbons, Mate. Res., Vol.13, No. 2, pp.129-134, 2010.

79- G. Ketsela, Z. Animen and A. Talema, Adsorption of lead (ii), cobalt (ii) and iron (ii) from aqueous solution by activated carbon prepared from white lupine (GIBITO) hsuk, J. Thermodyn. Cataly., Vol.11, No.2, pp. 1-8, 2020.

80- I.U.Salihi, S.R.M. Kutty and M. H. Isa, Adsorption of lead ions onto activated carbon derived from sugarcane bagasse, 7th International conference on key engineering materials (ICKEM 2017), IOP Conf. series: Materials Science and Engineering, Vol. 201, pp.1-7, 2017.

81- J.Samusolomon and P.M.Devaprasath, Removal of alizarin red s (dye) from aqueous media by using cynodon dactylon as an adsorbent, J. Chem. Pharm. Res., Vol.3, No.5, pp.478-490, 2011.

82- Z.A.Abdulnabi, Preparation,spectroscopic characterization, thermal study and biological activity of some complexes derived from schiff base and benzimidazole derived from 4-methylphenelendiamine , M.Sc Thesis , University of Basrah , 2013.

83- K.S.Khalikovich, A.S.Valievna and Z.S.Zafarovich, Extraction of fullerene C_{60} from the surface of the herbal pipe after combustion of coal and wood . Int. J. Modern Chem., Vol.11, No.1, pp.1-8, 2019.

84- M.Kigozi, R.K.Koech, O.Kingsley, I.Ojeaga , E.Tebandeke, G.N.Kasozi, A.P.Onwualu, Synthesis and characterization of graphene oxide from locally

mined graphite flakes and its supercapacitor applications, Results in Mate., Vol.7, No.100113, 2020.

85- S.K.Abdel-Aal, A.Lonov, R.N. Mozhchil and A.H.Naqvi, Simple synthesis of grapheme nanocomposites MgO-rGO and Fe_2O_3-rGO for multifunctional applications, Appl.Sci.A, Vol.124, pp.365, 2018.

86- A. N. A. Abdulwahhabb, H.Al-Agha. And M. A.Alheety, Addition of Some Primary and Secondary Amines to Graphene Oxide, and Studying Their Effect on Increasing its Electrical Properties, Bagh. Sci. J., Vol.13, No.1, pp.97-112, 2016.

87- N.A.-Carvajal, D.A.A.-Guzman, V.M.-Laguna, M.H.Farias, L.A.P.-Rey, E.A.-Morales, V.A.G.- Ramirez, V.A.Basiuk and E.V.Basiuk, One-step nondestructive functionalization of graphene oxide paper with amines, R.S.C. Adv., Vol.8, pp.15253-15265, 2018.

88- H.M.Marwani, H.M.Albishri, T.A.Jalal and E.M.Soliman, Activated carbon immobilized dithizone phase for selective adsorption and determination of gold(III), Desal. Wat. Treat., Vol.45, pp.128-135, 2012.

89- H.-M.Yu, H.Song and M.-L.Chen, Dithizone immobilized silica gel on-line preconcentration of trace copper with detection by flame atomic absorption spectrometry, Talanta, Vol.85, pp.625-630, 2011.

90- Y. Zhou, Q. Liu, P. Xu, H. Cheng and Q. Liu, Molecular structure and decomposition kinetics of kaolinite/alkylamine intercalation compounds, Front. Chem., Vol.6, Article No.310, 2018.

References

91- A.M.Kamil, F.H.Abdalrazak, A.F.Halbus and F.H.Hussein, Adsorption of Bismarck Brown R Dye Onto Multiwall Carbon Nanotubes, J. Env. Anal. Chem., Vol.1, No.1, 2014.

92- P.Bhatia, S.Pandey, R.Prakash and T. P.Nagaraja, Enhanced Anti-oxidant Activity as a Function of Selenium hyperaccumulation in Agaricus bisporus Cultivated on Se-rich Agri-residues , TBAP , Vol.4 , No.5 & 6 , pp. 354 -364, 2014.

93- J.Fu, X.Wang, J.Li, Y.Ding and L.Chen, Synthesis of multi-ion imprinted polymers based on dithizone chelation for simultaneous removal of Hg^{2+}, Cd^{2+}, Ni^{2+} and Cu^{2+} from aqueous solutions, R.S.C. Adv., Vol.6, pp.44087-44095, 2016.

94- H.P.Ebrahimi, J.S.Hadi, Z.A.Abdulnabi and Z.Bolandnazar, Spectroscopic, thermal analysis and DFT computational studies of salen-type Schiff base complexes , Spe.Acta Part A: Mol.Bio.Spe. , Vol.117 ,pp. 485–492, 2014.

95- A.I.Farounbi , P.K.Mensah, E.O.Olawode and N.P.Ngqwala, 1H-NMR Determination of Organic Compounds in MunicipalWastewaters and the Receiving Surface Waters in Eastern Cape Province of South Africa, Molecules, Vol.25, No.713, 2020.

96- T.Perera , P.A.Marzilli , F. R. Fronczek and L. G. Marzilli , NH NMR shifts of new, structurally characterized *fac*-[Re(CO)$_3$(polyamine)]$^{n+}$ complexes probed via outer-sphere H-bonding interactions to anions, including the paramagnetic[ReIVBr$_6$]$^{2-}$ anion , Inorg. Chem. , Vol. 49, No.12 , pp. 5560–5572, 2010.

97- P. R.-Ranjbar and I. Yavari, On the Structure of Dithizone, Organic magnetic resonance, Vol.16, No.2, pp.168-169, 1981.

98- C.Dagostino, M.D.Mantle and L.F.Gladden, In situ high-pressure $^{13}C/^{1}H$ NMR reaction studies of benzyl alcohol oxidation over a Pd/Al_2O_3 catalyst, React. Chem. Eng., Vol.5, pp.1053–1057, 2020.

99- M.A.R.Fresneda, J.D.Martin, J.G.Bolivar, M.V.F.Cantos, G.B.-Estévez, M.F.M.Moreno and M.L.Merroun, Green synthesis and biotransformation of amorphous Se nanospheres to trigonal 1D Se nanostructures: impact on Se mobility within the concept of radioactive waste disposal , Env.Sci.Nano , Vol.5 , pp. 2103-2116, 2018.

100- H.T.Abdulsahib, Synthesis and characterization of some polymers for the removal of some heavy metal ions and bentonite in waste waters , Ph.D Thesis , University of Basrah , 2015.

101- C.P.Shah, K.K.Singh, M.Kumar and P.N.Bajaj, Vinyl monomers-induced synthesis of polyvinyl alcohol-stabilized selenium nanoparticles , Mat. Res. Bull. , Vol. 45 , pp. 56-62, 2010.

102- B.Lafuente, R.T.Downs, H.Yang, N.Stone,2015, The power of databases: the RRUFF project. In: Highlights in Mineralogical Crystallography, T. Armbruster and R.M.Danisi, eds. Berlin, Germany, W. De Gruyter, pp.1-30,(https://rruff.info/selenium/R050656).

103- Mudasir, G. Raharjo, I. Tahir and E.T.Wahyuni, Immobilization of Dithizone onto Chitin Isolated from Prawn Seawater Shells (*P. merguensis*) and its Preliminary Study for the Adsorption of Cd(II) Ion , J. Phy. Sci., Vol.19, No.1, pp.63–78, 2008.

References

104- A.Mohammed and A.Abdullah, Scanning Electron Microscopy (SEM): A Review, Proceedings of International Conference on Hydraulics and Pneumatics – HERVEX, November 7-9, B ile Govora, Romania,2018.

105- A. Dulivo, L. Lampugnani, I. Sfetsios, R.Zamboni and C.Forte, Studies on the breakdown of organoselenium compounds in a hydrobromic acid–bromine digestion system, Analyst, Vol. 119, 1994.

106- M.Flak and P.A.Giguere, Infrared spectra and structure of selenious acid, Can. J. Chem. Vol. 36, pp.1680-1685, 1958.

107- T.R.Todorovic, A.Bacchi, N.O.Juranic, D.M.Sladic, G.Pelizzi, T.T.Bozˇic, N.R.Filipovic and K.K.Andelkovic, Synthesis and characterization of novel Cd(II), Zn(II) and Ni(II) complexes with 2-quinolinecarboxaldehyde selenosemicarbazone. Crystal structure of bis(2-quinolinecarboxaldehyde selenosemicarbazonato) nickel (II), Polyhedron, Vol.26, pp.3428-3436, 2007.

108- J.S.Hadi, Z.A.Abdulnabi and A.M.Dhumad, Synthesis, spectral characterization, thermal analysis and DFT computational studies of 2-(1H-indole-3-yl)-5-methyl-1H-benzimidazole and theeir Cu(II) , Zn(II) and Cd(II) complexes , Europ.J.Chem., Vol.8 , No.3 , pp.252-257, 2017.

109- S.R.Bakir, A.A.S.Al-hamdani, A.J.Jarad, Synthesis and Characterization of Mixed Ligands of Dithizone and Schiff Base Complexes with Selected Metal Ions, Diya. J. P. Sci, Vol.9, No.2, pp.82-95, 2013.

110- A.Gaber , A.A.M.Belal , I.M.El-Deen, N.Hassan , R.Zakaria, W.F.Alsanie, A.M.Naglah and M.S.Refat, Synthesis, Spectroscopic Characterization, and Biological Activities of New Binuclear Co(II), Ni(II), Cu(II), and Zn(II) Diimine Complexes, Crystals, Vol.11, No.300, 2021.

References

111- Ahmadi,R. A. , Hasanvand ,F. , Bruno ,G., Rudbari , H. A. and Amani ,S., Synthesis, Spectroscopy, and Magnetic Characterization of Copper(II) and Cobalt(II) Complexes with 2-Amino-5-bromopyridine as Ligand, ISRN Inorg.Chem., Vol.1, pp.1-7, 2013.

112- C.D'Agostino, P.Brauer, P.C.-Rajapark, M.D.Crouch and L.F.Gladden, Effect of paramagnetic species on T_1, T_2 and T_1/T_2 NMR relaxation times of liquids in porous $CuSO_4/Al_2O_3$, R.S.C. Adv., Vol.7, pp.36163–36167, 2017.

113- G.S.Kamble, S.S.Joshi, A.N.Kokare, S.B.Zanje, S.S.Kolekar, A.V.Ghule, S.H.Gaikwad and M.A.Anuse, A sensing behavior synergistic liquid–liquid extraction and spectrophotometric determination of nickel(II) by using 1-(2 ,4 dinitro aminophenyl)4,4,6-trimethyl-1,4dihydropyrimidine-2-thiol: Analysis of foundry and electroless nickel plating of waste water, Sepa. Sci. Techn., Vol.52, No.14, pp.2238-2251, 2017.

114- L.L.A.Ntoi And K.G.V.Eschwege, Spectrophotometry mole ratio and continuous variation experiments with dithizone, Afric. J. Chem. Edu., Vol.7, No.2, 2017.

115- A.Q.Waleed , Z.A-A.Khammas, A.S.Al-Ayash and F.Jasim, An Indirect Atomic Absorption Spectrophotometric Determination of Trifluoperazine Hydrochloride in Pharmaceuticals, Arab. J. Sci. Eng., vol.36, pp.553–563, 2011.

116- H.R.H.Ali, G.A.Saleha, S.A.Hussein and A.I.Hassan, Preparation, characterization and atomic absorption spectroscopic determination of some metal complexes of glipizide, Der Pharma Chemica, Vol.5, No.6, pp.156-163, 2013.

References

117- M.W.Woubie, Synthesis and characterization of ni(ii) and zn(ii) complexes of multidentate ligand derived from1,10-Phenanthroline-5,6-dione and O-phenylenediamine, M.Sc.Thesis , University of Addis Ababa , (2010) .

118- I. Ali, W. A.Wani and K. Saleem, Empirical Formulae to Molecular Structures of Metal Complexes by Molar Conductance, Syn. React. in Inorg., Metal-Org., and Nano-Metal Chem., Vol.43, pp.1162–1170, 2013.

119- J.S.Hadi and A.A.Abudl Kareem, Thermogravimetric Study of Some Schiff base Metal Complexes, SSRG Int. J. App. Chem., Vol.7, No. 1 , pp.34-44, 2020.

120- P.J.Haines, Introdution of thermal methods :Thermal Methods of Analysis ,Springer Science, 1995.

121- W.W.Wendlandt, Thermal analysis , ^{3th}Ed , John wliey&Sons, ISBN 0-471-88477-4, 1986.

122- H.Sahebalzamani, S.Ghammamy, K. Mehrani and F.Salimi, Synthesis, characterization and thermal analysis of Hg(II) complexes with hydrazide ligands, Der Chemica Sinica, Vol.1, No.1, pp.67-72, 2010.

123- S.Gopalakrishnan and R.Sujatha, Comparative thermoanalytical studies of polyurethanes using Coats-Redfern, Broido and Horowitz-Metzger methods, Der Chemica Sinica, Vol.2, No.5, pp.103-117, 2011.

124- C.-S.JOU , Expert system to retrieve optimal kinetic parameters for simple reactions, M.Sc Thesis , Texas Tech University, 1986.

125- A.A.M.ALY, A.H.Osman, M.A.El-Mottaleb and G.A.H. Gouda, Thermal stability and kinetic studies of cobalt (II), nickel (II), copper (II), cadmium

(II) and mercury (II) complexes derived from n-salicylidene schiff bases, J. Chil. Chem. Soc., Vol.54, No.4, 2009.

126- S. A.Abdl El-Latif, H. B. Hassib and Y.M. Issa, Studies on some salicylaldehyde Schiff base derivatives and their complexes with Cr(III), Mn(II), Fe(III), Ni(II) and Cu(II), Spectrochimica Acta Part A67,pp.950-957,(2007).

127- A. Aboulkas, K. El Harfi, Study of the kinetics and mechanisms of thermal decomposition of moroccan tarfaya oil shale and its kerogen, Oil Shale, Vol.25, No.4, pp.426-443, 2008.

128- A.Al-Mulla, Enthalpy-entropy compensation in polyester degradation reactions, Int. J. Chem. Eng., Vol.1, pp.1-8, 2012.

129- F. T. Senberber , E.M. Derun, Thermal kinetics and thermodynamics of the dehydration reaction of $Mg_3(PO_4)_2 \cdot 22H_2O$, Eurasian J. Bio. Chem. Sci., Vol.2, No.2, pp.47-51, 2019.

130- S.A.Aly, S.K.Fathalla, Preparation, characterization of some transition metal complexes of hydrazone derivatives and their antibacterial and antioxidant activities, Arab. J. Chem., Vol.13, pp.3735-3750, 2020.

131- **V.** Indira and G. Parameswaran, Thermal decomposition kinetics of schiff base complexes of copper(II) and palladium(II), Journal of ThermaI Ana., Vol. 32, pp.1151-1162, 1987.

132- V. Georgieva, D. Zvezdova and L. Vlaev, Non-isothermal kinetics of thermal degradation of chitosan, Chem. Cent. J., Vol.6, No.81, 2012.

133- A.P.d.S.Pereiraa, M.H.P.da Silvaa, É.P.L.Júniora, A.d.S.Paulaa and F.J.Tommasinia, Processing and characterization of pet composites reinforced with geopolymer concrete waste, Mate. Res., Vol.20, No. 2, pp.411-420, 2017.

134- P.A.Sheena, K.P.Priyanka, N.A.Sabu, B.Sabu, T.Varghese, Effect of calcination temperature on the structural and optical properties of nickel oxide nanoparticles, Nanosystems: Phy., Chem., Math., Vol.5, No. 3, pp.441-449, 2014.

135- A.A. Mizhir, A.A. Abdulwahid and H. S.Al-Lami, Chemical functionalization graphene oxide for the adsorption behavior of bismarck brown dye from aqueous solutions, Egypt.J.Chem.,Vol.63, No.5, pp.1679 - 1696, 2020.

136- S.Drewniak, R.Muzyka, A.Stolarczyk , T.Pustelny, M. K.-Moranska and M. Setkiewicz, Studies of reduced graphene oxide and graphite oxide in the aspect of their possible application in gas sensors, Sensors, Vol.16, No.103, pp. 1-16, 2016.

137- C.H.Manoratne, S.R.D.Rosa and I.R.M.KOTTEGODA, XRD-HTA, UV Visible, FTIR and SEM interpretation of reduced graphene oxide synthesized from high purity vein graphite, Mat. Sci. Res. India, Vol.14, No.1, pp.19-30, 2017.

138- D.L.Pavia, G.M.Lampman and G.S.Kriz, Introduction to spectroscopy, Thomson learning, [3th]Ed, ISBN 0-03-031961-7, 2001.

139- W.Gao, Graphite oxide: structure, reduction and applications, Ph.D Thesis, Rice University, Housi'on, Texas, 2012.

140- C.Panatarani, N.Muthahhari, A. Riant and I M. Joni, Purification and preparation of graphite oxide from natural graphite, The 4th International Conference on Theoretical and Applied Physics (ICTAP), AIP Conf. Proc. 1719, 030022-1–030022-6, 2016.

141- W. Gao, L.B.Alemany, L. Ci and P. M.Ajayan, New insights into the structure and reduction of graphite oxide, Nat.Chem., Doi: 10.1038/NCHEM.281, 2009.

142- B.Y.Yu and S.-Y.Kwak, Assembly of magnetite nanocrystals into spherical mesoporous aggregates with a 3-D wormhole-like pore structure, J. Mater. Chem., Vol.20, pp.8320-8328, 2010.

143- M. Gotic and S.Music, Mossbauer, FT-IR and FE SEM investigation of iron oxides precipitated from FeSO4 solutions, J. Mole. Stru., Vol.834–836, pp.445–453, 2007.

144- M. R. Karim and S. Hayami, Graphene Materials - Advanced Applications, Chapter 5: Chemical, Thermal, and Light-Driven Reduction of Graphene Oxide: Approach to Obtain Graphene and its Functional Hybrids, Intech, 2017.

145- M.J.Gros, M.MASRURI, R.T.Tjahjanto, A Green Method to Prepare Composite of Graphene Oxide- Manganese Oxide using a Modified Hummer's Method, The 2nd International Conference on Chemistry and Material Science, IOP Conf. Series: Materials Science and Engineering, Vol.833, 2020.

146- Q. Lai, S. Zhu, X. Luo, M. Zou and S. Huang, Ultraviolet-visible spectroscopy of graphene oxides, AIP Adv., Vol.2, No.032146, 2012.

147- S. Amutha and S.Sridhar, Green synthesis of magnetic iron oxide nanoparticle using leaves of *Glycosmis mauritiana* and their antibacterial activity against human pathogens, J. Innov. Pharma. Bio. Sci., Vol.5, No.2, pp.22-26, 2018.

148- K.Klacanova, P.Fodran, P.Simon, P.Rapta, R.Boca, V. Jorik, M. Miglierini, E. Kolek and L.Caplovic, Formation of Fe(0)-nanoparticles via reduction of Fe(II) compounds by amino acids and their subsequent oxidation to iron oxides, J.Chem., Vol.1, pp.1-10, 2013.

149- J.L. Figueiredo, M.F.R. Pereira, M.M.A. Freitas and J.J.M. Orfao, Modification of the surface chemistry of activated carbons, Carbon, Vol.37, pp.1379-1389, 1999.

150- P.J.M. Carrott, M.M.L. R. Carrott, P.A.M. Mourao and R.P. Lima, Preparation of activated carbons from cork by physical activation in carbon dioxide, Adsor. Sci. & Tech. Vol.21, No.7, pp.669-681, 2003.

151- M.S.Shamsuddin, N.R.N.Yusoff and M.A.Sulaiman, Synthesis and characterization of activated carbon produced from kenaf core fiber using H_3PO_4 activation, Procedia Chem., Vol.19, pp.558 - 565, 2016.

152- C. N. Tejada, D. Almanza, A. Villabona, F. Colpas and C. Granados, Characterization of activated carbon synthesized at low temperature from cocoa shell (Theobroma cacao) for adsorbing amoxicillin, Inge. Y Competitividad, Vol.19, No.2, pp.45 -54, 2017.

153- A. Mourhly, M. Khachani, A. El Hamidi, M.Kacimi, M.Halim and S. Arsalane, The Synthesis and Characterization of Low-cost Mesoporous Silica SiO2 from Local Pumice Rock, Nanomater Nanotechnol, Vol.5, No.35, 2015.

References

154- A. Purwanto, Yusmaniar, F. Ferdiani and R. Damayanti, Synthesis and Adsorption of Silica Gel Modified 3- aminopropyltriethoxysilane (APTS) from Corn Cobs against Cu(II) in Water, International Conference on Chemistry, Chemical Process and Engineering (IC3PE), AIP Conf. Proc. 1823, 020032-1–020032-8, 2017.

155- N. Bandara, Y. Esparza and J. Wu, Exfoliating nanomaterials in canola protein derived adhesive improves strength and water resistance, R.S.C. Adv., Vol.7, pp.6743–6752, 2017.

156- B.Lafuente, R.T.Downs, H.Yang, N.Stone,2015, The power of databases: the RRUFF project. In: Highlights in Mineralogical Crystallography, T. Armbruster and R.M.Danisi, eds. Berlin, Germany, W. De Gruyter, pp.1-30,(https://rruff.info/magnetite/R061111).

157- W. Wu, X. Xiao, S. Zhang, F. Ren and C. Jiang, Facile method to synthesize magnetic iron oxides/TiO2 hybrid nanoparticles and their photodegradation application of methylene blue, Nanoscale Res. Lett., Vol.6, pp.1-15, 2011.

158- G.Sangeetha, N.Usha, R.Nandhini, P.Kaviya, G.Vidhya And B.Chaithanya, A review on properties, applications and toxicities of metal nanoparticles, Int. J. App. Pharm., Vol. 12, No.5, pp.58-63, 2020.

159- S. L. Pal, U. Jana, P. K. Manna, G. P. Mohanta and R. Manavalan, Nanoparticle: An overview of preparation and characterization, J. Appli. Pharm. Sci., Vol.1, No.6, pp.228-234, 2011.

160- J. S. AZNAR, Characterization of activated carbon produced from coffee residues by chemical and physical activation, M.Sc Thesis, KTH Chemical Science and Engineering, 2011.

References

161- J.L.Rowlandson, Development of Nanoporous Carbons from Renewable Lignin Feedstocks for Sustainable Applications, Ph.D Thesis , University of Bristol, 2018.

162- O. P. O. Cancino, Experimental study of methane gas adsorption onto colombian shale and methane / carbon dioxide separation, Ph.D Thesis, University of Pau and Pays de l'Adour, 2018.

163- G.Wyasu, C.E.Gimba, E.B.Agbaji and G.I.Ndukwe, Thermo-gravimetry(TGA) and DSC of thermal analysis techniques in production of active carbon from lignocellulosic materials, Adv. Appl. Sci. Res., Vol.7, No.2, pp.109-115, 2016.

164- F.G.Okibe, C.E.Gimba, V.O.Ajibola and I.G.Ndukwe, Preparation and surface characteristics of activated carbon from brachystegia eurycoma and prosopis africana seed hulls, Int.J.Chem.Tech. Res., Vol.5, No.4, pp. 1991-2002, 2013.

165- J.Gaidukevic,R.Pauliukaite, G.Niaura, I.Matulaitiene, O.Opuchovic, A.Radzevic , G.Astromskas, V.Bukauskas and J.Barkauskas, Synthesis of reduced graphene oxide with adjustable microstructure using regioselective reduction in the melt of boric acid: relationship between structural properties and electrochemical performance, Nanomaterials, Vol.8, No.889, 2018.

166- K.Yin, H.Li, Y.Xia, H.Bi, J.Sun, Z.Liu, L.Sun, Thermodynamic and Kinetic Analysis of Lowtemperature Thermal Reduction of Graphene Oxide, Nano-Micro Lett., Vol.3, No.1, pp.51-55, 2011.

167- H.P.-Blanco, M.C.Zuluaga, L.A.Ortega , A.A.-Olazabal, J.J.C.-Ocampo and A.M.Salcedo, Mineralogical characterization of slags from the oiola site

(biscay, spain) to assess the development in bloomery iron smelting technology from the roman period to the middle ages, Minerals Vol.10, No.321, 2020.

168- A.Bazan, P.Nowicki, P.Połrolniczak and R.Pietrzak, Thermal analysis of activated carbon obtained from residue after supercritical extraction of hops, J. Therm. Anal. Calorim., Vol.125, pp.1199-1204, 2016.

169- C. F. d. Almeida, R. C. d. Andrade, G. F. de. Oliveira, P. H.Suegama, E.J. d.Arruda, J.A. Texeira and C. T. d. Carvalho, Study of porosity and surface groups of activated carbons produced from alternative and renewable biomass: buriti petiole, Orbital: Electron. J. Chem., Vol.9, No.1, pp.18-26, 2017.

170- S.arita Joshi and R. K. Srivastava, Characterization and Synthesis of Chitosan-Silica Gel and Chitosan-Bentonite Composites for Adsorption of Heavy Metals, Nature Env. Pollu. Tech., Vol.15, No. 4, 2016.

171- B. Charmas , K. Kucio, V. Sydorchuk, S. Khalameida, M. Ziezio and A. Nowicka, Characterization of Multimodal Silicas Using TG/DTG/DTA, Q-TG, and DSC Methods, Colloids Interfaces, Vol.3, No.6, 2019.

172- J.A.L.-Sanchez, G.Maties, C.G.-Arellano and A.M.D.-Pascual, Synthesis and characterization of graphene oxide derivatives via functionalization reaction with hexamethylene diisocyanate, Nanomaterials, Vol.8, No.870, 2018.

173- L.Guo, H.Yan, Z.Chen , Q.Lv , T.Bai and Y.Zhang, Graphene oxide grafted by hyperbranched polysiloxane to enhance mechanical and frictional properties of epoxy resin, SN Appl. Sci., Vol.2, No.473,(2020.

174- M.Ritu, A Simple and Effective Method of the Synthesis of Nanosized Fe_2O_3 particles, IOSR J. Appl. Chem. , Vol.4, No.6, pp.41-46, 2013.

175- D. Ouyang , Y. Zhuo, L. Hu, Q. Zeng, Y. Hu and Z. He, Research on the Adsorption Behavior of Heavy Metal Ions by Porous Material Prepared with Silicate Tailings, Minerals, Vol.9, No.291, 2019.

176- L.Ding, B.Zou, W.Gao, Q.Liu, Z. Wang, Y. Guo, X. Wang,Y. Liu, Adsorption of Rhodamine-B from aqueous solution using treated ricehusk-based activated carbon, Colloids and Surfaces A: Physicochem. Eng. Aspects, Vol.446, pp.1-7, 2014.

177- Q. Tang, N. Li, Q. Lu, X. Wang and Y. Zhu, Study on Preparation and Separation and Adsorption Performance of Knitted Tube Composite-Cyclodextrin/Chitosan Porous Membrane, Polymers, Vol.11, No.1737, 2019.

178- R.Kusumastuti, Sriyono, M.Pancoko, S.L.B.-Butar, G.E.Putra, H.Tjahjono, Study On The Mechanism of CO_2 Adsorption Process on zeolite 5A as a Molecular Sieve In RDE System: An Infrared Investigation, IOP Conf. Series: J. Phy.: Conf. Series Vol.1198, 2019.

179- M. H. Jnr, A. I.Spiff, Effects of temperature on the sorption of Pb^{2+} and Cd^{2+} from aqueous solution by *Caladium bicolor* (Wild Cocoyam) biomass, E. J. Biotechn., Vol.8, No.2, 2005.

180- A. H. Berger and A.S.Bhown, Comparing Physisorption and Chemisorption Solid Sorbents for use Separating CO_2 from Flue Gas using Temperature Swing Adsorption, Energy Procedia, Vol.4, pp.562-567, 2011.

181- N. C. Corda and M. S. Kini, A Review on Adsorption of Cationic Dyes using Activated Carbon, MATEC Web of Conferences 144, 02022, 2018.

182- K.Kusmierek and A. S.ٸtkowski, The influence of different agitation techniques on the adsorption kinetics of 4-chlorophenol on granular activated carbon, Reac. Kinet. Mech. Cat., Vol.116, pp.261-271, 2015.

183- M.ZAHOOR, Effect of Agitation Speed on Adsorption of Imidacloprid on Activated Carbon, J.Chem.Soc.Pak., Vol. 33, No.3, pp.305-312, 2011.

184- B. Priyadarshini, P. P. Rath, S. S. Behera, S. R. Panda, T. R. Sahoo and P. K. Parhi, Kinetics, thermodynamics and isotherm studies on adsorption of eriochrome black-t from aqueous solution using rutile TiO_2, IOP Conf. Series: Materials Science and Engineering Vol.310 ,2018.

185- M.S.I.Mozumder and M.A.Islam, Development of Treatment Technology for Dye Containing Industrial Wastewater, J. Sci. Res., Vol.2 No.3, pp.567-576, 2010.

186- H.Patel , R.T.Vashi, Removal of Congo Red dye from its aqueous solution using natural coagulants, J. Saudi Chem. Soc., Vol.16, pp.131-136, 2012.

187- A.Mlayah and S. Jellali, Study of continuous lead removal from aqueous solutions by marble wastes: efficiencies and mechanisms, Int. J. Env. Sci. Technol., Vol.12, pp.2965-2978, 2015.

188- R.Escudero, E.Espinoza and F.J. Tavera, Precipitation of Lead Species in a $Pb-H_2O$ System, Res. J. Recent Sci., Vol.2, No.9, pp.1-8, 2013.

189- Y. O. Khaniabadi, H. Basiri, H.Nourmoradi, M. J. Mohammadi, A.R.Yari, S. Sadeghi and A. Amrane, Adsorption of Congo Red Dye from Aqueous Solutions by Montmorillonite as a Low-cost Adsorbent, Int. J. Chem. Reac. Eng., 20160203, 2017.

References

190- M.A.Bedmohata, A.R.Chaudhari, S.P.Singh and M.D.Choudhary, Adsorption capacity of activated carbon prepared by chemical activation of lignin for the removal of methylene blue dye, Int. J. Advan. Res. Chem. Sci., Vol.2, No.8, pp.1-13, 2015.

191- S.Ramuthai,V.Nandhakumar, M.Thiruchelvi, S.Arivoli and V.Vijayakumaran, Rhodamine B adsorption- kinetic, mechanistic and thermodynamic studies, E-J. Chem., Vol.6, No.S1, pp. S363-S373, 2009.

192- D. Li, Q. Liu, S. Ma, Z. Chang and L. Zhang, Adsorption of Alizarin Red S onto Nano-sized Silica Modified with Aminopropyltriethoxysilane, Adso. Sci. & Techn., Vol.29, No.3, pp.289-300, 2011.

193- T.Sumathi and G.Alagumuthu, Adsorption Studies for Arsenic Removal Using Activated *Moringa oleifera*, Int. J. . Chem. Eng., Vol.1, pp.1-6, 2014.

194- A. Khenifi, Z. Bouberka, F. Sekrane, M. Kameche and Z. Derriche, Adsorption study of an industrial dye by an organic clay, Adsorption, Vol.13, pp.149–158, 2007.

195- Y.Cai, L.Liu, H.Tian, Z.Yang and X.Luo, Adsorption and Desorption Performance and Mechanism of Tetracycline Hydrochloride by Activated Carbon-Based Adsorbents Derived from Sugar Cane Bagasse Activated with $ZnCl_2$, Molecules, Vol.24, No.4534, 2019.

196- Momina , M.Rafatullah, S.Ismail and A.Ahmad, Optimization study for the desorption of methylene blue dye from clay based adsorbent coating, Water, Vol.11, No.1304, 2019.

197- J.Zhang, D.Cai, G.Zhang, C.Cai, C.Zhang, G.Qiu, K.Zheng and Z.Wu, Adsorption of methylene blue from aqueous solution onto multiporous

palygorskitemodified by ion beambombardment: Effect of contact time, temperature, pH and ionic strength, Appl. Clay Sci., Vol.83–84, pp.137–143, 2013.

198- Y.Kuang, X.Zhang and S.Zhou, Adsorption of Methylene Blue in Water onto Activated Carbon by Surfactant Modification, Water, Vol.12, No.587, pp.1-19, 2020.

199- L.A.Sepulveda and C.C.Santana, Effect of solution temperature, pH and ionic strength on dye adsorption onto Magellanic peat, Env. Techn., Vol.34, No.8, pp.967–977, 2013.

200- H.Benaïssa, Influence of ionic strength on methylene blue removal by sorption from synthetic aqueous solution using almond peel as a sorbent material: experimental and modelling studies, J. of Taibah University for Sci., Vol.4, pp.40-47, 2010.

201- M.Boumediene, H.Benaïssa, B.George, St.Molina and A.Merlin, Effects of pH and ionic strength on methylene blue removal from synthetic aqueous solutions by sorption onto orange peel and desorption study, J. Mate. Env. Sci., Vol.9, No.6, pp.1700-1711, 2018.

202- E.A.-García, G. Ma. C.-Camarillo and E. C.-Urbina, Effect of Ionic Strength and Coexisting Ions on the Biosorption of Divalent Nickel by the Acorn Shell of the Oak Quercus crassipes Humb. & Bonpl., Processes Vol.8, No.1229, pp.1-17, 2020.